Study of two-species chemotaxis models

Casimir Emako Kazianou

Université Pierre et Marie Curie – Paris 6 UFR 929 – Mathématiques

Etude de modèles de chimiotactisme à deux espèces

THÈSE

présentée et soutenue publiquement le 17 mars 2016

pour l'obtention du grade de

Docteur de l'Université Pierre et Marie Curie

Spécialité Mathématiques Appliquées

par

Casimir EMAKO KAZIANOU

Composition du jury

Rapporteurs :	Roberto NATALINI Magali RIBOT
Examinateurs :	Axel BUGUIN Vincent CALVEZ Marie DOUMIC
Directeurs de thèse :	Luis ALMEIDA Nicolas VAUCHELET

Laboratoire Jacques-Louis Lions — UMR 7598 Inria

Remerciements

On va se prêter à l'exercice périlleux des remerciements. Je tiens à remercier Benoît Perthame pour m'avoir fait découvrir les maths-bio au travers de son cours de Master 2 et m'avoir redirigé vers Luis Almeida et Nicolas Vauchelet, mes directeurs de thèse. Je tiens à exprimer toute ma reconnaissance envers Luis et Nicolas pour leur encadrement, disponibilité et conseils durant les trois années écoulées. C'est un honneur pour moi d'être le premier élève de Nicolas. J'espère avoir été à la hauteur et pu bénéficier de son expérience et de ses conseils. Grâce à leurs financements (ANR Kibord, ANR REGENR, programme Hubert Curien), j'ai pu voyager et participer à des conférences. Ces voyages ont été le fruit de collaborations avec Min Tang de l'Institut de Sciences Naturelles de l'Université Jiao Tong de Shanghai, Jie Liao du département de Mathématiques de East China University of Science and Technology, Pedro Patricio de l'IGC de Lisbonne. Je remercie mes collaborateurs pour m'avoir consacré de leur temps et rendu ces collaborations fructeuses.

Mes remerciements vont envers les membres de mon Jury. Merci d'avoir assité malgré votre emploi de tmeps chargé. Merci à Magali Ribot et Roberto Natalini pour avoir rapporté ma thèse. Merci pour vos commentaires sur les différents points abordés. C'est un immense plaisir de compter Vincent Calvez parmi mes examinateurs. Merci pour les séjours et invitations à Lyon. Dommage que notre collaboration n'ait pas pu abortir. Je remercie aussi Axel Buguin dont l'équipe a effectué les "jolies" expériences présentées au chapitre 3 qui m'ont permis d'illustrer notre étude théorique. Merci également à Marie Doumic de présider ce jury.

Ces trois années ont été partagées par les doctorants du laboratoire que je remercie. Un merci aux anciens pour l'intégration des premières années. Merci à (Charles, Mamadou, Pierre .L, Nicole, Magali, Anne-Cécile, Abdel, Benjamin, Waffah, Oana) Merci aux doctorants de mon année et aux plus jeunes (Guillaume, Philippe, Carlo, Jiamin, Eugénie, Jan, Sarah,Thibault.B, Thibault.L, Maxime, Pierre J.,)

J'associe aussi à ces remerciements les doctorants d'autres universités que j'ai rencontrés lors du Cemracs. Merci à (Ahmed, Lionel, Laurent V., Laurent M., Hélène, Rémi, Jean-Yves P.,). Il serait inimaginable d'oublier mes co-bureaux du 221 y compris ceux qui ont séjourné. Merci à (Malik, Guillaume, Shuyang, Bang, Ludovick, Giacomo,Tommaso, Slyvain, Carlos, Juliette, Jean-Paul, Camille) pour les discussions animées et la bonne ambiance dans le bureau. Merci également aux co-bureaux du (Laurent, Jean-François, Nicolas.S) Merci à la team Café (Sarah, Pierre-Antoine, Eric, Vincent, Alexandre, Joon). Rien de mieux qu'un petit café pour se changer les idées. Merci aux sécrétaires du laboratoire (Salima, Catherine, Nadine, Malika) pour les différentes démarches administratives. Un merci également au personnel informatique du laboratoire (Antoine, Khashayar, Altaïr, Hugues Stéphane).

Je remercie enfin mes amis(team 237(trop nombreux pour en dresser une liste exhaustive), Skipponts(Am, M'madi,Rémi, Paul, Pierre), team LDN (Ahcène, Simon, Charles, Marc)) et proches(parents, frères, soeurs, oncle, tantes et cousin(e)s) pour leur soutien indéfectible durant ces trois années.

Table des matières

Introduction générale

Introduction générale

Cette thèse porte sur l'étude de l'interaction de deux espèces sujettes au chimiotactisme. Ces deux espèces produisent et consomment les substances chimiques qui affectent leur déplacement par le processus de chimiotactisme. Les expériences menées par l'équipe d'Axel Buguin de l'Institut Curie révèlent le phénomène de synchronisation et de désynchronisation lors de la migration d'une population formée de deux espèces différentes d'E.Coli. Les travaux de Vincent Calvez, Jonathan Saragosti, Benoît Perthame et al. sur la migration d'une espèce d'E.Coli indiquent qu'elles ont un mouvement collectif de trajectoire rectiligne. Un tout autre phénomène est observé lorsqu'on met ensemble une population composée de deux espèces d'E.Coli nageant à des vitesses différentes. En fonction de la proportion de l'espèce la plus rapide dans la population, les deux espèces dans la population se déplacent ensemble ou non.
Une interprétation de ce phénomène par des modèles mathématiques est fournie ici, ainsi qu'une meilleure compréhension de l'impact des caractéristiques des deux espèces sur le comportement global de la population. Un phénomène similaire est aussi observé pour un modèle à deux espèces sans substance nutritive.
Cette introduction redéfinit dans un premier temps le chimiotactisme en insistant sur son rôle dans la migration collective de la bactérie Escherichia Coli et présente les résultats dans le cas d'une population constituée de deux espèces. Dans un deuxième temps, les modèles connus à une espèce sont rappelés ainsi que leurs résultats d'existence. Dans l'optique de bien simuler certains modèles en l'absence de solutions analytiques, il est indispensable que les schémas numériques possédent des propriétés réflétant certains aspects du modèle théorique. Ces propriétés sont introduites et certaines idées pour obtenir de tels schémas sont proposées. Enfin, les apports de cette thèse sont résumés.

1 Motivation biologique

Le chimiotactisme, phénomène sous-jacent à la migration cellulaire est expliqué. La migration de la bactérie E.coli étudiée par Calvez et Saragosti dans [115] est revisitée et les résultats obtenus pour la migration de deux espèces, point de départ de notre travail, sont exposés.

Chimiotactisme

Le chimiotactisme est le mécanisme par lequel les cellules se déplacent en réponse au changement chimique de l'environnement. Il permet à certains micro-organismes vivants de se mouvoir et s'adapter à différents environnements. Parmi les micro-organismes vivants chimiotactiques figurent la bactérie Escherichia Coli et l'amibe Dictyostelium discoideum. Ceux-ci réagissent différemment selon la nature du signal chimique extérieur (voir Figure 1) :

— Attraction par exemple par la substance nutritive,

— Répulsion par exemple par les substances nocives.

La richesse du chimiotactisme se traduit aussi par la diversité du mode de locomotion des cellules chimiotactiques. Celles-ci optent en général pour l'une des façons suivantes de se mouvoir.

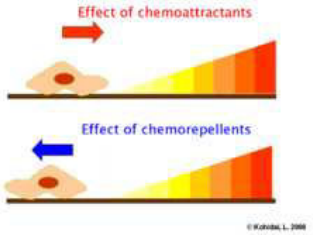

Figure 1 – Types de réponses au signal chimique extérieur

— **Nage** ("swimming") : Elle est employée par les cellules munies de flagelles pour se déplacer en milieu aqueux. La rotation des flagelles induit une propulsion de la cellule à une vitesse de l'ordre de dizaines de micromètre par seconde ($20 - 60 \mu m.s^{-1}$). Certaines espèces comme Escherichia coli ou Salmonella typhimurium avancent soit en ligne droite (phase de "run") ou bien tournent sur elles-mêmes (phase de "tumble"). Ces deux phases de mouvement sont illustrées à la Figure 2.

— **Essaimage** ("swarming") : Il traduit l'invasion des cellules sur une surface. Leurs filaments, organes externes, leur servent à se déplacer sur une surface dure. Cette structure d'essaim formée par les cellules est montrée à la Figure 3.

— **Rampage** ("Gliding") : Les bactéries non dotées d'organes externes comme les flagelles y recourent pour se propulser sur une surface.

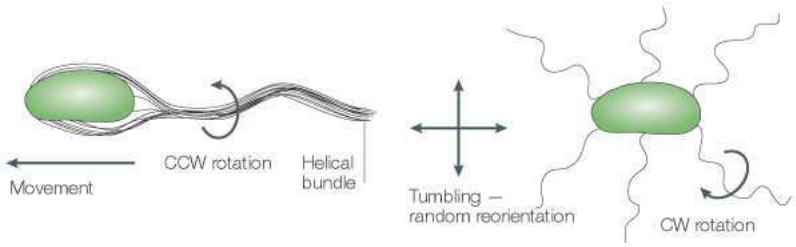

Figure 2 – Phases du mouvement de la bactérie E.Coli, image extraite de [19]

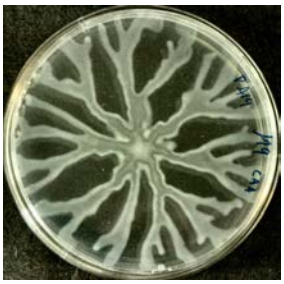

Figure 3 – Swarming de la bactérie Pseudomonas

La bactérie E.Coli, sujet de notre étude, est composée d'un corps ellipsoïdal muni de flagelles aléatoirement réparties à sa surface. Equipée de récepteurs de substances chimiques, elle est sensible à la variation du gradient temporel du stimuli. Ces récepteurs transmettent un signal aux membranes internes qui modifient le sens de rotation des flagelles et orientent la bactérie vers les zones favorables en nutriments.
Dans la section suivante, on montre que ce mouvement aléatoire des bactéries à l'échelle microscopique engendre un mouvement collectif à l'échelle macroscopique.

Du mouvement individuel d'E.Coli à la migration collective

Comme vu précédemment, la bactérie E.Coli alterne entre les phases de run et tumble pour se déplacer. Ce mouvement peut être perçu comme une marche aléatoire biasée : les longueurs des périodes de run dans les directions riches en nutriments sont plus grandes que celles dans les directions moins favorables. La bactérie préfère les directions riches en nutriments. Ceci est à l'origine de la formation d'ondes de concentration se propageant dans les microcanaux. Une telle expérience a été menée par l'équipe de Pascal Silberzan de l'Insitut Curie sur une souche de bactérie E.Coli dans [115].
Les bactéries sont initialement mises dans un microcanal de dimensions ($500\mu m \times 100\mu m \times 1.8cm$) riche en glucose et acides aminés. Celles-ci sont marquées de substances fluorescentes permettant leur observation par un stéréomicroscope. Le canal est ensuite fermé et centrifugé. Cette opération de centrifugation permet de confiner les bactéries à l'extrémité gauche du canal. Une fois la centrifugation terminée, le canal est observé à intervalles de temps réguliers. La figure 4 représente des images accolées du canal à différents instants. A un instant donné, le niveau de fluorescence rose traduisant la concentration maximale en bactéries, se déplace vers la droite du canal à une vitesse constante de quelques micromètres par seconde. Ce mouvement d'E.Coli présente trois caractéristiques majeures :

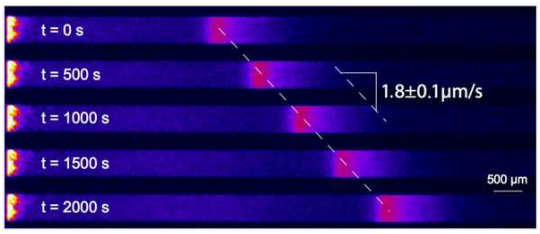

Figure 4 – Migration d'E.Coli constatée dans [115]

— La conservation du nombre de bactéries

— Le confinement de la population durant la propagation

— L'asymétrie du profil des bactéries : le nombre de bactéries se situant à droite du point central est supérieur à celui à gauche.

Cette asymétrie remarquable des profils distingue le résultat de Vincent Calvez, Jonathan Saragosti, Benoît Perthame et al. des travaux existants [2, 41, 85] sur la migration de bactérie.

Emergence d'un nouveau phénomène dans le cas de deux espèces d'E.Coli

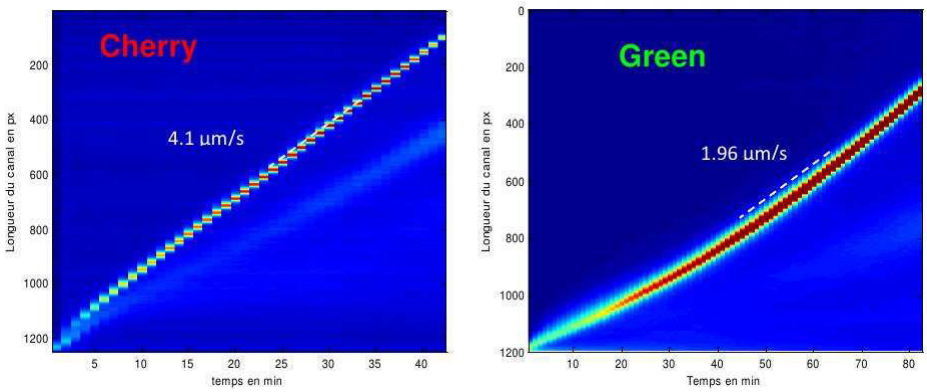

Figure 5 – Migration séparée des bactéries Cherry et Green

Dans les conditions semblables à l'expérience décrite ci-dessus, l'équipe d'Axel Buguin de l'Institut Curie a observé qu'un phénomène intéressant se produit dans le cas où la population est constituée de deux espèces de bactérie E.Coli : Cherry et Green. La figure 5 indique que séparément les bactéries Cherry forment une onde se déplaçant deux fois plus vite que les bactéries Green. Cependant, lorsque les deux

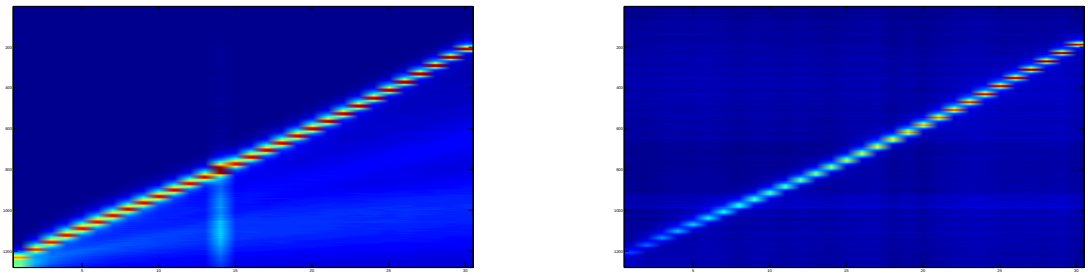

Figure 6 – Migration collective de Cherry et Green pour $\phi = 10\%$

espèces sont présentes dans la population, elles se synchronisent et se déplacent à la même vitesse ou séparément en fonction de la proportion de l'espèce la plus rapide ici Cherry. Lorsque la proportion de bactéries rapides (Cherry) est faible par exemple 10%, la population se déplace à la même vitesse comme l'atteste la Figure 6. La vitesse commume est proche de la vitesse des Green. Cependant la figure 7 montre que pour une proportion de bactéries Cherry élevée par exemple 90%, la population se sépare en deux. Les bactéries Cherry sont majoritairement dans le premier front et lesbactéries Green sont majoritaires dans le deuxième front. Les précédents modèles développés dans le cas d'une espèce de bactérie ne permettent

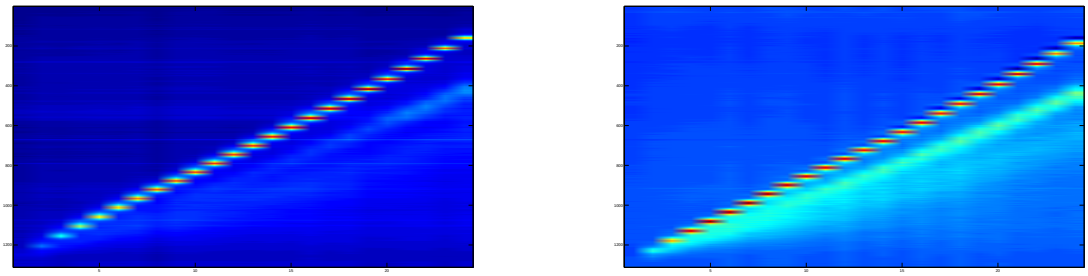

Figure 7 – Migration collective de Cherry et Green pour $\phi = 90\%$

pas de mettre en lumière la synchronisation de la population, encore moins la séparation des deux espèces.

2 Présentation et analyse de modèles de chimiotactisme à une espèce

Dans la première partie, on a montré qu'individuellement les bactéries décrivent une marche aléatoire biasée et qu'à l'échelle de la population, un mouvement collectif émerge. Ceci nous suggère deux points de vue de description du mouvement des cellules : microscopique et macroscopique. On distingue donc deux catégories de modèles. Dans cette partie, ces modèles sont présentés et les résultats d'existence et le phénomène d'explosion de leurs solutions sont enoncés. Bien que différents de part le point de vue considéré, les modèles microscopiques et macroscopiques sont liés par les limites diffusive et hyperbolique. En fonction du régime considéré, on peut préférer les modèles macroscopiques aux modèles microscopiques. Un des avantages des modèles macroscopiques réside dans une meilleure compréhension de phénomènes

macroscopiques. Par exemple, la recherche d'onde de transport dans le modèle parabolique permet de prédir et d'expliquer la migration collective d'E.Coli. Même lorsque les solutions analytiques ne peuvent pas être obtenues, comme dans la plupart des cas, les modèles macroscopiques sont moins coûteux à simuler que les modèles microscopiques (moins de variables). Cependant, ces modèles macroscopiques ne coincident avec les modèles micrososcopiques que dans un régime de validité des limites diffusives et hyperboliques. En dehors du régime de validité des limites diffusive et hyperbolique, il faut reconsidérer les modèles cinétiques qui englobent le comportement des modèles macroscopiques. La simulation de ces modèles constitue un défi de part le nombre de variables et la complexité de l'équation. Nous présentons quelques propriétés intéressantes qu'un bon schéma cinétique doit avoir.

2.1 Modèle cinétique

On introduit le modèle d'Othmer-Dunbar-Alt [99] qui décrit le mouvement microscopique de run et tumble de certaines bactéries. Dans ce modèle, les cellules sont caractérisées par leur distribution $f(x,v,t)$ des cellules de vitesse v à la position x à l'instant t. Cette distribution $f(x,v,t)$ évolue selon la dynamique :

$$\underbrace{\partial_t f + v\cdot\nabla_x f}_{\text{terme de run}} = \underbrace{\int_V \big(T[S](x,v,v',t)f(x,v',t) - T[S](x,v',v,t)f(x,v,t)\big)\,dv'}_{\text{terme de tumble}}, \tag{1}$$

où V, un sous-espace borné de $\mathbb{R}^d$, est le domaine de vitesses admissibles et $T[S]$ le noyau de réorientation des cellules.
Les deux membres de cette équation portent des significations différentes. Celui de gauche composé de la dérivée temporelle et de la dérivée spatiale représente le transport libre et donc la phase de run. Quant au membre de droite, il s'agit d'un terme intégral constitué d'un terme de gain et d'un terme de perte. Le terme de gain symbolise le nombre de bactéries qui passent de la vitesse v' à la vitesse v durant la phase de tumble. De même le terme de perte traduit le nombre de bactéries qui prennent la vitesse v'. Le noyau de réorientation $T[S](x,v,v',t)$ désigne la proportion de bactéries dont la vitesse passe de v' à v. Il dépend de la concentration de substance chimique (chimioattracteur) $S(x,t)$. Cette concentration en chimioattracteur satisfait une équation de réaction-diffusion :

$$\delta\partial_t S - \Delta S + \alpha S = \beta\rho, \quad \delta = 0,1, \tag{2}$$

avec δ,α,β des constantes et $\rho(x,t) := \displaystyle\int_V f(x,v,t)\,dv$.
Cette substance chimique est produite par les cellules elles-mêmes et provoque leur regroupement. L'équation (2) indique aussi que la substance chimique se diffuse dans le milieu et est dégradée.
Le système (1)–(2) a été l'objet de plusieurs recherches. Les questions d'existence des solutions sont explorées et les conditions d'explosion en temps sont déterminées.

Quelques résultats d'existence globale des solutions

Les résultats d'existence du système (1)–(2) dépendent des hypothèses sur le noyau de réorientation $T[S]$, de la dimension d du domaine d'étude et de la nature de l'équation (parabolique ou elliptique) sur S. Dans [28, 73], les auteurs choisissent l'hypothèse suivante sur $T[S]$

$$0 \le T[S](x,v,v',t) \le C\left(1 + S(x-v',t) + S(x+v,t)\right), \tag{3}$$

avec C une constante positive.
Cette hypothèse traduit la sensibilité des cellules à la concentration de la substance chimique. La tendance des cellules de passer de la vitesse v' à la vitesse v dépend des concentrations aux points $x+v$ et $x-v'$. La cellule localisée au point x mesure la concentration S le long de la future direction donnée par v et si celle-ci est élevée, sa propension à changer de direction est forte. De même, la cellule au point x évalue la

concentration S le long de l'actuelle direction v' et sa probabilité de se réorienter sera grande si celle-ci est faible.
Afin d'étudier le système (1)–(2), on le munit de la condition initiale f^{ini} choisie dans l'espace $L^1_+ \cap L^\infty(\mathbb{R}^d)$.
En dimension trois d'espace, dans le cas où (2) est elliptique ($\delta = 0$) avec $\beta = 0$, l'existence de solutions globales en temps $f \in L^\infty((0,\infty), L^1_+ \cap L^\infty(\mathbb{R}^3))$ et $S \in L^\infty((0,\infty), L^p(\mathbb{R}^3)$ pour $2 \leq p \leq +\infty$ est établie dans [28].
Ce résultat est étendu dans le cas où (2) est parabolique ($\delta = 1$) en dimension deux et trois d'espace dans [73] sans aucune restriction sur β.
Cependant, les cellules en réalité sont incapables de mesurer la concentration chimique, par contre elles peuvent détecter les variations du gradient en substance chimique. Ce qui pousse à substituer l'hypothèse (3) par la suivante :

$$0 \leq T[S](t,x,v,v') \leq C(1 + |\nabla_x S|\,(x+v,t) + |\nabla_x S|\,(x-v',t)). \tag{4}$$

Ces deux hypothèses (3)–(4) sur le noyau de réorientation $T[S]$ peuvent se résumer en une seule.

$$0 \leq T[S](t,x,v,v') \leq C_1 + C_2 S(x+v,t) + C_3 S(x-v',t) + C_4\,|\nabla_x S|\,(x+v,t) + C_5\,|\nabla_x S|\,(x-v',t), \tag{5}$$

où C_1, C_2, C_3, C_4, C_5 sont des constantes positives.
En rajoutant l'hypothèse supplémentaire sur $\nabla f^{ini} \in (L^1 \cap L^\infty)(\mathbb{R}^d \times V)$, Angela Stevens et al. (voir [74]) montrent l'existence des solutions $f \in (L^1_+ \cap L^\infty)(\mathbb{R}^d \times V)$ et $\nabla S \in L^\infty((0,\infty), L^p(\mathbb{R}^d))$ pour $1 \leq p \leq \infty$ en dimension deux d'espace pour le cas elliptique avec $\beta > 0$ et le cas parabolique avec $\beta > 0$.
Ce résultat en dimension deux peut être étendu à la dimension trois à condition que $C_3 = C_5 = 0$.
Une amélioration de ce résultat est fournie dans [18] dans le cas où les coefficients C_1, C_2, C_3, C_4 sont non nuls et $C_5 = 0$. Sous la condition de petitesse de la donnée initiale f^{ini}, une existence des solutions peut être obtenue dans le cas où C_1, C_2, C_3, C_4, C_5 sont non tous nuls.
D'autres formes plus réalistes du noyau de réorientation tiennent compte de la dépendance en la dérivée temporelle de la substance chimique le long de la trajectoire des cellules. Cette forme du noyau suggéré par [40] s'exprime de la façon suivante :

$$T[S](t,x,v,v') = \phi\left(\partial_t S + v' \cdot \nabla_x S\right), \tag{6}$$

où ϕ est une fonction décroissante et positive.
Sous cette hypothèse, Vauchelet prouve l'existence des solutions globales en temps dans [126] dans le cas d'un couplage de l'équation cinétique (1) avec une équation elliptique sur S.

Quelques résultats d'explosion en temps

Cependant pour certaines expressions du noyau de réorientation, une existence locale en temps des solutions régulières dans L^p du système (1)–(2) est obtenue en dimension supérieure à 2. Après ce temps, on assiste à la formation des solutions mesures. On parle alors d'une phénomène de blow-up (explosion). En dimension deux d'espace pour une donnée initiale f^{ini} à symétrie sphérique, pour le noyau de réorientation donnée par

$$T[S](t,x,v,v') = (v' \cdot \nabla_x S)^+, \tag{7}$$

on assiste à l'explosion des solutions pour une masse totale des cellules grande et un moment d'ordre 2 en espace petit dans [17].

Extension à des modèles à variable internes

Dans la modélisation du signal chimique extérieur, on peut inclure une variable interne y influant sur le noyau de réorientation. Un exemple de ce type de modèle est donné dans le cas où V est constitué de

deux vitesses $\pm v_0$ dans [117].

$$\begin{cases} \partial_t f^+ = -\partial_x(v_0 f^+) - \partial_m(G(a) f^+) - \dfrac{z(a)}{2}(f^+ - f^-), \\ \partial_t f^- = \partial_x(v_0 f^-) - \partial_m(G(a) f^-) + \dfrac{z(a)}{2}(f^+ - f^-). \end{cases}$$

Cette équation est couplée à la dynamique du taux de méthylation m

$$\frac{dm}{dt} = G(a) = k_R \left(1 - \frac{a}{a_0}\right),$$

où $a(m, S)$ désigne l'activité du récepteur dépendant du taux de méthylation m et de la concentration en chimioattracteur S.

$$a(m, S) = (1 + \exp(NE))^{-1},$$
$$E = -\alpha(m - m_0) + \ln\left(\frac{1 + S/K_I}{1 + S/K_A}\right).$$

Le noyau de réorientation z des cellules dépend cette fois-ci de l'activité des récepteurs a

$$z(a) = z_0 + \tau^{-1}(a/a_0)^H.$$

Dans ce modèle, $v_0, m_0, a_0, N, K_I, K_A, k_R, \tau, H$ sont des constantes positives. Ce modèle se généralise au cas d'un domaine continu en vitesses V

$$\partial_t f = -v \cdot \nabla_x f - \partial_m(G(a) f) + Q(f, z),$$

où $Q(f, z)$ est défini par

$$Q(f, z) = \frac{1}{|V|}\int_V z(m, S, v, v') f(x, v', m, t) dv' - \frac{1}{|V|}\int_V z(m, S, v', v) f(x, v, m, t) dv'.$$

D'autres modèles continus à variables internes sont proposés dans [40, 44]. A partir de ce modèle, on retrouve le modèle cinétique (1) dans le cas d'une adaptation rapide.

$$\partial_t f^\varepsilon + v \cdot \nabla_x f^\varepsilon + \frac{1}{\varepsilon}\partial_m(G(m - S) f^\varepsilon) = Q_\varepsilon[m, S](f^\varepsilon),$$

avec $Q_\varepsilon[m, S]$

$$Q_\varepsilon[m, S](f^\varepsilon) = \int_V \left(\Lambda(\frac{m - S}{\varepsilon}, v, v') f^\varepsilon(x, v', m, t) - \Lambda(\frac{m - S}{\varepsilon}, v', v) f^\varepsilon(x, v, m, t)\right) dv',$$

avec Λ une généralisation du noyau de réorientation $T[S]$.
Il a été démontré dans [107] que lorsque ε tend vers zéro,

$$\overline{f^\varepsilon} = \int_{\mathbb{R}} f^\varepsilon dm \rightharpoonup \overline{f^0} = \int_{\mathbb{R}} f^0 dm \quad \text{converge faible* dans } L^\infty([0, T] \times \mathbb{R}^d \times V),$$

où $f^0 = \overline{f^0}\delta(m = S)$ satisfait l'équation cinétique (1) avec le noyau de réorientation

$$T(u, v, v') = \Lambda(-\frac{u}{\widetilde{G}(0)}, v, v'), \text{avec } \widetilde{G} = -\frac{G}{y} \in C_b^1(\mathbb{R}).$$

2.2 Modèles macroscopiques

Au lieu de regarder la distribution des bactéries ayant une vitesse donnée, on cherche à caractériser l'ensemble des cellules à une position donnée dans $\mathbb{R}^d$, la densité des bactéries ρ. Pour ce faire, on emploie deux classes de modèles macroscopiques : modèle parabolique et modèle hyperbolique.
Le modèle parabolique le plus connu est le modèle de Patlak-Keller-Segel ([102]) ou Keller-Segel ([85]) dont la dynamique s'écrit :

$$\begin{cases} \partial_t \rho = \Delta \rho - \chi \nabla \cdot (\rho \nabla_x S), \\ \delta \partial_t S = \Delta S + \beta \rho - \alpha S, \end{cases} \tag{8}$$

avec χ, δ, α des constantes positives.
Ce modèle signifie que les cellules diffusent dans l'environnement et se dirigent selon le gradient de la substance chimique S. Il permet d'interpréter la formation des agrégats dans [41]. Les cellules présentes à une position favorable sécretent une substance chimique qui attirent les autres cellules. Ceci participe à l'apparition d'une accumulation de cellules.
En dimension deux d'espace, Dolbeaut et Perthame dans [12] ont déterminé une condition d'existence globale des solutions dépendant de la masse totale M des cellules et du coefficient de sensibilité χ . Si $\chi M < 8\pi$, la solution existe en temps long. Par contre, pour $\chi M > 8\pi$, on assiste à l'explosion en temps fini. En dimension supérieure, on peut citer les résultats d'existence de [21, 129] pour des données intiales petites.
On peut aussi considérer des modèles paraboliques dont la vitesse est bornée. Ce qui prévient l'explosion en temps des solutions (voir [32]).
Une autre extension du modèle (8) est le rajout d'une substance chimique extérieure aux cellules jouant le rôle de nutriments. Le système (8) prend la forme suivante :

$$\begin{cases} \partial_t \rho = \Delta \rho - \chi^S \nabla \cdot (\rho \nabla_x S) - \chi^N \nabla \cdot (\rho \nabla_x N), \\ \delta \partial_t S = \Delta S + \beta \rho - \alpha S, \\ \partial_t N = \Delta N - \gamma \rho N, \end{cases}$$

où $\chi^S, \chi^N, \alpha, \gamma, \delta, \beta$ sont des constantes positives.
Ces modèles interviennent dans les phénomènes de propagation des cellules attirées par la nourriture (voir [115]). Cependant, les modèles paraboliques ne permettent pas d'expliquer certains mécanismes observés comme la formation de réseaux. Les modèles hyperboliques développés dans [66] rendent compte de ce phénomène où ρ désigne la densité et u la vitesse moyenne. L'évolution de ces quantités est donnée par des équations de conservation.

$$\begin{cases} \partial_t \rho + \nabla \cdot (\rho u) = 0, \\ \partial_t (\rho u) + \nabla \cdot (\rho u \otimes u) + \nabla_x P(\rho) = \rho \nabla_x S - \tau_0 \rho u, \\ \delta \partial_t S - \Delta S + \alpha S = \beta \rho, \end{cases}$$

avec τ_0 la constante positive traduisant la friction et P le terme de pression.
La deuxième équation, celle sur ρu, constitue le bilan des forces appliquées au système et indique que ce dernier est soumis aux forces de pression, friction et d'attraction par la substance chimique S . Ce type de modèle est analysé numériquement par Natalini-Ribot dans [98]. Il permet d'étudier la formation des vaisseaux sanguins lors du développement embryonnaire.
Sous certaines hypothèses sur la vitesse ρu, cette équation peut se réduire à l'équation suivante

$$\partial_t \rho + \nabla \cdot (a[S]\rho) = 0,$$

avec a une fonction dépendant de la concentration S.
Dans ce modèle, le phénomène d'explosion en temps est aussi présent (voir [23, 10]). L'existence des solutions mesures est prouvée dans [76, 23] par les méthodes de flot-gradient et de dualité.

2.3 Liens entre le modèle cinétique et les modèles macroscopiques

Dans cette partie, on effectue le lien entre le modèle cinétique et les modèles macroscopiques par les changements d'échelle parabolique et hyperbolique. Une fois le changement d'échelle réalisé, on passe à la limite et on obtient les modèles parabolique et hyperbolique présentés ci-haut.

Limite diffusive

Effectuons le changement de variable suivant $\widetilde{x} = \varepsilon x, \widetilde{t} = \varepsilon^2 t$ avec ε un petit paramètre. Après ommission des tildes sur les variables, on obtient

$$\varepsilon^2 \partial_t f^\varepsilon + \varepsilon v \cdot \nabla_x f^\varepsilon = \int_V \left(T^\varepsilon[S^\varepsilon](x,v,v',t) f^\varepsilon(x,v',t) - T^\varepsilon[S^\varepsilon](x,v',v,t) f^\varepsilon(x,v,t) \right) dv',$$

$$\delta \partial_t S^\varepsilon = \Delta S^\varepsilon - \frac{\alpha^\varepsilon}{\varepsilon^2} S^\varepsilon + \frac{\beta^\varepsilon}{\varepsilon^2} \rho^\varepsilon.$$

On considère que le noyau de réorientation $T^\varepsilon[S]$ est une petite pertubation d'un noyau constant ψ :

$$T^\varepsilon[S](x,v,v',t) = \psi \times (1 + \varepsilon \phi(v' \cdot \nabla_x S)), \tag{9}$$

avec ψ une constante positive et ϕ une fonction décroissante.
La dégradation et la production de la substance chimique S sont supposées lentes et α^ε et β^ε peuvent s'écrire sous la forme suivante

$$\alpha^\varepsilon = \varepsilon^2 \alpha, \quad \beta^\varepsilon = \varepsilon^2 \beta.$$

Dans ces circonstances, réalisons le développement asymptotique formel de f^ε et S^ε :

$$\begin{aligned} f^\varepsilon &= f^0 + \varepsilon f^1 + O(\varepsilon^2), \\ S^\varepsilon &= S^0 + \varepsilon S^1 + O(\varepsilon^2). \end{aligned} \tag{10}$$

On remplace (10) dans l'équation de S^ε. Il en découle que S^0 est solution de

$$\delta \partial_t S^0 = \Delta S^0 - \alpha S^0 + \beta \int_V f^0(x,v,t) dv.$$

Injectons dès à présent (10) dans l'équation sur f^ε et comparons les deux membres de l'équation à différents ordres. Il en résulte qu'au premier ordre f^0 est donné par

$$f^0 = \frac{\int_V f^0 dv}{|V|} = \frac{\rho^0}{|V|},$$

avec $|V|$ la mesure du domaine V.
A l'ordre suivant, on obtient f^1

$$f^1 = \rho_1 + \frac{1}{|V|} \int_V \phi(v \cdot \nabla_x S^0) dv - \frac{v}{\psi |V|^2} \cdot \nabla_x \rho^0 - \frac{\phi(v \cdot \nabla_x S^0)}{|V|} \rho^0.$$

Déterminer ρ^0 nécessite une équation de fermeture du système. Cette dernière est obtenue en intégrant l'équation sur f^ε sur tout le domaine de vitesse V et en remarquant que le second membre disparaît

$$\partial_t \rho^\varepsilon + \nabla \cdot (J^\varepsilon) = 0, \tag{11}$$

avec $J^\varepsilon := \frac{1}{\varepsilon} \int_V v f^\varepsilon dv$.
Comme le premier moment de f^0 s'annule, l'expression de f^1 nous indique que

$$J^\varepsilon = -D \nabla_x \rho^0 + u[S] \rho^0 + O(\varepsilon),$$

avec

$$D = \frac{1}{\psi |V|^2} \int_V v \otimes v \, dv, \quad u[S] = -\int_V \frac{v}{|V|} \phi(v \cdot \nabla_x S^0) \, dv.$$

En passant à la limite dans l'équation de conservation de ρ^ε (11), on s'aperçoit que ρ^0 vérifie l'équation de type Keller-Segel

$$\partial_t \rho^0 = \nabla \cdot (D \nabla_x \rho^0 - u[S] \rho^0).$$

Cette dérivation formelle a été réalisée dans [100]. Une justification rigoureuse pour des formes de noyaux $T[S]$ plus générales est apportée dans [28, 73, 74] où un sens est donné à la convergence de f^ε et S^ε.

Limite hyperbolique

Après le changement d'échelle $\widetilde{t} = t\varepsilon, \widetilde{x} = x\varepsilon$, (1) s'écrit

$$\varepsilon \partial_t f^\varepsilon + \varepsilon v \cdot \nabla_x f^\varepsilon = \int_V \left(T^\varepsilon[S^\varepsilon](x, v, v', t) f^\varepsilon(x, v', t) - T^\varepsilon[S^\varepsilon](x, v', v, t) f^\varepsilon(x, v, t) \right) dv'.$$

Dans ce cas, on considère que le couplage de l'équation sur f^ε avec une équation elliptique sur S^ε.

$$\Delta S^\varepsilon - \frac{\alpha^\varepsilon}{\varepsilon^2} S^\varepsilon + \frac{\beta^\varepsilon}{\varepsilon^2} \rho^\varepsilon = 0.$$

En fonction de l'hypothèse sur $T^\varepsilon[S]$, on obtient soit un système d'équations satisfait par la densité limite ρ^0 et la vitesse moyenne u ou bien une équation que sur ρ. Considérons le modèle dans une dimension d'espace et dans le cas d'un domaine de vitesses $V = \{-1, 1\}$.
Supposons que les deux termes qui constituent le noyau de réorientation $T^\varepsilon[S]$ sont du même ordre de grandeur contrairement à (9)

$$T^\varepsilon[S](t, x, v', v) = \psi \times (1 + \varepsilon \phi(v' \partial_x S)).$$

En additionnant et soustrayant l'équation sur f^ε pour $v = \pm 1$, on obtient

$$\begin{aligned} &\partial_t \rho^\varepsilon + \partial_x J^\varepsilon = 0, \\ &\partial_t J^\varepsilon + \partial_x \rho^\varepsilon = -2 \frac{\psi}{\varepsilon} \left(J^\varepsilon + \phi(\partial_x S^\varepsilon) \rho^\varepsilon \right). \end{aligned}$$

On en déduit que J^ε admet le développement asymptotique :

$$J^\varepsilon = -\phi(\partial_x S^0) \rho^0 + O(\varepsilon).$$

Le passage à la limite dans la première équation donne

$$\partial_t \rho^0 + \partial_x (a[S^0] \rho^0) = 0,$$

avec $a[S] = -\phi(\partial_x S)$.
Cette dérivation formelle est effectuée rigouresement dans [76]. Dans le cas où les deux termes constituant le noyau de réorientation sont d'ordre différent comme dans (9), des calculs similaires montrent que le système limite est formé de deux équations de conservation. La justification théorique de ce résultat se trouve dans [50, 66, 40].

2.4 Ondes de concentration dans un modèle macroscopique

Lors de l'analyse de modèle macroscopique, on s'intéresse généralement aux solutions sous la forme d'ondes de transport ("traveling waves"). Plusieurs travaux ([69, 97]) concernent l'existence des solutions d'ondes de transport dans les équations d'advection-réaction-diffusion. Ces ondes de transport sont causées par le phénomène de croissance ou la présence de substances nutritives. Afin d'expliquer la migration

des bactéries E.Coli dans les microcanaux, Saragosti, Calvez et al. ont proposé un modèle macroscopique à deux espèces chimiques.

$$\begin{cases} \partial_t \rho = D\Delta\rho - \nabla\cdot(u[S]\rho + u[N]\rho), \\ \partial_t S = D_S \Delta S - \alpha S + \beta\rho, \\ \partial_t N = D_N \Delta N - \gamma N \rho. \end{cases} \tag{12}$$

Dans cette équation, $u[S]$ et $u[N]$ modélisent la réponse des cellules au signal chimique induit par le chimioattracteur S et le nutriment N. Ce système d'équations peut être considéré comme la limite diffusive d'un modèle macroscopique. On exprime ainsi $u[S]$ et $u[N]$ en fonction des caractéristiques microscopiques.

$$u[S] = -\int_V v\phi^S(v\cdot\nabla_x S)\frac{dv}{|V|}, \quad u[N] = -\int_V v\phi^N(v\cdot\nabla_x N)\frac{dv}{|V|},$$

avec ϕ_S, ϕ_N des pertubations du premier ordre du noyau de réorientation. Des solutions analytiques des ondes de concentration ont été obtenues dans [115]. pour des fonctions $u[S], u[N]$ de la forme

$$u[S] = \chi^S \operatorname{sgn}\partial_x S, \quad u[N] = \chi^N \operatorname{sgn}\partial_x N,$$

où sgn est la fonction signe.

Définition 1. *On dit que ρ est une **onde de concentration**, s'il existe une fonction $\widetilde{\rho}$ croissante pour les valeurs négatives, décroissante pour les valeurs positives et nulle à l'infini tel que*

$$\rho = \widetilde{\rho}(x - \sigma t),$$

où $\sigma > 0$ désigne la vitesse de l'onde.

Le modèle (12) admet des ondes de concentration :

$$\rho = \widetilde{\rho}(x-\sigma t), \quad S = \widetilde{S}(x-\sigma t), \quad N = \widetilde{N}(x-\sigma t),$$

avec ρ, S des ondes de concentration données par

$$\widetilde{\rho} = \rho^0 \begin{cases} \exp(\lambda_- z), & \lambda_- = \dfrac{\chi^N + \chi^S - \sigma}{D} \quad z<0, \\ \exp(\lambda_+ z), & \lambda_+ = \dfrac{\chi^N - \chi^S - \sigma}{D} \quad z>0, \end{cases}, \qquad \widetilde{S} = K * \widetilde{\rho},$$

où ρ^0 est une constante positive, $K := \exp\left(-\dfrac{\sigma}{2D_S}z - \dfrac{\sqrt{\sigma^2+4\alpha D_S}}{2D_S}|z|\right)$ et $\widetilde{N}$ est déterminé numériquement.
La vitesse σ de l'onde est unique et donnée par la formule implicite suivante.

$$\chi^N - \sigma = \chi^S \frac{\sigma}{\sqrt{\sigma^2+4\alpha D_S}}.$$

Sur la figure 8, les solutions théoriques tracées en noir se superposent parfaitement aux courbes expérimentales en bleu, rouge et vert prises à trois instants différents.

2.5 Schémas numériques du modèle cinétique

Après changements d'échelle dans le modèle cinétique (1), ce dernier prend la forme d'un modèle multi-échelle $\mathcal{F}^\varepsilon$ avec ε un paramètre prenant ses valeurs dans l'intervalle $[0,1]$. Les solutions f^ε du modèle $\mathcal{F}^\varepsilon$ admettent un comportement différent en fonction des valeurs de ε. Dans le cas d'un changement d'échelle parabolique, les solutions ont un comportement diffusif pour des valeurs petites de ε et un comportement hyperbolique pour des valeurs modérées de ε. Afin de différencier ces deux comportements numériquement, les schémas de discrétisation de $\mathcal{F}^\varepsilon$ doivent posséder les deux propriétés suivantes :

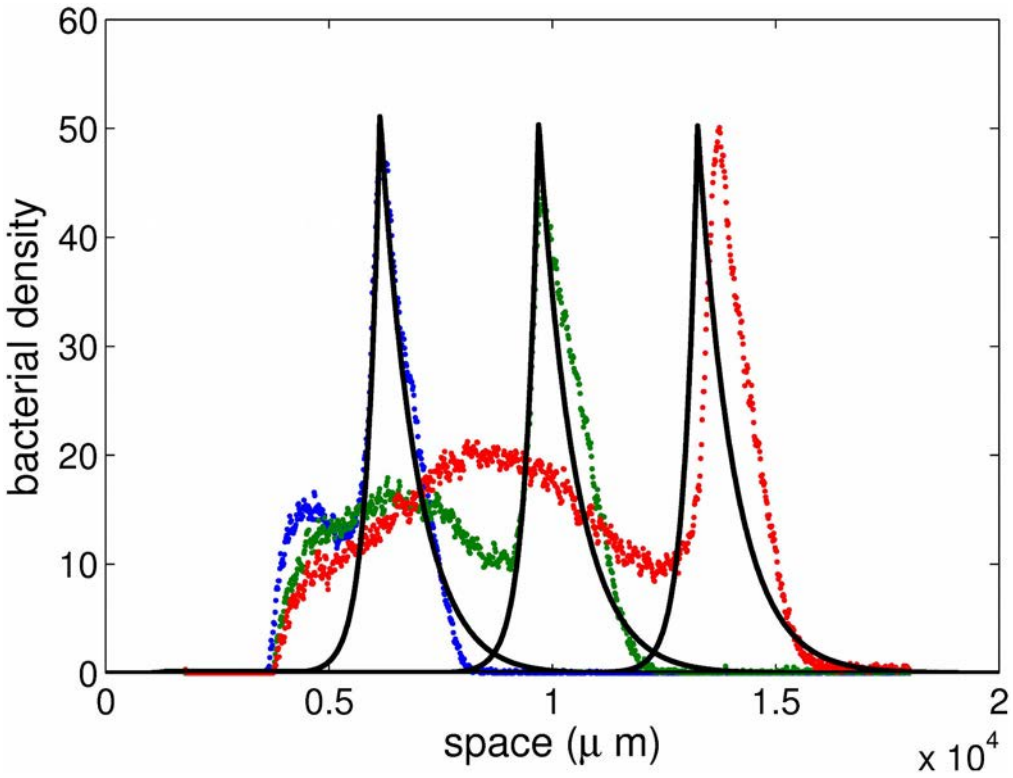

Figure 8 – Profils expérimental et théorique des bactéries dans [115]

— La première préservant l'asymptotique retrouve le comportement diffusif théorique pour des valeurs de ε petites.
— La deuxième préservant l'équilibre permet d'obtenir le comportement en temps long du système pour $\varepsilon = 1$.

Schémas préservant l'asymptotique

Les schémas préservant l'asymptotique sont des méthodes numériques pour résoudre le problème $\mathcal{F}^\varepsilon$. L'hypothèse indispensable pour la construction de tel schéma est la convergence de la solution f^ε vers la solution f^0 du problème limite $\mathcal{F}^0$ généralement vérifiée grâce aux théorèmes de convergence dans [28, 73]. Cependant, une discrétisation naïve du problème $\mathcal{F}^\varepsilon$ imposerait des contraintes très restrictives sur les pas de discrétisation temporel et spatial $\Delta t, \Delta x$ du type $\Delta t, \Delta x \sim O(\varepsilon)$ ou bien $\Delta t, \Delta x \sim O(\varepsilon^2)$ pour des raisons de stabilité. Ceci s'avère coûteux numériquement et hors de portée en grande dimension d'espace.
Ces schémas ont été introduits par Shi Jin dans [79, 81, 80] pour des modèles cinétiques dans le régime diffusif. Ils permettent une résolution du problème $\mathcal{F}^\varepsilon$ ainsi que celui de $\mathcal{F}^0$ avec une précision indépendante de ε.
Avant de définir un schéma préservant l'équilibre, quelques notations utilisées dans la définition sont rappelées.

— $\delta = (\Delta t, \Delta x)$ pas de discrétisation temporel et spatial du schéma numérique,
— $\mathcal{F}_\delta^\varepsilon$: discrétisation du modèle $\mathcal{F}^\varepsilon$,
— $\mathcal{F}_\delta^0$: discrétisation du modèle limite $\mathcal{F}^0$.

Définition 2 ([79]). *On dit que le schéma numérique $\mathcal{F}_\delta^\varepsilon$ préserve l'asymptotique si et seulement s'il satisfait les trois conditions suivantes*

— $\mathcal{F}_\delta^\varepsilon$ *est une discrétisation consistente de l'équation* $\mathcal{F}^\varepsilon$,
— *Pour* δ *fixé,* $\mathcal{F}_\delta^\varepsilon$ *tend vers la discrétisation consistente* $\mathcal{F}_\delta^0$ *quand* $\varepsilon \to 0$,
— *La condition de stabilité du schéma* $\mathcal{F}_\delta^\varepsilon$ *est indépendante de* ε.

Le diagramme de la Figure 9 résume bien cette propriété. A gauche, figurent les discrétisations consistentes des équations continues de droite. Les flèches verticales correspondent aux limites d'échelle.
L'idée principale pour construire de tels schémas consiste à transformer le problème $\mathcal{F}^\varepsilon$ en un problème équivalent $A\mathcal{F}^\varepsilon$ dont la résolution numérique est plus aisée. Illustrons cette idée dans le cas d'un modèle cinétique à deux vitesses $v = \pm 1$.

$$\partial_t u + \frac{1}{\varepsilon}\partial_x u = \frac{1}{\varepsilon^2}(v-u),$$
$$\partial_t v - \frac{1}{\varepsilon}\partial_x v = \frac{1}{\varepsilon^2}(u-v).$$

Si on considére les variables d'intérêt $\rho = u + v$ et $J = (u-v)/\varepsilon$, les nouvelles équations sur ρ et J s'écrivent

$$\begin{aligned} &\partial_t \rho + \partial_x J = 0, \\ &\partial_t J + \frac{1}{\varepsilon^2}\partial_x \rho = -\frac{2}{\varepsilon^2} J. \end{aligned} \tag{13}$$

Dans le modèle précédent, le paramètre ε n'apparaît que dans la deuxième équation. Une étude théorique de ce modèle à deux vitesses indique que la limite de J, J^0, est donnée par

$$J^0 = -\partial_x \rho^0,$$

où la limite de ρ, ρ^0, est solution de l'équation de diffusion

$$\partial_t \rho^0 - \partial_{xx}\rho^0 = 0. \tag{14}$$

Construisons un schéma qui permet d'obtenir (14) à la limite avec la bonne limite du J correspondant. L'intégration de l'équation (13) sur J entre $[t^n, t^{n+1}]$ au moyen d'un intégrateur exponentiel comme dans [48] donne :

$$J(x,t^{n+1}) = J(x,t^n)\exp\left(-2\frac{\Delta t}{\varepsilon^2}\right) - \frac{1}{\varepsilon^2}\int_{t^n}^{t^{n+1}} (\partial_x\rho)(x,u)\exp\left(\frac{2(u-t^{n+1})}{\varepsilon^2}\right)du.$$

En effectuant l'approximation $(\partial_x\rho)(x,u) \approx (\partial_x\rho)(x,t^{n+1})$ pour tout $u \in [t^n, t^{n+1}]$ au point $x_{i+1/2}$ du maillage en x, on obtient

$$J_{i+1/2}^{n+1} = J_{i+1/2}^n \exp\left(-2\frac{\Delta t}{\varepsilon^2}\right) - (\partial_x\rho)_{i+1/2}^{n+1}\left(1 - \exp\left(-2\frac{\Delta t}{\varepsilon^2}\right)\right), \tag{15}$$

avec la notation $g_{i+1/2}^n := g(x_{i+1/2}, t^n)$.
Cette formule indique que lorsque ε tend vers zéro, on récupére la bonne limite du flux J comme dans la partie limite diffusive. Pour obtenir le schéma global, il suffit d'appliquer la méthode des volumes finis à la première équation

$$\frac{\rho_i^{n+1} - \rho_i^n}{\Delta t} + \frac{J_{i+1/2}^n - J_{i-1/2}^n}{\Delta x} = 0,$$

où le flux $J_{i+1/2}^n$ est donné par (4.23).
Le passage à la limite quand $\varepsilon \to 0$ donne la discrétisation explicite de l'équation limite (14)

$$\frac{\rho_i^{n+1} - \rho_i^n}{\Delta t} - \frac{\rho_{i-1}^n - 2\rho_i^n + \rho_{i+1}^n}{(\Delta x)^2} = 0.$$

Pour des valeurs du paramètre ε proches de zéro, la condition de stabilité du schéma est donnée par

$$\Delta t < \frac{\Delta x^2}{2}.$$

Cette stratégie peut être étendue dans le cas d'un modèle avec un domaine de vitesse continu grâce à la formule de Duhamel qui donne une réprésentation de la solution du modèle cinétique sous la forme d'une intégrale en temps (voir [132, 95]). Pour des modèles plus complexes, l'intégration en temps ne peut se faire analytiquement et on doit utiliser des schémas d'intégration en temps numériques. Afin d'éviter une condition de stabilité restrictive, on emploie des schémas semi-implicites ([39, 80, 81, 79]) dans lesquels les termes en $\frac{1}{\varepsilon}$ ou bien $\frac{1}{\varepsilon^2}$ sont traités de façon implicite en temps.

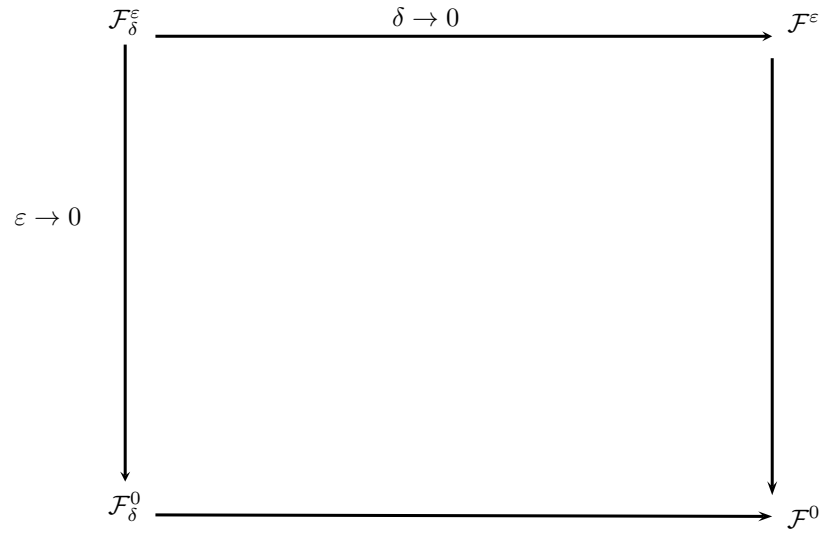

Figure 9 – Propriétés des schémas préservant l'asymptotique

Schémas préservant l'équilibre

Le comportement en temps long d'un modèle suscite autant d'intérêt que le comportement diffusif pour des petites valeurs ε. Préserver l'état d'équilibre est donc indispensable pour observer numériquement le comportement correct en temps long du modèle.

Définition 3. *On dit qu'un schéma numérique préserve l'équilibre si en temps long la solution numérique est proche de la solution théorique.*

Les schémas préservant l'équilibre ont été introduis pour les équations hyperboliques avec terme source comme les équations de Saint-Venant, Shallow-water par Greenberg-Leroux dans [62], Perthame-Siméoni dans [103], Bouchut dans [15] et Gosse-Leroux dans [60]. Dans ses récents travaux [58, 57, 61, 56], Laurent Gosse a proposé une stratégie pour traiter les modèles cinétiques issus du chimiotactisme. La plupart de ces modèles se mettent sous la forme suivante

$$\partial_t f + v\partial_x f = \mathcal{T}[S](f),$$

où $\mathcal{T}[S](f)$ est un opérateur.
Cette méthode pour développer des schémas préservant l'équilibre, s'appuie sur le calcul des états stationnaires de l'équation. A chaque itération, le problème stationnaire de l'équation est calculé sur la cellule $[x_i, x_{i+1}]$.

$$v\partial_x \widetilde{f} = \mathcal{T}[S](\widetilde{f}).$$

On impose les conditions aux bords entrantes :

$$\begin{cases} \widetilde{f}(x_{i+1}) = f_{i+1}^n, & v < 0, \\ \widetilde{f}(x_i) = f_i^n, & v > 0. \end{cases}$$

Ce problème stationnaire permet donc de calculer $\widetilde{f}_{i+1/2}$ pour $v < 0, v > 0$ donné par

$$\begin{aligned} \widetilde{f}_{i+1/2} &= \widetilde{f}(x_i), \quad v < 0 \\ \widetilde{f}_{i+1/2} &= \widetilde{f}(x_{i+1}), \quad v > 0. \end{aligned}$$

Le schéma préservant l'équilibre est alors construit de la manière suivante

$$\begin{cases} f_i^{n+1} = f_i^n - v\dfrac{\Delta t}{\Delta x}\left(f_i^n - \widetilde{f}_{i-1/2}\right), & v > 0 \\ f_i^{n+1} = f_i^n - v\dfrac{\Delta t}{\Delta x}\left(\widetilde{f}_{i+1/2} - f_i^n\right), & v < 0, \end{cases} \tag{16}$$

Remarque. Dans (16), on voit que si la solution à l'itération n, f^n est une solution du problème stationnaire, alors les valeurs de $\widetilde{f}$ sont données par

$$\begin{aligned} \widetilde{f}_{i+1/2} &= f_i^n, \quad v < 0 \\ \widetilde{f}_{i+1/2} &= f_{i+1}^n, \quad v > 0. \end{aligned}$$

Ce qui assure que $f_i^{n+1} = f_i^n$ au moins si la méthode numérique de résolution du probléme stationnaire est exacte. En général, f_i^{n+1} sera autant proche de f_i^n que la méthode numérique soit précise.

3 Contributions de la thèse

Cette thése s'intéresse à des modèles de chimiotactisme à deux espèces. Elle met en lumière les phénomènes qui se produisent lors de l'interaction de ses deux espèces. Bien qu'on se limite aux espèces issus de la même famille, leur interaction fait apparaître des phénomènes de synchronisation ou de désynchronisation. Selon les proportions des espèces dans la population, La population se comporte comme une seule entité ou bien comme deux entités distinctes.
Elle s'articule autour de quatre axes. Dans le premier chapitre, on introduit un modèle microscopique de chimiotactisme, vu comme une extension du modèle d'Othmer Dunbar et Alt. Le résultat d'existence des solutions à un système formé d'équations cinétiques couplées à une équation parabolique est prouvé. Les noyaux de réorientation des équations cinétiques incorporent la dérivée temporelle en temps de la substance chimique. La dérivation rigoureuse de l'équation de Keller-Segel multi-espèces est effectuée. Dans le second chapitre, la limite hyperbolique du modèle microscopique de chimiotactisme introduit dans le chapitre 1 est réalisée. Ceci nous permet de définir les solutions au sens de dualité du modèle hyperbolique à deux espèces en une dimension d'espace. On construit un schéma numérique convergeant vers la solution théorique afin d'étudier la dynamique du système. Le phénomène de synchronisation et de désynchronisation s'opére quand des espèces distinctes allant en sens opposé se rencontrent. Sous certaines conditions ellucidées dans ce chapitre, elles vont ensemble ou se séparent après la collision. Le troisième chapitre porte sur la recherche d'ondes de concentration dans un modèle à deux espèces avec nutriments. Le nutriment est à l'origine de la formation de l'onde. On montre théoriquement l'existence d'une onde de concentration en deçà d'une proportion de l'espèce la plus rapide. Au delà de ce seuil, les deux espèces se séparent et on retrouve le comportement observé au chapitre précédent. Le résultat théorique est conforté par les expériences discutées dans l'introduction. Le dernier chapitre définit des schémas numériques qui préservent à la fois l'asymptotique et l'équilibre. Ces schémas sont applicables au modèle cinétique couplé à une équation macroscopique. De tels modèles se retrouvent dans le chimiotactisme, le transfert radiatif et plein d'autres domaines.

Notations

Dans cette partie, on introduit les notations des espaces de fonctions qui apparaitront dans les chapitres de cette thèse.

— $L^1_+(\mathbb{R})$ est l'espace de fonctions positives de $L^1(\mathbb{R})$.

— $C_0(\mathbb{R})$ est l'ensemble des fonctions qui s'annulent à l'infini.

— $\mathcal{M}_{\mathrm{loc}}(\mathbb{R})$ est l'ensemble des mesures de Borel, $\mathcal{M}_{\mathrm{b}}(\mathbb{R})$ à variation totale bornée :

$$\mathcal{M}_b(\mathbb{R}) = \{\mu \in \mathcal{M}_{\mathrm{loc}}(\mathbb{R}), |\mu|(\mathbb{R}) < +\infty\}.$$

— $\mathcal{S}_{\mathcal{M}} = C([0,T], \mathcal{M}_{\mathrm{b}}(\mathbb{R}) - \sigma(\mathcal{M}_{\mathrm{b}}(\mathbb{R}), C_0(\mathbb{R})))$ est l'ensemble des mesures de Borel à temps continu muni de la topologie faible.

— $\mathcal{P}_2(\mathbb{R})$ est l'espace de Wasserstein d'ordre 2 :

$$\mathcal{P}_2(\mathbb{R}) = \left\{ \mu \quad \text{mesures de Borel positives de } \mathbb{R} \quad \text{tel que} |\mu|(\mathbb{R}) = 1, \int_{\mathbb{R}} |x|^2 \mu(dx) < \infty \right\}.$$

— Pour $M \in C(\mathbb{R}\backslash\{0\})$, on définit $\widehat{M}$:

$$\widehat{M} = \begin{cases} M(x), & \text{pour } x \neq 0, \\ 0, & \text{autre.} \end{cases}$$

Chapitre 1 : Existence et limite diffusive d'un modèle cinétique

Dans ce chapitre, on introduit le modèle cinétique multi-échelle à deux espèces. Dans ce modèle, les deux espèces se déplacent soit en ligne droite ou bien se réorientent sous l'influence d'une substance commune appelée chimioattracteur produit par les deux espèces.

$$\begin{cases} \varepsilon^2 \partial_t f_i^\varepsilon + \varepsilon v \cdot \nabla_x f_i^\varepsilon = -\mathcal{T}_i^\varepsilon[S^\varepsilon](f_i^\varepsilon), \\ f_i^\varepsilon(x, v, t=0) = f_i^{ini}(x, v), \quad \text{pour} \quad i = 1, 2, \end{cases} \tag{17}$$

avec

$$\mathcal{T}_i^\varepsilon[S](f) := \int_V (T_i^\varepsilon[S](x, v', v, t) f(x, v, t) - T_i^\varepsilon[S](x, v, v', t) f(x, v', t))\, dv'.$$

Dans l'équation (17), f_i^ε représente la distribution en vitesses v des espèces i pour $i = 1, 2$ et $\varepsilon > 0$ un paramètre du modèle. Les espèces se réorientent en fonction du noyau $T_i^\varepsilon[S]$ qui intégre la dépendance temporelle en S

$$\forall x \in \mathbb{R}^d,\ v, v' \in V,\ t > 0, \quad T_i^\varepsilon[S](x, v, v', t) := \phi_i^\varepsilon(\varepsilon \partial_t S + v' \cdot \nabla_x S), \quad \text{pour } i = 1, 2. \tag{18}$$

où ϕ_i^ε pour $i = 1, 2$ sont des fonctions décroissantes. Ce modèle cinétique est couplé au modèle macroscopique sur S

$$\begin{cases} \delta \partial_t S^\varepsilon - \Delta S^\varepsilon + S^\varepsilon = \displaystyle\int_V f_1^\varepsilon dv + \int_V f_2^\varepsilon dv, & \delta = 0, 1, \\ S^\varepsilon(x, t=0) = 0, & \text{pour } \delta = 1. \end{cases} \tag{19}$$

Le permier résultat concerne l'existence des solutions du modèle (17)–(19).

Théorème 1. *Soit $\varepsilon > 0$ et considérons des noyaux de réorientation $T_1^\varepsilon, T_2^\varepsilon$ de la forme* (18) *avec $\phi_1^\varepsilon, \phi_2^\varepsilon$ des fonctions positives bornées et lipschitziennes.*

Si les données initiales f_1^{ini}, f_2^{ini} sont dans $L^1_+(\mathbb{R}^d \times V) \cap L^\infty(\mathbb{R}^d \times V)$, alors il existe une solution unique globale en temps au système (17)–(19) *tel que*

$$\begin{aligned} &f_1^\varepsilon, f_2^\varepsilon \in L^\infty((0, \infty), L^1_+ \cap L^\infty(\mathbb{R}^d \times V)), \\ &S^\varepsilon \in L^\infty((0, \infty), L^p(\mathbb{R}^d)), \quad \textit{pour } 1 \leq p \leq \infty. \end{aligned}$$

Ce résultat étend le résultat d'existence des solutions aux équations cinétiques prouvées dans [126]. Dans notre cas, le noyau de réorientation dépend de la dérivée temporelle en temps de S^ε. De plus, le couplage de l'équation sur f_i^ε avec une équation parabolique sur S^ε est considérée.

Idée de la preuve :

La preuve de ce résultat s'articule en trois étapes :

1. Résolution explicite de l'équation sur S^ε (19) en fonction de $(f_1^\varepsilon, f_2^\varepsilon)$
   S^ε s'exprime comme une convolution d'un noyau G dans le cas elliptique et K dans le cas parabolique avec $\rho_i^\varepsilon = \displaystyle\int_V f_i^\varepsilon$
2. Existence locale en temps des solutions $(f_1^\varepsilon, f_2^\varepsilon, S)$ par la méthode de point fixe de Banach
   On construit itérativement des solutions d'un système "linéaire" proche du système initial. La contractivité de l'application ainsi construite découle du fait que ϕ_i^ε sont lipschitziens.
3. Existence globale obtenue grâce à des estimées uniformes en temps fini sur f_i^ε. L'existence locale en temps est étendue à l'existence globale en temps grâce à des estiméees uniformes en temps fini sur f_i^ε.

On s'intéresse à présent à la limite du système (17)–(19) quand ε tend vers zéro. On effectue une hypothèse supplémentaire sur la décomposition du noyau ϕ_i^ε pour des ε petit.

Hypothèse asymptotique sur les fonctions ϕ_i^ε du noyau de réorientation $T_i^\varepsilon[S]$ pour $i = 1, 2$

On considère que les fonctions ϕ_i^ε dans (18) admettent le développement suivant lorsque ε est petit :

$$\phi_i^\varepsilon(z) = \psi_i\big(1 + \varepsilon\theta_i(z)\big), \quad \text{pour } i = 1, 2 \tag{20}$$

avec ψ_i une constante positive et $\theta_i \in C^{0,1}(\mathbb{R}) \cap L^\infty(\mathbb{R})$ une fonction décroissante telle que $\|\theta_i\|_{L^\infty(\mathbb{R})} < 1$. On détermine formellement dans un permier temps les limites de $(f_1^\varepsilon, f_2^\varepsilon, S^\varepsilon)$ ainsi que les équations satisfaites par ces limites. Après, on justifie rigoureusement ces limites.

Dérivation formelle du modèle macroscopique

Une dérivation formelle similaire au cas une espèce indique que

$$\begin{aligned} f_i^\varepsilon &= \rho_i^0 F(v) + O(\varepsilon), \quad \text{pour } i = 1, 2, \\ S^\varepsilon &= S^0 + O(\varepsilon), \end{aligned}$$

où F est la distribution donnée par

$$F(v) := \frac{\mathbb{1}_{v \in V}}{|V|},$$

$|V|$ est la mesure du domaine V.
Les limites ρ_1^0, ρ_2^0, S^0 sont solutions du modèle macroscopique à deux espèces type Keller-Segel

$$\begin{cases} \partial_t \rho_1 = \nabla \cdot (D_1 \nabla_x \rho_1 - \chi_1[\nabla_x S]\rho_1), \\ \partial_t \rho_2 = \nabla \cdot (D_2 \nabla_x \rho_2 - \chi_2[\nabla_x S]\rho_2), \\ \delta \partial_t S = \Delta S - S + \rho_1 + \rho_2, \quad \delta = 0, 1, \end{cases} \tag{21}$$

où D_i et $\chi_i[\nabla S]$ sont définis pour $i = 1, 2$ par

$$D_i = \frac{1}{|V|^2 \psi_i} \left(\int_V v_1^2 \, dv \right) I_d, \quad \chi_i[\nabla S] = -\frac{\nabla_x S}{|\nabla_x S|} \int_V v_1 \, \theta_i(v_1 \, |\nabla_x S|) \frac{dv}{|V|}, \tag{22}$$

v_1 est la première composante de la vitesse v dans V et I_d la matrice identité. La justification rigoureuse de ce passage à la limite est donnée par le théorème qui suit.

Théorème 2. *Supposons l'hypothèse* (20) *vraie et que les données initiales* f_1^{ini}, f_2^{ini} *sont dans* $L^1_+(\mathbb{R}\times V)\cap L^\infty(\mathbb{R}\times V)$. *Alors, il existe une sous-suite de* $(f_1^\varepsilon, f_2^\varepsilon, S^\varepsilon)$ *de solution de* (17)–(19) *convergente au sens où*

$$(f_1^\varepsilon, f_2^\varepsilon) \overset{*}{\rightharpoonup} (\rho_1^0 F, \rho_2^0 F) \quad \textit{dans } L^\infty_{loc}((0,\infty), L^q(\mathbb{R}\times V)), \quad 1<q<\infty,$$
$$(S^\varepsilon, \nabla_x S^\varepsilon) \to (S^0, \nabla_x S^0) \quad \textit{dans } L^p_{loc}(\mathbb{R}^d\times(0,\infty)), \quad 1\le p\le\infty.$$

Idée de la preuve :

L'extension au cas de deux espèces du Théorème 5 de [28] est prouvée ici. La démonstration de ce résultat s'effectue en deux étapes.

1. Dérivation des estimées uniformes en ε de $(f_1^\varepsilon, f_2^\varepsilon, S^\varepsilon)$
   La conservation de la norme de f_i^ε dans $L^1(\mathbb{R}\times V)$ fournit une première estimation uniforme. L'estimée uniforme sur S^ε découle des estimées des solutions d'équations elliptiques ou parabolique du type (19).
2. Lemme de compacité d'**Aubin-Lions**
   Ce lemme permet d'extraire des sous-suites fortement convergentes en temps à partir des sous-suites faiblement convergentes.

Chapitre 2 : Dynamiques synchrones ou asynchrones dans un modèle d'agrégation à deux espèces

Le modèle hyperbolique d'agrégation à deux espèces considéré est l'analogue du modèle parabolique (21).

$$\partial_t\rho_\alpha + \chi_\alpha\partial_x\left(a(\rho)\rho_\alpha\right) = 0, \quad \text{pour } \alpha = 1,2, \tag{23}$$

avec

$$a(\rho) := \int_{\mathbb{R}} \partial_x K(x-y)\rho(t,dy), \quad \rho := \theta_1\rho_1 + \theta_2\rho_2,$$

et $\theta_\alpha, \chi_\alpha$ pour $\alpha = 1,2$ des constantes positives.
Contrairement au cas parabolique, on a une perte de régularité des solutions à cette équation car le noyau K irrégulier en zéro satisfait les hypothèses suivantes :

(H1) $K\in C^1(\mathbb{R}\backslash\{0\})$.

(H2) $\forall x\in\mathbb{R}, \quad K(x) = K(-x)$.

(H3) $\partial_x K\in L^\infty(\mathbb{R})$.

(H4) K est λ-concave avec $\lambda>0$ c'est-à-dire,

$$\forall x,y\in\mathbb{R}^*, \quad \left(\partial_x K(x) - \partial_x K(y)\right)(x-y) \le \lambda(x-y)^2.$$

Dans le cas où ρ_α est une mesure, le produit $a(\rho)\rho_\alpha$ n'est pas défini car $\partial_x K$ peut être discontinu en 0. Il est donc primordial de donner un sens à ce produit. De plus (23) est donc une équation à coefficients discontinus. Nous utliserons donc la théorie des solutions en dualité, développée dans [14] pour définir des solutions mesures.

Définition 4. *On dit que* $(\rho_1,\rho_2)\in C([0,T],\mathcal{M}_b(\mathbb{R})^2)$ *est une solution au sens de la dualité de* (23) *s'il existe* $\hat a(\rho)\in L^\infty((0,T)\times\mathbb{R})$ *et* $\gamma\in L^1_{loc}([0,T])$ *satisfait* $\partial_x\hat a\le\gamma$ *au sens des distributions, tel que pour* $0<t_1<t_2<T$,

$$\partial_t\rho_\alpha + \chi_\alpha\partial_x(\hat a(\rho)\rho_\alpha) = 0, \quad \textit{pour } \alpha=1,2, \quad \rho = \theta_1\rho_1+\theta_2\rho_2, \tag{24}$$

au sens de la dualité dans (t_1,t_2) *et* $\hat a(\rho) = \partial_x K * \rho$ *presque partout. On insiste que la donnée finale de* (24) *doit être* t_2 *au lieu de* T.

Le théorème suivant fournit l'existence et l'unicité des solutions en dualité.

Théorème 3. *Soit $T > 0$ et $(\rho_1^{ini}, \rho_2^{ini}) \in \mathcal{P}_2(\mathbb{R})^2$. Sous les hypothèses (H1)–(H4), il existe une unique solution en dualité $(\rho_1, \rho_2) \in C([0,T], \mathcal{P}_2(\mathbb{R})^2)$ de (23) selon la définition 4 avec $(\rho_1, \rho_2)(t=0) = (\rho_1^{ini}, \rho_2^{ini})$ tel que*

$$\hat{a}(\rho) := \int_{\mathbb{R}} \widehat{\partial_x K}(x-y)\rho(t,dy), \quad \rho = \theta_1\rho_1 + \theta_2\rho_2. \tag{25}$$

La solution au sens de la dualité est équivalente à la solution flot-gradient définie dans [36].

Idée de la preuve :

La difficulté du problème vient de la singularité du potentiel $\partial_x K$ en zéro. Dans un premier temps, on régularise le noyau $\partial_x K$ en considérant la suite de fonctions $\partial_x K^n$ continues coincidant avec $\partial_x K$ en dehors de zéro et linéaire autour de zéro. De plus, on définit a_n par

$$a^n(\rho) = \int_{\mathbb{R}} \partial_x K^n(x-y)\rho(t,dx), \tag{26}$$

On considère alors le problème approché :

$$\partial_t \rho_\alpha^n + \chi_\alpha \partial_x \left(a^n(\theta_1\rho_1^n + \theta_2\rho_2^n)\rho_\alpha^n\right) = 0, \quad \text{for } \alpha = 1,2. \tag{27}$$

La preuve s'effectue en trois étapes :

1. Existence des solutions de dualité du problème approché (27)
2. Calcul de la limite $a^n(\theta_1\rho_1^n + \theta_2\rho_2^n)\rho_\alpha^n$
   Cette étape est importante dans la démonstration et fait l'objet du lemme central du chapitre 2. Il permet aussi le passage à la limite du modèle microscopique au modèle hyperbolique.
3. Passage à la limite et stabilité des solutions de dualité.

Le lien entre modèle microscopique et modèle macorscopique est étudié par la suite. On propose comme modèle microscopique une version simplifiée du modèle cinétique (17) introduit dans le permier chapitre.

$$\begin{cases} \partial_t f_\alpha^\varepsilon + v\,\partial_x f_\alpha^\varepsilon = \dfrac{1}{\varepsilon}\displaystyle\int_V \left(T_\alpha[S](v',v)f_\alpha^\varepsilon(v') - T_\alpha[S](v,v')f_\alpha^\varepsilon(v)\right)dv', \quad \alpha = 1,2,\ v \in V = \{\pm 1\}, \\ -\partial_{xx}S^\varepsilon + S^\varepsilon = \theta_1\left(f_1^\varepsilon(1) + f_1^\varepsilon(-1)\right) + \theta_2\left(f_2^\varepsilon(1) + f_2^\varepsilon(-1)\right), \end{cases} \tag{28}$$

où $f_\alpha^\varepsilon(x,v,t)$ représente la distribution en vitesse de l'espèce α à l'instant t à la position x, $S^\varepsilon(t,x)$ la concentration de l'espèce chimique, $T_\alpha[S](v,v')$ le noyau de réorientation de la direction $v \in V$ à la direction $v' \in V$ et $\varepsilon > 0$ un paramètre.
On opte pour un noyau $T_\alpha[S]$ dépendant du gradient en la substance chimique

$$T_\alpha[S](v,v') = \psi_\alpha\left(1 - \chi_\alpha v \partial_x S\right), \tag{29}$$

où ψ_α est une constante positive et χ_α est la sensibilité à la substance chimique S.
La convergence du modèle microscopique (28) vers le modèle macroscopique (23) est énoncée par le théorème suivant.

Théorème 4. *Soit $T > 0$ et supposons que $\chi_\alpha(\theta_1 + \theta_2) < 1$ pour $\alpha = 1,2$. Soit $(f_\alpha^\varepsilon, S^\varepsilon)$ la solution de l'équation cinétique (28) tel que $f_\alpha^\varepsilon(t=0) = f_\alpha^{ini}$ et $f_\alpha^{ini} \in L^\infty \cap L_+^1(\mathbb{R})$ et $\displaystyle\int_{\mathbb{R}} x^2 f_\alpha^{ini} dx < \infty$.*
Alors, quand $\varepsilon \to 0$, $(f_\alpha^\varepsilon, S^\varepsilon)$ converges vers (ρ_α, S) au sens où :

$$\begin{aligned} &\rho_\alpha^\varepsilon := f_\alpha^\varepsilon(1) + f_\alpha^\varepsilon(-1) \rightharpoonup \rho_\alpha \quad \textit{faiblement dans} \quad \mathcal{S}_M, \quad \textit{pour } \alpha = 1,2, \\ &S^\varepsilon \rightharpoonup S \quad \textit{faiblement dans} \quad C([0,T], W^{1,\infty}(\mathbb{R})), \end{aligned}$$

où ρ_α est l'unique solution de dualité de (23) et $S = K * (\theta_1\rho_1 + \theta_2\rho_2)$ donné par le Théorème 3.

Idée de la preuve :

A partir de (28), on définit les dynamiques de $\rho_\alpha^\varepsilon := f_\alpha^\varepsilon(1) + f_\alpha^\varepsilon(-1)$ et $J_\alpha^\varepsilon := f_\alpha^\varepsilon(1) - f_\alpha^\varepsilon(-1)$. On utilise le résultat du calcul de la limite du produit $\hat{a}(\theta_1\rho_1^\varepsilon + \theta_2\rho_2^\varepsilon)\rho_\alpha^\varepsilon$ et on conclue par passage à la limite dans les équations de ρ_α^ε et J_α^ε.

Après avoir prouvé l'existence des solutions au sens de dualité de (23) et établi le lien entre ce modèle et le modèle microscopique (28), on s'intéresse à la simulation numérique de (23).

Considérons une grille cartésienne de pas de temps Δt et d'espace Δx dont les points sont $x_j = j\Delta x, j \in \mathbb{Z}, t^n = n\Delta t, n \in \mathbb{N}$. La discrétisation de $\rho_\alpha(t^n, x_j)$ notée $\rho_{\alpha,j}^n$ est construite par la méthode de volumes finis dont le flux $F_{\alpha,j-1/2}^n$ est donné par la méthode de splitting de flux. Etant donné $(\rho_{\alpha,j}^n)$ connu au temps t^n, on calcule $\rho_{\alpha,j}^{n+1}$ par le schéma suivant :

$$\begin{cases} \dfrac{\rho_{\alpha,j}^{n+1} - \rho_{\alpha,j}^n}{\Delta t} + \dfrac{F_{\alpha,j+1/2}^n - F_{\alpha,j-1/2}^n}{\Delta x} = 0 \quad \text{pour } \alpha = 1,2 \text{ et } j \in \mathbb{Z}, \\ F_{\alpha,j-1/2}^n = \chi_\alpha \left((\hat{a}_{j-1}^n)^+ \rho_{\alpha,j-1}^n + (\hat{a}_j^n)^- \rho_{\alpha,j}^n \right), \\ \hat{a}_j^n = \displaystyle\sum_{i \neq j} \partial_x K(x_j - x_i) \left(\theta_1 \rho_{1,i}^n + \theta_2 \rho_{2,i}^n \right), \end{cases} \tag{30}$$

où $(\cdot)^+ := \max\{(\cdot), 0\}$ et $(\cdot)^- := \min\{(\cdot), 0\}$ désignent respectivement la partie positive et négative de $(\cdot)$.
Le schéma numérique assure la conservation de la masse des espèces et du centre de masses ponderés par les sensibilités χ_α.

Théorème 5. *Soient $T > 0$, $\Delta x > 0$ et $\Delta t > 0$ tels que la condition de stabilité $\max(\chi_1, \chi_2)\|\partial_x K\|_{L^\infty}(\theta_1 + \theta_2)\frac{\Delta t}{\Delta x} < 1$ soit satisfaite et notons $N_t = \frac{T}{\Delta t}$. Soit $\rho_\alpha^{ini} \in \mathcal{P}_2(\mathbb{R})$, on définit*

$$\rho_{\alpha,j}^0 = \int_{x_{j-\frac{1}{2}}}^{x_{j+\frac{1}{2}}} \rho_\alpha^{ini}(dx), \qquad j \in \mathbb{Z}.$$

On définit $\rho_{\alpha,\Delta x} \in \mathcal{M}_b([0,T] \times \mathbb{R})$ par

$$\rho_{\alpha,\Delta x}(t,x) = \sum_{n=0}^{N_t - 1} \sum_{j \in \mathbb{Z}} \rho_{\alpha,j}^n \mathbb{1}_{[t^n, t^{n+1}[}(t) \delta_{x_j}(x), \tag{31}$$

où $(\rho_{\alpha,j}^n)_{j,n}$ est calculé par (37).
Alors, on a

$$\rho_{\alpha,\Delta x} \rightharpoonup \rho_\alpha \quad \textit{converge faiblement dans} \quad \mathcal{M}_b([0,T] \times \mathbb{R}) \quad \textit{quand} \quad \Delta x \to 0,$$

où ρ_α est la solution en dualité du Théorème 3 avec la donnée initiale ρ_α^{ini}.

Idée de la preuve :

Dans cette démonstration, on s'appuie aussi sur le lemme de la limite du produit $\hat{a}(\theta_1\rho_1^n + \theta_2\rho_2^n)\rho_\alpha^n$.

Dans un modèle similaire à (23), on observe la formation en temps fini d'un agrégat unique dont la position est donnée par le centre de masse ponderés par les sensibilités χ_α. On présente deux situations. Dans la première situation, on assiste à la formation des masses de dirac des espèces. Ces masses de dirac se déplacent pour former l'agrégat commun. Lors de leur déplacement, les masses de dirac d'espèces différentes se recontrent et se déplacent ensemble (voir Figure 10). On parle du phénomène de synchronisation. Par contre, dans la deuxième situation, après leurs collisions, les masses de dirac se déplacent indépendamment l'une de l'autre (voir Figure 11). Dans ce cas, il s'agit plutôt d'une désynchronisation.

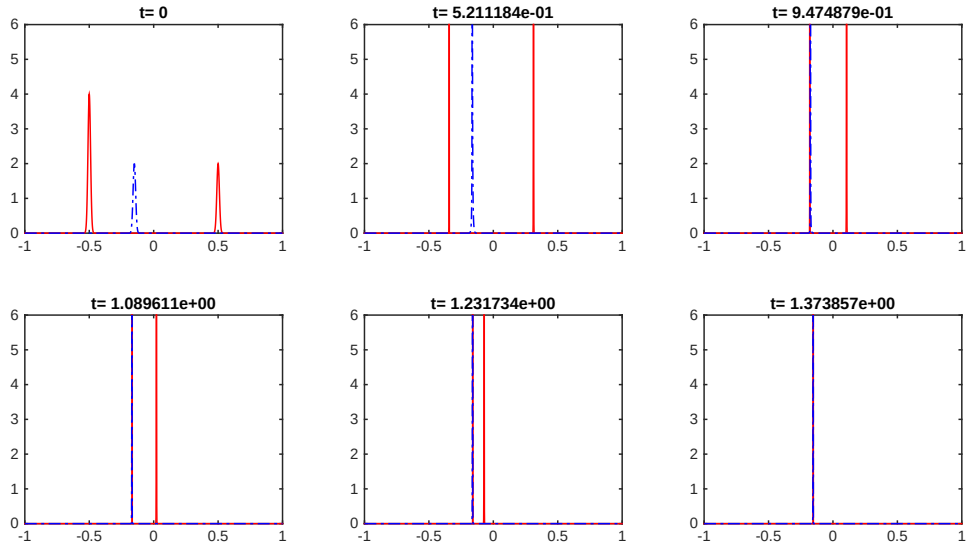

Figure 10 – Phénomène de synchronisation après collisions. ρ_1 en rouge et en ligne et ρ_2 en bleu et en pointillés.

Chapitre 3 : Description mathématique de la migration collective de deux espèces d'E.Coli

Ce chapitre étudie la migration d'une population de deux bactéries différentes dans des microcanaux. On propose un modèle à deux espèces de type Keller Segel semblable à (21). La différence avec le modèle (21) est la présence d'une seconde substance chimique consommée par les bactéries. Elle garantit la formation d'une onde de concentration comme vu dans le cas d'une espèce. Le modèle étudié se met sous la forme suivante

$$\begin{cases} \partial_t \rho_1 = D_1 \rho_1 - \nabla \cdot (\rho_1 (u_1[S] + u_1[N])), \\ \partial_t \rho_2 = D_2 \Delta \rho_2 - \nabla \cdot (\rho_2 (u_2[S] + u_2[N])), \\ \partial_t S = D_S \Delta S - \alpha S + \rho_1 + \rho_2, \\ \partial_t N = D_N \Delta N - \gamma_1 \rho_1 N - \gamma_2 \rho_2 N, \end{cases} \tag{32}$$

avec $D_1, D_2, D_S, D_N, \alpha, \gamma_1, \gamma_2$ des constantes positives.
Dans (32), ρ_1, ρ_2 décrivent respectivement les densités des bactéries de type 1 et 2 dans la population. S joue le rôle de la substance chimique "attractative". N est la source nutritive des bactéries.
On se restreint aux formes particulières de $u_i[S], u_i[N]$ suivantes.

$$u_i[S] = \chi_i^S \operatorname{sgn}(\partial_x S), \quad u_i[N] = \chi_i^N \operatorname{sgn}(\partial_x N), \qquad i = 1, 2, \tag{33}$$

avec χ_i^S, χ_i^N, les sensibilités chimiotactiques de la sous-population i au chimioattracteur S et nutriment N. On prouve le théorème suivant sur l'existence et la non-existence d'ondes de concentration de (32). Il démontre l'existence de deux régimes en fonction de la fraction de la bactérie la plus rapide dans la population. Ce résultat fait écho aux observations numériques du chapitre 2.

Théorème 6. *Supposons que séparément les deux sous-populations se déplacent en formant une onde de concentration prédite par le modèle à une espèce de Saragosti-Calvez et al. Nommons σ_1 la vitesse de l'espèce la plus lente et σ_2 celle de l'espèce la plus rapide. Soit M_i le nombre d'individus de la sous-population i, $\phi_{cherry} = \frac{M_2}{M_1+M_2}$ le pourcentage de la sous-population rapide et I_i l'intervalle $[\chi_i^N - \chi_i^S, \chi_i^N + \chi_i^S]$ pour $i = 1, 2$.*

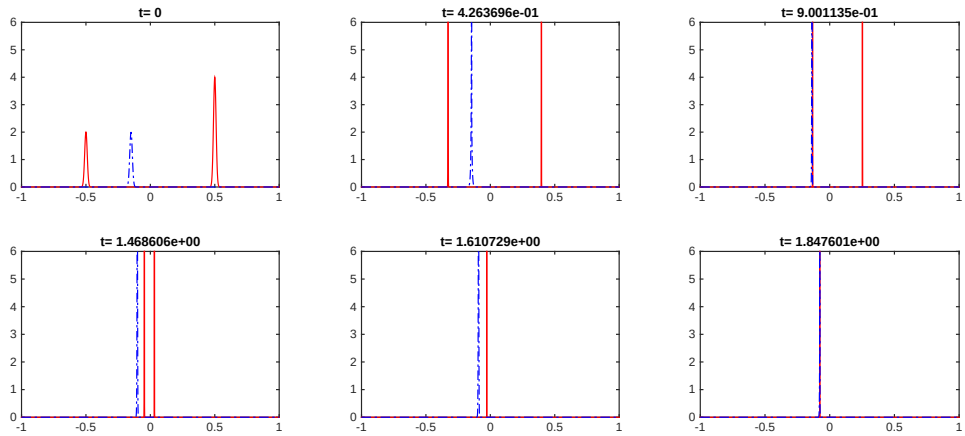

Figure 11 – Phénomène de désynchronisation après collisions. ρ_1 en rouge et en ligne et ρ_2 en bleu et en pointillés.

Si l'hypothèse suivante est satisfaite

$$I_1 \cap I_2 \neq \varnothing, \quad \text{et } \sigma_2, \chi_2^N - \chi_2^S \notin I_1 \cap I_2.$$

Alors il existe une fraction $\phi^*_{cherry} \in]0,1[$ *telle que*

— *Pour* $\phi_{cherry} \leq \phi^*_{cherry}$, *il existe une onde de concentration de vitesse* σ *comprise entre* σ_1 *et* σ_2 *solution de l'équation*

$$(\sigma - \chi_1^N) + \chi_1^S \frac{\sigma}{\sqrt{\sigma^2 + 4\alpha D_S}} + \frac{\phi_{cherry}}{1-\phi_{cherry}} H(\sigma) \left((\sigma - \chi_2^N) + \chi_2^S \frac{\sigma}{\sqrt{\sigma^2 + 4\alpha D_S}} \right) = 0, \tag{34}$$

où H *est une fonction positive définie dans cette section.*

— *Pour* $\phi_{cherry} > \phi^*_{cherry}$, *il n'existe pas d'onde de concentration.*

Idée de la preuve :

Elle repose sur la construction des profils de ρ_1, ρ_2 sous la forme de double exponentielle. On impose la condition selon laquelle le profil en S est maximal en zéro. On obtient ainsi la condition que doit vérifier la vitesse d'onde σ. L'étude de cette fonction permet d'exhiber une condition dépendant de la ϕ_{red} sur l'existence ou la non existence de σ.

La figure 12 compare les résultats théoriques aux simulations numériques du modèle pour des proportions différentes. La figure 13 représente la vitesse des deux sous-populations Cherry et Green en fonction de la proportion ϕ_{cherry}. Cette figure compare les résultats expérimentaux aux résultats théoriques. On observe que le modèle proposé est en adéquation avec les résultats expérimentaux.

Chapitre 4 : Schémas numériques asymptotiques et préservant les équilibres pour les modèles cinétiques

On propose un schéma numérique qui préserve à la fois l'équilibre et l'asymptotique pour les modèles cinétiques similaires à (1)–(2).

$$\varepsilon^2 \partial_t f^\varepsilon + \varepsilon v \partial_x f^\varepsilon = \mathcal{T}[S](f^\varepsilon),$$

avec $\mathcal{T}[S](f^\varepsilon)$ le terme intégral.
Ce schéma se décompose en deux étapes.

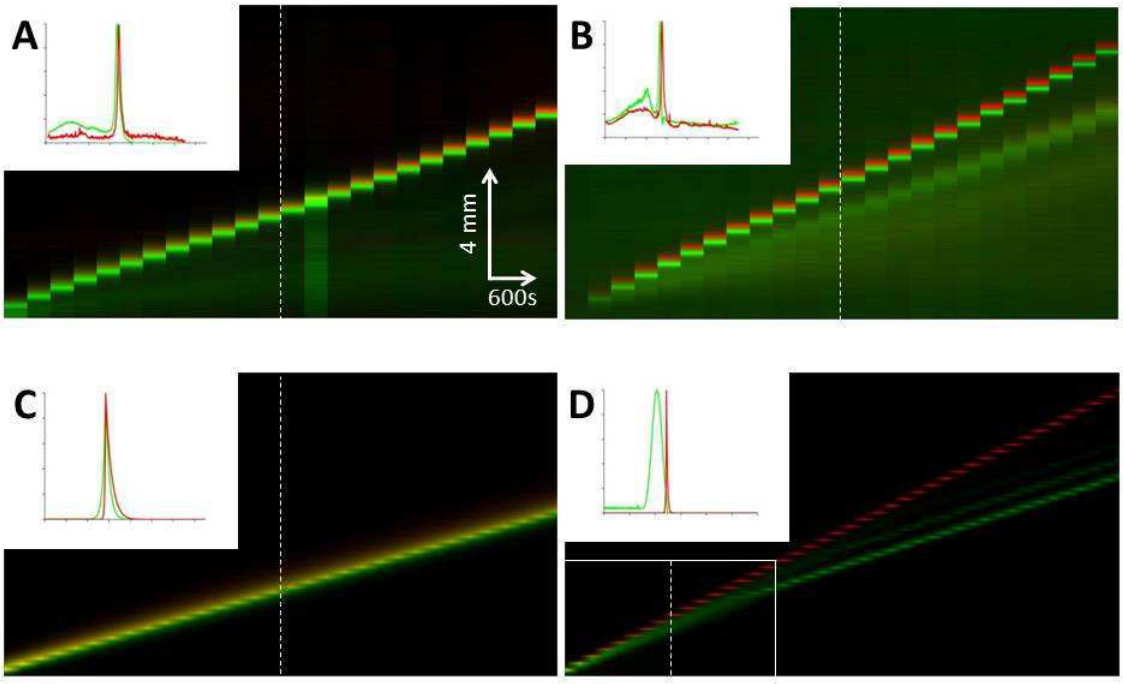

Figure 12 – Kymographes illustrant le comportement de l'onde pour des proportions différentes. (A) Résultat expérimental obtenu pour $\phi_{cherry} = 10\%$. (B) Résultat expérimental obtenu pour $\phi_{cherry} = 90\%$. (C) Simulation numérique du modèle pour $\phi_{cherry} = 10\%$ (D) Simulation numérique du modèle pour $\phi_{cherry} = 90\%$. Le rectangle en blanc dans le coin gauche correspond à la taille des images A, B et C. Pour l'image D, la simulation est réalisée pour des temps longs au delà du régime transitoire où les pics sont bien séparés. Les profils des espèces rouges et vertes sont représentés dans le carré blanc de gauche.

— **Prédiction** : A cette étape, on impose la propriété de conservation de l'asymptotique. A partir de la variable microscopique f_i^n et la variable macroscopique ρ_i^n obtenus à l'itération précédente, on en déduit la variable microscopique $\widetilde{f}_i^{n+1}$ et la variable macroscopique $\widetilde{\rho}_i^{n+1}$ en effectuant un pas d'un schéma préservant l'asymptotique.

— **Résolution du problème stationnaire** : Pour chaque cellule $[x_i, x_{i+1}]$, les états stationnaires sont calculés en considérant le problème :

$$v\partial_x \hat{f}^\varepsilon = \frac{1}{\varepsilon}\mathcal{T}[S](\hat{f}^\varepsilon). \tag{35}$$

Cette équation (35) est munie des conditions aux bords entrantes

$$\begin{cases} \hat{f}(x_i, v) & = (1-\widetilde{\alpha})f_i^n + \widetilde{\alpha}\widetilde{f}_i^{n+1}, \quad v > 0, \\ \hat{f}(x_{i+1}, v) & = (1-\widetilde{\alpha})f_{i+1} + \widetilde{\alpha}\widetilde{f}_{i+1}^{n+1}, \quad v < 0, \end{cases}$$

avec $\widetilde{\alpha} = \min(1, \frac{\Delta t}{\varepsilon})$ et $\widetilde{f}_i^{n+1}$ donné par l'étape de prédiction. On définit alors $\hat{f}_{i+1/2}$ par :

$$\begin{aligned} \hat{f}_{i+1/2} &= \hat{f}(x_{i+1}, v), \quad v > 0 \\ \hat{f}_{i+1/2} &= \hat{f}(x_i, v), \quad v < 0. \end{aligned} \tag{36}$$

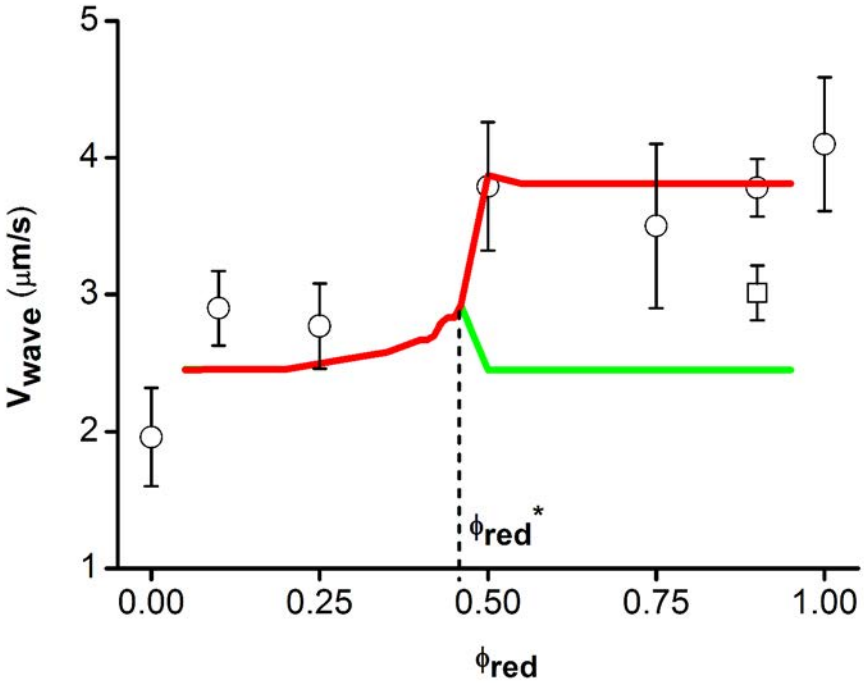

Figure 13 – Vitesse de l'onde en fonction de la proportion ϕ_{cherry} : les résultats expérimentaux sont représentés par leurs moyennes (cercles) et leurs écarts types (barres d'erreur). On dispose d'au moins une dizaine de points pour chaque valeur. Les résultats expérimentaux sont comparés aux simulations (courbes rouge et verte). On observe une séparation des deux espèces autour de la valeur $\phi_{cherry} = 50\%$. Le carré correspond à la vitesse moyenne de l'onde verte observée à la figure 12 D.

Le schéma numérique s'écrit donc :

$$\begin{aligned} &\frac{f_i^{n+1} - f_i^n}{\Delta t} + \frac{v}{\varepsilon \Delta x}\left((1-\widetilde{\alpha}) f_i^n + \widetilde{\alpha} f_i^{n+1} - \hat{f}_{i-1/2}\right) = 0, \quad v > 0, \\ &\frac{f_i^{n+1} - f_i^n}{\Delta t} + \frac{v}{\varepsilon \Delta x}\left(\hat{f}_{i+1/2} - \left((1-\widetilde{\alpha}) f_i^n + \widetilde{\alpha} f_i^{n+1}\right)\right) = 0, \quad v < 0, \end{aligned} \tag{37}$$

où $\hat{f}_{i+1/2}$ est solution du problème (36).

Proposition 7. *Lorsque le schéma préservant l'asymptotique est utilisé pour l'étape de prédiction et le schéma préservant l'équilibre employé pour la résolution du problème stationnaire,*
alors le schéma numérique proposé en (37) *préserve à la fois l'équilibre et l'asymptotique.*

Cette méthode de dérivation des schémas qui présevent à la fois l'état d'équilibre et l'asymptotique peut être employée à d'autres équations cinétiques. Elle peut aussi être adaptée afin d' obtenir des schémas d'ordre élevé en temps.

4 Perspectives

La première perspective de notre travail concerne l'étude de modèle hyperbolique à deux espèces avec $a(\rho)$ non-linéaire par rapport à ρ.

4.1 Etude de modèles hyperboliques à deux espèces avec a non-linéaire

On considère maintenant uen généralisation de l'équation hyperbolique à deux espèces (23)

$$\partial_t \rho_\alpha + \chi_\alpha \partial_x \left(a(\rho) \rho_\alpha \right) = 0, \quad \text{pour } \alpha = 1, 2, \tag{38}$$

avec

$$a(\rho) := \phi \left(\int_{\mathbb{R}} \partial_x K(x-y) \rho(t, dy) \right), \quad \rho := \theta_1 \rho_1 + \theta_2 \rho_2,$$

ϕ est une fonction non-linéaire.
Ce cas a été traité dans le cas d'une espèce dans [76] où l'existence d'une entropie permet de définir le produit $a(\rho)\rho$ et d'obtenir l'unicité des solutions de dualité. Dans le cas de deux espèces, il n'existe pas d'entropie et la technique employée dans le cas d'une espèce est inapplicable. De plus, les outils de flot-gradient sont inutilisables à cause de la non-linéarité de ϕ.
Si l'on suit l'approche utilisée dans le cas où ϕ est linéaire, on se heurte au problème du calcul de la limite de $a(\theta_1 \rho_1^n + \theta_2 \rho_2^n)\rho_\alpha^n$. L'existence de solutions dans ce cas reste un problème ouvert.

4.2 Existence d'ondes de concentration à l'échelle cinétique

L'existence d'ondes de transport a déjà été étudiée au niveau macroscopique. On se demande si ce type d'onde existe au niveau microscopique dans le cas d'un modèle à une espèce.

$$\begin{cases} \partial_t f + v\, \partial_x f = \displaystyle\int_V \left(T[S](v', v) f(v') - T[S](v, v') f(v) \right) dv' + \int_V \left(T[N](v', v) f(v') - T[N](v, v') f(v) \right) dv', \; v \in V, \\ \partial_t S = D_S \Delta S - \alpha S + \rho, \\ \partial_t N = D_N \Delta N - \gamma \rho N, \end{cases} \tag{39}$$

où D_S, D_N, α, γ sont des constantes positives et les noyaux de réorientation $T[S], T[N]$ sont donnés par

$$\begin{aligned} T[S] &= \psi \left(1 - \chi^S \operatorname{sgn}(v \partial_x S) \right), \\ T[N] &= \psi \left(1 - \chi^N \operatorname{sgn}(v \partial_x N) \right), \end{aligned} \tag{40}$$

ψ, χ^S, χ^N sont des constantes positives.
Ce problème consiste à prouver l'existence de $\sigma > 0$ et de profils $f(z, v)$ tel que

$$\begin{cases} (v - \sigma) \partial_z f = \displaystyle\int_V \left(T[S](v', v) f(v') - T[S](v, v') f(v) \right) dv' + \int_V \left(T[N](v', v) f(v') - T[N](v, v') f(v) \right) dv', \\ -\sigma S' = D_S S'' - \alpha S + \rho, \\ -\sigma N' = D_N N'' - \gamma \rho N, \end{cases}$$

avec

$$T[S] = \psi \left(1 - \chi^S \operatorname{sgn}(vz) \right), \quad T[N] = \psi \left(1 - \chi^N \operatorname{sgn}(v) \right).$$

Dans le cas où V se réduit à deux vitesses ($V = \{\pm 1\}$), l'existence d'ondes de transport peut être obtenue de la même façon que dans le cas macroscopique. En effet, le calcul analytique de f est rendu possible par le changement de variable ρ et J.
Cependant, ce problème s'avère compliquée dans le cas d'un continum de vitesse car on ne peut plus calculer analytiquement la relation implicite que doit verifier σ même après avoir fait des hypothèses de décroissance exponentielle en x de f.
Même en s'inpirant de la méthode utilisée dans [22] pour démontrer l'existence des solutions stationnaires ($\sigma = 0$ sans l'équation sur N), on se heurte à des difficultés pour prouver la croissance et décroissance du profil ρ assurant ainsi l'existence d'une onde de transport.
D'autre part, prouver la positivté de σ et en donner une borne supérieure demeure un écueil de plus à surmonter.

4.3 Extension du schéma numérique WB-AP au cas 2D

On se demande si on peut généraliser la stratégie d'obtention des schémas numériques WB-AP en dimension 2. Dans ce cas, on considérerait la version 2D des équations de chimiotactisme.

$$\varepsilon^2 \partial_t f^\varepsilon + \varepsilon \nabla \cdot (v f^\varepsilon) = \mathcal{T}[S](f^\varepsilon), \tag{41}$$

avec $\mathcal{T}[S](f^\varepsilon)$ le terme intégral.
On peut suivre la même démarche. Cependant, on se doit de proposer des schémas WB en 2D. Les schémas WB constituent une extension du solveur de Riemannn des équations hyperboliques. Cependant, obtenir un solveur de Riemmann s'avère délicat en 2D étant donné l'interaction de plusieurs ondes. De même, la constitution de schémas WB s'avère compliquée en 2D.

Existence and diffusive limit of a two-species kinetic model of chemotaxis

Ce travail est réalisé en collaboration avec Luís Almeida et Nicolas Vauchelet. Il introduit le modèle cinétique de chimiotactisme à deux espèces permettant de décrire le comportement individuel d'une population à deux espèces. Il étend les résultats d'existence prouvés dans le cadre d'une population à une espèce à une population à deux espèces et pour des noyaux de réorientation présentant une dépendance temporelle du signal chimique. La limite diffusive du modèle conduit à des équations aux dérivées partielles nonlinéaires et couplées du type Keller-Segel.

Article publié dans *Kinetic Related Models*, Vol. 8, no 2 (2015), pp 359-380. doi:10.3934/krm.2015.8.359.

Chapter 1

Existence and diffusive limit of a two-species kinetic model of chemotaxis

Abstract

In this chapter, we propose a kinetic model describing the collective motion by chemotaxis of two species in interaction emitting the same chemoattractant. Such model can be seen as a generalisation to several species of the Othmer-Dunbar-Alt model which takes into account the run-and-tumble process of bacteria. Existence of weak solutions for this two-species kinetic model is studied and the convergence of its diffusive limit towards a macroscopic model of Keller-Segel type is analysed.

Contents

1.1 Introduction

Chemotaxis is the biological mechanism by which organisms sense their environment and react to chemical stimuli. It induces a motion towards the attractant (positive chemotaxis) or away from the repellent (negative chemotaxis). One consequence of positive chemotaxis is the formation of patterns and aggregates as observed in [41, 101, 68, 84] for motile bacteria Escherichia coli or Dictyostelium discoideum mold. Many mathematical models have been proposed to explain this aggregation phenomenon.Among them, we can distinguish between microscopic and macroscopic models depending on the level of description.

In [99], Othmer, Dunbar and Alt choose the microscopic setting in which cells are represented by their velocity distribution $f(x, v, t)$ and the chemical attractant (chemoattractant) by its concentration

$S(x,t)$. The dynamics of f is given by

$$\partial_t f + v\cdot\nabla_x f = \int_V \big(T[S](x,v,v',t)f(x,v',t) - T[S](x,v',v,t)f(x,v,t)\big)\,dv', \tag{1.1}$$

with V a bounded domain of $\mathbb{R}^d$. This kinetic equation points out the *run-and-tumble* process which characterises the individual motion of cells (see [72]). The left-hand side is associated to the run phase during which cells move in a straight line at a constant speed v. The right-hand side includes loss and gain terms resulting from the reorientation phase (tumble). Cells reorient from v to v' with the probability per unit of time $T[S](x,v',v,t)/\int_V T[S](x,v',v,t)\,dv'$. This justifies why $T[S]$ is called the tumbling rate or kernel. Many choices of $T[S]$ are possible.

Since cells are able to respond to temporal changes of the gradient of the chemical substance S along their pathways, we opt for the form of $T[S]$ proposed in [40]:

$$\forall x\in\mathbb{R}^d,\ v,v'\in V,\ t>0,\quad T[S](x,v',v,t) := \phi(\partial_t S + v\cdot\nabla_x S), \tag{1.2}$$

where ϕ is decreasing in order to take into account the preference for favourable regions. This model has shown to be efficient to describe the traveling pulse behaviour of bacteria observed experimentally in [116]. Finally, the chemoattractant is emitted by the cells themselves, diffuses into the medium and is naturally degraded. Then, the chemoattracttant concentration S appearing in (1.1) solves the following reaction-diffusion equation:

$$\delta\partial_t S - \Delta S + S = \int_V f(x,v,t)\,dv := \rho(x,t),\quad \delta = 0,1. \tag{1.3}$$

At a macroscopic level, the dynamics of cells is described by their density $\rho(t,x)$. The well-known Keller-Segel [85] system has been widely used to describe aggregation by chemotaxis. This model describes the dynamics of cells thanks to a parabolic equation with an oriented drift depending on the spatial gradient of the chemoattractant:

$$\begin{cases} \partial_t\rho = \nabla\cdot\left(D\nabla_x\rho - \chi\rho\nabla_x S\right), \\ \delta\partial_t S - \Delta S + S = \rho,\quad \delta = 0,1, \end{cases} \tag{1.4}$$

where D and χ are positive constants called the diffusivity and the chemosensivity of the species to the chemoattractant.

In the mathematical literature both elliptic ($\delta = 0$) and parabolic ($\delta = 1$) cases are encountered. Although the point of view of microscopic and macroscopic models is different, it has been proved that the Keller-Segel model (1.4) can be derived as the diffusion limit of the Othmer-Dunbar-Alt model (1.1)–(1.3) (see [9, 8, 28, 74, 73, 115, 105]). The hyperbolic limit can also be considered [40, 50, 76] leading to the same kind of macroscopic model with small diffusion. As a consequence, coefficients D and χ of (1.4) depend on microscopic parameters which can be measured. This allows one to fit the model with experimental data as done in [115]. Other advantages of (1.4) are understanding of collective effects emerging from individual behaviours and its simple simulation compared to (1.1)–(1.3). However, the microscopic approach provides a general framework of chemotaxis models which encompasses macroscopic models including hyperbolic models obtained by a momentum method from kinetic models (see e.g. [63, 66, 67, 38]). In this work, we focus on the modelling of the chemotactic behaviour of two-interacting species. Existing two-species models (see e.g. [70, 130, 47, 37]) concern the macroscopic scale. For instance, the following Keller-Segel two-species model is considered:

$$\begin{cases} \partial_t\rho_1 = \nabla\cdot\big(D_1\nabla_x\rho_1 - \chi_1\rho_1\nabla_x S\big), \\ \partial_t\rho_2 = \nabla\cdot\big(D_2\nabla_x\rho_2 - \chi_2\rho_2\nabla_x S\big), \\ \delta\partial_t S - \Delta S + S = \rho_1+\rho_2,\quad \delta = 0,1, \end{cases} \tag{1.5}$$

where D_1, D_2 and χ_1, χ_2 are the diffusivities and chemosensivities of the two species 1, 2 to the common chemoattractant S. This can happen in case we consider two closely related types of cells. Many

theoretical issues arise from (1.5). The question of global existence of solutions and understanding of the blow-up are addressed in [?, 33, 45] in the two-dimensional case. These results are validated by numerical simulations carried out in [89]. In addition, traveling wave solutions of a two-species model like (1.5) are studied in [93]. In this paper, we address the question of the derivation of such macroscopic model from a kinetic point of view. We propose the following microscopic model in which the dynamics of the distribution function $f_i(x,v,t)$ for the i-th species, $i=1,2$, is governed by the two following kinetic equations:

$$\begin{cases} \partial_t f_i + v\cdot\nabla_x f_i = \displaystyle\int_V \left(T_i[S](x,v,v',t)f_i(x,v',t) - T_i[S](x,v',v,t)f_i(x,v,t)\right)dv', \\ f_i(x,v,t=0) = f_i^{ini}(x,v), \quad \text{for } i=1,2. \end{cases} \tag{1.6}$$

The position $x\in\mathbb{R}^d$, velocity $v\in V$ (where V is a bounded set of $\mathbb{R}^d$) and time $t\geq 0$. As previously, the tumbling rate $T_i[S]$ takes into account temporal changes of the chemoattractant concentration along the path of cells and reads:

$$\forall x\in\mathbb{R}^d,\ v,v'\in V,\ t>0, \quad T_i[S](x,v',v,t) := \phi_i(\partial_t S + v\cdot\nabla_x S), \quad \text{for } i=1,2, \tag{1.7}$$

where ϕ_i is a decreasing function.

We consider the case where species 1 and 2 involved in (1.6) emit the same attracting chemical substance S, whose dynamics is given by the parabolic ($\delta=1$) or elliptic ($\delta=0$) system:

$$\begin{cases} \delta\partial_t S - \Delta S + S = \displaystyle\int_V f_1(x,v,t)dv + \int_V f_2(x,v,t)dv := \rho_1(x,t)+\rho_2(x,t),\ \delta=0,1, \\ S(x,t=0)=0, \qquad \text{if } \delta=1. \end{cases} \tag{1.8}$$

We determine the drift-diffusion limit of (1.6)–(1.8) by performing a diffusive scaling of space and time $\widetilde{x}=\varepsilon x$, $\widetilde{t}=\varepsilon^2 t$. After dropping the tilde, system (3.19) now reads

$$\begin{cases} \varepsilon^2\partial_t f_i^\varepsilon + \varepsilon v\cdot\nabla_x f_i^\varepsilon = -\mathcal{T}_i^\varepsilon[S^\varepsilon](f_i^\varepsilon), \\ f_i^\varepsilon(x,v,t=0) = f_i^{ini}(x,v), \quad \text{for} \quad i=1,2, \end{cases} \tag{1.9}$$

with

$$\mathcal{T}_i^\varepsilon[S](f) := \int_V \left(T_i^\varepsilon[S](x,v',v,t)f(x,v,t) - T_i^\varepsilon[S](x,v,v',t)f(x,v',t)\right)dv',$$

where we consider as above

$$\forall x\in\mathbb{R}^d,\ v,v'\in V,\ t>0, \quad T_i^\varepsilon[S](x,v,v',t) := \phi_i^\varepsilon(\varepsilon\partial_t S + v'\cdot\nabla_x S), \quad \text{for } i=1,2. \tag{1.10}$$

The difference of scale between terms $\partial_t S$ and $v\cdot\nabla_x S$ comes from the scaling between space and time. Since the production and degradation rates are slow, we can assume prior to the microscopic scaling that the equation for S writes

$$\begin{cases} \delta\partial_t S - \Delta S = \varepsilon^2\left(\rho_1+\rho_2-S\right), \qquad \delta=0,1, \\ S(x,t=0)=0, \qquad \text{if } \delta=1. \end{cases}$$

By performing the diffusive scaling, the equation for S^ε states now as

$$\begin{cases} \delta\partial_t S^\varepsilon - \Delta S^\varepsilon + S^\varepsilon = \rho_1^\varepsilon + \rho_2^\varepsilon, \qquad \delta=0,1, \\ S^\varepsilon(x,t=0)=0, \qquad \text{if } \delta=1. \end{cases} \tag{1.11}$$

We first prove the global-in-time existence of solution (f_1,f_2,S) of (1.9)–(1.11).Then, we prove convergence when $\varepsilon\to 0$ of solutions to (1.9)–(1.11) towards a macroscopic model of Keller-Segel type. The proof relies on uniform estimates on $f_1^\varepsilon, f_2^\varepsilon, S^\varepsilon$ which allow us to use the Aubin-Lions-Simon compactness

Lemma [118]. We only focus on the case of bounded tumbling kernel T for which no blow-up of solutions in finite time is expected both at the microscopic and macroscopic levels. This non blow-up has been proved in the one species case in [32]. Bounded tumbling kernels might seem too restrictive but they are significant for the applications we have in mind since they allow to obtain good agreement with experimental results (see [115, 116]). In particular, in [115] this hypothesis yields the correct experimental profile of the bacterial traveling pulses. For single species, existence results for the kinetic model were shown in the case of unbounded kernels in [74, 18].

The paper is organised as follows. The following section presents the two main results: the global-in-time existence theorem of solutions to (1.9)–(1.11) for fixed $\varepsilon > 0$ and the convergence as $\varepsilon \to 0$ of this solution towards a macroscopic model, i.e. the drift-diffusion limit of (1.9)–(1.11). We also formally derive in this section the equation verified by the limit. By a fixed-point argument, global existence of solutions to the kinetic model is proved in Section 1.3. Section 1.4 is devoted to the proof of the drift-diffusion limit stated in Theorem 1.2.3.

1.2 Main results

Before stating our main results, we introduce some notations. We denote $\Omega := \mathbb{R}^d \times V$ where V is a bounded and rotationally invariant domain of $\mathbb{R}^d$.
We define the following abbreviations which are used throughout the paper:

$$\begin{aligned} &f_i^\varepsilon := f_i^\varepsilon(x,v,t), \quad f_i'^\varepsilon := f_i^\varepsilon(x,v',t), \\ &T_i^\varepsilon[S] := T_i^\varepsilon[S](x,v',v,t), \quad T_i^{*,\varepsilon}[S] := T_i^\varepsilon[S](x,v,v',t), \qquad \text{for } i=1,2. \end{aligned}$$

1.2.1 Main results

In this paper, we consider tumbling rates $T_i^\varepsilon[S]$ of the form (1.10) which meet the following requirement for $i = 1, 2$

(H1) $\phi_i^\varepsilon(z) = \psi_i\big(1+\varepsilon\theta_i(z)\big)$, with $\psi_i \in \mathbb{R}_+^*$ and $\theta_i \in C^{0,1}(\mathbb{R}) \cap L^\infty(\mathbb{R})$ is nonincreasing and satisfies $\|\theta_i\|_{L^\infty(\mathbb{R})} < 1$.

Remark 1.2.1. *This hypothesis is realistic since it was observed experimentally in [116] that for bacteria E. Coli, an external stimulus modifies their natural constant tumbling kernel by adding an anisotropic small term.*

Note that the condition on the L^∞-norm of θ_i ensures that T_i^ε is positive at least for ε smaller than 1, which will always be the case here since we focus on the asymptotic limit $\varepsilon \to 0$. The positivity and the boundness of $T_i^\varepsilon[S]$ come from its physical meaning.

If F denotes the uniform distribution on V

$$F(v) := \frac{\mathbb{1}_{v\in V}}{|V|}, \tag{1.12}$$

with $|V|$ the measure of the velocity set V, the symmetry assumption of V implies that

$$\int_V F(v)dv = 1 \quad \text{and} \quad \int_V vF(v)dv = 0. \tag{1.13}$$

As in [28], we define the symmetric and anti-symmetric parts of $\mathcal{T}_i^\varepsilon$ by

$$\begin{aligned} \phi_i^{S,\varepsilon}[S] :&= \frac{T_i^\varepsilon[S] + T_i^{*,\varepsilon}[S]}{2} = \psi_i\left(1 + \frac{\varepsilon}{2}\big(\theta_i(\varepsilon\partial_t S + v'\cdot\nabla_x S) + \theta_i(\varepsilon\partial_t S + v\cdot\nabla_x S)\big)\right), \\ \phi_i^{A,\varepsilon}[S] :&= \frac{T_i^\varepsilon[S] - T_i^{*,\varepsilon}[S]}{2} = \psi_i\frac{\varepsilon}{2}\big(\theta_i(\varepsilon\partial_t S + v'\cdot\nabla_x S) - \theta_i(\varepsilon\partial_t S + v\cdot\nabla_x S)\big). \end{aligned} \tag{1.14}$$

From Assumption (H1), $\phi_i^{S,\varepsilon}$ and $\phi_i^{A,\varepsilon}$ satisfy the following inequalities which are useful to derive uniform estimates in ε:

$$\begin{aligned} \phi_i^{S,\varepsilon} &\geq \psi_i\big(1-\varepsilon\,\|\theta_i\|_{L^\infty(\mathbb{R})}\big), \\ \int_V \frac{(\phi_i^{A,\varepsilon})^2}{\phi_i^{S,\varepsilon}} dv' &\leq \varepsilon^2 \psi_i\,|V|\,\|\theta_i\|^2_{L^\infty(\mathbb{R})}\,. \end{aligned} \tag{1.15}$$

The expansion of $\mathcal{T}_i^\varepsilon[S]$ now reads:

$$\mathcal{T}_i^\varepsilon[S] = \mathcal{T}_i^0 + \varepsilon \mathcal{T}_i^1[S], \tag{1.16}$$

with

$$\begin{aligned} \mathcal{T}_i^0(f) &:= \psi_i\left(|V|\,f-\rho\right), \\ \mathcal{T}_i^1[S](f) &:= \psi_i\big(\,|V|\,\theta_i(\varepsilon\partial_t S + v\cdot\nabla_x S)f - \int_V \theta_i(\varepsilon\partial_t S + v'\cdot\nabla_x S)f'\,dv'\big). \end{aligned} \tag{1.17}$$

Our first result concerns the global-in-time existence of solution of (1.9)–(1.11).

Theorem 1.2.2. *Let $\varepsilon>0$ and assume that tumbling rates $T_1^\varepsilon, T_2^\varepsilon$ are given by (1.10) where $\phi_1^\varepsilon, \phi_2^\varepsilon$ are positive, bounded and Lipschitz continuous functions.*

If the initial data f_1^{ini}, f_2^{ini} are in $L^1_+(\Omega)\cap L^\infty(\Omega)$, then there exists a unique global solution of (1.9)–(1.11) such that

$$\begin{aligned} f_1^\varepsilon, f_2^\varepsilon &\in L^\infty((0,\infty), L^1_+\cap L^\infty(\Omega)), \\ S^\varepsilon &\in L^\infty((0,\infty), L^p(\mathbb{R}^d)), \quad \textit{for all } 1\leq p\leq\infty. \end{aligned}$$

Then we establish the diffusive limit $\varepsilon\to 0$ of these solutions. The limiting system is the following two-species Keller-Segel type equation:

$$\begin{cases} \partial_t\rho_1 = \nabla\cdot\left(D_1\nabla\rho_1 - \chi_1[\nabla S]\rho_1\right), \\ \partial_t\rho_2 = \nabla\cdot\left(D_2\nabla\rho_2 - \chi_2[\nabla S]\rho_2\right), \\ \delta\partial_t S = \Delta S - S + \rho_1+\rho_2, \quad \delta=0,1, \end{cases} \tag{1.18}$$

where D_i and $\chi_i[\nabla S]$ are given for $i=1,2$ by

$$D_i = \frac{1}{|V|^2\,\psi_i}\left(\int_V v_1^2\,dv\right) I_d, \quad \chi_i[\nabla S] = -\frac{\nabla_x S}{|\nabla_x S|}\int_V v_1\,\theta_i(v_1\,|\nabla_x S|)\frac{dv}{|V|}, \tag{1.19}$$

with v_1 the first component of the velocity v in V and I_d the identity matrix. The intial conditions of this system are

$$\rho_1^{ini} = \int_V f_1^{ini} dv, \quad \rho_2^{ini} = \int_V f_2^{ini} dv \quad \text{and } S^{ini}=0 \quad \text{if } \delta=1.$$

Theorem 1.2.3. *Let (H1) hold. Assume that the initial data f_1^{ini}, f_2^{ini} belong to $L^1_+(\Omega)\cap L^\infty(\Omega)$. Then, there exists a subsequence $(f_1^\varepsilon, f_2^\varepsilon, S^\varepsilon)$ of solutions of (1.9)–(1.11) that converges when ε tends to zero and we have*

$$\begin{aligned} &(f_1^\varepsilon, f_2^\varepsilon) \overset{*}{\rightharpoonup} (\rho_1^0 F, \rho_2^0 F) \quad \textit{in } L^\infty_{loc}((0,\infty), L^q(\Omega)), \quad 1<q<\infty \\ &(S^\varepsilon, \nabla_x S^\varepsilon) \to (S^0, \nabla_x S^0) \quad \textit{in } L^p_{loc}(\mathbb{R}^d\times(0,\infty)), \quad 1\leq p\leq\infty, \end{aligned}$$

where F is the equilibrium distribution defined in (1.12) and $(\rho_1^0, \rho_2^0, S^0)$ the solution of (1.18).

Remark 1.2.4. *Note that D_i is a diagonal and positive definite matrix, thanks to the symmetry assumption on V, and $\chi_i[\nabla S]$ is bounded. This ensures that the macroscopic equation (1.18) subject to the previous initial condition admits a unique and global-in-time solution. We refer the reader to the appendix for details.*

1.2.2 Formal derivation of drift-diffusion limits

For the sake of clarity, we first derive formally the limit equation (1.18). We consider Hilbert expansions of $f_1^\varepsilon, f_2^\varepsilon$:

$$f_i^\varepsilon = f_i^0 + \varepsilon f_i^1 + \varepsilon^2 f_i^2 + o(\varepsilon^2), \quad \text{for } i = 1, 2. \tag{1.20}$$

Assume $S^\varepsilon = S^0$ is independent of ε and given by (1.11) with the right-hand side $\rho_1^0 + \rho_2^0$ and consider in this part that θ_i is smooth for $i = 1, 2$.

Injecting (1.20) into the equation for f_i^ε (1.9)–(1.16)–(1.17) and identifying the terms in $O(1)$ and $O(\varepsilon)$ leads to,

$$\begin{aligned} f_i^0 &= \frac{1}{|V|}\int_V f_i^0 dv = \rho_i^0 F, \\ f_i^1 &= \rho_i^1 - \frac{v\cdot\nabla_x f_i^0}{|V|\,\psi_i} + \frac{1}{|V|}\left(\int_V \theta_i(v'\cdot\nabla_x S^0) f_i^0(v')dv' - |V|\,\theta_i(v\cdot\nabla_x S^0) f_i^0(v)\right), \end{aligned}$$

for $i = 1, 2$. Replacing f_i^0 in the expression of f_i^1 yields

$$f_i^1 = \rho_i^1 - \frac{v\cdot\nabla_x \rho_i^0}{|V|^2\,\psi_i} + \frac{\rho_i^0}{|V|}\left(\int_V \theta_i(v'\cdot\nabla_x S^0)\frac{dv'}{|V|} - \theta_i(v\cdot\nabla_x S^0)\right), \quad \text{for } i = 1, 2. \tag{1.21}$$

Then for the $O(\varepsilon^2)$ term, we have that

$$-\psi_i(|V| f_i^2 - \rho_i^2) = \partial_t \rho_i^0 + v\cdot\nabla_x f_i^1 + \psi_i U_i, \quad \text{for } i = 1, 2, \tag{1.22}$$

where

$$\begin{aligned} U_i(v) = \; & |V|\theta_i(v\cdot\nabla_x S^0) f_i^1 - \int_V \theta_i(v'\cdot\nabla_x S^0) f_i^1(v')\,dv' \\ & + \partial_t S^0\Big(|V|\theta_i'(v\cdot\nabla_x S^0) f_i^0 - \int_V \theta_i'(v'\cdot\nabla_x S^0) f_i^0(v')\,dv'\Big). \end{aligned}$$

We notice that $\int_V U_i\,dv = 0$. Equation (1.22) admits a solution provided the integral over V of the right-hand side vanishes. This implies the conservation law:

$$\partial_t \rho_i^0 + \nabla\cdot J_i^1 = 0,$$

where $J_i^1 := \displaystyle\int_V v f_i^1 dv$, for $i = 1, 2$. Using (1.21) and formulas of D_i and $\chi_i[\nabla S]$ (1.19), it follows that

$$J_i^1 = -D_i \nabla_x \rho_i^0 + \chi_i[\nabla S]\rho_i^0, \qquad \text{for } i = 1, 2.$$

The formula of $\chi_i[\nabla S]$ follows from the invariant rotationally property of the domain V. This gives the equation for ρ_i^0 for $i = 1, 2$.

1.3 Global existence of solutions of the kinetic model

The purpose of this section is to prove the global existence for System (1.9)–(1.11). The Green representation formula allows us to decouple (1.11) and (1.9). This gives a system which depends only on f_i^ε. The fixed-point argument gives the uniqueness and local existence in time of solutions. Thanks to a-priori estimates on f_i^ε, we recover global-in-time existence. Without loss of generality, and for the sake of simplicity of the notation, we fix $\varepsilon = 1$ and denote $\phi_i^{max} := \max \phi_i^\varepsilon$.

1.3.1 A-priori estimates

We recall that using Bessel potential (see [46]), the solution S of elliptic/parabolic equation (1.8) is given by

$$\begin{aligned} S(x,t) &= \int_{\mathbb{R}^d} G(y)\,(\rho_1+\rho_2)\,(x-y,t)\,dy, \quad \delta = 0, \\ S(x,t) &= \int_0^t\!\!\int_{\mathbb{R}^d} K(y,s)\,(\rho_1+\rho_2)\,(x-y,t-s)\,dy\,ds, \quad \delta = 1, \end{aligned} \tag{1.23}$$

with

$$\begin{aligned} G(x) &:= \frac{1}{2}e^{-|x|}, \quad d=1, \\ G(x) &:= \frac{1}{4\pi}\int_0^\infty \exp\big(-\pi\frac{|x|^2}{4s} - \frac{s}{4\pi}\big)\, s^{\frac{2-d}{2}}\frac{ds}{s}, \quad d\geq 2, \\ K(x,t) &:= \frac{1}{(4\pi t)^{d/2}}\exp\big(-\frac{|x|^2}{4t} - t\big), \quad d\geq 1. \end{aligned} \tag{1.24}$$

We review some classical results on the integrability of kernels G, K and their gradients.

Lemma 1.3.1 (Estimates on G and K). *Let $t>0$. If $d=1$, then there exists a constant C_1 such that*

$$\|G\|_{L^1(\mathbb{R})} = 1, \quad \int_0^t \|K(\cdot,s)\|_{L^1(\mathbb{R})}\,ds \leq 1, \tag{1.25}$$

$$\|\nabla_x G\|_{L^1(\mathbb{R})} = 1, \quad \int_0^t \|\nabla_x K(\cdot,s)\|_{L^1(\mathbb{R})}\,ds \leq C_1\, t^{\frac{1}{2}}. \tag{1.26}$$

For $d\geq 2$, there exists constants $C_p, C_p^{'}$ such that

$$\|G\|_{L^p(\mathbb{R}^d)} \leq C_p, \quad \int_0^t \|K(\cdot,s)\|_{L^p(\mathbb{R}^d)}\,ds \leq C_p\, t^{\frac{d(1-p)}{2p}+1}, \quad 1\leq p < \frac{d}{d-2}, \tag{1.27}$$

$$\|\nabla_x G\|_{L^p(\mathbb{R}^d)} \leq C_p^{'}, \quad \int_0^t \|\nabla_x K(\cdot,s)\|_{L^p(\mathbb{R}^d)}\,ds \leq C_p^{'}\, t^{\frac{d(1-p)+p}{2p}}, \quad 1\leq p < \frac{d}{d-1}. \tag{1.28}$$

Proof. For $d=1$, simple computations give the result for G and $\nabla_x G$. For $\|K(\cdot,s)\|_{L^1(\mathbb{R})}$, the transformation $y = \frac{x}{\sqrt{2s}}$ leads to

$$\|K(\cdot,t)\|_{L^1(\mathbb{R})} = e^{-t}.$$

It follows that

$$\int_0^t \|K(\cdot,s)\|_{L^1(\mathbb{R})}\,ds \leq 1.$$

By similar computations, we show that

$$\|\nabla_x K(\cdot,s)\|_1 = \frac{1}{4\pi^{d/2}}\left\| y\mapsto y e^{-\frac{|y|^2}{2}}\right\|_{L^1(\mathbb{R})} s^{-\frac{1}{2}}e^{-s}.$$

By integrating with respect to s in $(0,t)$, we obtain the result.

We now suppose that $d\geq 2$ and compute L^p-norms of G and K.

$$\|G\|_{L^p(\mathbb{R}^d)} = \frac{1}{4\pi}\int_0^\infty \left\| x\mapsto e^{-\pi\frac{|x|^2}{4s}}\right\|_{L^p(\mathbb{R}^d)} e^{-\frac{s}{4\pi}}\, s^{\frac{2-d}{2}}\frac{ds}{s}.$$

Performing the change of variable $y = \sqrt{\frac{\pi}{2s}}x$ and simplifying yields

$$\|G\|_{L^p(\mathbb{R}^d)} = \frac{2^{d(\frac{2}{p}-1)}}{p^{d/2p}\pi^{\frac{d}{2}(1-\frac{1}{p})}}\int_0^\infty e^{-u}\, u^{\frac{d}{2}(\frac{1}{p}-1)}\,du.$$

After straightforward computations, we deduce that for all $1 \leq p < \frac{d}{d-2}$

$$\|G\|_{L^p(\mathbb{R}^d)} \leq \frac{2^{d(\frac{2}{p}-1)}}{p^{d/2p}\pi^{\frac{d}{2}(1-\frac{1}{p})}}\Gamma\left(1+\frac{d-dp}{2p}\right).$$

A similar transformation applied to $\|K(\cdot,s)\|_{L^p(\mathbb{R}^d)}$ gives

$$\|K(\cdot,s)\|_{L^p(\mathbb{R}^d)} = \frac{2^{d(\frac{1}{p}-1)}}{\pi^{\frac{d}{2}(1-\frac{1}{p})}} s^{\frac{d}{2}(\frac{1}{p}-1)} e^{-s}.$$

We conclude that for all $1 \leq p < \frac{d}{d-2}$

$$K(\cdot,s) \in L^p(\mathbb{R}^d) \quad \text{and} \quad \int_0^t \|K(\cdot,s)\|_{L^p(\mathbb{R}^d)}\, ds \leq C\, t^{\frac{d(1-p)}{2p}+1}.$$

For the estimates on the gradients, we have

$$\|\nabla_x G\|_{L^p(\mathbb{R}^d)} = \frac{1}{4\pi}\int_0^\infty \frac{\pi}{2s}\left\| x e^{-\pi\frac{|x|^2}{4s}}\right\|_{L^p(\mathbb{R}^d)} e^{-\frac{s}{4\pi}}\, s^{\frac{2-d}{2}}\frac{ds}{s}.$$

We apply the two successive transformations $y = \sqrt{\frac{\pi}{2s}}x, t = \frac{s}{4\pi}$ and simplify. We see that for all $1 \leq p < \frac{d}{d-1}$

$$\|\nabla_x G\|_{L^p(\mathbb{R}^d)} = \frac{2^{3d/2p-(2d+3)/2}}{\pi^{d/2}}\Gamma\left(1/2-\frac{d}{2}(1-1/p)\right)\left\| y e^{-\frac{|y|^2}{2}}\right\|_{L^p(\mathbb{R}^d)}.$$

Similar computations applied to $\nabla_x K$ give

$$\|\nabla_x K(\cdot,s)\|_{L^p(\mathbb{R}^d)} = \frac{2^{\frac{d}{2}(1/p-1)-d}}{\pi^{d/2}}\left\| y e^{-\frac{|y|^2}{2}}\right\|_{L^p(\mathbb{R}^d)} s^{\frac{d}{2p}-\frac{d+1}{2}} e^{-s}.$$

Integrating with respect to s leads to the result. □

Lemma 1.3.2. *Fix $\tau > 0$ and v in V. Let ϕ be a Lipschitz continuous function and $f, \widetilde{f}$ be in $L^\infty([0,\tau), L^\infty(\Omega)\cap L^1(\Omega))$ such that $f, \widetilde{f}$ coincide at the time $t = 0$ and satisfy in a weak sense*

$$\partial_t \rho(f) + \nabla \cdot J(f) = 0, \tag{1.29}$$

where J is a linear and bounded operator on $L^\infty(\Omega)$. Let S and $\widetilde{S}$ denote

$$S(x,\tau) := G * \rho(f),\ \widetilde{S}(x,\tau) := G * \rho(\widetilde{f}), \quad \text{for } \delta = 0,$$
$$S(x,\tau) := \int_0^\tau K(\cdot,s) * \rho(f)(\cdot,\tau-s)ds,\ \widetilde{S}(x,\tau) := \int_0^\tau K(\cdot,s) * \rho(\widetilde{f})(\cdot,\tau-s)ds, \text{ for } \delta = 1.$$

Then, there exists a positive constant C such that

$$\|\phi(\partial_t S + v\cdot\nabla_x S) - \phi(\partial_t \widetilde{S} + v\cdot\nabla_x \widetilde{S})\|_{L^\infty(\Omega)} \leq C\|\phi\|_{C^{0,1}(\mathbb{R})}\|\nabla_x G\|_{L^1(\mathbb{R}^d)}\,\|(f-\widetilde{f})(\cdot,\tau)\|_{L^\infty(\Omega)}$$

for $\delta = 0$, and

$$\|\phi(\partial_t S + v\cdot\nabla_x S) - \phi(\partial_t \widetilde{S} + v\cdot\nabla_x \widetilde{S})\|_{L^\infty(\Omega)}$$
$$\leq C\|\phi\|_{C^{0,1}(\mathbb{R})}\int_0^\tau \|\nabla_x K(\cdot,s)\|_{L^1(\mathbb{R}^d)}\|(f-\widetilde{f})(\cdot,\tau-s)\|_{L^\infty(\Omega)}ds, \quad \text{for } \delta = 1.$$

Proof. For $\delta = 0$, recalling the expression of $S = G * \rho(f)$, differentiating with respect to t and using the conservation equation (1.29), we get from Green's formula

$$\partial_t S = \int_{\mathbb{R}^d} \nabla_x G(y) \cdot J(f)(x-y,\tau)\, dy.$$

We proceed in the same way for $\nabla_x S$. Putting together $\partial_t S$ and $\nabla_x S$ terms, one obtains

$$\partial_t S + v \cdot \nabla_x S = \int_{\mathbb{R}^d} \nabla_x G(y) \cdot (J - v\rho)(f)(x-y,\tau)\, dy.$$

This formula combined with the Lipschitz continuity of ϕ implies

$$\begin{aligned}\left|\phi(\partial_t S + v\cdot\nabla_x S) - \phi(\partial_t \widetilde{S} + v\cdot\nabla_x \widetilde{S})\right| &\le \|\phi\|_{C^{0,1}(\mathbb{R})} \left|\partial_t(S-\widetilde{S}) + v\cdot\nabla_x(S-\widetilde{S})\right| \\ &\le \|\phi\|_{C^{0,1}(\mathbb{R})} \left|\nabla_x G * (J - v\rho)(f - \widetilde{f})\right|.\end{aligned}$$

By applying Young's inequality and using either (1.26) or (1.28), it follows that

$$\left|\phi(\partial_t S + v\cdot\nabla_x S) - \phi(\partial_t \widetilde{S} + v\cdot\nabla_x \widetilde{S})\right| \le \|\phi\|_{C^{0,1}(\mathbb{R})} \|\nabla_x G\|_{L^1(\mathbb{R}^d)} \|(J - v\rho)(f-\widetilde{f})\|_{L^\infty(\Omega)}.$$

From the assumption, J is bounded on $L^\infty(\Omega)$. Since V is a bounded domain, the linear operator ρ is also bounded on $L^\infty(\Omega)$. Then, we conclude that

$$\left|\phi(\partial_t S + v\cdot\nabla_x S) - \phi(\partial_t \widetilde{S} + v\cdot\nabla_x \widetilde{S})\right| \le C\|\phi\|_{C^{0,1}(\mathbb{R})} \|\nabla_x G\|_{L^1(\mathbb{R}^d)} \|(f-\widetilde{f})(\cdot,\tau)\|_{L^\infty(\Omega)}.$$

The case $\delta = 1$ is treated similarly. The slight difference comes from the additional term appearing in the expression of $\partial_t S$:

$$\partial_t S = \int_{\mathbb{R}^d} K(y,\tau)\rho(f)(x-y,0)\, dy + \int_0^\tau\!\!\int_{\mathbb{R}^d} K(s,y)\partial_t\rho(f)(x-y,\tau-s)\, dy \quad \text{in a weak sense.}$$

Then $\partial_t S + v\cdot\nabla_x S$ becomes

$$\partial_t S + v\cdot\nabla_x S = \int_{\mathbb{R}^d} K(y,\tau)\rho(f)(x-y,0)\, dy + \int_0^\tau\!\!\int_{\mathbb{R}^d} \nabla_x K(y,s)(J-v\rho)(f)(x-y,\tau-s)\, dy\, ds.$$

The substraction between $\partial_t S + v\cdot\nabla_x S$ and $\partial_t \widetilde{S} + v\cdot\nabla_x \widetilde{S}$ has the same form as in the elliptic setting since $f(\cdot,0) = \widetilde{f}(\cdot,0)$. Therefore,

$$\begin{aligned}\left|\phi(\partial_t S + v\cdot\nabla_x S) - \phi(\partial_t \widetilde{S} + v\cdot\nabla_x \widetilde{S})\right| \le C\|\phi\|_{C^{0,1}(\mathbb{R})} \int_0^\tau &\|\nabla_x K(\cdot,s)\|_{L^1(\mathbb{R}^d)} \\ &\times \|(f-\widetilde{f})(\cdot,\tau-s)\|_{L^\infty(\Omega)} ds.\end{aligned}$$

□

Lemma 1.3.3 (A-priori bounds on f_1, f_2)**.** *Let $\tau > 0$ and (f_1, f_2) be a weak solution of (1.6) such that f_1, f_2 are in $L^1((0,\tau), L^1_+ \cap L^\infty(\Omega))$. We assume that tumbling rates $T_1[S], T_2[S]$ defined by (1.7) are positive and bounded.*

If the inital data (f_1^{ini}, f_2^{ini}) belongs to $L^\infty(\Omega)\times L^\infty(\Omega)$, then there exists a constant $C > 0$ such that for $i = 1,2$ and $t \in (0,\tau)$, we have

$$\begin{aligned}&\|f_i(\cdot,t)\|_{L^1(\Omega)} = \left\|f_i^{ini}\right\|_{L^1(\Omega)}, \\ &\|f_i(\cdot,t)\|_{L^\infty((0,\tau),L^\infty(\Omega))} \le C\left\|f_i^{ini}\right\|_{L^\infty(\Omega)} e^{|V|\phi_i^{max}\tau}.\end{aligned}$$

Proof. By integrating the equation for f_i (1.6) with respect to v, we see that ρ_i satisfies the conservation law :

$$\partial_t \rho_i + \nabla \cdot J_i = 0, \tag{1.30}$$

with $J_i := \int_V v f_i$. It follows that the L^1-norm of ρ_i is conserved. We show the second inequality by using the Duhamel representation formula and the Gronwall lemma. Since each equation for $i = 1$ and 2 can be treated separately, the proof is identical to the single-species case. We refer the reader to [126]. □

1.3.2 Proof of Theorem 1.2.2

We now prove the global-in-time existence. It is standard that if they exist, the solutions f_1^ε and f_2^ε are nonnegative provided the initial data are nonnegative. Since ρ_i satisfies the conservation law (1.30), by the proof of Lemma 1.3.2, $\partial_t S + v \cdot \nabla_x S$ is given for $\delta = 0$ and $\delta = 1$, respectively, by

$$\begin{aligned}
\partial_t S + v \cdot \nabla_x S &= \int_{\mathbb{R}^d} \nabla_x G(y) \cdot (J - v\rho)(f_1 + f_2)(x - y, t)\, dy, \\
\partial_t S + v \cdot \nabla_x S &= \int_{\mathbb{R}^d} K(y, t)\rho(f_1 + f_2)(x - y, 0)\, dy \\
&\quad + \int_0^t \int_{\mathbb{R}^d} \nabla_x K(y, s)(J - v\rho)(f_1 + f_2)(x - y, t - s)\, dy\, ds.
\end{aligned}$$

Replacing $\partial_t S + v \cdot \nabla_x S$ in (1.6) yields in the case $\delta = 0$

$$\begin{cases}
\partial_t f_i + v \cdot \nabla_x f_i = \displaystyle\int_V \phi_i \left(\nabla_x G * (J - v'\rho)(f_1 + f_2)\right) f_i' dv' \\
\qquad\qquad\qquad\qquad - |V|\, \phi_i \left(\nabla_x G * (J - v\rho)(f_1 + f_2)\right) f_i, \\
f_i(x, v, t = 0) = f_i^{ini}, \quad \text{for } i = 1, 2.
\end{cases} \tag{1.31}$$

For $\delta = 1$, we obtain

$$\begin{cases}
\partial_t f_i + v \cdot \nabla_x f_i = \displaystyle\int_V \phi_i \left(K * \rho(f_1^{ini} + f_2^{ini})\right. \\
\qquad\qquad\qquad\qquad \left. + \displaystyle\int_0^t \nabla_x K(\cdot, s) * (J - v'\rho)(f_1 + f_2)(\cdot, t - s) ds\right) f_i' dv' \\
\qquad\qquad\qquad\qquad - |V|\, \phi_i \left(K * \rho(f_1^{ini} + f_2^{ini})\right. \\
\qquad\qquad\qquad\qquad \left. + \displaystyle\int_0^t \nabla_x K(\cdot, s) * (J - v\rho)(f_1 + f_2)(\cdot, t - s) ds\right) f_i, \\
f_i(x, v, t = 0) = f_i^{ini}, \quad \text{for } i = 1, 2.
\end{cases} \tag{1.32}$$

Here, we define the convolution between two vector-valued functions $M, H : \mathbb{R} \to \mathbb{R}^d$ as

$$M * H = \sum_{j=0}^{d} M_j * H_j,$$

where M_j, H_j are components of M and H.

We fix $\tau > 0$ and introduce the Banach space $(X^\tau, \|\cdot\|_{X^\tau})$ given by

$$\begin{aligned}
X^\tau &:= L^1((0, \tau), L^\infty(\Omega)) \times L^1((0, \tau), L^\infty(\Omega)), \\
\|f\|_{X^\tau} &:= \int_0^\tau \left(\|f_1(\cdot, s)\|_{L^\infty(\Omega)} + \|f_2(\cdot, s)\|_{L^\infty(\Omega)}\right) ds \quad \text{for } f = (f_1, f_2) \in X^\tau.
\end{aligned}$$

We build fixed-point operators $\mathcal{F}(f) = (\mathcal{F}_1(f), \mathcal{F}_2(f))$ for Systems (1.31), (1.32) on X^τ. Since these systems are different, we need to consider two cases and treat them separately.

1.3.2.1 Proof of the elliptic case, $\delta = 0$

$(\mathcal{F}_1(f), \mathcal{F}_2(f))$ is the weak solution of the system:

$$\begin{cases} \partial_t \mathcal{F}_i + v \cdot \nabla_x \mathcal{F}_i = \displaystyle\int_V \phi_i \left(\nabla_x G * (J - v'\rho)(f_1 + f_2)\right) \mathcal{F}_i^{'} \, dv' \\ \qquad\qquad\qquad\qquad - |V| \, \phi_i \left(\nabla_x G * (J - v\rho)(f_1 + f_2)\right) \mathcal{F}_i, \\ \qquad \mathcal{F}_i(\cdot, t = 0) = f_i^{ini}, \quad \text{for } i = 1, 2, \end{cases} \tag{1.33}$$

with $\mathcal{F}_i := \mathcal{F}_i(f)(x, v, t)$ and $\mathcal{F}_i^{'} := \mathcal{F}_i(f)(x, v', t)$.

For $f = (f_1, f_2)$ and $g = (g_1, g_2)$ in X^τ, we define the mapping $\mathcal{F}^{fg} := \mathcal{F}(f) - \mathcal{F}(g)$ whose components $\mathcal{F}_i^{fg}$ are defined by

$$\mathcal{F}_i^{fg} := \mathcal{F}_i(f) - \mathcal{F}_i(g), \quad \text{for } i = 1, 2.$$

Substracting equations for $\mathcal{F}_i(f)$ and $\mathcal{F}_i(g)$ and collecting terms leads to

$$\begin{cases} \partial_t \mathcal{F}_i^{fg} + v \cdot \nabla_x \mathcal{F}_i^{fg} + |V| \, \phi_i (\nabla_x G * (J - v\rho)(f_1 + f_2)) \mathcal{F}_i^{fg} = \mathcal{G}_i^{fg}, \\ \mathcal{F}_i^{fg}(\cdot, t = 0) = 0, \quad \text{for } i = 1, 2, \end{cases} \tag{1.34}$$

where $\mathcal{G}_i^{fg}$ is defined by

$$\begin{aligned} \mathcal{G}_i^{fg}(x, v, t) := & \int_V \phi_i \left(\nabla_x G * (J - v'\rho)(f_1 + f_2)\right) \mathcal{F}_i^{fg}(v') \, dv' \\ & - \mathcal{F}_i(g) \, |V| \left(\phi_i \left(\nabla_x G * (J - v\rho)(f_1 + f_2)\right) - \phi_i \left(\nabla_x G * (J - v\rho)(g_1 + g_2)\right)\right) \\ & + \int_V \mathcal{F}_i(g)(v') \left(\phi_i \left(\nabla_x G * (J - v'\rho)(f_1 + f_2)\right)\right. \\ & \left. - \phi_i \left(\nabla_x G * (J - v'\rho)(g_1 + g_2)\right)\right) dv'. \end{aligned} \tag{1.35}$$

By similar computations performed at Lemma 1.3.2 and applying it to $f = f_1 + f_2$ and $g = g_1 + g_2$, we find that

$$\begin{aligned} \left|\mathcal{G}_1^{fg}(x, v, s)\right| \leq \phi_1^{max} & \int_V \left|\mathcal{F}_1^{fg}(x, v', s)\right| dv' \\ & + C \|\phi_1\|_{C^{0,1}(\mathbb{R})} \|\nabla_x G\|_{L^1(\mathbb{R}^d)} \left(|\mathcal{F}_1(g)| + \int_V |\mathcal{F}_1(g)|\right) \sum_{i=1,2} \|(f_i - g_i)(\cdot, s)\|_{L^\infty(\Omega)}. \end{aligned}$$

Hence,

$$\begin{aligned} \left\|\mathcal{G}_1^{fg}(\cdot, s)\right\|_{L^\infty(\Omega)} \leq \phi_1^{max} & |V| \, \|\mathcal{F}_1^{fg}(\cdot, s)\|_{L^\infty(\Omega)} \\ & + C\big(1 + |V|\big) \|\phi_1\|_{C^{0,1}(\mathbb{R})} \|\nabla_x G\|_{L^1(\mathbb{R}^d)} \|\mathcal{F}_1(g)(\cdot, s)\|_{L^\infty(\Omega)} \sum_{i=1,2} \|(f_i - g_i)(\cdot, s)\|_{L^\infty(\Omega)}. \end{aligned}$$

Thanks to the Duhamel formula, $\mathcal{F}_i^{fg}$ writes

$$\begin{aligned} \mathcal{F}_i^{fg}(x, v, t) = \int_0^t \exp & \left(- \int_s^t \phi_i (\nabla_x G * (J - v\rho)(f_1 + f_2))(x - v(s - u), u) du\right) \\ & \times \mathcal{G}_i^{fg}(x - v(t - s), v, s) \, ds. \end{aligned} \tag{1.36}$$

Taking the L^∞-norm on Ω of both sides and using the fact that ϕ_1 is nonnegative gives

$$\left\|\mathcal{F}_1^{fg}(\cdot, t)\right\|_{L^\infty(\Omega)} \leq \int_0^t \left\|\mathcal{G}_1^{fg}(\cdot, s)\right\|_{L^\infty(\Omega)}.$$

Recalling the estimate on $\left\|\mathcal{G}_1^{fg}(\cdot,s)\right\|_{L^\infty(\Omega)}$ above, it follows that

$$\left\|\mathcal{F}_1^{fg}(\cdot,t)\right\|_{L^\infty(\Omega)} \leq \phi_1^{max}\,|V| \int_0^t \|\mathcal{F}_1^{fg}(\cdot,s)\|_{L^\infty(\Omega)} ds + C_1 \int_0^t \|\mathcal{F}_1(g)(\cdot,s)\|_{L^\infty(\Omega)} \sum_{i=1,2} \|(f_i-g_i)(\cdot,s)\|_{L^\infty(\Omega)}\, ds.$$

The bound on $\|\mathcal{F}_1(g)(\cdot,s)\|_{L^\infty(\Omega)}$ is similar to the one given by Lemma 1.3.3. By using this estimate, we get

$$\left\|\mathcal{F}_1^{fg}(\cdot,t)\right\|_{L^\infty(\Omega)} \leq \phi_1^{max}\,|V| \int_0^t \left\|\mathcal{F}_1^{fg}(\cdot,s)\right\|_{L^\infty(\Omega)} ds + C_1' e^{\phi_1^{max}|V|t} \int_0^t \sum_{i=1,2} \|(f_i-g_i)(\cdot,s)\|_{L^\infty(\Omega)}\, ds.$$

The Gronwall lemma asserts that

$$\int_0^\tau \left\|\mathcal{F}_1^{fg}(\cdot,t)\right\|_{L^\infty(\Omega)} dt \leq C_1'\big(e^{\phi_1^{max}|V|\tau}-1\big) \int_0^\tau \sum_{i=1,2} \|(f_i-g_i)(\cdot,t)\|_{L^\infty(\Omega)}\, dt.$$

We obtain a similar estimate on $\mathcal{F}_2^{fg}$ by replacing ϕ_1^{max} by ϕ_2^{max}. Summing the estimates on $\mathcal{F}_i^{fg}$ for $i=1,2$, we deduce that

$$\int_0^\tau \sum_{i=1,2} \|\mathcal{F}_i^{fg}(\cdot,t)\|_{L^\infty(\Omega)} dt \leq C\big(e^{\phi^{max}\tau}-1\big) \int_0^\tau \sum_{i=1,2} \|(f_i-g_i)(\cdot,t)\|_{L^\infty(\Omega)}\, dt,$$

with $\phi^{max} = \max(\phi_1^{max},\phi_2^{max})$. Recalling the definition of the X^τ-norm, we conclude that

$$\|\mathcal{F}(f)-\mathcal{F}(g)\|_{X^\tau} \leq C\big(e^{\phi^{max}\tau}-1\big)\|f-g\|_{X^\tau}.$$

Therefore, there exists a sufficiently small time $\tau_0 > 0$ such that $\mathcal{F}$ is a contraction mapping on $X^{\tau_0} = L^1((0,\tau_0),L^\infty(\Omega)) \times L^1((0,\tau_0),L^\infty(\Omega))$. Thus, Banach fixed-point Theorem gives the existence and uniqueness of weak solution $f=(f_1,f_2)$ of (1.9)–(1.11) in X^{τ_0}.

From the a-priori estimates of Lemma 1.3.3, we see that $f(\cdot,\tau_0)$ is bounded in $L^1(\Omega)\cap L^\infty(\Omega)$. We now consider our problem with the initial condition $f(\cdot,\tau_0)$, apply the same strategy and obtain the existence up to the time $2\tau_0$. By iterating this procedure, we extend the solution to $L^1((0,\tau),L^\infty(\Omega)) \times L^1((0,\tau),L^\infty(\Omega))$.

1.3.2.2 Proof of the parabolic case, $\delta = 1$

In this case, $(\mathcal{F}_1(f),\mathcal{F}_2(f))$ verifies

$$\begin{cases} \partial_t \mathcal{F}_i + v\cdot\nabla_x \mathcal{F}_i = \displaystyle\int_V \phi_i \left(K*(\rho_1^{ini}+\rho_2^{ini}) + \int_0^t \nabla_x K(\cdot,s) * (J - v'\rho)(f_1+f_2)(\cdot,t-s)\,ds\right) \mathcal{F}_i' dv,' \\ \qquad\qquad - |V|\,\phi_i \left(K*(\rho_1^{ini}+\rho_2^{ini}) + \displaystyle\int_0^t \nabla_x K(\cdot,s) * (J - v\rho)(f_1+f_2)(\cdot,t-s)\,ds\right) \mathcal{F}_i, \\ \mathcal{F}_i(\cdot,t=0) = f_i^{ini}, \quad \text{for } i=1,2. \end{cases} \tag{1.37}$$

Therefore, $(\mathcal{F}_1^{fg},\mathcal{F}_2^{fg})$ satisfies

$$\begin{cases} \partial_t \mathcal{F}_i^{fg} + v\cdot\nabla_x \mathcal{F}_i^{fg} + |V|\,\phi_i\big(K*(\rho_1^{ini}+\rho_2^{ini}) + \displaystyle\int_0^t \nabla_x K(\cdot,s) * (J-v\rho)(f_1+f_2)(\cdot,t-s)\,ds\big)\mathcal{F}_i^{fg} = \mathcal{G}_i^{fg}, \\ \mathcal{F}_i^{fg}(\cdot,t=0) = 0, \quad \text{for } i=1,2, \end{cases}$$

where $\mathcal{G}_i^{fg}$ is defined by

$$\begin{aligned}\mathcal{G}_i^{fg}(x,v,t) := &\int_V \phi_i(K*(\rho_1^{ini}+\rho_2^{ini}) + \int_0^t \nabla_x K(\cdot,s)*(J-v'\rho)(f_1+f_2)(\cdot,t-s)ds)\mathcal{F}_i^{fg}(v')dv' \\ &- \mathcal{F}_i(g)\Big(\phi_i(K*(\rho_1^{ini}+\rho_2^{ini}) + \int_0^t \nabla_x K(\cdot,s)*(J-v\rho)(f_1+f_2)(\cdot,t-s)ds) \\ &\quad -\phi_i(K*(\rho_1^{ini}+\rho_2^{ini}) + \int_0^t \nabla_x K(\cdot,s)*(J-v\rho)(g_1+g_2)(\cdot,t-s)ds))\Big) \\ &+ \mathcal{F}_i(g)(v')\Big(\phi_i(K*(\rho_1^{ini}+\rho_2^{ini}) + \int_0^t \nabla_x K(\cdot,s)*(J-v'\rho)(f_1+f_2)(\cdot,t-s)ds) \\ &\quad -\phi_i(K*(\rho_1^{ini}+\rho_2^{ini}) + \int_0^t \nabla_x K(\cdot,s)*(J-v'\rho)(g_1+g_2)(\cdot,t-s)ds)\Big)\,dv'.\end{aligned}$$

By the same strategy as in the elliptic case, one can show that

$$\begin{aligned}\|\mathcal{G}_1^{fg}(\cdot,s)\|_{L^\infty(\Omega)} \le \phi_1^{max}|V|\,\|\mathcal{F}_1^{fg}(\cdot,s)\|_{L^\infty(\Omega)} + C(1+|V|)\|\phi_1\|_{C^{0,1}(\mathbb{R})} \\ \times \|\mathcal{F}_1(g)(\cdot,s)\|_{L^\infty(\Omega)}\int_0^s \|\nabla_x K(\cdot,r)\|_{L^1(\mathbb{R}^d)}\sum_{i=1,2}\|(f_i-g_i)(\cdot,s-r)\|_{L^\infty(\Omega)}\,dr. \quad (1.38)\end{aligned}$$

By the Duhamel formula, we obtain the expression of $\mathcal{F}_i^{fg}(x,v,t)$

$$\begin{aligned}\mathcal{F}_i^{fg}(x,v,t) = &\int_0^t \exp\big(-\int_s^t \phi_i\big(\int_0^u \nabla_x K(\cdot,r)*(J-v\rho)(f_1+f_2)(x-v(s-u),u-r)dr\big)du\big) \\ &\times \mathcal{G}_i^{fg}(s,x-v(t-s),v)\,ds. \quad (1.39)\end{aligned}$$

As previously, from (1.39), we get that

$$\|\mathcal{F}_1^{fg}(\cdot,t)\|_{L^\infty(\Omega)} \le \int_0^t \|\mathcal{G}_1^{fg}(\cdot,s)\|_{L^\infty(\Omega)}ds.$$

Using the bound on $\|\mathcal{G}_1^{fg}(\cdot,s)\|_{L^\infty(\Omega)}$ (1.38) yields

$$\begin{aligned}\Big\|\mathcal{F}_1^{fg}(\cdot,t)\Big\|_{L^\infty(\Omega)} \le \phi_1^{max}|V|\int_0^t \Big\|\mathcal{F}_1^{fg}(\cdot,s)\Big\|_{L^\infty(\Omega)}ds + C_1\int_0^t \|\mathcal{F}_1(g)(\cdot,s)\|_{L^\infty(\Omega)} \\ \times\left(\int_0^s \|\nabla_x K(\cdot,r)\|_{L^1(\mathbb{R}^d)}\sum_{i=1,2}\|(f_i-g_i)(\cdot,s-r)\|_{L^\infty(\Omega)}\,dr\right)ds.\end{aligned}$$

By using the estimate on $\|\mathcal{F}_1(g)(\cdot,s)\|_{L^\infty(\Omega)}$ which is the same as in Lemma 1.3.3, we have

$$\begin{aligned}\Big\|\mathcal{F}_1^{fg}(\cdot,t)\Big\|_{L^\infty(\Omega)} \le \phi_1^{max}|V|\int_0^t \Big\|\mathcal{F}_1^{fg}(\cdot,s)\Big\|_{L^\infty(\Omega)}ds \\ + C_1' e^{\phi_1^{max}|V|t}\int_0^t\int_0^s \|\nabla_x K(\cdot,r)\|_{L^1(\mathbb{R}^d)}\sum_{i=1,2}\|(f_i-g_i)(s-r,\cdot,\cdot)\|_{L^\infty(\Omega)}\,dr\,ds.\end{aligned}$$

We bound the integral over $(0,s)$ by the integral over $(0,t)$. By applying a change of variable and the Fubini Theorem, it follows that

$$\begin{aligned}\Big\|\mathcal{F}_1^{fg}(\cdot,t)\Big\|_{L^\infty(\Omega)} \le \phi_1^{max}|V|\int_0^t \Big\|\mathcal{F}_1^{fg}(\cdot,s)\Big\|_{L^\infty(\Omega)}ds \\ + C_1' e^{\phi_1^{max}|V|t}\left(\int_0^t \|\nabla_x K(\cdot,r)\|_{L^1(\mathbb{R}^d)}dr\right)\left(\int_0^t \sum_{i=1,2}\|(f_i-g_i)(\cdot,s)\|_{L^\infty(\Omega)}\,ds\right).\end{aligned}$$

By Lemma 1.3.1, $\|\nabla_x K(\cdot,r)\|_{L^1(\mathbb{R}^d)}$ is integrable and we have

$$\left\|\mathcal{F}_1^{fg}(\cdot,t)\right\|_{L^\infty(\Omega)} \leq \phi_1^{max}\,|V| \int_0^t \left\|\mathcal{F}_1^{fg}(\cdot,s)\right\|_{L^\infty(\Omega)} ds + C_1' e^{\phi_1^{max}|V|t} t^{1/2} \int_0^t \sum_{i=1,2} \|(f_i-g_i)(\cdot,s)\|_{L^\infty(\Omega)}\, ds.$$

Applying the Gronwall Lemma gives a bound on $\left\|\mathcal{F}_1^{fg}(\cdot,t)\right\|_{L^\infty(\Omega)}$ and the rest of the proof is analogous to the elliptic case.

1.4 Rigorous proof of Drift-diffusion limit

In this section, we investigate the diffusive limit of the kinetic model, i.e we prove Theorem 1.2.3. We start by giving estimates on S for given functions ρ_1, ρ_2 and useful inequalities. Afterwards, we state a proposition which gives uniform estimates on $f_1^\varepsilon, f_2^\varepsilon, S^\varepsilon$. Finally, we conclude by using Aubin-Lions-Simon compactness lemma [118].

1.4.1 A-priori estimates

Lemma 1.4.1 (Estimates on S^ε)**.** *Fix $\tau > 0$. Let p, q, α be such that $1 < p < \infty, d < q < \infty, 0 < \alpha < 1 - \frac{d}{q}$. Assume that $\rho_1^\varepsilon, \rho_2^\varepsilon \in L^\infty([0,\tau], L^1(\mathbb{R}^d) \cap L^q(\mathbb{R}^d))$. Then, we have*

— *For $\delta = 0$, $S^\varepsilon(\cdot,t)$ is bounded in $C^{1,\alpha}(\mathbb{R}^d)$ for all $t \in [0,\tau]$ and there exists a constant c independent of ε and t such that*

$$\|S^\varepsilon(\cdot,t)\|_{C^{1,\alpha}(\mathbb{R}^d)} \leq c\left(\|(\rho_1^\varepsilon+\rho_2^\varepsilon)(\cdot,t)\|_{L^1(\mathbb{R}^d)} + \|(\rho_1^\varepsilon+\rho_2^\varepsilon)(\cdot,t)\|_{L^q(\mathbb{R}^d)}\right).$$

— *For $\delta = 1$, S^ε is bounded in $L^\infty([0,\tau], C^{1,\alpha}(\mathbb{R}^d)) \cap L^\infty([0,\tau], W^{1,p}(\mathbb{R}^d))$ and there exists a constant c_τ independent of ε such that*

$$\|S^\varepsilon\|_{L^\infty([0,\tau],W^{1,p}(\mathbb{R}^d))} + \|S^\varepsilon\|_{L^\infty([0,\tau],C^{1,\alpha}(\mathbb{R}^d))} \leq c_\tau\big(\|\rho_1^\varepsilon+\rho_2^\varepsilon\|_{L^\infty([0,\tau],L^1(\mathbb{R}^d))} + \|\rho_1^\varepsilon+\rho_2^\varepsilon\|_{L^\infty([0,\tau],L^q(\mathbb{R}^d))}\big).$$

Proof. The result for the case $\delta = 0$ is classical and follows from the elliptic regularity. We refer the reader to [20, chapter 9] for details. We just give main arguments and derive bounds for S^ε. By the elliptic regularity, we know that $S^\varepsilon(\cdot,t)$ is bounded in $W^{2,q}(\mathbb{R}^d)$ and the following estimate holds.

$$\|S^\varepsilon(\cdot,t)\|_{W^{2,q}(\mathbb{R}^d)} \leq C\,\|(\rho_1^\varepsilon+\rho_2^\varepsilon)(\cdot,t)\|_{L^q(\mathbb{R}^d)}.$$

By the Morrey theorem, $W^{2,q}$ is continuously embedded into $C^{1,\gamma}$ with $\gamma = 1 - \frac{d}{q}$.

$$W^{2,q}(\mathbb{R}^d) \hookrightarrow C^{1,\gamma}(\mathbb{R}^d).$$

The interpolation between L^1 and L^q implies that for all $d \leq p \leq q$, $(\rho_1^\varepsilon+\rho_2^\varepsilon)(\cdot,t)$ are bounded in L^p and by elliptic regularity $S^\varepsilon(\cdot,t)$ is bounded in $W^{2,p}$. Thus, the $W^{2,p}$-norm of S^ε is bounded by L^p-norms of ρ_1^ε and ρ_2^ε.

$$\|S^\varepsilon(\cdot,t)\|_{W^{2,p}(\mathbb{R}^d)} \leq C\,\|(\rho_1^\varepsilon+\rho_2^\varepsilon)(\cdot,t)\|_{L^p(\mathbb{R}^d)}.$$

By the Morrey Theorem, we conclude that for all $0 < \alpha < 1 - \frac{d}{q}$, $S(\cdot,t)$ belongs to $C^{1,\alpha}$ and we have the estimate

$$\|S^\varepsilon(\cdot,t)\|_{C^{1,\alpha}(\mathbb{R}^d)} \leq C\,\|S^\varepsilon(\cdot,t)\|_{W^{2,p}(\mathbb{R}^d)},$$

where p is given by $1-\frac{d}{p}=\alpha$.

We now deal with the case $\delta=1$. We recall that S is given by the convolution with the kernel K defined in (1.24). Applying Young's inequality and using Lemma 1.3.1 yields for all t in $[0,\tau]$

$$\|S^\varepsilon(\cdot,t)\|_{L^\infty(\mathbb{R}^d)} \le \left(\int_0^\tau \|K(\cdot,s)\|_{L^{q'}(\mathbb{R}^d)}\,ds\right)\|\rho_1^\varepsilon+\rho_2^\varepsilon\|_{L^\infty([0,\tau],L^q(\mathbb{R}^d))},$$
$$\|\nabla S^\varepsilon(\cdot,t)\|_{L^\infty(\mathbb{R}^d)} \le \left(\int_0^\tau \|\nabla K(\cdot,s)\|_{L^{q'}(\mathbb{R}^d)}\,ds\right)\|\rho_1^\varepsilon+\rho_2^\varepsilon\|_{L^\infty([0,\tau],L^q(\mathbb{R}^d))}.$$

Similarly, we have

$$\|S^\varepsilon(\cdot,t)\|_{L^1(\mathbb{R}^d)} \le \left(\int_0^\tau \|K(\cdot,s)\|_{L^1(\mathbb{R}^d)}\,ds\right)\|\rho_1^\varepsilon+\rho_2^\varepsilon\|_{L^\infty([0,\tau],L^1(\mathbb{R}^d))},$$
$$\|\nabla S^\varepsilon(\cdot,t)\|_{L^1(\mathbb{R}^d)} \le \left(\int_0^\tau \|\nabla K(\cdot,s)\|_{L^1(\mathbb{R}^d)}\,ds\right)\|\rho_1^\varepsilon+\rho_2^\varepsilon\|_{L^\infty([0,\tau],L^1(\mathbb{R}^d))}.$$

By an interpolation argument, we deduce that S^ε is bounded in $L^\infty([0,\tau],W^{1,p}(\mathbb{R}^d))$ for any p between 1 and ∞. Thanks to the Morrey theorem, S^ε belongs to $L^\infty([0,\tau],C^{0,\alpha}(\mathbb{R}^d))$ with $0<\alpha\le 1-\frac{d}{q}$.

Fix x and x' in $\mathbb{R}^d$ and set $r:=|x-x'|$. For the sake of simplicity, we define $\rho^\varepsilon:=\rho_1^\varepsilon+\rho_2^\varepsilon$. Let us prove that ∇S^ε is bounded in $L^\infty([0,\tau],C^{0,\alpha}(\mathbb{R}^d))$. We split the integral into two parts I_1 and I_2.

$$\begin{aligned}\nabla S^\varepsilon(x,t)-\nabla S^\varepsilon(x',t) &= \int_0^t\int_{\mathbb{R}^d}\big(\nabla K(x-y,t-s)-\nabla K(x'-y,t-s)\big)\\ &\quad\times(\rho_1^\varepsilon+\rho_2^\varepsilon)(y,s)\,dy\,ds\\ &= I_1+I_2,\end{aligned}$$

with

$$I_1 := \int_0^t\int_{B_x(2r)}\big(\nabla K(x-y,t-s)-\nabla K(x'-y,t-s)\big)(\rho_1^\varepsilon+\rho_2^\varepsilon)(y,s)\,dy\,ds,$$
$$I_2 := \int_0^t\int_{\mathbb{R}^d\setminus B_x(2r)}\big(\nabla K(x-y,t-s)-\nabla K(x'-y,t-s)\big)(\rho_1^\varepsilon+\rho_2^\varepsilon)(y,s)\,dy\,ds.$$

We now estimate I_1. Using the definition of ∇K and the triangle inequality, we get

$$\begin{aligned}I_1 \le &\frac{1}{2(4\pi)^{d/2}}\int_0^t\int_{B_x(2r)} e^{-\frac{|x-y|^2}{4(t-s)}-(t-s)}\frac{|x-y|}{(t-s)^{d/2+1}}\rho^\varepsilon(y,s)\,dy\,ds\\ &+\frac{1}{2(4\pi)^{d/2}}\int_0^t\int_{B_x(2r)} e^{-\frac{|x'-y|^2}{4(t-s)}-(t-s)}\frac{|x'-y|}{(t-s)^{d/2+1}}\rho^\varepsilon(y,s)\,dy\,ds.\end{aligned}$$

These two terms are identical and we will be treated in the same manner. We just carry out computations for the first one. Since y belongs to $B_x(2r)$, $r=|x-x'|$, we have

$$\begin{aligned}\int_0^t\int_{B_x(2r)} e^{-\frac{|x-y|^2}{4(t-s)}-(t-s)}\frac{|x-y|}{(t-s)^{d/2+1}}\rho^\varepsilon(y,s)\,dy\,ds &\le 2^\alpha|x-x'|^\alpha\\ &\quad\times\int_0^t\int_{B_x(2r)} e^{-\frac{|x-y|^2}{4(t-s)}-(t-s)}\frac{|x-y|^{1-\alpha}}{(t-s)^{d/2+1}}\rho^\varepsilon(y,s)\,dy\,ds.\end{aligned}$$

Therefore, I_1 reads

$$\begin{aligned}I_1 \le \frac{2^{\alpha-1}}{(4\pi)^{d/2}}|x-x'|^\alpha\Bigg(&\int_0^t\int_{B_x(2r)} e^{-\frac{|x-y|^2}{4(t-s)}-(t-s)}\frac{|x-y|^{1-\alpha}}{(t-s)^{d/2+1}}\rho^\varepsilon(y,s)\,dy\,ds\\ &+\int_0^t\int_{B_x(2r)} e^{-\frac{|x'-y|^2}{4(t-s)}-(t-s)}\frac{|x'-y|^{1-\alpha}}{(t-s)^{d/2+1}}\rho^\varepsilon(y,s)\,dy\,ds\Bigg).\end{aligned}$$

We conclude by bounding the integral over the ball $B_x(2r)$ by the integral over the whole space. We now deal with I_2. We first compute the hessian $D_x^2 K$ of the kernel K.

$$D_x^2 K(x,t) = \frac{1}{(4\pi t)^{d/2}}(-\frac{I_d}{t} + \frac{x\otimes x}{t^2})e^{-\frac{|x|^2}{4t}-t}.$$

We decompose $D_x^2 K$ into two parts :

$$D_x^2 K(x,t) = \frac{1}{(4\pi)^{d/2}}\left(-I_d + \frac{x}{\sqrt{t}}\otimes\frac{x}{\sqrt{t}}\right)e^{-\frac{1}{8}\left|\frac{x}{\sqrt{t}}\right|^2} \times \frac{e^{-\frac{|x|^2}{8t}-t}}{t^{d/2+1}}.$$

By using the change of variable $u = \frac{x}{\sqrt{t}}$, we notice that the first part of the rhs is bounded by a nonnegative constant C. Thus,

$$\left|D_x^2 K\right|(x,t) \le \frac{C}{t^{d/2+1}}e^{-\frac{|x|^2}{8t}-t}.$$

Moreover, we remark that for all y in $\mathbb{R}^d \setminus B_x(2r)$ and u in $[0,1]$

$$|x-y+u(x'-x)| \ge |x-y| - u\,|x-x'| \ge (1-u/2)\,|x-y|\,.$$

We infer that for all y in $\mathbb{R}^d \setminus B_x(2r)$ and u in $[0,1]$

$$\left|D_x^2 K\right|(x-y+u(x'-x),t-s) \le \frac{C}{(t-s)^{d/2+1}}\exp\left(-\frac{|x-y|^2}{32(t-s)} - (t-s)\right).$$

Hence,

$$I_2 \le C\,|x-x'|\int_0^t\!\!\int_{\mathbb{R}^d\setminus B_x(2r)} \frac{1}{(t-s)^{d/2+1}}\exp\left(-\frac{|x-y|^2}{32(t-s)} - (t-s)\right)\rho^\varepsilon(y,s)\,dy\,ds.$$

We deduce that

$$\begin{aligned} I_2 &\le C'\,|x-x'|^\alpha \int_0^t\!\!\int_{\mathbb{R}^d\setminus B_x(2r)} \frac{|x-y|^{1-\alpha}}{(t-s)^{d/2+1}}\exp\left(-\frac{|x-y|^2}{32(t-s)} - (t-s)\right)\rho^\varepsilon(y,s)\,dy\,ds,\\ &\le C'\,|x-x'|^\alpha \int_0^t\!\!\int_{\mathbb{R}^d} \frac{|x-y|^{1-\alpha}}{(t-s)^{d/2+1}}\exp\left(-\frac{|x-y|^2}{32(t-s)} - (t-s)\right)\rho^\varepsilon(y,s)\,dy\,ds. \end{aligned}$$

Then using Young's inequality, we have for any positive constant c and any $p \in (d,q)$,

$$\begin{aligned} \int_0^t\int_{\mathbb{R}^d}\frac{e^{-(t-s)}}{(t-s)^{d/2+1}}\,|x-y|^{1-\alpha}\,e^{-\frac{c|x-y|^2}{t-s}}\rho^\varepsilon(y,s)dy\,ds \le \int_0^t \frac{e^{-(t-s)}}{(t-s)^{d/2+1}}\\ \|\,|y|^{1-\alpha}\,e^{-\frac{c|y|^2}{t-s}}\|_{L^{p'}(\mathbb{R}^d)}\|\rho^\varepsilon\|_{L^p(\mathbb{R}^d)}ds. \end{aligned}$$

It is clear that

$$\|y\mapsto |y|^{1-\alpha}\exp\Big(-\frac{c\,|y|^2}{t-s}\Big)\|_{L^{p'}(\mathbb{R}^d)} \le C(t-s)^{\frac{1-\alpha}{2}+\frac{d}{2p'}}.$$

This implies that for all $\alpha < 1-\frac{d}{q}$ and all $d<p<q$

$$\begin{aligned} \int_0^t\int_{\mathbb{R}^d}\frac{e^{-(t-s)}}{(t-s)^{d/2+1}}\,|x-y|^{1-\alpha}\,e^{-\frac{c|x-y|^2}{t-s}}\rho^\varepsilon(y,s)\,dy\,ds \le C\left(\int_0^\tau t^{\frac{1-\alpha}{2}-\frac{d}{2p'}}e^{-t}dt\right)\\ \times\|\rho^\varepsilon\|_{L^\infty([0,\tau],L^p(\mathbb{R}^d))} < \infty. \end{aligned}$$

So, the $C^{1,\alpha}$ bound of S^ε follows. □

Lemma 1.4.2. *Fix $S \geq 0$ and let f be a velocity distribution and $q > 1$. Then, we have*

$$\left|\phi_i^{A,\varepsilon}[S](f+f')(f^{q-1}-(f')^{q-1})\right| \leq \frac{1}{2}\phi_i^{S,\varepsilon}[S](f-f')(f^{q-1}-(f')^{q-1}) + \frac{\phi_i^{A,\varepsilon}[S]^2}{2\phi_i^{S,\varepsilon}[S^\varepsilon]}\frac{(f+f')^2(f^{q-1}-(f')^{q-1})}{f-f'}, \quad (1.40)$$

where $\phi_i^{S,\varepsilon}[S], \phi_i^{A,\varepsilon}[S]$ are the symmetric and anti-symmetric parts of $\mathcal{T}_i^\varepsilon[S]$ defined in (1.14)*. There also exists a constant c_q depending on q such that*

$$\frac{(f+f')^2(f^{q-1}-(f')^{q-1})}{f-f'} \leq c_q(f^q+(f')^q). \quad (1.41)$$

Proof. For (1.40), we observe that

$$\left(\phi_i^{S,\varepsilon}[S](f-f') \pm \phi_i^{A,\varepsilon}[S](f+f')\right)^2 \geq 0.$$

Expanding this inequality and dividing both sides by $(f^{q-1}-(f')^{q-1})/(f-f')$ gives the result.
To prove (1.41), we show that for $a \geq 0$, the following function A is bounded

$$A : a \longmapsto \frac{(1+a)^2(1-a^{q-1})}{(1-a)(1+a^q)}.$$

In fact, we have $\lim_{a\to 1} A(a) = 2(q-1) > 0$. Then A can be continuously extended to $[0,\infty[$. Since A tends to 1 at infinity and is positive, A is bounded by a positive constant. □

Proposition 1.4.3. *Assume that the initial data f_1^{ini} and f_2^{ini} belong to $L^1_+(\Omega)\cap L^\infty(\Omega)$. Under Assumption (H1), the solution of* (1.9)–(1.11) *admits uniform estimates in ε in the following spaces :*

$$\begin{cases} f_1^\varepsilon, f_2^\varepsilon \in L^\infty_{loc}((0,\infty), L^q(\Omega)), \quad 1 \leq q < \infty, \\ r_1^\varepsilon, r_2^\varepsilon \in L^2(\Omega\times(0,\infty)), \\ S^\varepsilon \in L^\infty_{loc}((0,\infty), C^{1,\alpha}(\mathbb{R}^d)\cap W^{1,p}(\mathbb{R}^d)), \quad 1 \leq p \leq \infty,\ 0<\alpha<1, \end{cases}$$

where r_i^ε is given by

$$r_i^\varepsilon := \frac{f_i^\varepsilon - \rho_i^\varepsilon F}{\varepsilon}.$$

We skip the proof of this result since it is a straightforward adapation of the single-species case done in [28, Theorem 2]. The proof uses all lemmas shown below.

1.4.2 Proof of Theorem 1.2.3

We prove the theorem in the parabolic setting $\delta = 1$. The proof in the elliptic one is analogous.

We first recall the following Aubin-Lions-Simon compactness lemma.

Lemma 1.4.4 (Aubin-Lions-Simon, [118]). *Let $\tau > 0$ and p, q be such that $1 < p \leq \infty, 1 \leq q \leq \infty$. Let V, E, F be Banach spaces such that*

$$V \overset{c}{\hookrightarrow} E \hookrightarrow F.$$

If A is bounded in $W^{1,p}((0,\tau),F)\cap L^q((0,\tau),V)$, then A is relatively compact in $L^q((0,\tau),E)$.

Proof of Theorem 1.2.3. Let us fix $1 < q < \infty$, $1 < p \leq \infty$ and $\tau > 0$. We decomposed the proof into three steps.

Step 1 : Uniform estimates for $\partial_t(\nabla S^\varepsilon)$ and $\partial_t(S^\varepsilon)$. We differentiate the conservation law of ρ_i^ε with respect to x.

$$\partial_t \rho_i^\varepsilon + \nabla \cdot J_i^\varepsilon = 0, \tag{1.42}$$

with $J_i^\varepsilon := \dfrac{1}{\varepsilon}\displaystyle\int_V v f_i^\varepsilon dv$.

$$\partial_t \nabla_x \rho_i^\varepsilon + \nabla_x \nabla \cdot J_i^\varepsilon = 0.$$

Summing these equalities for $i = 1, 2$ gives

$$\partial_t \nabla_x (\rho_1^\varepsilon + \rho_2^\varepsilon) + \nabla_x \nabla \cdot (J_1^\varepsilon + J_2^\varepsilon) = 0.$$

By multiplying by the kernel $K(t-s, x-y)$ and integrating by parts, one gets

$$\partial_t(\nabla_x S^\varepsilon) + \nabla_x(\nabla \cdot S^{J,\varepsilon}) = \nabla_x \left(\int_{\mathbb{R}^d} K(t,y)(\rho_1 + \rho_2)(0, x-y)\, dy \right), \tag{1.43}$$

where $S^{J,\varepsilon}$ denotes

$$S^{J,\varepsilon} := \int_0^t \int_{\mathbb{R}^d} K(t-s, x-y)(J_1^\varepsilon + J_2^\varepsilon)(s,y)\, dy\, ds.$$

From Proposition 1.4.3, r_i^ε is uniformly bounded in $L^2(\Omega \times [0,\tau])$. Since $J_i^\varepsilon = \int_V v r_i^\varepsilon\, dv$, we deduce by the Cauchy-Schwarz inequality that J_i^ε is also bounded in $L^2(\Omega \times [0,\tau])$.

The mathematical form of $S^{J,\varepsilon}$ implies that $S^{J,\varepsilon}$ satisfies the same parabolic equation as S^ε with the right-hand side $J_1^\varepsilon + J_2^\varepsilon$. Using the parabolic regularity, we conclude that

$$S^{J,\varepsilon} \in L^2((0,\tau], H^2_{\mathrm{loc}}(\mathbb{R}^d)).$$

Then, from (1.43), we get that

$$\partial_t(\nabla S^\varepsilon) \in L^2((0,\tau], L^2_{\mathrm{loc}}(\mathbb{R}^d)).$$

Moreover, we know the expression of $\partial_t S^\varepsilon$ from Lemma 1.3.2.

$$\partial_t S^\varepsilon = \int_{\mathbb{R}^d} K(y,\tau)(\rho_1^{ini} + \rho_2^{ini})(x-y)\, dy + \int_0^\tau \int_{\mathbb{R}^d} \nabla_x K(y,s)(J_1^\varepsilon + J_2^\varepsilon)(x-y, \tau-s)\, dy\, ds.$$

The same conclusion holds for $\partial_t S^\varepsilon$:

$$\partial_t S^\varepsilon \in L^2((0,\tau], L^2_{\mathrm{loc}}(\mathbb{R}^d)).$$

Step 2 : Extraction of subsequences. By the Ascoli Theorem, we have the following embeddings :

$$C^{0,\alpha}_{\mathrm{loc}}(\mathbb{R}^d) \overset{c}{\hookrightarrow} L^p_{\mathrm{loc}}(\mathbb{R}^d) \hookrightarrow L^2_{\mathrm{loc}}(\mathbb{R}^d), \quad 2 \leq p \leq \infty.$$

From the Aubin-Lions-Simon Lemma 1.4.4, there exists subsequences $(S^\varepsilon)_\varepsilon$ and $(\nabla S^\varepsilon)_\varepsilon$ that strongly converge in $L^p_{\mathrm{loc}}(\mathbb{R}^d \times (0,\tau])$. This result is extended to p between 1 and 2 by the continuous embedding of L^∞_{loc} into L^p_{loc}. The extraction of weak-* convergent subsequences of $f_1^\varepsilon, f_2^\varepsilon$ and weak convergent subsequences $r_1^\varepsilon, r_2^\varepsilon$ follows from the separability or reflexivity property of Banach spaces $L^\infty((0,\tau], L^q(\Omega))$, $L^2(\Omega \times (0,\tau])$.

We find a subsequence of $(f_1^\varepsilon, f_2^\varepsilon, S^\varepsilon)$ which satisfies

$$\begin{aligned}
&f_1^\varepsilon \overset{*}{\rightharpoonup} f_1^0, \quad f_2^\varepsilon \overset{*}{\rightharpoonup} f_2^0 \quad \text{in } L^\infty((0,\tau], L^q(\Omega)),\\
&r_1^\varepsilon \rightharpoonup r_1^0, \quad r_2^\varepsilon \rightharpoonup r_2^0, \quad \text{in } L^2(\Omega \times (0,\tau]),\\
&S^\varepsilon \to S^0, \quad \nabla_x S^\varepsilon \to \nabla_x S^0 \quad \text{in } L^p_{\mathrm{loc}}(\mathbb{R}^d \times (0,\tau]),
\end{aligned}$$

for any p, q such that $1 < q < \infty$ and $1 \le p \le \infty$.
As a consequence, ρ_i^ε converges weakly-* in $L^\infty((0,\tau], L^q(\mathbb{R}^d))$.

$$(\rho_1^\varepsilon, \rho_2^\varepsilon) \overset{*}{\rightharpoonup} \left(\int_V f_1^0 dv, \int_V f_2^0 dv \right) \quad \text{in } L^\infty((0,\tau_0), L^q(\mathbb{R}^d)).$$

Step 3 : Passing to the limit. This step consists in identifying limits $f_1^0, f_2^0, r_1^0, r_2^0$. We now operate in either $L^2_{\text{loc}}((0,\tau], L^2(\mathbb{R}^d))$ or $L^2_{\text{loc}}((0,\tau], L^2(\Omega))$. We pass to the limit in the relation $f_i^\varepsilon = \rho_i^\varepsilon F + \varepsilon r_i^\varepsilon$ to get

$$f_1^0 = \rho_1^0 F \quad \text{and} \quad f_2^0 = \rho_2^0 F \quad \text{in } L^2_{\text{loc}}((0,\tau], L^2(\Omega)).$$

We replace f_i^ε by $\rho_i^\varepsilon F + \varepsilon r_i^\varepsilon$ into $\mathcal{T}_i^0(f_i^\varepsilon)$, the equation for f_i^ε (1.9) now reads

$$\varepsilon \partial_t f_i^\varepsilon + v \cdot \nabla_x f_i^\varepsilon = -|V|\, \psi_i r_i^\varepsilon + \psi_i \left(\int_V \theta_i (\varepsilon \partial_t S^\varepsilon + v' \cdot \nabla_x S^\varepsilon) f_i^{\varepsilon'} dv' \right. \\ \left. - |V|\, \theta_i (\varepsilon S^\varepsilon + v \cdot \nabla_x S^\varepsilon) f_i^\varepsilon \right). \quad (1.44)$$

From the previous study, we have

$$\partial_t S^\varepsilon \text{ is uniformly bounded in } L^2((0,\tau], L^2_{\text{loc}}(\mathbb{R}^d)),$$

and

$$\nabla_x S^\varepsilon \to \nabla_x S^0 \text{ in } L^2((0,\tau], L^2_{\text{loc}}(\mathbb{R}^d)).$$

Since θ_i is Lipschitz continuous, we deduce that

$$\theta_i(\varepsilon \partial_t S^\varepsilon + v \cdot \nabla_x S^\varepsilon) \to \theta_i(v \cdot \nabla_x S^0) \text{ in } L^2((0,\tau], L^2_{\text{loc}}(\Omega)).$$

We also know that

$$f_i^\varepsilon \rightharpoonup \rho_i^0 F \text{ in } L^2((0,\tau], L^2_{\text{loc}}(\Omega)).$$

The combination of these arguments gives

$$\int_V \theta_i (\varepsilon \partial_t S^\varepsilon + v' \cdot \nabla_x S^\varepsilon) f_i^{\varepsilon'} dv' \rightharpoonup \rho_i^0 \int_V \theta_i (v' \cdot \nabla_x S^0) \frac{dv'}{|V|} \quad \text{in } L^2((0,\tau], L^2_{\text{loc}}(\Omega)),$$
$$\theta_i (\varepsilon \partial_t S^\varepsilon + v \cdot \nabla_x S^\varepsilon) f_i^\varepsilon \rightharpoonup \rho_i^0 \theta_i (v \cdot \nabla_x S^0) \frac{\mathbb{1}_{v \in V}}{|V|} \quad \text{in } L^2((0,\tau], L^2_{\text{loc}}(\Omega)).$$

By passing to the limit in (1.44), we obtain r_i^0.

$$r_i^0 = -\frac{v \cdot \nabla_x \rho_i^0}{\psi_i |V|^2} + \frac{\rho_i^0}{|V|} \left(\int_V \theta_i (v' \cdot \nabla_x S^0) \frac{dv'}{|V|} - \theta_i (v \cdot \nabla_x S^0) \right).$$

We deduce that J_i^ε converges weakly in $L^2((0,\tau], L^2_{\text{loc}}(\mathbb{R}^d))$.

$$J_i^\varepsilon = \frac{1}{\varepsilon} \int_V v\, f_i^\varepsilon = \int_V v\, r_i^\varepsilon \rightharpoonup \int_V v r_i^0.$$

By passing to the limit in the conservation law (1.42), we find the equation for ρ_i^0.

$$\partial_t \rho_i^0 + \nabla \cdot \int_V v\, r_i^0 = 0.$$

Next, the equation for S^0 is obtained by passing to the limit in (1.11).

Synchronising and Non-synchronising dynamics for a two-species aggregation model

Ce travail est réalisé en collaboration avec Jie Liao et Nicolas Vauchelet. Il est consacré à l'analyse de la limite hyperbolique du modèle cinétique de chimiotactisme à deux espèces présenté dans le premier chapitre. Dans cette étude, on se restreint au cas unidimensionnel et dans le cas à deux vitesses. La démarche employée permet de prouver l'existence et l'unicité des solutions au sens de dualité d'un modèle hyperbolique à deux espèces. On propose une méthode numérique qui converge vers la solution théorique et étudie la dynamique de formation d'agrégats dans ce modèle. Le phénomène de synchronisation ou de désynchronisation inexistant dans le cas d'une population à une espèce apparaît. Il traduit le comportement des masses de diracs qui s'opère lors de leurs collisions. En fonction des paramètres du modèle, les masses de diracs d'espèces différentes vont ensemble ou se séparent.
Article soumis

Chapitre 2

Synchronising and Non-synchronising dynamics for a two-species aggregation model

Abstract

This chapter deals with analysis and numerical simulations of a one-dimensional two-species hyperbolic aggregation model. This model is formed by a system of transport equations with nonlocal velocities, which describes the aggregate dynamics of a two-species population in interaction appearing for instance in bacterial chemotaxis. Blow-up of classical solutions occurs in finite time. This raises the question to define measure-valued solutions for this system. To this aim, we use the duality method developed for transport equations with discontinuous velocity to prove the existence and uniqueness of measure-valued solutions. The proof relies on a stability result. In addition, this approach allows to study the hyperbolic limit of a kinetic chemotaxis model. Moreover, we propose a finite volume numerical scheme whose convergence towards measure-valued solutions is proved. It allows for numerical simulations capturing the behaviour after blow up. Finally, numerical simulations illustrate the complex dynamics of aggregates until the formation of a single aggregate: after blow-up of classical solutions, aggregates of different species are synchronising or nonsynchronising when collide, that is move together or separately, depending on the parameters of the model and masses of species involved.

Contents

2.1 Introduction

Aggregation phenomena for a population of individuals interacting through an interaction potential are usually modelled by the so-called aggregation equation which is a nonlocal nonlinear conservation equation. This equation governs the dynamics of the density of individuals subject to an interaction potential K. In this work, we are interested in the case where the population consists of two species which respond to the interaction potential in different ways. In the one-dimensional case, the system of equations writes:

$$\partial_t \rho_\alpha + \chi_\alpha \partial_x \left(a(\rho)\rho_\alpha\right) = 0, \quad \text{for } \alpha = 1, 2, \tag{2.1}$$

with

$$a(\rho) := \int_{\mathbb{R}} \partial_x K(x-y)\rho(t,dy), \quad \rho := \theta_1\rho_1 + \theta_2\rho_2,$$

where $\theta_\alpha, \chi_\alpha$ for $\alpha = 1, 2$ are positive constants.

In this work, we are interested in the case where the interaction potential K in (2.1) is *pointy* i.e. satisfies the following assumptions:

(H1) $K \in C^1(\mathbb{R}\backslash\{0\})$.

(H2) $\forall x \in \mathbb{R}, \quad K(x) = K(-x)$.

(H3) $\partial_x K \in L^\infty(\mathbb{R})$.

(H4) K is λ-concave with $\lambda > 0$ i.e.,

$$\forall x, y \in \mathbb{R}^*, \quad \left(\partial_x K(x) - \partial_x K(y)\right)(x-y) \leq \lambda (x-y)^2.$$

The aggregation equation arises in several applications in biology and physics. In fact, it is encountered in the modelling of cells which move in response to chemical cues. The velocity of cells $a(\rho)$ depending on the distribution of nearby cells represents the gradient of the chemical substance which triggers the motion. Cells gather and form accumulations near regions more exposed to oxygen as observed in [96, 115]. We can also describe the movement of pedestrians using the aggregation equation as in [65] where the velocity of pedestrians is influenced by the distribution of neighbours. This equation can also be applied to model opinion formation (see [121]) where interactions between different opinions can be expressed by a convolution with the kernel K.

From the mathematical point of view, it is known that solutions to the aggregation equation with a pointy potential blow up in finite time (see e.g [36, 23, 10]). Then global-in-time existence for weak measure solutions has been investigated. In [23], existence of weak solutions for single species model has been obtained as a gradient flow. This technique has been extended to the two-species model at hand in [36]. Another approach of defining weak solution for such kind of model has been proposed in [76, 75] for the single species case. In this approach, the aggregation equation is seen as a transport equation with a discontinuous velocity $a(\rho)$. Then solutions in the sense of duality have been defined for the aggregation equation.

Duality solutions has been introduced for linear transport equations with discontinuous velocity in the one-dimensional space in [14]. Then it has been adapted to the study of nonlinear transport equations in [16, 76, 75]. In [76, 75], the authors use this notion of duality solutions for the one-species aggregation equation. Such solutions are constructed by approximating the problem with particles, i.e. looking for a solution given by a finite sum of Dirac delta functions. Particles attract themselves through the interacting potential K, when two particles collide, they stick to form a bigger particle.

In this work, we extend this approach to the two species case. To do so, we need to modify the strategy to the problem at hand. Indeed, collisions between particles of different species are more complex: particles can move together or separately after collision. This synchronising or non-synchronising dynamics implies several difficulties for the treatment of the dynamics of particles. In fact, particles of different species can not stick when they collide. Then an approximate problem is constructed by considering the transport equation with the a regularized velocity. Then measure valued solutions are constructed by using a stability result.

An important advantage of this approach is that it allows to prove convergence of finite volume schemes. Numerical simulations of the aggregation equation for the one-species case, which corresponds to the particular case of (2.1) when setting $\rho_2 = 0$, have been investigated by several authors. In [27] the authors propose a finite volume method consistent with the gradient flow structure of the equation, but no convergence result has been obtained. In [34], a Lagrangian method is proposed (see also the recent work [26]). For the dynamics after blow up, a finite volume scheme which converges to the theoretical solution is proposed in [77, 24]. In the two-species case, the behaviour is more complex since the interaction between the two species can occur and they may synchronise or not i.e. move together or separately depending on the parameters of the models and the masses of species. A numerical scheme illustrating this interesting synchronising or non-synchronising dynamics is provided in Section 6. In addition, a theoretical result on the convergence of the numerical approximation obtained with our numerical scheme towards the duality solution is given. Such complex interactions phenomena have been observed experimentally in [42].

System (2.1) can be derived from a hyperbolic limit of a kinetic chemotaxis model. In the case of two-velocities and in one space dimension, the kinetic chemotaxis model is given by

$$\begin{cases} \partial_t f_\alpha^\varepsilon + v\,\partial_x f_\alpha^\varepsilon = \dfrac{1}{\varepsilon}\displaystyle\int_V (T_\alpha[S](v',v) f_\alpha^\varepsilon(v') - T_\alpha[S](v,v') f_\alpha^\varepsilon(v))\,dv', \quad \alpha = 1,2,\ v \in V = \{\pm 1\}, \\ -\partial_{xx} S^\varepsilon + S^\varepsilon = \theta_1 \left(f_1^\varepsilon(1) + f_1^\varepsilon(-1)\right) + \theta_2 \left(f_2^\varepsilon(1) + f_2^\varepsilon(-1)\right), \end{cases} \tag{2.2}$$

where $f_\alpha^\varepsilon(x,v,t)$ stands for the distribution function of α-th species at time t, position x and velocity v, $S^\varepsilon(t,x)$ is the concentration of the chemical substance, $T_\alpha[S](v,v')$ is the tumbling kernel from direction $v \in V$ to direction $v' \in V$ and $\varepsilon > 0$ is a small parameter. This tumbling kernel being affected by the gradient of the chemoattractant, is chosen as in [40]

$$T_\alpha[S](v,v') = \psi_\alpha \left(1 - \chi_\alpha v \partial_x S\right), \tag{2.3}$$

where ψ_α is a positive constant called the natural tumbling kernel and χ_α is the chemosensitivity to the chemical S. This kinetic model for chemotaxis has been introduced in [99] to model the run-and-tumble process. Existence of solutions to this two species kinetic system has been studied in [43].

Summing and substracting equations (2.2) with respect to $v = \pm 1$ for f_α^ε yields

$$\partial_t \rho_\alpha^\varepsilon + \partial_x J_\alpha^\varepsilon = 0, \tag{2.4}$$

$$\partial_t J_\alpha^\varepsilon + \partial_x \rho_\alpha^\varepsilon = \frac{2\psi_\alpha}{\varepsilon}(\chi_\alpha \partial_x S^\varepsilon \rho_\alpha^\varepsilon - J_\alpha^\varepsilon), \quad \alpha = 1,2, \tag{2.5}$$

where $\rho_\alpha^\varepsilon := f_\alpha^\varepsilon(1) + f_\alpha^\varepsilon(-1)$ and $J_\alpha^\varepsilon := (f_\alpha^\varepsilon(1) - f_\alpha^\varepsilon(-1))$. Taking formally the limit $\varepsilon \to 0$ in (2.5), we deduce that $J_\alpha^\varepsilon \rightharpoonup \chi_\alpha \partial_x S^0 \rho_\alpha^0$ in the sense of distributions. Injecting in (2.4), we deduce formally that ρ_α^0 satisfies the limiting equation:

$$\partial_t \rho_\alpha^0 + \chi_\alpha \partial_x((\partial_x S^0)\rho_\alpha^0) = 0, \tag{2.6}$$

where S^0 satisfies the elliptic equation:

$$-\partial_{xx} S^0 + S^0 = \theta_1 \rho_1^0 + \theta_2 \rho_2^0.$$

This latter equation can be solved explicitly on $\mathbb{R}$ and S^0 is given by

$$S^0 = K * (\theta_1 \rho_1^0 + \theta_2 \rho_2^0), \quad K = \frac{1}{2} e^{-|x|}. \tag{2.7}$$

Then we recover system (2.1). This formal computation can be made rigorous. The rigorous derivation of (2.6) from system (2.2) will be proved in this work.

The paper is organized as follows. We first recall some basic notations and notions about the duality solutions and state our main results. Section 3 is devoted to the derivation of the macroscopic velocity used to define properly the product $a(\rho)\rho_\alpha$ and duality solutions. Existence and uniqueness of duality solutions are proved in Section 4, as well as its equivalence to gradient flow solutions. The convergence of the kinetic model (2.2) as $\varepsilon \to 0$ towards the aggregation model (2.6)-(2.7) is shown in Section 5. Finally, a numerical scheme that captures the synchronising and non-synchronising behaviour of the aggregate equation is studied in Section 6, as well as several numerical examples showing the synchronising and non-synchronising dynamics.

2.2 Notations and main results

2.2.1 Notations

We will make use of the following notations. Let $T > 0$, we denote

— $L^1_+(\mathbb{R})$ is the space of nonnegative functions of $L^1(\mathbb{R})$.

— $C_0(\mathbb{R})$ is the space of continuous functions that vanish at infinity.

— $\mathcal{M}_{\mathrm{loc}}(\mathbb{R})$ is the set of local Borel measures, $\mathcal{M}_{\mathrm{b}}(\mathbb{R})$ those whose total variation is finite:

$$\mathcal{M}_b(\mathbb{R}) = \{\mu \in \mathcal{M}_{\mathrm{loc}}(\mathbb{R}), |\mu|(\mathbb{R}) < +\infty\}.$$

— $\mathcal{S}_{\mathcal{M}} = C([0,T], \mathcal{M}_{\mathrm{b}}(\mathbb{R}) - \sigma(\mathcal{M}_{\mathrm{b}}(\mathbb{R}), C_0(\mathbb{R})))$ is the space of time-continuous bounded Borel measures endowed with the weak topology.

— $\mathcal{P}_2(\mathbb{R})$ is the Wasserstein space of order 2:

$$\mathcal{P}_2(\mathbb{R}) = \left\{ \mu \quad \text{nonnegative borel measures in } \mathbb{R} \quad \text{s.t } |\mu|(\mathbb{R}) = 1, \int_{\mathbb{R}} |x|^2 \mu(dx) < \infty \right\}.$$

— For $H \in C(\mathbb{R}\backslash\{0\})$, we define $\widehat{H}$:

$$\widehat{H} = \begin{cases} H(x), & \text{for } x \neq 0, \\ 0, & \text{else.} \end{cases}$$

We notice that if K satisfies (H2) and (H4), we have by taking $y = -x$ in (H4) and using (H2) that, $\forall\, x \in \mathbb{R}$, $\partial_x K(x) x \leq \lambda x^2$. We deduce that (H4) holds for $\widehat{\partial_x K}$ i.e.:

$$\forall\, x, y \in \mathbb{R}, \quad (\widehat{\partial_x K}(x) - \widehat{\partial_x K}(y))(x - y) \leq \lambda (x - y)^2. \tag{2.8}$$

We recall a compactness result on $\mathcal{M}_{\mathrm{b}}(\mathbb{R}) - \sigma(\mathcal{M}_{\mathrm{b}}(\mathbb{R}), C_0(\mathbb{R}))$. If there exists a sequence of bounded measures $\mu^n \in \mathcal{M}_{\mathrm{b}}(\mathbb{R})$ such that their total variations $|\mu^n|(\mathbb{R})$ are uniformly bounded, then there exists a subsequence of μ^n that converges weakly to μ in $\mathcal{M}_{\mathrm{b}}(\mathbb{R})$.

2.2.2 Duality solutions

For the sake of completeness, we recall the notion of duality solutions which has been introduced in [14] for one dimensional linear scalar conservation law with discontinuous coefficients. Let us then consider the linear conservation equation:

$$\partial_t \rho + \partial_x (b(t,x)\rho) = 0, \quad \text{in }]0,T[\times\mathbb{R}, \tag{2.9}$$

with $T > 0$. We assume weak regularity of the velocity field $b \in L^\infty(]0,T[\times\mathbb{R})$ and b satisfies the so-called one-sided Lipschitz (OSL) condition:

$$\partial_x b \leq \gamma(t), \gamma \in L^1(]0,T[), \quad \text{in the sense of distributions.} \tag{2.10}$$

In order to define duality solutions, we introduce the related backward problem

$$\begin{cases} \partial_t p + b\partial_x p = 0, \\ p(T,\cdot) = p^T \in Lip_{loc}(\mathbb{R}). \end{cases} \tag{2.11}$$

We define the set of exceptional solutions $\mathcal{E}$ as follows

$$\mathcal{E} := \left\{ p \in Lip_{loc}(]0,T[\times\mathbb{R}) \quad \text{solution to (2.11) with } p^T = 0 \right\}.$$

Definition 2.2.1 (*Reversible solutions* to (2.11))**.** *We say that p is a reversible solution to* (2.11) *if and only if $p \in Lip_{loc}(]0,T[\times\mathbb{R})$ satisfies* (2.11) *and is locally constant on $\mathcal{V}_e$, where $\mathcal{V}_e$ is defined by*

$$\mathcal{V}_e := \{(t,x) \in]0,T[\times\mathbb{R};\ \exists p_e \in \mathcal{E}\ p_e(t,x) \neq 0\}.$$

Definition 2.2.2 (*Duality solutions* to (2.9), see [14])**.** *We say $\rho \in \mathcal{S}_\mathcal{M}$ is a duality solution to* (??) *in $]0,T[$ if for any $0 < \tau \leq T$, and any p reversible solution to* (2.11) *compactly supported in x, the function $t \to \int_{\mathbb{R}} p(t,x)\rho(t,dx)$ is constant on $[0,\tau]$.*

The following result shows existence and weak stability for duality solutions provided that the velocity field satisfied the one-sided-Lipschitz condition.

Theorem 2.2.1 (Theorem 2.1 in [14])**.**

1. *Given $\rho^{ini} \in \mathcal{M}_b(\mathbb{R})$. Under the assumption* (2.10)*, there exists a unique $\rho \in \mathcal{S}_\mathcal{M}$, duality solution to* (2.9)*, such that $\rho(0,\cdot) = \rho^{ini}$.*
2. *There exists a bounded Borel function $\hat{b}$, called universal representative of b such that $\hat{b} = b$ a. e., and for any duality solution ρ,*

$$\partial_t \rho + \partial_x(\hat{b}\rho) = 0, \quad \text{in the distributional sense.}$$

3. *Let $(b_n)_{n\in\mathbb{N}}$ be a bounded sequence in $L^\infty(]0,T[\times\mathbb{R})$, with $b_n \rightharpoonup b$ in $L^\infty(]0,T[\times\mathbb{R}) - w*$. Assume that $\partial_x b_n \leq \gamma^n(t)$, where $(\gamma^n)_{n\in\mathbb{N}}$ is bounded in $L^1(]0,T[)$. Consider a sequence $\rho_n \in \mathcal{S}_\mathcal{M}$ of duality solutions to*

$$\partial_t \rho_n + \partial_x(b_n\rho_n) = 0, \quad \text{in }]0,T[\times\mathbb{R},$$

such that $\rho_n(0,\cdot)$ is bounded in $\mathcal{M}_b(\mathbb{R})$, and $\rho_n(0,\cdot) \rightharpoonup \rho^{ini} \in \mathcal{M}_b(\mathbb{R})$. Then $\rho_n \rightharpoonup \rho$ in $\mathcal{S}_\mathcal{M}$, where $\rho \in \mathcal{S}_\mathcal{M}$ is the duality solution to

$$\partial_t \rho + \partial_x(b\rho) = 0, \quad \text{in }]0,T[\times\mathbb{R}, \quad \rho(0,\cdot) = \rho^{ini}.$$

Moreover, $\hat{b}_n\rho_n \rightharpoonup \hat{b}\rho$ weakly in $\mathcal{M}_b(]0,T[\times\mathbb{R})$.

2.2.3 Main results

Up to a rescaling, we can assume without loss of generality that the total mass of each species is normalized to 1. Then we will work in the space of probabilities for densities.

The first theorem states the existence and uniqueness of duality solutions for system (2.1) and its equivalence with the gradient flow solution considered in [36].

Definition 2.2.3. *(Duality solutions for system* (2.1)*) We say that* $(\rho_1, \rho_2) \in C([0,T], \mathcal{M}_b(\mathbb{R})^2)$ *is a duality solution to* (2.1) *if there exists* $\hat{a}(\rho) \in L^\infty((0,T)\times\mathbb{R})$ *and* $\gamma \in L^1_{loc}([0,T])$ *satisfying* $\partial_x \hat{a} \le \gamma$ *in the sense of distributions, such that for all* $0 < t_1 < t_2 < T$,

$$\partial_t \rho_\alpha + \chi_\alpha \partial_x(\hat{a}(\rho)\rho_\alpha) = 0, \quad \text{for } \alpha = 1,2, \quad \rho = \theta_1\rho_1 + \theta_2\rho_2, \tag{2.12}$$

in the sense of duality on (t_1, t_2) *and* $\hat{a}(\rho) = \partial_x K * \rho$ *a.e. We emphasize that the final datum for* (2.12) *should be* t_2 *instead of* T.

Then, we have the following existence and uniqueness result:

Theorem 2.2.2 (Existence, uniqueness of duality solution and equivalence to gradient flow solution)**.** *Let* $T > 0$ *and* $(\rho_1^{ini}, \rho_2^{ini}) \in \mathcal{P}_2(\mathbb{R})^2$. *Under assumptions (H1)–(H4), there exists a unique duality solution* $(\rho_1, \rho_2) \in C([0,T], \mathcal{P}_2(\mathbb{R})^2)$ *to* (2.1) *in the sense of Definition 2.2.3 with* $(\rho_1, \rho_2)(t=0) = (\rho_1^{ini}, \rho_2^{ini})$ *such that*

$$\hat{a}(\rho) := \int_{\mathbb{R}} \widehat{\partial_x K}(x-y)\rho(t,dy), \quad \rho = \theta_1\rho_1 + \theta_2\rho_2. \tag{2.13}$$

This duality solution is equivalent to the gradient flow solution defined in [36].

In our second main result, we prove the convergence of the kinetic model (2.2) towards the aggregation model.

Theorem 2.2.3 (Hydrodynamical limit of the kinetic model)**.** *Assume that* $\chi_\alpha(\theta_1+\theta_2) < 1$ *for* $\alpha = 1,2$. *Let* $T > 0$ *and* $(f_\alpha^\varepsilon, S^\varepsilon)$ *be a solution to the kinetic-elliptic equation* (2.2) *such that* $f_\alpha^\varepsilon(t=0) = f_\alpha^{ini}$ *and* $f_\alpha^{ini} \in L^\infty \cap L^1_+(\mathbb{R})$ *and* $\int_{\mathbb{R}} x^2 f_\alpha^{ini} dx < \infty$.
Then, as $\varepsilon \to 0$, $(f_\alpha^\varepsilon, S^\varepsilon)$ *converges in the following sense:*

$$\rho_\alpha^\varepsilon := f_\alpha^\varepsilon(1) + f_\alpha^\varepsilon(-1) \rightharpoonup \rho_\alpha \quad \text{weakly in} \quad \mathcal{S}_M, \quad \text{for } \alpha = 1,2,$$
$$S^\varepsilon \rightharpoonup S \quad \text{in} \quad C([0,T], W^{1,\infty}(\mathbb{R})) - \text{weak},$$

where ρ_α *is the unique duality solution of* (2.6) *and* $S = K * (\theta_1\rho_1 + \theta_2\rho_2)$ *given in Theorem 2.2.2.*

The condition $\chi_\alpha(\theta_1+\theta_2) < 1$ in the previous theorem is needed to guarantee that the tumbling kernel $T_\alpha[S]$ defined in (2.3) is positive.

To conclude this Section on the main results, we emphasize that, a finite volume scheme to simulate (2.12) is proposed in Section 6 and its convergence towards duality solutions is stated in Theorem 2.6.3.

2.3 Macroscopic velocity

In this section, we find the representative $\hat{a}$ of a for which existence and uniqueness of duality solutions hold. To this end, we consider the similar system of transport equations to (2.1) associated to the velocity a^n which converges to a. Next, the limit of the product $a^n(\rho_\alpha^n)\rho_\beta^n$ for $\alpha, \beta = 1,2$ is computed.

2.3.1 Regularisation

We build a sequence $(a^n)_{n\in\mathbb{N}}$ which converges to a by considering the sequence of regularised kernels $\partial_x K^n$ approaching $\partial_x K$.

Lemma 2.3.1. *Let $(\partial_x K^n)_{n\in\mathbb{N}}$ be the sequence of regular kernels defined by*

$$\partial_x K^n(x) = \begin{cases} \partial_x K(x), & \text{for } |x| > \dfrac{1}{n}, \\ n\partial_x K\left(\dfrac{1}{n}\right) x, & \text{else.} \end{cases}$$

Then

$$\partial_x K^n \in C^0(\mathbb{R}), \quad \forall x \in \mathbb{R}, \quad \partial_x K^n(-x) = -\partial_x K^n(x),$$

and

$$\|\partial_x K^n\|_\infty \leq \|\partial_x K\|_\infty, \quad \partial_{xx} K^n \leq \lambda \quad \text{in the distributional sense.}$$

Proof. From (H1), $\partial_x K \in C^0(\mathbb{R}\backslash\{0\})$ and since $\partial_x K^n$ is continuous at $\pm\frac{1}{n}$, we conclude that $\partial_x K^n \in C^0(\mathbb{R})$. From (H2), we deduce that $\partial_x K$ is an odd function. Using the definition of $\partial_x K^n$ and (H3), we get that $\|\partial_x K^n\|_\infty \leq \|\partial_x K\|_\infty$. From the construction of $\partial_x K^n$, we have that $\partial_x K^n = \partial_x K$ outside the interval $[-\frac{1}{n}, \frac{1}{n}]$ and from (H4) one sees $\partial_{xx} K^n \leq \lambda$ in $\mathbb{R}\backslash(-\frac{1}{n}, \frac{1}{n})$ in the sense of distributions. In addition, if we take $x = -\frac{1}{n}$ and $y = \frac{1}{n}$ in (H4), we have that

$$n\partial_x K\left(\frac{1}{n}\right) \leq \lambda.$$

Since $\partial_{xx} K^n = n\partial_x K\left(\frac{1}{n}\right)$ in $[-\frac{1}{n}, \frac{1}{n}]$, we conclude that $\partial_{xx} K^n \leq \lambda$ in $[-\frac{1}{n}, \frac{1}{n}]$ in the sense of distributions. Finally, we obtain that $\partial_{xx} K^n \leq \lambda$ in the sense of distributions. □

In the rest of the paper, the notation $\partial_x K^n$ will refer to the regularised kernels of Lemma 2.3.1. Given $\partial_x K^n$, the velocity a^n is defined similarly to (2.13) as

$$\forall \rho \in \mathcal{S}_\mathcal{M}, \quad a^n(\rho) := \int_{\mathbb{R}} \partial_x K^n(x-y)\rho(t,dy). \tag{2.14}$$

In the following lemma, we show that if ρ_α^n and ρ_β^n admit weak limits ρ_α and ρ_β respectively in $\mathcal{S}_\mathcal{M}$, then the limit of the product $a^n(\rho_\alpha^n)\rho_\beta^n$ is $\hat{a}(\rho_\alpha)\rho_\beta$. Contrary to [111] where the two-dimensional case is considered, this limiting measure does not charge the diagonal.

Lemma 2.3.2. *For $\alpha = 1, 2$, let $\{\rho_\alpha^n\} \in \mathcal{S}_\mathcal{M}$ be a sequence such that $\forall n \in \mathbb{N}, \forall t \in [0,T], |\rho_\alpha^n|(t,\mathbb{R}) = M_\alpha$. Suppose that there exists ρ_α in $\mathcal{S}_\mathcal{M}$ such that*

$$\rho_\alpha^n \rightharpoonup \rho_\alpha \quad \text{weakly in } \mathcal{S}_\mathcal{M},$$

Then, we have

$$a^n(\rho_\alpha^n)\rho_\beta^n \rightharpoonup \hat{a}(\rho_\alpha)\rho_\beta \quad \text{weakly in } \mathcal{M}_b([0,T]\times\mathbb{R}), \quad \alpha, \beta = 1, 2,$$

where $a^n(\cdot)$ and $\hat{a}(\cdot)$ are defined in (2.13),(2.14) respectively. That is for $\phi \in C_0([0,T]\times\mathbb{R})$,

$$\int_0^T \int_{\mathbb{R}^2} \partial_x K^n(x-y)\rho_\alpha^n(t,dx)\rho_\beta^n(t,dy)\phi(t,x)dt \to \int_0^T \int_{\mathbb{R}^2} \widehat{\partial_x K}(x-y)\rho_\alpha(t,dx)\rho_\beta(t,dy)\phi(t,x)dt.$$

Proof. Before starting the proof of the lemma, we first introduce some notations which simplify the computations

$$\begin{aligned} &\mu^n(t,dx,dy) := \rho_\alpha^n(t,dx) \otimes \rho_\beta^n(t,dy), \quad E_n := \left\{(x,y) \in \mathbb{R}^2, x \neq y, |x-y| \leq \frac{1}{n}\right\}, \\ &\mu(t,dx,dy) := \rho_\alpha(t,dx) \otimes \rho_\beta(t,dy). \end{aligned} \tag{2.15}$$

For $\phi \in C_0([0,T]\times\mathbb{R})$, we denote

$$A_n(t) := \int_{\mathbb{R}^2} \partial_x K^n(x-y)\mu^n(t,dx,dy)\phi(t,x) - \int_{\mathbb{R}^2} \widehat{\partial_x K}(x-y)\mu(t,dx,dy)\phi(t,x),$$

Step 1: Convergence almost everywhere in time of $A_n(t)$.

Since $\partial_x K^n(0) = 0$, we have

$$\begin{aligned} A_n(t) &= \int_{\mathbb{R}^2} \widehat{\partial_x K^n}(x-y)\mu^n(t,dx,dy)\phi(t,x) - \int_{\mathbb{R}^2} \widehat{\partial_x K}(x-y)\mu(t,dx,dy)\phi(t,x), \\ &= \mathrm{I}_n(t) + \mathrm{II}_n(t), \end{aligned}$$

where $\mathrm{I}_n(t)$ and $\mathrm{II}_n(t)$ are defined by

$$\begin{aligned} \mathrm{I}_n(t) &:= \int_{\mathbb{R}^2} \left(\widehat{\partial_x K^n}(x-y) - \widehat{\partial_x K}(x-y)\right) \mu^n(t,dx,dy)\phi(t,x), \\ \mathrm{II}_n(t) &:= \int_{\mathbb{R}^2} \widehat{\partial_x K}(x-y)\left(\mu^n(t,dx,dy) - \mu(t,dx,dy)\right)\phi(t,x). \end{aligned}$$

From the definition of $\partial_x K^n$ in Lemma 2.3.1, it follows that

$$\mathrm{I}_n(t) = \int_{E_n} \left(\partial_x K^n(x-y) - \partial_x K(x-y)\right)\mu^n(t,dx,dy)\phi(t,x).$$

The estimate on $\|\partial_x K^n\|_{L^\infty}$ in Lemma 2.3.1 and (H3) imply that

$$|\mathrm{I}_n(t)| \leq 2\|\phi\|_{L^\infty}\|\partial_x K\|_{L^\infty}\mu^n(t,E_n),$$

with μ^n and E_n defined in (2.15).
Let $\varepsilon > 0$. Since the set E_n converges to the empty set, there exists $N \in \mathbb{N}$ such that $\forall n \geq N$,

$$\mu(t,E_n) \leq \varepsilon. \tag{2.16}$$

For all $n \geq N$, we observe that $E_n \subset E_N$, we have

$$\mu^n(t,E_n) \leq \mu^n(t,E_N) \leq (\mu^n - \mu)(t,E_N) + \mu(t,E_N). \tag{2.17}$$

From the weak convergence of ρ^n_α, $\alpha = 1,2$, we note that the sequence $\mu^n(t,\cdot)$ converges weakly to $\mu(t,\cdot)$. Since the total variation of $\mu^n(t,\cdot)$ is constant in n, the tight convergence is achieved. Then, there exists N' such that $\forall n \geq N' \geq N$

$$|\mu^n - \mu|\,(t,E_N) \leq \varepsilon.$$

From (2.17) and (2.16), we conclude that $\forall n \geq N' \geq N$,

$$\mu^n(t,E_n) \leq 2\varepsilon.$$

Hence, for all $n \geq N'$, we get

$$|\mathrm{I}_n(t)| \leq 2\|\phi\|_{L^\infty}\|\partial_x K\|_{L^\infty}\mu^n(t,E_n) \leq 4\|\phi\|_{L^\infty}\|\partial_x K\|_{L^\infty}\ \varepsilon. \tag{2.18}$$

We deduce that $\mathrm{I}_n(t) \longrightarrow 0$.

Next, we show that $\mathrm{II}_n(t)$ tends to zero.

$$\begin{aligned} \mathrm{II}_n(t) &= \int_{\mathbb{R}^2} (\widehat{\partial_x K}(x-y) - \widehat{\partial_x K^R}(x-y))\phi(t,x)(\mu^n(t,dx,dy) - \mu^n(t,dx,dy)) \\ &+ \int_{\mathbb{R}^2} \widehat{\partial_x K^R}(x-y)\phi(t,x)(\mu^n(t,dx,dy) - \mu(t,dx,dy)), \\ &:= \mathrm{II}^1_n(t) + \mathrm{II}^2_n(t), \end{aligned}$$

where R is an integer which will be fixed later. From the construction of $\partial_x K^R$ in Lemma 2.3.1, we get

$$\mathrm{II}^1_n = \int_{E_R} (\partial_x K(x-y) - \partial_x K^R(x-y))\phi(t,x)(\mu^n(t,dx,dy) - \mu(t,dx,dy)).$$

Therefore, one has

$$\left|\mathrm{II}_n^1(t)\right| \leq 2\|\partial_x K\|_{L^\infty}\|\phi\|_{L^\infty}\left(\mu^n(t,E_R)+\mu(t,E_R)\right).$$

Let $\varepsilon>0$. Using (2.17), by the same token as previously, there exists N such that for all $n\geq N$,

$$\mu^n(t,E_N)\leq 2\varepsilon, \quad \mu(t,E_n)\leq\varepsilon,$$

Setting $R=N$, we conclude that for all $n\geq N$,

$$\left|\mathrm{II}_n^1(t)\right| \leq 6\varepsilon\|\partial_x K\|_{L^\infty}\|\phi\|_{L^\infty}.$$

For $\mathrm{II}_n^2(t)$, we notice that $\partial_x K^N(x-y)\phi(t,x)$ is a continuous function that vanishes on the diagonal (x,x) and we have

$$\int_{\mathbb{R}^2}\widehat{\partial_x K^N}(x-y)\phi(t,x)(\mu^n-\mu)(t,dx,dy)=\int_{\mathbb{R}^2}\partial_x K^N(x-y)\phi(t,x)(\mu^n-\mu)(t,dx,dy).$$

The tight convergence of μ^n to μ implies that there exists $N''>0$ such that for all $n\geq N''$

$$\left|\int_{\mathbb{R}^2}\widehat{\partial_x K^M}(x-y)\phi(t,x)(\mu^n-\mu)(t,dx,dy)\right|\leq\varepsilon.$$

Therefore for all $n\geq\max\{N',N''\}$, one has

$$|\mathrm{II}_n(t)|\leq\varepsilon(1+6\|\partial_x K\|_{L^\infty}\|\phi\|_{L^\infty}). \tag{2.19}$$

This implies that $\mathrm{II}_n(t)$ converges to 0.
Combining (2.18) and (2.19), we deduce that for almost every $t\in[0,T]$, A_n converges to 0.

Step 2: Lebesgue's dominated convergence theorem

For all $t\in[0,T]$, we have that

$$|A_n(t)|\leq 2\|\phi\|_{L^\infty}\|\partial_x K\|_{L^\infty}M_\alpha M_\beta.$$

Since A_n converges almost everywhere to 0, $\int_0^T A_n(t)dt$ converges to zero from Lebesgue's dominated convergence theorem. □

2.3.2 OSL condition on the macrosocopic velocity

Proposition 2.3.3. *Let T,M be positive constants and $\rho\in\mathcal{S}_{\mathcal{M}}$ be a positive measure such that $\forall t\in[0,T], |\rho|(t,\mathbb{R})=M$. Let K be such that assumption (H4) hold. Let $\hat{a}(\rho)$ and $a^n(\rho)$ be defined in* (2.13) *and* (2.14) *respectively. Then, there exists $\kappa\in L^1([0,T])$ such that*

$$\partial_x\hat{a}(t,x)\leq\kappa(t), \quad \partial_x a^n(t,x)\leq\kappa(t), \quad \textit{in the sense of distributions.}$$

Proof. For $x,y\in\mathbb{R}$, we compute:

$$(\hat{a}(\rho)(t,x)-\hat{a}(\rho)(t,y))(x-y) = \int_{\mathbb{R}}(\widehat{\partial_x K}(x-z)-\widehat{\partial_x K}(y-z))(x-y)\rho(t,dz).$$

Using the λ-concavity of K, we deduce from (2.8)

$$(\hat{a}(\rho)(t,x)-\hat{a}(\rho)(t,y))(x-y)\leq\lambda(x-y)^2\int_{\mathbb{R}}\rho(t,dz)\leq\lambda M(x-y)^2.$$

Since K^n is also λ concave from the proof of Lemma 2.3.1, we get the one-sided Lipschitz estimate on a^n by the same token as for a. □

2.4 Existence and uniqueness of duality solutions

2.4.1 Proof of the existence of duality solutions in Theorem 2.2.2

The proof is divided into several steps. First, we construct an approximate problem for which the existence of duality solutions holds. Then, we pass to the limit in the approximate problem to get the existence of duality solutions thanks to the weak stability of duality solutions stated in Theorem 2.2.1 and recover Equation (2.12) from Lemma 2.3.2. Finally, we recover the bound on the second order moment.

Step 1: Existence of duality solutions for the approximate problem

The macroscopic velocity a is replaced by an approximation a^n defined in (2.14) and the following system is considered:

$$\partial_t \rho_\alpha^n + \chi_\alpha \partial_x \left(a^n(\theta_1\rho_1^n + \theta_2\rho_2^n)\rho_\alpha^n\right) = 0, \quad \text{for } \alpha = 1, 2. \tag{2.20}$$

Since $\partial_x K^n$ is not Lipschitz continuous, we first consider $\partial_x K^{n,m}$ an approximation of $\partial_x K^n$ obtained by a convolution with a molifier. The solution $\rho_\alpha^{n,m}$ to the following equation is investigated.

$$\partial_t \rho_\alpha^{n,m} + \chi_\alpha \partial_x \left(a^{n,m}(\theta_1\rho_1^{n,m} + \theta_2\rho_2^{n,m})\rho_\alpha^{n,m}\right) = 0, \quad \text{for } \alpha = 1, 2, \tag{2.21}$$

where $a^{n,m}$ is given by

$$a^{n,m}(\rho) := \int_{\mathbb{R}} \partial_x K^{n,m}(x-y)\rho(t,dy).$$

Applying Theorem 1.1 in [35] gives the existence of solutions $\rho_\alpha^{n,m}$ in $L^\infty([0,T], \mathcal{M}_b(\mathbb{R}))$ and $|\rho_\alpha^{n,m}|(t,\mathbb{R}) = \left|\rho_\alpha^{ini}\right|(\mathbb{R}) = 1$. Since the velocity field $a^{n,m}$ is Lipschitz, $\rho_\alpha^{n,m}$ is a duality solution. In addition, for $\phi \in C_c^\infty(\mathbb{R})$ we have for $\alpha = 1, 2$ the following estimate:

$$\frac{d}{dt}\left(\int_{\mathbb{R}} \rho_\alpha^{n,m}(t,dx)\phi(x)\right) = \int_{\mathbb{R}^2} \partial_x K^{n,m}(x-y)(\theta_1\rho_1^{n,m}(t,dy) + \theta_2\rho_2^{n,m}(t,dy))\rho_\alpha^{n,m}(t,dx)\partial_x\phi(x).$$

Then,

$$\left|\frac{d}{dt}\left(\int_{\mathbb{R}} \rho_\alpha^{n,m}(t,dx)\phi(x)\right)\right| \leq \|\partial_x\phi\|_{L^\infty}\|\partial_x K\|_{L^\infty}(\theta_1+\theta_2). \tag{2.22}$$

Using (2.22) and the density of $C_c^\infty(\mathbb{R})$ in $C_0(\mathbb{R})$, we deduce that $\rho_\alpha^{n,m} \in \mathcal{S}_\mathcal{M}$. Moreover, the equicontinuity of $\rho_\alpha^{n,m}$ in $\mathcal{S}_\mathcal{M}$ follows from (2.22) and the density of $C_c^\infty(\mathbb{R})$ in $C_0(\mathbb{R})$. Since $|\rho_\alpha^{n,m}|(t,\mathbb{R}) = \left|\rho_\alpha^{ini}\right|(\mathbb{R}) = 1$, Ascoli Theorem gives the existence of a subsequence in m of $\rho_\alpha^{n,m}$ which converges to a limit named ρ_α^n in $\mathcal{S}_\mathcal{M}$. We pass to the limit when m tends to infinity in Equation (2.21) and obtain that ρ_α^n satisfies (2.20).

Step 2 : Extraction of a convergent subsequence of ρ_α^n and existence of duality solutions.

As above, there exists a subsequence of ρ_α^n in $\mathcal{S}_\mathcal{M}$ such that

$$\rho_\alpha^n \rightharpoonup \rho_\alpha \quad \text{weakly in } \mathcal{S}_\mathcal{M}, \quad \text{for } \alpha = 1, 2.$$

Let us find the equation satisfied by ρ_α in the distributional sense. Let ϕ be in $C_c^\infty([0,T]\times\mathbb{R})$. Since ρ_α^n satisfies (2.20) in the distributional sense, we have

$$\int_0^T \int_{\mathbb{R}} \partial_t\phi(t,x)\rho_\alpha^n(t,dx)dt + \chi_\alpha \int_0^T \int_{\mathbb{R}} a^n(\theta_1\rho_1^n + \theta_2\rho_2^n)\rho_\alpha^n(t,dx)\phi(t,x)dt = 0.$$

Using Lemma 2.3.2, we can pass to the limit in the latter equation and obtain,

$$\int_0^T \int_{\mathbb{R}} \partial_t\phi(t,x)\rho_\alpha(t,dx)dt + \chi_\alpha \int_0^T \int_{\mathbb{R}} \hat{a}(\theta_1\rho_1 + \theta_2\rho_2)\rho_\alpha(t,dx)\phi(t,x)dt = 0.$$

Thus ρ_α satisfies (2.12) in the sense of distributions. From Proposition 2.3.3, the macroscopic velocity $a^n(\rho^n)$ satisfies an uniform OSL condition. Then, by weak stability of duality solutions in (see Theorem 2.2.1 (3)), we deduce that

$$\partial_t \rho_\alpha + \chi_\alpha \partial_x(\hat{a}(\rho)\rho_\alpha) = 0, \quad \text{for } \alpha = 1,2, \quad \text{in the sense of duality in }]0,T[\times\mathbb{R}.$$

Step 3 : Finite second order moment.

From Equation (2.12), we deduce that the first and second moments satisfy in the sense of distributions

$$\frac{d}{dt}\left(\int |x|\,\rho_\alpha(t,dx)\right) = -\int \mathrm{sgn}(x)\hat{a}(\rho)\rho_\alpha(t,dx),$$
$$\frac{d}{dt}\left(\int |x|^2\,\rho_\alpha(t,dx)\right) = -2\int \hat{a}(\rho)\rho_\alpha(t,dx), \quad \text{for } \alpha = 1,2.$$

Since $\rho_\alpha^{ini} \in \mathcal{P}_2(\mathbb{R})$ and $\hat{a}(\rho)$ is bounded from ((H2)), we deduce that the first two moments of ρ_α are finite, then $\rho_\alpha(t) \in \mathcal{P}_2(\mathbb{R})$ for $t > 0$. □

Remark 2.4.1. *If we define the weighted center of mass of the system x_c as follows:*

$$x_c(t) := \frac{\theta_1}{\chi_1}\int_{\mathbb{R}} x\rho_1(t,dx) + \frac{\theta_2}{\chi_2}\int_{\mathbb{R}} x\rho_2(t,dx).$$

We remark from straightforward computation that $\frac{d}{dt}x_c = 0$. Then the weighted center of mass is conserved for this system.

2.4.2 Proof of the uniqueness of duality solutions in Theorem 2.2.2

Uniqueness relies on a stability estimate in Wasserstein distance, which is the metric endowed in $\mathcal{P}_2(\mathbb{R})$. This Wasserstein distance d_W is defined by (see e.g. [127, 128])

$$d_W(\nu,\mu) = \inf_{\gamma\in\Gamma(\nu,\mu)}\left\{\int_{\mathbb{R}^2} |y-x|^2\,\gamma(dx,dy)\right\}^{1/2},$$

where $\Gamma(\mu,\nu)$ is the set of measures on $\mathbb{R}^2\times\mathbb{R}^2$ with marginals μ and ν, i.e.,

$$\Gamma(\nu,\mu) = \Big\{\gamma\in\mathcal{P}_2(\mathbb{R}\times\mathbb{R}), \forall\xi\in C_0(\mathbb{R}\times\mathbb{R}), \int_{\mathbb{R}^2}\xi(y_0)\gamma(dy_0,dy_1) = \int_{\mathbb{R}}\xi(y_0)\mu(dy_0),$$
$$\int_{\mathbb{R}^2}\xi(y_1)\gamma(dy_0,dy_1) = \int_{\mathbb{R}}\xi(y_1)\nu(dy_1)\Big\}.$$

The Wasserstein distance d_W takes a more pratical form in the one-dimensional setting. Indeed, in one space dimension, we have (see e.g [112, 127])

$$d_W(\nu,\mu)^2 = \int_0^1 \left|F_\nu^{-1}(z) - F_\mu^{-1}(z)\right|^2 dz,$$

where F_ν^{-1} and F_μ^{-1} are the generalised inverse of cumulative distributions of ν and μ, defined by

$$F_\nu^{-1}(z) = \inf\Big\{x\in\mathbb{R}, \nu((-\infty,x)) > z\Big\}, \quad F_\mu^{-1}(z) = \inf\Big\{x\in\mathbb{R}, \mu((-\infty,x)) > z\Big\}.$$

This Wasserstein distance can be extended to the product space $\mathcal{P}_2(\mathbb{R})\times\mathcal{P}_2(\mathbb{R})$. In the case at hand, we define $W_2(\nu,\mu)$ by

$$W_2(\nu,\mu)^2 = \int_0^1 \left|F_{\nu_1}^{-1}(z) - F_{\mu_1}^{-1}(z)\right|^2 dz + \frac{\chi_1\theta_2}{\chi_2\theta_1}\int_0^1 \left|F_{\nu_2}^{-1}(z) - F_{\mu_2}^{-1}(z)\right|^2 dz, \tag{2.23}$$

where $\nu = \begin{pmatrix}\nu_1\\ \nu_2\end{pmatrix}, \mu = \begin{pmatrix}\mu_1\\ \mu_2\end{pmatrix} \in \mathcal{P}_2(\mathbb{R}) \times \mathcal{P}_2(\mathbb{R})$ and $F^{-1}_{\nu_\alpha}$, $F^{-1}_{\mu_\alpha}$ are the generalised inverse of cumulative distributions of ν_α and μ_α for $\alpha = 1, 2$, respectively. Using W_2 we prove a contraction inequality between duality solutions of (2.1).

Proposition 2.4.2. *Let* $\mu^{ini} = \begin{pmatrix}\mu_1^{ini}\\ \mu_2^{ini}\end{pmatrix}$ *and* $\nu^{ini} = \begin{pmatrix}\nu_1^{ini}\\ \nu_2^{ini}\end{pmatrix}$ *be in* $\mathcal{P}_2(\mathbb{R})^2$. *We define* $\mu = \begin{pmatrix}\mu_1\\ \mu_2\end{pmatrix}$ *and* $\nu = \begin{pmatrix}\nu_1\\ \nu_2\end{pmatrix}$ *duality solutions of* (2.1) *with respectively the initial data* μ^{ini}, ν^{ini}.
Then $W_2(\mu, \nu)$ *defined in* (2.23) *is bounded and satisfies the estimate:*

$$W_2(\mu, \nu) \leq W_2(\mu^{ini}, \nu^{ini}) \exp\left(2\lambda(\chi_1 + \chi_2)(\theta_1 + \theta_2)t\right).$$

Proof. Since $(\mu, \nu) \in \mathcal{P}_2(\mathbb{R})^2 \times \mathcal{P}_2(\mathbb{R})^2$, $W_2(\mu, \nu)$ is bounded. For the sake of clarity in the proof, we denote

$$F^{-1}_\alpha := F^{-1}_{\nu_\alpha}, \quad G^{-1}_\alpha := F^{-1}_{\mu_\alpha}, \quad \text{for } \alpha = 1, 2.$$

We also omit the argument t in notations $F^{-1}_\alpha(t, x)$ and $G^{-1}_\alpha(t, x)$. Computing the derivative of $W_2(\mu, \nu)^2$ with respect to time,

$$\begin{aligned}\partial_t W_2(\mu, \nu)^2 = 2 \int_0^1 \big(F_1^{-1}(x) - G_1^{-1}(x)\big)\big(\partial_t F_1^{-1}(x) - \partial_t G_1^{-1}(x)\big)dx \\ + 2\frac{\chi_1\theta_2}{\chi_2\theta_1} \int_0^1 \big(F_2^{-1}(x) - G_2^{-1}(x)\big)\big(\partial_t F_2^{-1}(x) - \partial_t G_2^{-1}(x)\big)dx.\end{aligned}$$

Straightforward and standard computations give that

$$\partial_t F^{-1}_\alpha(x) = \chi_\alpha \hat{a}(t, F^{-1}_\alpha(x)), \quad \partial_t G^{-1}_\alpha = \chi_\alpha \hat{a}(t, G^{-1}_\alpha(x)), \quad \text{for } \alpha = 1, 2.$$

From the definition of $\hat{a}$ in (2.13), we get

$$\partial_t F_1^{-1}(x) = \chi_1\theta_1 \int_0^1 \widehat{\partial_x K}(F_1^{-1}(x) - z)\mu_1(t, dz) + \chi_1\theta_2 \int_0^1 \widehat{\partial_x K}(F_1^{-1}(x) - z)\mu_2(t, dz).$$

Setting $z = F_1^{-1}(y)$ in the first integral and $z = F_2^{-1}(y)$ in the second one yields

$$\partial_t F_1^{-1}(x) = \chi_1\theta_1 \int_0^1 \widehat{\partial_x K}(F_1^{-1}(x) - F_1^{-1}(y))dy + \chi_1\theta_2 \int_0^1 \widehat{\partial_x K}(F_1^{-1}(x) - F_2^{-1}(y))dy.$$

Similarly, we get

$$\partial_t G_1^{-1}(x) = \chi_1\theta_1 \int_0^1 \widehat{\partial_x K}(G_1^{-1}(x) - G_1^{-1}(y))dy + \chi_1\theta_2 \int_0^1 \widehat{\partial_x K}(G_1^{-1}(x) - G_2^{-1}(y))dy.$$

Using the oddness of $\partial_x K$, we can symmetrise the terms in the right-hand side of $\partial_t F_1^{-1}$, $\partial_t G_1^{-1}$. One gets

$$\begin{aligned}\int_0^1 \big(F_1^{-1}(x) - G_1^{-1}(x)\big)\big(\partial_t F_1^{-1}(x) - \partial_t G_1^{-1}(x)\big)dx = \\ \frac{1}{2}\chi_1\theta_1 \int_0^1 \int_0^1 \Big(\widehat{\partial_x K}(F_1^{-1}(x) - F_1^{-1}(y)) - \widehat{\partial_x K}(G_1^{-1}(x) - G_1^{-1}(y))\Big) \times \\ \big(F_1^{-1}(x) - G_1^{-1}(x) - \big(F_1^{-1}(y) - G_1^{-1}(y)\big)\big)\, dx\, dy \\ + \chi_1\theta_2 \int_0^1 \int_0^1 \Big(\widehat{\partial_x K}(F_1^{-1}(x) - F_2^{-1}(y)) - \widehat{\partial_x K}(G_1^{-1}(x) - G_2^{-1}(y))\Big)\big(F_1^{-1}(x) - G_1^{-1}(x)\big)dy\, dx.\end{aligned}$$

Similar computations can be carried out for $\int_0^1 \big(F_2^{-1}(t,x)-G_2^{-1}(t,x)\big)\big(\partial_t F_2^{-1}(t,x)-\partial_t G_2^{-1}(t,x)\big)$. Finally, $\partial_t W_2(\nu,\mu)^2$ reads

$$\begin{aligned}\partial_t W_2(\nu,\mu)^2 &= \chi_1\theta_1\int_0^1\int_0^1 \Big(\widehat{\partial_x K}(F_1^{-1}(x)-F_1^{-1}(y))-\widehat{\partial_x K}(G_1^{-1}(x)-G_1^{-1}(y))\Big)\times\\ &\quad \big(F_1^{-1}(x)-G_1^{-1}(x)-\big(F_1^{-1}(y)-G_1^{-1}(y)\big)\big)\,dx\,dy\\ &\quad +\frac{\chi_1\theta_2^2}{\theta_1}\int_0^1\int_0^1 \Big(\widehat{\partial_x K}(F_2^{-1}(x)-F_2^{-1}(y))-\widehat{\partial_x K}(G_2^{-1}(x)-G_2^{-1}(y))\Big)\times\\ &\quad \big(F_2^{-1}(x)-G_2^{-1}(x)-\big(F_2^{-1}(y)-G_2^{-1}(y)\big)\big)\,dx\,dy\\ &\quad +2\chi_1\theta_2\int_0^1\int_0^1 \Big(\widehat{\partial_x K}(F_1^{-1}(x)-F_2^{-1}(y))-\widehat{\partial_x K}(G_1^{-1}(x)-G_2^{-1}(y))\Big)\times\\ &\quad \big(F_1^{-1}(x)-F_2^{-1}(y)-\big(G_1^{-1}(x)-G_2^{-1}(y)\big)\big)\,dx\,dy.\end{aligned} \tag{2.24}$$

Applying inequality (2.8) to (2.24) and using Young's inequality yields

$$\partial_t W_2(\nu,\mu)^2 \le 4\chi_1\lambda\times\left((\theta_1+\theta_2)\int_0^1 (F_1^{-1}(x)-G_1^{-1}(x))^2dx+(\theta_2+\frac{\theta_2^2}{\theta_1})\int_0^1 (F_2^{-1}(x)-G_2^{-1}(x))^2dx\right).$$

By definition of W_2 (2.23), we conclude

$$\partial_t W_2(\nu,\mu)^2 \le 4\lambda(\chi_1+\chi_2)(\theta_1+\theta_2)W_2(\nu,\mu)^2.$$

Then the result follows from Gronwall's Lemma. □

Proof of uniqueness. From Proposition 2.4.2, it is clear that if $\mu^{ini}=\nu^{ini}$, then $\mu=\nu$. We deduce uniqueness of duality solution in Theorem 2.2.2.

2.4.3 Equivalence with gradient flow

We recall that $\mu\in AC^2([0,T],\mathcal{P}_2(\mathbb{R})\times\mathcal{P}_2(\mathbb{R}))$ if μ is locally Hölder continuous of exponent $1/2$ with respect to the Wasserstein distance W_2 in $\mathcal{P}_2(\mathbb{R})\times\mathcal{P}_2(\mathbb{R})$.

Proposition 2.4.3. *Let assumptions of Theorem 2.2.2 hold. Given* $\rho^{ini}=\begin{pmatrix}\rho_1^{ini}\\ \rho_2^{ini}\end{pmatrix}\in\mathcal{P}_2(\mathbb{R})\times\mathcal{P}_2(\mathbb{R})$. *Let* $\rho=\begin{pmatrix}\rho_1\\ \rho_2\end{pmatrix}$ *and* $\widetilde{\rho}=\begin{pmatrix}\widetilde{\rho}_1\\ \widetilde{\rho}_2\end{pmatrix}$ *be respectively the duality and gradient flow solution. Then, we have* $\rho\in AC^2([0,T],\mathcal{P}_2(\mathbb{R})\times\mathcal{P}_2(\mathbb{R}))$ *and* $\rho=\widetilde{\rho}$.

Proof. We have that $\begin{pmatrix}\hat{a}(\rho)\\ \hat{a}(\rho)\end{pmatrix}\in L^1([0,T],L^2(\rho_1\otimes\rho_2,\mathbb{R}^2))$. This comes from the fact that $\partial_x K$ is bounded and

$$\left|\int_{\mathbb{R}}\widehat{\partial_x K}(x-y)(\theta_1\rho_1(t,dy)+\theta_2\rho_2(t,dy))\right|\le\|\partial_x K\|_{L^\infty}(\theta_1+\theta_2).$$

From Theorem 8.3.1 in [5], we deduce that $\rho\in AC^2([0,T],\mathcal{P}_2(\mathbb{R})\times\mathcal{P}_2(\mathbb{R}))$. Since ρ satisfies (2.12) in the distributional sense, we deduce by uniqueness of such solution that $\widetilde{\rho}$ is a gradient flow solution.

Conversely, we suppose that $\widetilde{\rho}$ is a gradient flow solution, we have that $\rho\in C([0,T],\mathcal{P}_2(\mathbb{R})\times\mathcal{P}_2(\mathbb{R}))$ and ρ verifies (2.12)–(2.13). By uniqueness of the solution in Theorem 2.2.2, we deduce that $\rho=\widetilde{\rho}$. □

2.5 Convergence for the kinetic model

The convergence of the kinetic model (2.2) towards the aggregation model is analysed in this section.

Proof of Theorem 2.2.3. From the assumption $\chi^\alpha(\theta_1+\theta_2)<1$ for $\alpha=1,2$, we obtain that $T_\alpha[S]$ defined in (2.3) is positive. Since $T_\alpha[S]$ is a bounded and Lipschitz continuous function, we get the global in time existence of solutions to (2.2) and we have that $f_\alpha^\varepsilon \in C([0,T],L^\infty\cap L_1^+(\mathbb{R}))$ and $\int x^2 f_\alpha^\varepsilon dx<\infty$.
To prove the convergence result stated in Theorem 2.2.3, we consider the zeroth and first order moments of the distribution $f_\alpha^\varepsilon(x,v,t)$ introduced previously.

$$\rho_\alpha^\varepsilon := f_\alpha^\varepsilon(1)+f_\alpha^\varepsilon(-1), \quad J_\alpha^\varepsilon := (f_\alpha^\varepsilon(1)-f_\alpha^\varepsilon(-1)), \quad \text{for } \alpha=1,2.$$

From (2.2), these moments satisfy the following equations

$$\begin{aligned} &\partial_t\rho_\alpha^\varepsilon+\partial_x J_\alpha^\varepsilon=0,\\ &\partial_t J_\alpha^\varepsilon+\partial_x\rho_\alpha^\varepsilon=\frac{2}{\varepsilon}(\chi_\alpha\partial_x S^\varepsilon\rho_\alpha^\varepsilon-J_\alpha^\varepsilon), \quad \text{for } \alpha=1,2. \end{aligned} \tag{2.25}$$

From the first equation of (2.25), we deduce that $\forall t\in[0,T]$, $|\rho_\alpha^\varepsilon|(t,\mathbb{R})=\left|\rho_\alpha^{ini}\right|(\mathbb{R})$. Therefore, for all $t\in[0,T]$ the sequence $(\rho_\alpha^\varepsilon(t,\cdot))_\varepsilon$ is relatively compact in $\mathcal{M}_b(\mathbb{R})-\sigma(\mathcal{M}_b(\mathbb{R}),C_0^0(\mathbb{R}))$. Since J_α^ε is uniformly bounded in $C^0([0,T],L^1(\mathbb{R}))$, using the same token as in the proof of the existence, there exists $\rho_\alpha\in\mathcal{S}_\mathcal{M}$ such that

$$\rho_\alpha^\varepsilon \rightharpoonup \rho_\alpha \quad \text{weakly in } \mathcal{S}_\mathcal{M}, \quad \text{for } \alpha=1,2.$$

From the second equation of (2.25), we have

$$\begin{aligned} J_\alpha^\varepsilon &= \chi_\alpha\partial_x S^\varepsilon\rho_\alpha^\varepsilon-\frac{\varepsilon}{2}\left(\partial_t J_\alpha^\varepsilon+\partial_x\rho_\alpha^\varepsilon\right), \quad \text{in the distributional sense}\\ &:= A^\varepsilon+R^\varepsilon. \end{aligned}$$

We have that R^ε converges weakly to zero in the sense of distributions. From Lemma 2.3.2, one obtains

$$\int_0^T\int_{\mathbb{R}}\hat{a}(\theta_1\rho_1^\varepsilon+\theta_2\rho_2^\varepsilon)\phi(t,x)\rho_\alpha^\varepsilon(t,dx)dt\to\int_0^T\int_{\mathbb{R}}\hat{a}(\theta_1\rho_1+\theta_2\rho_2)\phi(t,x)\rho_\alpha(t,dx)dt.$$

We conclude that

$$J_\alpha^\varepsilon\rightharpoonup\chi_\alpha\hat{a}(\theta_1\rho_1+\theta_2\rho_2)\rho_\alpha \quad \text{in the sense of distributions.}$$

Passing to the limit in the first equation of (2.25), we deduce that ρ_α satisfies (2.12) in the sense of distributions. We use uniqueness of duality solutions to conclude the proof. □

2.6 Numerical simulations

This section is devoted to the numerical simulation of system (2.12). We provide a numerical scheme which preserves basic properties of the system such as positivity, conservation of mass for each species and conservation of the weighted center of mass. Moreover, we prove the convergence of the numerical approximation towards the duality solution defined in Theorem 2.2.2.

2.6.1 Numerical scheme and properties

Let us consider a cartesian grid of time step Δt and space step Δx. We denote $x_j=j\Delta x, j\in\mathbb{Z}, t^n=n\Delta t, n\in\mathbb{N}$. An approximation of $\rho_\alpha(t^n,x_j)$ denoted $\rho_{\alpha,j}^n$ is computed by using a finite volume approach

where the flux $F^n_{\alpha,j-1/2}$ is given by the flux vector splitting method (see [59]). Assuming that $(\rho^n_{\alpha,j})$ are known at time t^n, we compute $\rho^{n+1}_{\alpha,j}$ by the scheme:

$$\begin{cases} \dfrac{\rho^{n+1}_{\alpha,j}-\rho^n_{\alpha,j}}{\Delta t}+\dfrac{F^n_{\alpha,j+1/2}-F^n_{\alpha,j-1/2}}{\Delta x}=0 \quad \text{for } \alpha=1,2 \text{ and } j\in\mathbb{Z}, \\ F^n_{\alpha,j-1/2}=\chi_\alpha\left((\hat{a}^n_{j-1})^+\rho^n_{\alpha,j-1}+(\hat{a}^n_j)^-\rho^n_{\alpha,j}\right), \\ \hat{a}^n_j=\displaystyle\sum_{i\neq j}\partial_x K(x_j-x_i)\left(\theta_1\rho^n_{1,i}+\theta_2\rho^n_{2,i}\right), \end{cases} \tag{2.26}$$

where $(\cdot)^+:=\max\{(\cdot),0\}$, $(\cdot)^-:=\min\{(\cdot),0\}$ are respectively the positive and negative part of $(\cdot)$. Then we reconstruct

$$\rho_{\alpha,\Delta x}(t,x)=\sum_{n=0}^{N_t-1}\sum_{j\in\mathbb{Z}}\rho^n_{\alpha,j}\mathbb{1}_{[t^n,t^{n+1}[}(t)\delta_{x_j}(x),$$

where δ_{x_j} is the Dirac delta function at $x_j=j\Delta x$. We first verify that this scheme allows the conservation of the mass and of the weighted center of mass.

Proposition 2.6.1. *Let us consider $(\rho^{ini}_1,\rho^{ini}_2)\in\mathcal{P}_2(\mathbb{R})^2$ such that for $\alpha=1,2$, $\rho^{ini}_\alpha=\sum_{j\in\mathbb{Z}}\rho^0_{\alpha,j}\delta_{x_j}$. We assume that for $n\in\mathbb{N}^*$, $(\rho^n_{\alpha,j})_{j,n}$ are given by the numerical scheme (2.26). Then the conservation of the mass of each species and of the weighted center of mass hold:*

$$\forall n\in\mathbb{N},\quad \sum_{j\in\mathbb{Z}}\rho^{n+1}_{\alpha,j}=\sum_{j\in\mathbb{Z}}\rho^n_{\alpha,j}\quad \text{for } \alpha=1,2, \tag{2.27}$$

$$\forall n\in\mathbb{N},\quad \frac{\theta_1}{\chi_1}\sum_{j\in\mathbb{Z}}x_j\rho^{n+1}_{1,j}+\frac{\theta_2}{\chi_2}\sum_{j\in\mathbb{Z}}x_j\rho^{n+1}_{2,j}=\frac{\theta_1}{\chi_1}\sum_{j\in\mathbb{Z}}x_j\rho^n_{1,j}+\frac{\theta_2}{\chi_2}\sum_{j\in\mathbb{Z}}x_j\rho^n_{2,j}. \tag{2.28}$$

Proof. Identity (2.27) can be obtained directly by summing over $j\in\mathbb{Z}$ the first equation in (2.26).

We now show (2.28). Multiplying by x_j the first equation in (2.26) and summing over $j\in\mathbb{Z}$, one gets

$$\begin{aligned}\frac{1}{\chi_\alpha}\sum_{j\in\mathbb{Z}}x_j\rho^{n+1}_{\alpha,j}=\frac{1}{\chi_\alpha}\sum_{j\in\mathbb{Z}}x_j\rho^n_{\alpha,j}-\frac{\Delta t}{\Delta x}\sum_{j\in\mathbb{Z}}x_j(\hat{a}^n_j)^+\rho^n_{\alpha,j}+\frac{\Delta t}{\Delta x}\sum_{j\in\mathbb{Z}}x_j(\hat{a}^n_{j-1})^+\rho^n_{\alpha,j-1}\\ +\frac{\Delta t}{\Delta x}\sum_{j\in\mathbb{Z}}x_j(\hat{a}^n_j)^-\rho^n_{\alpha,j}-\frac{\Delta t}{\Delta x}\sum_{j\in\mathbb{Z}}x_j(\hat{a}^n_{j+1})^-\rho^n_{\alpha,j+1},\quad \text{for } \alpha=1,2.\end{aligned}$$

Using a discrete integration by parts, one gets

$$\frac{1}{\chi_\alpha}\sum_{j\in\mathbb{Z}}x_j\rho^{n+1}_{\alpha,j}=\frac{1}{\chi_\alpha}\sum_{j\in\mathbb{Z}}x_j\rho^n_{\alpha,j}+\Delta t\sum_{j\in\mathbb{Z}}\left((\hat{a}^n_j)^++(\hat{a}^n_j)^-\right)\rho^n_{\alpha,j}=\frac{1}{\chi_\alpha}\sum_{j\in\mathbb{Z}}x_j\rho^n_{\alpha,j}+\Delta t\sum_{j\in\mathbb{Z}}\hat{a}^n_j\rho^n_{\alpha,j}.$$

Finally, we get

$$\frac{\theta_1}{\chi_1}\sum_{j\in\mathbb{Z}}x_j\rho^{n+1}_{1,j}+\frac{\theta_2}{\chi_2}\sum_{j\in\mathbb{Z}}x_j\rho^{n+1}_{2,j}=\frac{\theta_1}{\chi_1}\sum_{j\in\mathbb{Z}}x_j\rho^n_{1,j}+\frac{\theta_2}{\chi_2}\sum_{j\in\mathbb{Z}}x_j\rho^n_{2,j}+\Delta t\sum_{j\in\mathbb{Z}}\hat{a}^n_j\left(\theta_1\rho^n_{1,j}+\theta_2\rho^n_{2,j}\right).$$

From (2.26), we have that

$$\sum_{j\in\mathbb{Z}}\hat{a}^n_j\left(\theta_1\rho^n_{1,j}+\theta_2\rho^n_{2,j}\right)=\sum_{i\neq j}\partial_x K(x_j-x_i)\left(\theta_1\rho^n_{1,j}+\theta_2\rho^n_{2,j}\right)\left(\theta_1\rho^n_{1,i}+\theta_2\rho^n_{2,i}\right).$$

Swapping indices i and j and using the oddness of $\partial_x K$ yields

$$\sum_{j\in\mathbb{Z}}\hat{a}^n_j\left(\theta_1\rho^n_{1,j}+\theta_2\rho^n_{2,j}\right)=0.$$

Then (2.28) follows. □

Lemma 2.6.2. *Let $(\rho_1^{ini}, \rho_2^{ini})$ be in $\mathcal{P}_2(\mathbb{R})^2$ such that $\rho_\alpha^{ini} = \sum_{j\in\mathbb{Z}} \rho_{\alpha,j}^0 \delta_{x_j}$ with $\sum_{j\in\mathbb{Z}} \rho_{\alpha,j}^0 = 1$ and $\rho_{\alpha,j} \geq 0$ for $\alpha = 1, 2$. Assuming that for $n \in \mathbb{N}^*$, $(\rho_{\alpha,j}^n)_{j,n}$ are given by the numerical scheme (2.26). If the following CFL condition holds*

$$\max(\chi_1, \chi_2)\|\partial_x K\|_{L^\infty}(\theta_1 + \theta_2)\frac{\Delta t}{\Delta x} < 1, \tag{2.29}$$

Then for all $n \in \mathbb{N}$, $\rho_{\alpha,j}^n \geq 0$ and we have $\sup_{j,n} \left|\hat{a}_j^n\right| \leq \|\partial_x K\|_{L^\infty}(\theta_1 + \theta_2)$.

Proof. This result is proved by induction. Let us assume that at time n, for all $j \in \mathbb{Z}$, $\rho_{\alpha,j}^n$ is positive and $\sup_j \left|\hat{a}_j^n\right| \leq \|\partial_x K\|_{L^\infty}(\theta_1 + \theta_2)$. From (2.26), it follows that

$$\rho_{\alpha,j}^{n+1} = \left(1 - \chi_\alpha \frac{\Delta t}{\Delta x}\left|\hat{a}_j^n\right|\right)\rho_{\alpha,j}^n + \chi_\alpha \frac{\Delta t}{\Delta x}(\hat{a}_{j-1}^n)^+ \rho_{\alpha,j-1}^n - \chi_\alpha \frac{\Delta t}{\Delta x}(\hat{a}_{j+1}^n)^- \rho_{\alpha,j+1}^n. \tag{2.30}$$

Using the condition (2.29) and the fact that $\sup_j \left|\hat{a}_j^n\right| \leq \|\partial_x K\|_{L^\infty}(\theta_1 + \theta_2)$, we get that $\chi_\alpha \frac{\Delta t}{\Delta x}\left|\hat{a}_j^n\right| < 1$. Therefore $\rho_{\alpha,j}^{n+1}$ is positive as a linear combinaison of positive numbers.

Then, recalling the expression of $\hat{a}_j^n$ given in (2.26), using the fact that $\rho_{\alpha,j}^{n+1}$, $j \in \mathbb{Z}$, are positive and the conservation of the mass, (2.27) yields

$$\left|\hat{a}_j^{n+1}\right| \leq \|\partial_x K\|_{L^\infty}(\theta_1 + \theta_2).$$

□

2.6.2 Convergence of the numerical solution to the theoretical solution

In this part, we prove that the numerical scheme given in (2.26) converges to the duality solution obtained in Theorem 2.2.2.

Theorem 2.6.3 (Convergence of the numerical scheme)**.** *Let $T > 0$, $\Delta x > 0$ and $\Delta t > 0$ such that (2.29) is satisfied and denote $N_t = \frac{T}{\Delta t}$. Let $\rho_\alpha^{ini} \in \mathcal{P}_2(\mathbb{R})$, we define*

$$\rho_{\alpha,j}^0 = \int_{x_{j-\frac{1}{2}}}^{x_{j+\frac{1}{2}}} \rho_\alpha^{ini}(dx), \qquad j \in \mathbb{Z}.$$

Let us define $\rho_{\alpha,\Delta x} \in \mathcal{M}_b([0,T]\times\mathbb{R})$ by

$$\rho_{\alpha,\Delta x}(t,x) = \sum_{n=0}^{N_t-1}\sum_{j\in\mathbb{Z}} \rho_{\alpha,j}^n \mathbb{1}_{[t^n,t^{n+1}[}(t)\delta_{x_j}(x), \tag{2.31}$$

where $(\rho_{\alpha,j}^n)_{j,n}$ computed by (2.26).
Then, we have

$$\rho_{\alpha,\Delta x} \rightharpoonup \rho_\alpha \quad \text{weakly in} \quad \mathcal{M}_b([0,T]\times\mathbb{R}) \quad \text{as} \quad \Delta x \to 0,$$

where ρ_α is the duality unique solution of Theorem 2.2.2 with initial data ρ_α^{ini}.

Proof of Theorem 2.6.3. For the initial data, it is clear that when $\Delta x \to 0$, we have $\rho_{\alpha,\Delta x}(t=0) \rightharpoonup \rho_\alpha^{ini}$ weakly. From Lemma 2.6.2, we get that for all $j \in \mathbb{Z}, n \in \mathbb{N}$, values of $\rho_{\alpha,j}^n$ are positive.

Step 1: Extraction of a convergent subsequence
Equation (2.27) implies that the total variation of $\rho_{\alpha,\Delta x}$ is fixed and independant of Δx.

$$|\rho_{\alpha,\Delta x}|([0,T]\times\mathbb{R}) = T\sum_{j\in\mathbb{Z}} \rho_{\alpha,j}^{ini}.$$

Therefore, there exists a subsequence of $\rho_{\alpha,\Delta x}$ that converges weakly to $\rho_\alpha \in \mathcal{M}_b([0,T]\times\mathbb{R})$.

Step 2: Modified equation satisfied by $\rho_{\alpha,\Delta x}$
Let be $\phi \in C_c^\infty((0,T)\times\mathbb{R})$. From the definition of $\rho_{\alpha,\Delta x}$ in (2.31), we have

$$< \partial_t \rho_{\alpha,\Delta x}, \phi >= -\int_{[0,T]\times\mathbb{R}} \rho_{\alpha,\Delta x}\partial_t\phi = -\sum_{n=0}^{N_t-1}\sum_{j\in\mathbb{Z}} \rho_{\alpha,j}^n \int_{t^n}^{t^{n+1}} \partial_t\phi(x_j,t)dt,$$

Here and below we use $< \cdot,\cdot >$ to denote the dual product in the sense of distributions. Discrete integration by parts yields

$$< \partial_t \rho_{\alpha,\Delta x}, \phi >= -\sum_{n=0}^{N_t-1}\sum_{j\in\mathbb{Z}} \rho_{\alpha,j}^n(\phi_j^{n+1}-\phi_j^n) = \sum_{n=1}^{N_t}\sum_{j\in\mathbb{Z}}(\rho_{\alpha,j}^n - \rho_{\alpha,j}^{n-1})\phi_j^n,$$

where we use the notation $\phi_j^n := \phi(x_j,t^n)$. Using (2.30) and applying transformations to indices yields

$$< \partial_t \rho_{\alpha,\Delta x}, \phi >= \chi_\alpha \frac{\Delta t}{\Delta x}\sum_{n=0}^{N_t-1}\sum_{j\in\mathbb{Z}}(\hat{a}_j^n)^+\rho_{\alpha,j}^n(\phi_{j+1}^{n+1}-\phi_j^{n+1}) + \chi_\alpha\frac{\Delta t}{\Delta x}\sum_{n=0}^{N_t-1}\sum_{j\in\mathbb{Z}}(\hat{a}_j^n)^-\rho_{\alpha,j}^n(\phi_j^{n+1}-\phi_{j-1}^{n+1}).$$

Taylor expansions gives the existence of ζ^j in (x_j,x_{j+1}) and $\hat{\zeta}^j$ in (x_{j-1},x_j) such that

$$\phi_{j+1}^{n+1} = \phi_j^{n+1} + \Delta x\partial_x\phi_j^{n+1} + \frac{(\Delta x)^2}{2}\partial_{xx}\phi(\zeta^j,t^{n+1}),$$
$$\phi_{j-1}^{n+1} = \phi_j^{n+1} - \Delta x\partial_x\phi_j^{n+1} + \frac{(\Delta x)^2}{2}\partial_{xx}\phi(\hat{\zeta}^j,t^{n+1}).$$

Putting together, one obtains

$$< \partial_t \rho_{\alpha,\Delta x}, \phi >= \Delta t\chi_\alpha\sum_{n=0}^{N_t-1}\sum_{j\in\mathbb{Z}}\hat{a}_j^n\rho_{\alpha,j}^n\partial_x\phi_j^{n+1} + \chi_\alpha R_\alpha^1(\Delta x,\Delta t),$$

where $R_\alpha^1(\Delta x,\Delta t)$ is given by

$$\begin{aligned}R_\alpha^1(\Delta x,\Delta t) :=& \frac{\Delta t}{\Delta x}\sum_{n=0}^{N_t-1}\sum_{j\in\mathbb{Z}}(\hat{a}_j^n)^+\rho_{\alpha,j}^n\left(\frac{(\Delta x)^2}{2}\partial_{xx}\phi(\zeta^j,t^{n+1})\right)\\ &-\frac{\Delta t}{\Delta x}\sum_{n=0}^{N_t-1}\sum_{j\in\mathbb{Z}}(\hat{a}_j^n)^-\rho_{\alpha,j}^n\left(\frac{(\Delta x)^2}{2}\partial_{xx}\phi(\hat{\zeta}^j,t^{n+1})\right).\end{aligned}$$

From (2.31) and the definition of $\hat{a}$ in (2.13), we have

$$\hat{a}(\theta_1\rho_{1,\Delta x}+\theta_2\rho_{2,\Delta x}) = \sum_{n=0}^{N_t-1}\sum_{j\in\mathbb{Z}}\hat{a}_j^n\mathbb{1}_{[t^n,t^{n+1}[}(t)\delta_{x_j}(x).$$

where $\hat{a}_j^n$ are defined in (2.26). We get that

$$< \hat{a}(\theta_1\rho_{1,\Delta x}+\theta_2\rho_{2,\Delta x})\rho_{\alpha,\Delta x}, \partial_x\phi >= -\sum_{n=0}^{N_t-1}\sum_{j\in\mathbb{Z}}\hat{a}_j^n\rho_{\alpha,j}^n\int_{t^n}^{t^{n+1}}\partial_x\phi(x_j,t)dt.$$

From the Taylor expansion of $\partial_x\phi(x_j,t)$:

$$\partial_x\phi(x_j,t) = \partial_x\phi(x_j,t^{n+1}) + (t-t^{n+1})\partial_{xt}\phi(x_j,\tau_t^n),$$

with $\tau_t^n \in (t, t^{n+1})$, one sees that

$$< \hat{a}(\theta_1\rho_{1,\Delta x} + \theta_2\rho_{2,\Delta x})\rho_{\alpha,\Delta x}, \partial_x\phi >= -\Delta t \sum_{n=0}^{N_t-1}\sum_{j\in\mathbb{Z}} \hat{a}_j^n \rho_{\alpha,j}^n \partial_x\phi_j^{n+1} + R_\alpha^2(\Delta x, \Delta t),$$

where $R_\alpha^2(\Delta x, \Delta t)$ is defined as follows:

$$R_\alpha^2(\Delta x, \Delta t) := -\sum_{n=0}^{N_t-1}\sum_{j\in\mathbb{Z}} \hat{a}_j^n \rho_{\alpha,j}^n \int_{t^n}^{t^{n+1}} (t - t^{n+1})\partial_{xt}\phi(x_j, \tau_t^n)dt.$$

The modified equation satisfied by $\rho_{\alpha,\Delta x}$ in the distributional sense writes:

$$\int_0^T\int_{\mathbb{R}} \rho_{\alpha,\Delta x}\partial_t\phi(t,x) + \chi_\alpha \int_0^T\int_{\mathbb{R}} \hat{a}(\theta_1\rho_{1,\Delta x} + \theta_2\rho_{2,\Delta x})\rho_{\alpha,\Delta x}\partial_x\phi = \chi_\alpha R_\alpha^1(\Delta x, \Delta t) + \chi_\alpha R_\alpha^2(\Delta x, \Delta t).$$

From Lemma 2.6.2, we deduce that the terms R_α^1 and R_α^2 satisfy the estimates:

$$\left|R_\alpha^1\right| \le CT\Delta x\|\partial_{xx}\phi\|_{L^\infty}, \qquad \left|R_\alpha^2\right| \le CT\Delta x\|\partial_{tx}\phi\|_{L^\infty},$$

where C stands for a nonnegative constant. Passing to the limit and using the technical Lemma 2.3.2, we conclude that the limit ρ_α satisfies (2.12) in the distributional sense with the expression (2.13) for the velocity. By uniqueness result in Theorem 2.2.2, we deduce that ρ_α is the unique duality solution of (2.1). □

2.6.3 Dynamics of aggregates and numerical simulations

In this part, we carry out simulations of Equation (2.12) obtained thanks to scheme (2.26). Before numerically simulating the hydrodynamic behavior of the chemotaxis model, we first clarify the aggregate dynamics of this model, especially on the synchronising dynamics between aggregates of different species.

For the sake of simplicity, we choose $\theta_1 = \theta_2 = 1$ and $K = \frac{1}{2}e^{-|x|}$ in (2.12), which corresponds to the particular case of bacterial chemotaxis (see (2.7)). To illustrate the synchronising dynamics of the aggregates for (2.12), we consider the initial data given by sums of aggregates

$$\rho_1^0 = \sum_k \mu_k\delta_{x_k^0}, \quad \rho_2^0 = \sum_k \nu_k\delta_{y_k^0},$$

and look for a solution in the form

$$\rho_1(t,x) = \sum_k \mu_k\delta_{x_k(t)}, \quad \rho_2(t,x) = \sum_k \nu_k\delta_{y_k(t)}.$$

We denote by u_1 and u_2 antiderivatives of ρ_1 and ρ_2, respectively. Then the equation (2.12) reads

$$\partial_t u_\alpha + \chi_\alpha\hat{a}\rho_\alpha = 0, \qquad \alpha = 1, 2, \tag{2.32}$$

in the sense of distributions. Direct computation shows that

$$\hat{a}\rho_1 = \sum_{k,\ell} \mu_k(\mu_\ell\widehat{\partial_x K}(x_k - x_\ell) + \nu_\ell\widehat{\partial_x K}(x_k - y_\ell))\delta_{x_k},$$
$$\hat{a}\rho_2 = \sum_{k,\ell} \nu_k(\mu_\ell\widehat{\partial_x K}(y_k - x_\ell) + \nu_\ell\widehat{\partial_x K}(y_k - y_\ell))\delta_{y_k}.$$

Injecting these expressions into equation (2.32), the positions x_k and y_k satisfy the system of ODEs

$$x_k'(t) = \chi_1 \sum_\ell (\mu_\ell \widehat{\partial_x K}(x_k - x_\ell) + \nu_\ell \widehat{\partial_x K}(x_k - y_\ell)),$$
$$y_k'(t) = \chi_2 \sum_\ell (\mu_\ell \widehat{\partial_x K}(y_k - x_\ell) + \nu_\ell \widehat{\partial_x K}(y_k - y_\ell)).$$

We recover the same system for particle solutions as in DiFrancesco and Fagioli [36] for two species. See also similar aggregate dynamics for single species in [23, 76]. In the case of one single species, the system of ODEs is determinant before any collision of aggregates, and after each collision, one can always 'restart' the particle system till final collapse of all aggregates. However, the case of collisions between particles of different species is more complex, since it does not necessarily imply whether the particles of different species will synchronise or not after colliding. In fact, as observed in the following simulations, both 'synchronising'(colliding particles of different species staying together) and 'non-synchronising' cases can occur, and the transitions between the synchronising types may happen, depending on the weighted attraction of other aggregates acting on them.

For illustration, we assume that two points of different species collide at a time t_0. For instance, take $x_k(t_0) = y_k(t_0)$ for some k, then at this time t_0 we have

$$x_k'(t_0) = \chi_1 \gamma_k(t_0), \qquad y_k'(t_0) = \chi_2 \gamma_k(t_0), \qquad \gamma_k = \sum_{\ell,k} (\mu_\ell \widehat{\partial_x K}(x_k - x_\ell) + \nu_\ell \widehat{\partial_x K}(x_k - y_\ell)). \tag{2.33}$$

Note that γ_k characterises external weighted attraction on ν_k and μ_k, depending on chemo-sensitivities, distances to other aggregates and the masses of all other aggregates.

Thus if $\chi_1 \neq \chi_2$ the velocity of species 1 and 2 is not the same at this time t_0. However, with the special case at hand, $K(x) = \frac{1}{2}e^{-|x|}$, we have $\partial_x K(x_k - y_k) \to \frac{1}{2}$ when $x_k \xrightarrow{<} y_k$; and $\partial_x K(x_k - y_k) \to -\frac{1}{2}$ when $x_k \xrightarrow{>} y_k$. We deduce that when $x_k < y_k$ and $x_k \to y_k$ we have

$$(y_k - x_k)'(t) = -\frac{1}{2}(\chi_1 \nu_k + \chi_2 \mu_k) + (\chi_2 - \chi_1)\gamma_k(t).$$

Obviously, in this case, particles μ_k and ν_k stay together if $(y_k - x_k)'(t) \leq 0$. On the other hand, when $y_k < x_k$ and $y_k \to x_k$ we have

$$(x_k - y_k)'(t) = -\frac{1}{2}(\chi_1 \nu_k + \chi_2 \mu_k) + (\chi_1 - \chi_2)\gamma_k(t).$$

In this case, particles μ_k and ν_k stay together when $(x_k - y_k)'(t) \leq 0$. Finally, to keep $x_k(t) = y_k(t)$ for $t \geq t_0$, we need the condition

$$|(\chi_1 - \chi_2)\gamma_k(t)| \leq \frac{1}{2}(\chi_1 \nu_k + \chi_2 \mu_k), \tag{2.34}$$

where $\gamma_k(t)$ is defined in (2.33). This relation characterises the weighted attraction of other aggregates acting on them. If the external weighted attraction on ν_k and μ_k (the left hand side of (2.34)) is small, they will stay together. When the external weighted attraction is big, the attraction between ν_k and μ_k is relatively weak and they will move separately, the one with bigger motility will move faster than the other.

We call (2.34) the synchronising condition for μ_k and ν_k. Similarly, we can get the synchronising condition for any μ_i and ν_j, $\forall i, j$. If more than two aggregates collide simultaneously, we can simply replace them by two aggregates of each species, each aggregate accumulating the total mass of each species.

In conclusion, according to the dynamics defined above, we can see that the initial aggregates will collapse such that they eventually form a single aggregate of the two species. The final aggregate can not separate, which is similar but illustrate more complex behaviour as one species case discussed in [76].

Now we give some numerical examples showing "synchronising", "non-synchronising", transitions between "synchronising" and "non-synchronising" dynamical behaviours for the hydrodynamic model (2.12).

Example 1: Synchronising dynamics. Take the chemosensitivity constants $\chi_1 = 10$, $\chi_2 = 1$ in (2.12), and consider initial data

$$\rho_1^0 = 4e^{-5000(x+0.5)^2} + 2e^{-5000(x-0.5)^2}, \quad \rho_2^0 = 2e^{-5000(x+0.15)^2}.$$

It corresponds to small bumps located at position $x_1(0) = -0.5$, $y_1(0) = -0.15$, $x_2(0) = 0.5$, with mass $\mu_1 = 4m_0$, $\mu_2 = 2m_0$, $\nu_1 = 2m_0$, where $m_0 = \int_{\mathbb{R}} e^{-5000x^2} dx$. Figure 2.1 displays numerical results

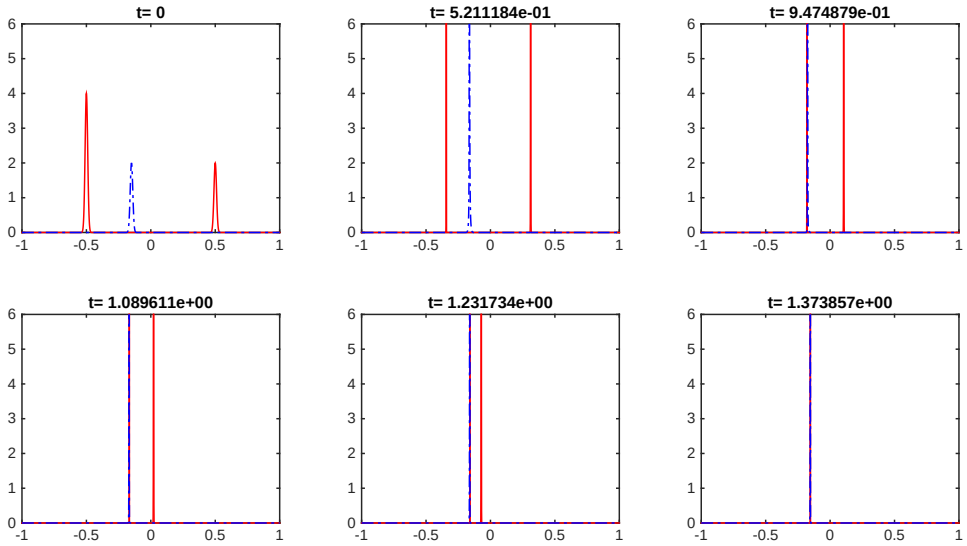

Figure 2.1: Snapshots of ρ_1 (red solid line) and ρ_2 (blue dashdot). The evolution shows the synchronising dynamics after first collision.

obtained thanks to the scheme (2.26) defined above. We first observe the fast blow-up with the formation of Dirac deltas. Then, the numerical simulation shows that μ_1 and ν_1 collapse for the first time at $t_1 \approx 0.947$, with $x_1(t_1) = y_1(t_1) \approx -0.18$, and $x_2(t_1) \approx 0.12$. We check the "synchronising condition" (2.34):

$$LHS = |(\chi_1 - \chi_2)\gamma_1(t_1)| = (10-1) \times 2 \times \frac{1}{2} e^{-(x_2 - x_1)} = 9e^{-(x_2-x_1)} < 9, \quad \forall x_1, x_2,$$
$$RHS = \frac{1}{2}(\chi_1\nu_1 + \chi_2\mu_1) = \frac{1}{2}(10 \times 2 + 1 \times 4) = 12.$$

Thus the "synchronising condition" (2.34) is always satisfied, then they will move together afterwards till final collapse with μ_2. This evolutionary dynamics is shown in Figure 2.1. The numerical result confirms the synchronising dynamics of the aggregates.

Example 2: Non-synchronising dynamics. Take the chemosensitivity constants $\chi_1 = 10$, $\chi_2 = 1$ in (2.12), and consider initial data

$$\rho_1^0 = 2e^{-5000(x+0.5)^2} + 4e^{-5000(x-0.5)^2}, \quad \rho_2^0 = 2e^{-5000(x+0.15)^2}.$$

It corresponds to small bumps located at position $x_1(0) = -0.5$, $y_1(0) = -0.15$, $x_2(0) = 0.5$, with mass $\mu_1 = 2m_0$, $\mu_2 = 4m_0$, $\nu_1 = 2m_0$, where $m_0 = \int_{\mathbb{R}} e^{-5000x^2} dx$. The numerical simulation in Figure 2.2

shows that μ_1 and ν_1 collapse for the first time at $t_1 \approx 0.9$, $x_1(t_1) = y_1(t_1) \approx -0.15$, and $x_2(t_1) \approx 0.25$. Direct computation shows that

$$LHS = |(\chi_1 - \chi_2)\gamma_1(t_1)| = (10-1) \times 4 \times \frac{1}{2} e^{-(x_2 - x_1)} \approx 18e^{-0.4} \approx 12.066,$$
$$RHS = \frac{1}{2}(\chi_1\nu_1 + \chi_2\mu_1) = \frac{1}{2}(10 \times 2 + 1 \times 2) = 11,$$

thus the "synchronising condition" (2.34) is not satisfied, then they will change their order after intersection and travel separately. The simulation shows μ_1 will collapse with μ_2 at time $t_2 \approx 1.61$, and finally collapse with ν_1 at time $t_3 \approx 1.85$. This dynamics is shown in Figure 2.2. The numerical result confirms the non-synchronising dynamics of the aggregates.

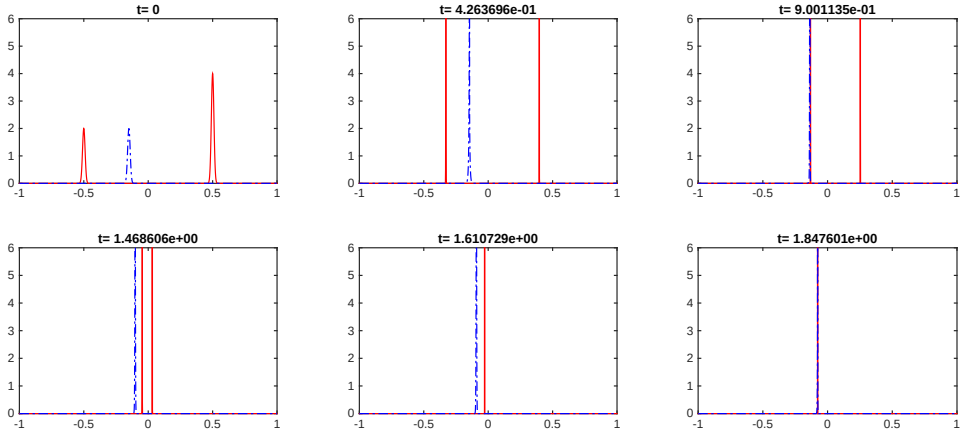

Figure 2.2: Snapshots of ρ_1 (red solid line) and ρ_2 (blue dashdot). The evolution shows the non-synchronising dynamics after first collision.

Example 3: Transition from synchronising to non-synchronising dynamics. Take the chemosensitivity constants $\chi_1 = 10$, $\chi_2 = 1$ in (2.12), and slightly modify the initial data of Example 2 to

$$\rho_1^0 = 2e^{-5000(x+0.5)^2} + 4e^{-5000(x-0.5)^2}, \quad \rho_2^0 = 2e^{-5000(x+0.3)^2}.$$

It corresponds to small bumps located at position $x_1(0) = -0.5$, $y_1(0) = -0.3$, $x_2(0) = 0.5$, with mass $\mu_1 = 2m_0$, $\mu_2 = 4m_0$, $\nu_1 = 2m_0$. The numerical simulation displayed in Figure 2.3 shows that μ_1 and ν_1 collapse for the first time at $t_1 \approx 0.47$ with $x_1(t_1) = y_1(t_1) \approx -0.29$, and $x_2(t_1) \approx 0.39$. Direct computation shows that

$$LHS = |(\chi_1 - \chi_2)\gamma_1(t_1)| = (10-1) \times 4 \times \frac{1}{2} e^{-(x_2 - x_1)} \approx 18e^{-0.68} \approx 9.1191,$$
$$RHS = \frac{1}{2}(\chi_1\nu_1 + \chi_2\mu_1) = \frac{1}{2}(10 \times 2 + 1 \times 2) = 11,$$

thus the "synchronising condition" (2.34) is satisfied, then they will move together toward μ_2. The interesting phenomenon is that, as their distance to μ_2 is decreasing, the LHS of the "synchronising condition" (2.34) is increasing and finally greater than the RHS. The simulation shows that, at $t_2 \approx 1.04$, $x_1(t_2) = y_1(t_2) \approx -0.26$, and $x_2(t_2) \approx 0.23$, then

$$LHS = |(\chi_1 - \chi_2)\gamma_1(t_1)| = (10-1) \times 4 \times \frac{1}{2} e^{-(x_2 - x_1)} \approx 18e^{-0.49} \approx 11 = RHS,$$

then after this time t_2, the interaction type has been changed: the "synchronising condition" (2.34) is no longer satisfied, then they will travel separately. Further simulation shows that μ_1 collapses with μ_2 at

time $t_3 \approx 2.037$, and finally collapse with ν_1 at time $t_4 \approx 2.32$. The full dynamics is shown in Figure 2.3. The numerical result shows the transition from synchronising to non-synchronising dynamics of the aggregates.

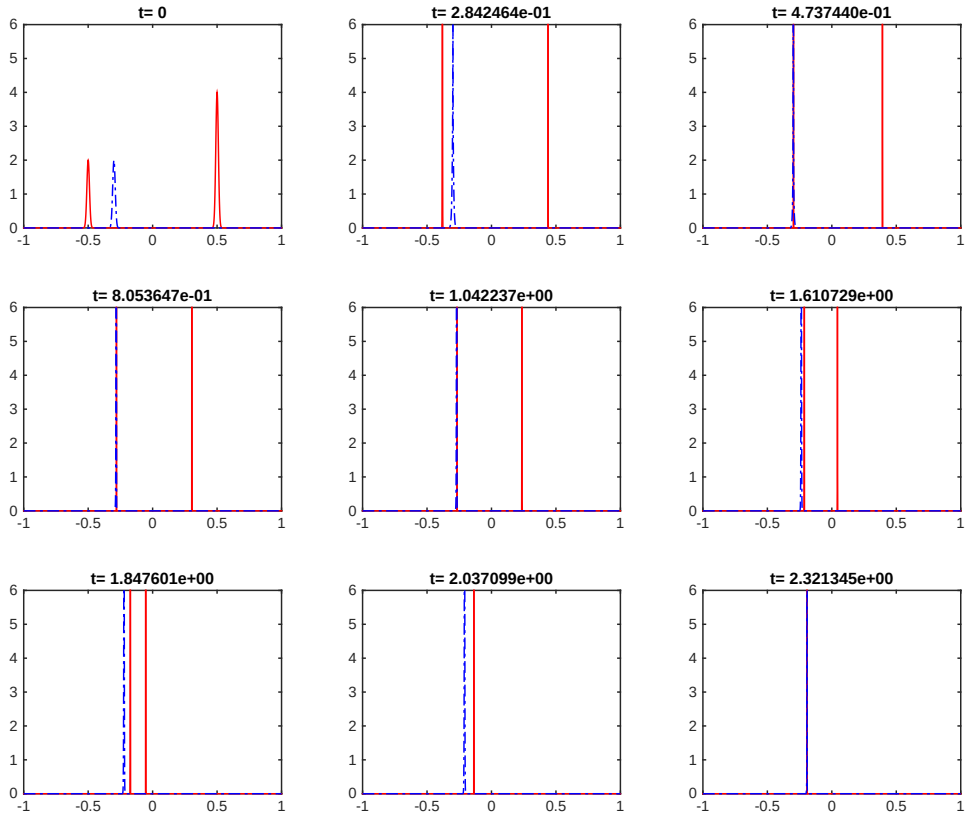

Figure 2.3: Snapshots of ρ_1 (red solid line) and ρ_2 (blue dashdot). From time $t_0 = 0$ to $t_1 \approx 0.47$, μ_1 moves toward ν_1. From time $t_1 \approx 0.47$ to $t_2 \approx 1.04$, μ_1 and ν_1 travel together. The synchronising type changed at t_2. After time t_2, μ_1 overtakes ν_1 and collapse with μ_2 at $t_3 \approx 2.037$, and finally all the aggregates collapse at $t_4 \approx 2.32$. The evolution shows the transition from synchronising to non-synchronising dynamics.

Example 4: More complex transition. Take the chemosensitivity constants $\chi_1 = 10$, $\chi_2 = 1$ in (2.12), and consider initial data

$$\rho_1^0 = 3e^{-5000(x+0.8)^2} + 1.5e^{-5000(x+0.02)^2}, \quad \rho_2^0 = 3.5e^{-5000(x-0.02)^2} + 8.5e^{-5000(x-0.5)^2}.$$

It corresponds to small bumps located at position $x_1(0) = -0.8$, $x_2(0) = -0.02$, $y_1(0) = 0.02$, $y_2(0) = 0.5$, with mass $\mu_1 = 3m_0$, $\mu_2 = 1.5m_0$, $\nu_1 = 3.5m_0$, $\nu_2 = 8.5m_0$. The snapshots of ρ_1 and ρ_2 are shown in Figure 2.4. We observe that μ_2 and ν_1 meet for the first time at $t_1 \approx 0.0459$ and satisfy non-synchronising condition so they separate after t_1. See the snapshot at $t_2 \approx 0.4288$ for evidence. They meet for the second time at $t_3 \approx 0.9494$ but the synchronising type has been changed: now they satisfy synchronising condition thus they travel together afterwards. At time $t_4 \approx 1.04$, μ_1 catches μ_2 and ν_1. Now we treat them as $(\mu_1 + \mu_2)$ and ν_1: they satisfy non-synchronising condition and separate, see snapshot at $t_5 \approx 1.256$ for evidence. At time $t_6 \approx 1.684$, $(\mu_1 + \mu_2)$ collapse with ν_2, satisfying synchronising condition

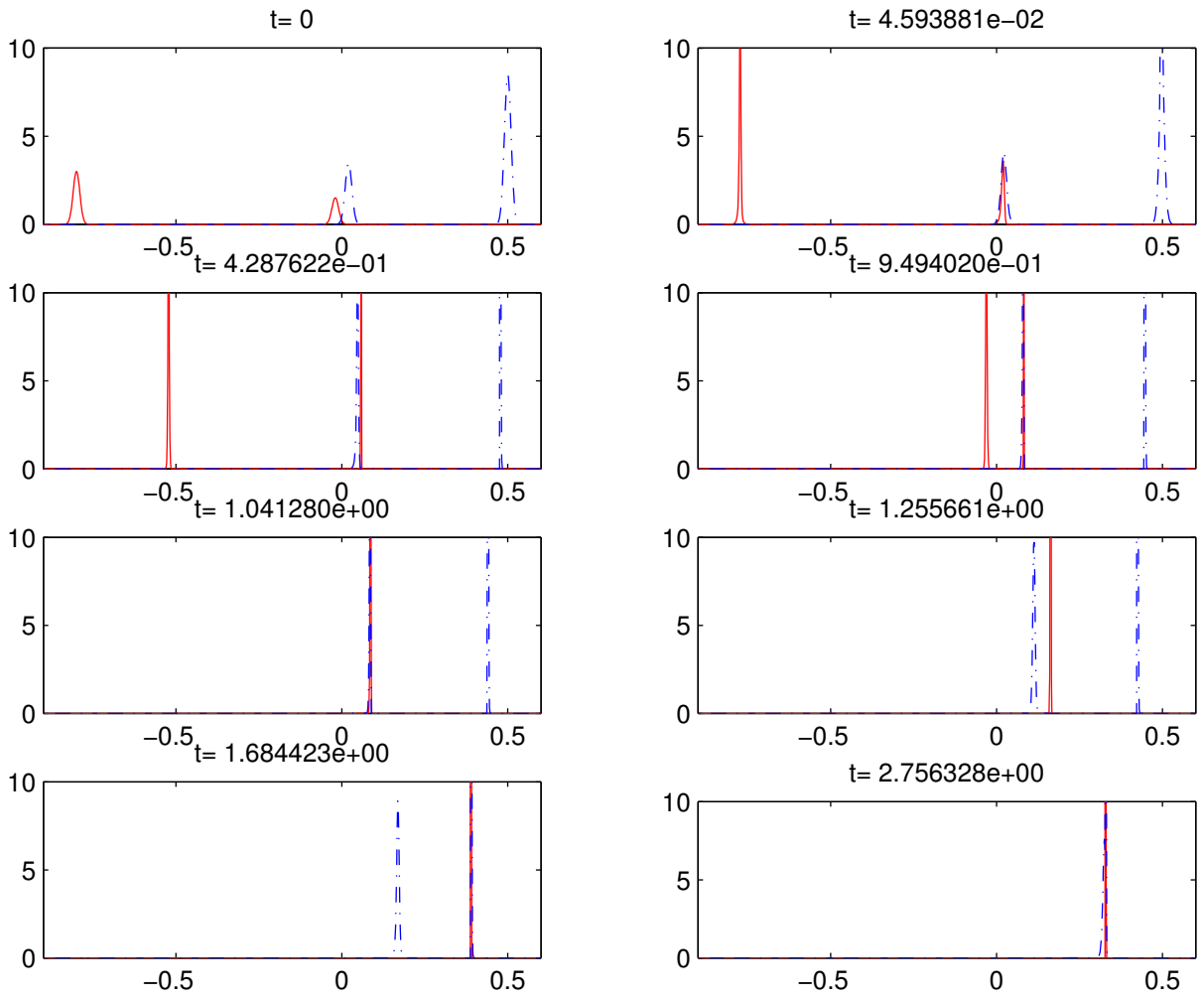

Figure 2.4: Snapshots of ρ_1 (red solid line) and ρ_2 (blue dashdot).

and staying together till final collapse with ν_1 at $t_7 \approx 2.756$. The illustration shows the complex changing of interaction types for the aggregate dynamics of two species chemotaxis model.

Traveling pulses for a two-species chemotaxis model

Ce travail est réalisé en collaboration avec Luis Almeida, Nicolas Vauchelet, Axel Buguin, Charlène Gayrard de l'Institut Curie. Il traite de la recherche d'ondes de concentration dans un modèle parabolique à deux espèces. Le résultat principal est le phénomène de synchronisation et de désynchronisation inexistant dans le cas d'un modèle à une espèce. Dans une population composée de deux espèces avec des vitesses de nage différente, si la proportion de l'espèce rapide est minoritaire alors la population se déplace à la même vitesse. Par contre, si la proportion de l'espèce rapide est dominante, alors les deux espèces se déplacent à des vitesses différentes. Ce résultat théorique est en conformité avec les résultats expérimentaux obtenus sur des souches de bactéries E.Coli par Axel Buguin et Charlène Gayrard de l'Institut Curie.
Article soumis

Chapitre 3

Traveling pulses for a two-species chemotaxis model

Abstract

Mathematical models have been widely used to describe the collective movement of bacteria by chemotaxis. In particular, concentration waves traveling in a narrow channel have been experimentally observed and can be precisely described thanks to a mathematical model at the macroscopic scale. Such model was derived in [116] using a kinetic model based on an accurate description of the mesoscopic run-and-tumble process through a kinetic model. We extend this approach to study the behaviour of the interaction between two populations of E. Coli. Separately, each population travels with its own speed in the channel. When put together, a synchronisation of the speed of the traveling pulses can be observed. We show that this synchronisation depends on the fraction of the fast population. Our approach is based on mathematical analysis of a macroscopic model of partial differential equations. Numerical simulations in comparison with experimental observations show qualitative agreement.

Contents

Author Summary

The use of mathematical tools to describe self-organization of bacterial communities has raised a lot of interest since it permits a precise description of experimentally observed phenomena. In the last 40 years a hierarchy of mathematical models for the dynamics of a single bacterial population has been proposed. These models have progressively taken into account more precise aspects of individual bacterial behaviour (like the run and tumble behaviour).

Nowadays, a natural and challenging issue is to use such models to describe the interaction between different populations of bacteria. In this work, we consider a macroscopic system of equations derived from the mesoscopic scales to describe the interaction between two populations of bacteria. The prediction obtained thanks to this model is compared to experimental observations concerning the behaviour of traveling pulses of bacteria in a channel.

3.1 Introduction

The ability of microorganisms to sense their environment helps them to colonize regions by using chemical cues to move towards favorable areas (e.g. with higher concentration in nutrients like in the present study). This biological process called chemotaxis has been extensively studied. Since pioneering works of Adler [2] (see also [41, 85]), we know that many bacteria like E.Coli may gather, feel the nutrient (oxygen, glucose) and move towards it. Many models including the famous Keller-Segel system (see [86, 66, 122, 106]) were proposed to describe mathematically this behaviour. In [115], Saragosti and al. described the propagation of bacterial concentration waves in microchannels using a macroscopic model. This model (3.1) gives the dynamics of the density of cells $\rho(x,t)$ and the concentrations in chemoattractant $S(x,t)$ and nutrients $N(x,t)$

$$\begin{cases} \partial_t \rho = D\Delta\rho - \nabla\cdot\left(\rho\left(u[S]+u[N]\right)\right), \\ \partial_t S = D_S\Delta S - \alpha S + \rho, \\ \partial_t N = D_N\Delta N - \gamma\rho N, \end{cases} \tag{3.1}$$

where $u[S], u[N]$ are given by

$$u[S] = \chi^S \operatorname{sgn}(\partial_x S), \quad u[N] = \chi^N \operatorname{sgn}(\partial_x N),$$

with $D, D_S, D_N, \chi^S, \chi^N, \alpha, \gamma$ positive constants. Here sgn is the sign function:

$$\operatorname{sgn}(x) = \begin{cases} 1, & \text{if } x > 0, \\ -1, & \text{if } x < 0. \end{cases}$$

Initially put on the left of a channel filled with nutrients, the bacteria consume nutrients located at this side. This creates a gradient of nutrients (oriented) towards the right which induces the motion of bacteria represented by the drift term $u[N]$ in the equation for ρ (see Figure 3.1). Figure 3.1 shows in A a schematic view of a micro-channel of height=100 μm, width = 500 μm and length = 1.5 cm. The channel filled with a homogeneous suspension of bacteria is then centrifuged to accumulate bacteria on the left end. Few minutes after the centrifugation has been stopped, a concentration wave of bacteria propagates at constant velocity from left to right. The concentration "wave" of E. coli chemotactic bacteria observed by fluorescence microscopy. is seen in Figure 3.1 B. The population migrates at a constant velocity (Vwave=2.2 μm/s for this particular experiment). While traveling in the channel, bacteria stay together thanks to the chemoattractant S they produce. In such a model, the existence of traveling waves is

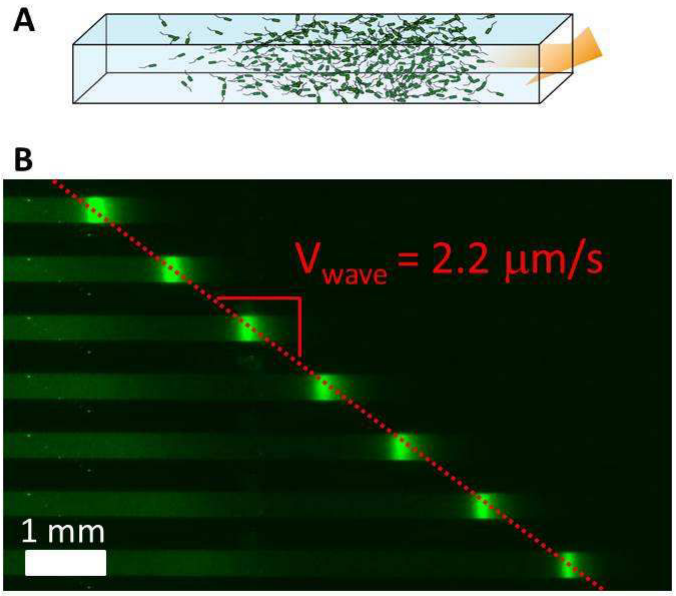

Figure 3.1: Collective migration of Escherichia coli in a PDMS micro-channel

proved, analytical forms for ρ and S are provided and the speed of the wave σ satisfies the following relationship

$$\chi^N - \sigma = \chi^S \frac{\sigma}{\sqrt{4D_S\alpha + \sigma^2}}. \tag{3.2}$$

This model predicts the double asymmetric exponential shape of ρ and the speed σ as observed experimentally. However, when we have two different strains of bacteria simultaneously, new behaviours emerge and this model is no longer valid. For instance for the two strains we used in this study, we observed that even if separately they travel at different speeds, when they are in presence of each other they may form a single band and travel together.
In this work, we study the case of a population composed of two different subpopulations of E.Coli that, when they are alone, form bands traveling at different speeds (subppopulation 1, green, being the one traveling at a slower speed σ_1 and subpopulation 2, red, being the one traveling at a higher speed σ_2, see Figure 3.2).The mean wave velocities obtained from about 15 experiments for each color, are respectively Vgreen=1.9 μm/s and Vred=4.1 μm/s.
Our experiments show that when the ratio between the number of individuals of type 2 (fast subpopulation) and the number of individuals of type 1 (slow subpopulation) is sufficiently small, there is a single band (i.e the two subpopulations travel together with an intermediate speed σ such that $\sigma_1 < \sigma < \sigma_2$. We provide a mathematical model to describe this behaviour and handle the dependency of the speed of the wave on relative sizes of subpopulations. On the contrary, when this ratio is big, our experiments and our numerical simulations (Figure 3.3) show that the two subpopulations travel at different speeds.

3.2 Results

3.2.1 Description of the experiments

When confined at one end of a microchannel, large enough populations of swimming bacteria E. Coli propagate as concentration waves. To perform such experiments, we simply fill a microchannel,

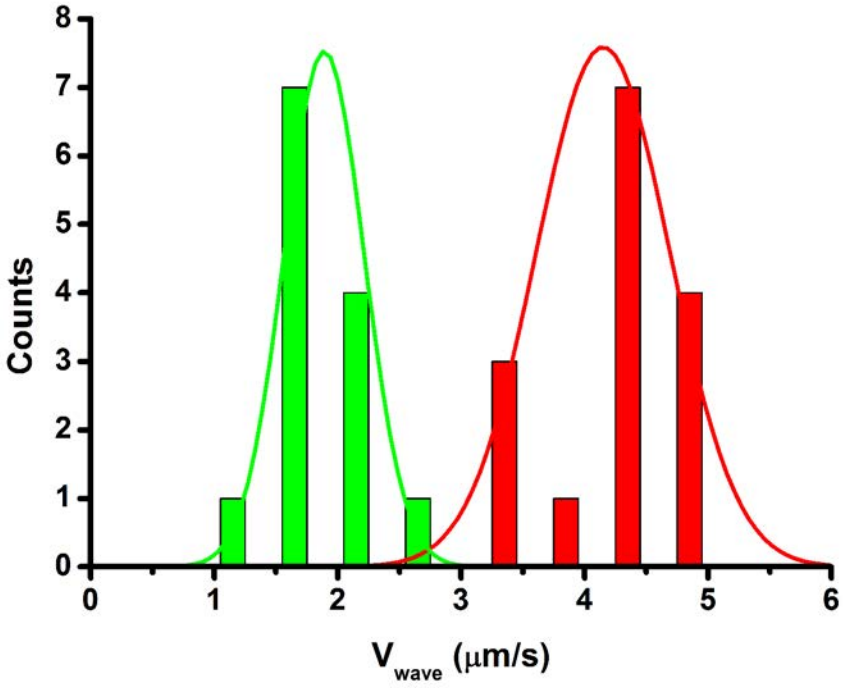

Figure 3.2: Wave velocity distribution for two different bacteria

microfabricated using soft lithography [131], of typical size 100 μm and length 1 cm with a homogeneous solution of bacteria grown up to the mid-log phase (5×10^8 bacteria/mL). The channel is then closed at both ends using epoxy glue and gently centrifuged to accumulate motile bacteria at one end of the channel. When the centrifugation is stopped a concentration wave propagates along the channel at a velocity of few μm/s. We use fluorescently labelled bacteria and thus it is possible to characterize the concentration profile of the travelling pulse using fluorescence video microscopy. These experiments are reported in previous publications [116, 115]. If we start now from a mix of two bacterial strains having different swimming speeds what happens? Do they swim together? How does one population affects the other? This is the type of questions we want to address in the present paper. To do so we have used two types of bacteria: one carrying a plasmid expressing GFP (green) and the other carrying a plasmid expressing mCherry (red). The concentration waves obtained with the red ones are two times faster than the concentration waves of the green ones (see Figure 3.2). We propose to study and to interpret the behavior of the concentration waves obtained for different ratios of the two sub-populations keeping constant the total number of bacteria. More details about the experiments are provided in material and methods.

3.2.2 Description of the model

We study the migration of a bacterial population composed of two subpopulations which react to two common chemical substances: the chemoattractant S and the nutrient N. These two chemical substances play different roles since bacteria produce the same chemoattractant which gathers the population and at the same time they consume the common nutrient which triggers the motion. Each species is represented by its density at position $x \in \mathbb{R}^d$ and time $t > 0$, $\rho_i(x,t)$ for $i = 1, 2$. The chemoattractant and the nutrient are described respectively by their concentration $S(x,t)$ and $N(x,t)$. Dynamics of ρ_1, ρ_2, S, N

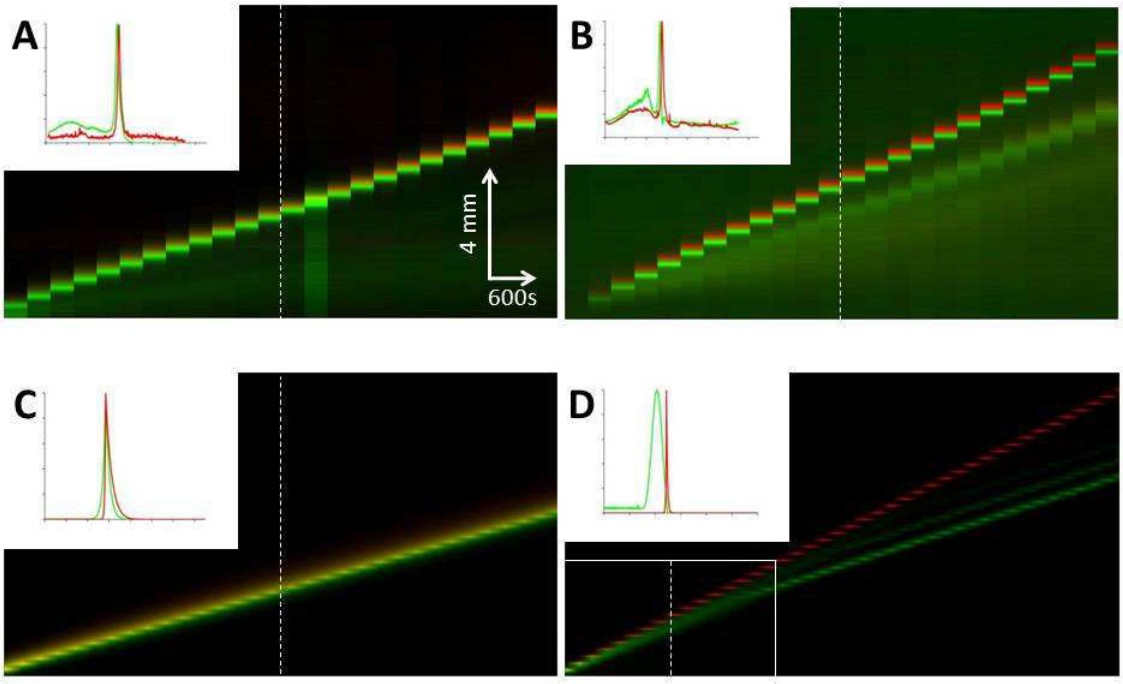

Figure 3.3: Kymographs showing the wave behavior for different bacterial compositions ϕ_{red} corresponds to the ratio of red bacteria over the total number of bacteria at the beginning of an experiment. (A) Experimental result obtained with $\phi_{red} = 10\%$. (B) Experimental result obtained with $\phi_{red} = 90\%$. (C) Simulation based on our model with $\phi_{red} = 10\%$. (D) Simulation with $\phi_{red} = 90\%$.

are given by coupled advection-diffusion-reaction equations:

$$\begin{cases} \partial_t \rho_1 = D_1 \Delta \rho_1 - \nabla \cdot (\rho_1 \left(u_1[S] + u_1[N]\right)), \\ \partial_t \rho_2 = D_2 \Delta \rho_2 - \nabla \cdot (\rho_2 \left(u_2[S] + u_2[N]\right)), \\ \partial_t S = D_S \Delta S - \alpha S + \rho_1 + \rho_2, \\ \partial_t N = D_N \Delta N - \gamma_1 \rho_1 N - \gamma_2 \rho_2 N, \end{cases} \tag{3.3}$$

where $D_1, D_2, D_S, D_N, \alpha, \gamma_1, \gamma_2$ are positive constants.
The model is an extension to the two subpopulation case of the single population model (3.1). The starting point of the modelling is the Othmer-Dunbar-Alt model which illustrates the run-and-tumble process characterising the motion of individual bacteria. Then, the macroscopic equation is recovered by drift-diffusion limits (see part 3.4.6). By this means, we derive our model (3.3) from kinetic equations describing the phenomenon at the microscopic scale (see [43]) and obtain expressions for $u_i[S], u_i[N]$

$$u_i[S] = -\frac{1}{|V|} \int_{v \in V} v \, \phi_i^S (v \cdot \nabla_x S) dv, \quad u_i[N] = -\frac{1}{|V|} \int_{v \in V} v \, \phi_i^N (v \cdot \nabla_x N) dv, \quad i = 1, 2. \tag{3.4}$$

where V is the set of admissible velocities and ϕ_i^S, ϕ_i^N are decreasing functions corresponding to the first order pertubations of the tumbling kernel of subpopulation i.
Since the phenomenon we are considering at is uni-directional, we restrict our study to one dimension in space ($d = 1$) and for computational purposes, we consider the following particular forms of $u_i[S]$ and $u_i[N]$

$$u_i[S] = \chi_i^S \operatorname{sgn}(\partial_x S), \quad u_i[N] = \chi_i^N \operatorname{sgn}(\partial_x N), \qquad i = 1, 2, \tag{3.5}$$

with χ_i^S, χ_i^N, the chemotatic sensivities of subpopulation i to the chemoattractant S and the nutrient N. We recall that sgn is the sign function.

3.2.3 Bifurcation theoretical result

Separately, the two subpopulations travel at different speeds and we name σ_1 the slow speed and σ_2 the fast one. We denote M_i the size of the subpopulation i, $\phi_{red} = \frac{M_2}{M_1+M_2}$ the percentage of the fast subpopulation (bacteria mCherry) and I_i the interval $[\chi_i^N - \chi_i^S, \chi_i^N + \chi_i^S]$ for $i = 1, 2$.
We can prove our **main result**: if the following assumption holds

$$I_1 \cap I_2 \neq \varnothing, \quad \text{and } \sigma_2, \chi_2^N - \chi_2^S \notin I_1 \cap I_2, \quad \text{where } I_i := [\chi_i^N - \chi_i^S, \chi_i^N + \chi_i^S], \tag{3.6}$$

Then there exists $\phi_{red}^* \in]0, 1[$ such that

— for $\phi_{red} \leq \phi_{red}^*$, there exist traveling pulses. Moreover, the speed of the wave σ is between σ_1 and σ_2 and satisfies

$$(\sigma - \chi_1^N) + \chi_1^S \frac{\sigma}{\sqrt{\sigma^2 + 4\alpha D_S}} + \frac{\phi_{red}}{1 - \phi_{red}} H(\sigma) \left((\sigma - \chi_2^N) + \chi_2^S \frac{\sigma}{\sqrt{\sigma^2 + 4\alpha D_S}} \right) = 0, \tag{3.7}$$

where H is defined in (3.18).

— for $\phi_{red} > \phi_{red}^*$, there do not exist single-speed traveling pulses

We remark that the speed of the wave σ is given by an implicit equation depending on the parameters of the model and the subpopulation sizes M_i. Note that in the case of a single population ($\phi_{red} = 0$), we recover the single-species equation for σ (3.2).

3.2.4 After the bifurcation point : numerical insights

We complete the theoretical analysis with numerical simulations. This allows us to see what happens after the bifurcation point. We clearly observe in Figure 3.3 that the subpopulations 1 and 2 split. After a transitory regime, they move separately at their own speed. We notice that it might take a long time for the separation to be completed in order to have a well defined speed for each pulse. Then, to define these speeds we consider the density profiles of the green and red subpopulations at each later time and notice that both subpopulations have a clear peak around their maximum density. It is the spatial position of this maximum point at each time that is used to define the position of the corresponding subpopulation pulse. This position is then used to compute the speed of each subpopulation pulse.

3.3 Discussion

3.3.1 Quantitative and qualitative conclusions

In this work we derive a macroscopic model (3.3) from microscopic assumptions on the run and tumble motion of individual bacteria (in the spirit of [115]). This model extends the one proposed in [115] for the one species case. The analytical study of the model enables us to determine the profiles of the traveling wave solutions and that they travel with a speed σ given by (3.7). Moreover, we prove the existence of a critical proportion ϕ_{red}^* of the red subpopulation above which the single traveling wave solution no longer exists.

We discretise Equation (3.3) by a finite difference semi-implicit scheme. The numerical simulations (Fig 3.4) show that, for small values of ϕ_{red}, the two subpopulations travel together in a single wave of speed σ given in Equation (3.7) as predicted by our theoretical study. For higher values of ϕ_{red} there is clearly a bifurcation at the proportion ϕ_{red}^* beyond which the two subpopulations travel in separate waves with different speeds. The experimental results (Figure 3.3) confirm this separation of the two subpopulations for high values of ϕ_{red} but our experiments are not sufficiently precise to enable us to look for the experimental bifurcation point (for intermediate values of ϕ_{red} the experimental data on the population density are diffuse and do not have clear peaks).

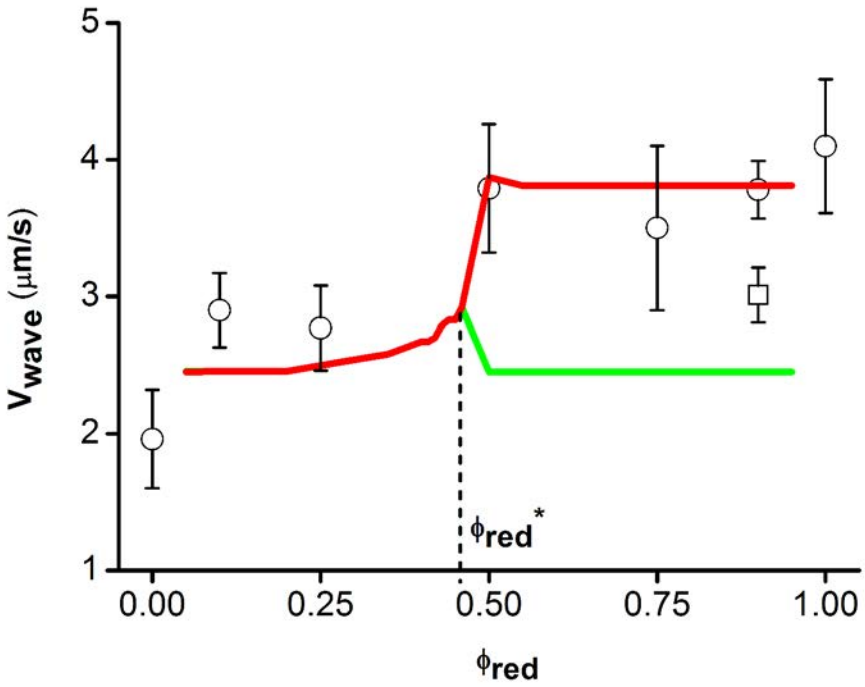

Figure 3.4: Mean wave velocity of red bacteria as a function of bacterial composition ϕ_{red}: the experimental results are represented by their means (open circles) and standard deviations (error bars). We use at least ten values for each point. These experimental results are compared to the simulation (red and green curves). One observes a separation of the two strains around $\phi_{red} = 50\%$. The square corresponds to the mean velocity of the green wave observed in Figure 3D

In Figure 3.3, we notice that for $\phi_{red} = 0.9$ the experimental point corresponding to the red subpopulation is below the red curve and the one corresponding to the Green subpopulation is above the Green curve. This should be due to the fact that our experimental channel is probably not long enough. In fact, in the simulation (see Figure 3.3D), the experimental setting corresponds to the white rectangle in the lower left corner, while the full separation of the pulses only happens for later times (further to the right in Figure 3.3 D). Therefore, the experimental measurement might still be influenced by the transitory regime which would lead to overestimating the speed of the green pulse (due to the presence or interaction with the red subpopulation).

3.3.2 Perspectives

Unfortunately, our present experimental setting does not allow us to do sufficiently precise measurements of the population density, in particular for intermediate values of ϕ_{red} where the distribution we obtain is very diffuse. This prevents us from being able to experimentally study the bifurcation and the two branches of solutions in detail. We hope that it will be possible to do the appropriate experiments in the near future since they would provide us with important information to support the predictions of our model (and make it evolve if necessary).

As in [115], we could do the analytical study only in the case where the functions $u_i[S], u_i[N]$ have the particular form (3.5). lt would be extremely interesting, but very challenging, to be able to extend this study to more general cases.

3.4 Materials and Methods

3.4.1 Bacterial Strain and Cell culture

We used the strain RP437 considered wild type for motility and chemotaxis. The strains were transformed by heat shock with PZE1R-GFP and PZE1R-mCherry plasmids. Cells were cultured in 3 mL LB medium (Sigma) with ampicilin at 33 °C, with shaking, up to mid-exponential phase (Optical density $OD_{600} = 0.5$), and re-suspended after centrifugation in the medium used for the experiments: M9 Minimal Salts, 5× supplemented with 1 g.L^{-1} Bacto Casamino Acids (both from Difco Laboratories, Sparks), 4 g.L^{-1} D-Glucose, and 1 mM MgSO4. The two types of bacteria were cultured independently before being mixed at the desired ratio at a final concentration corresponding to $OD_{600} = 0.5$.

3.4.2 Micro fabrication and centrifugation

The micro-channels were prepared using usual soft lithography techniques [131]. 100μm-high patterns were microfabricated on silicon wafers using SU-8 100 resin (MICROCHEM). The PDMS was molded on the wafer and peeled off after curing. A clean glass slide and the micro patterned PDMS were plasma treated for 30s and directly placed in contact thereby forming an array of 8 PDMS/glass parallel microchannels (width=500μm, height=100μm, length=1.8cm). They were then filled by capillarity with the homogeneous suspension of motile bacteria and sealed with a fast curing epoxy resin. The glass slide was gently centrifuged (800rpm, rotor diameter 20cm) at room temperature for half an hour. The bacteria accumulated at one end of the channels and stayed motile.

3.4.3 Video Microscopy

The channels were then immediately placed in a closed chamber maintained at constant temperature (33 °C). Few minutes after centrifugation had been stopped the concentration waves of bacteria started to propagate inside the channels (Figure 3.1). The observations were performed with a Leica MZ16F stereomicroscope equipped with two fluorescence sets: a green one, GFP2 (Leica) Ex480/Em510 and a red one, G (Leica) Ex546/Em590. Images were recorded on a CCD camera (CoolSnapHQ, Roper Scientific) at a framerate of one image per minute for both fluorescence signals. The image stacks were then post-processed using ImageJ and Matlab.

3.4.4 Analytical forms of ρ_i and S

Experiments show that bacteria are concentrated locally in space while traveling. Therefore, traveling pulses (see [69, 97]) are particularly interesting to study. By definition, we say that Equation (3.3) admits traveling pulses if and only if ρ_i, S, N are traveling waves i.e functions satisfying the ansatz

$$\rho_1(t,x) = \widetilde{\rho}_1(z), \quad \rho_2(t,x) = \widetilde{\rho}_2(z), \quad S(t,x) = \widetilde{S}(z), \quad N(t,x) = \widetilde{N}(z), \quad \text{where } z = x - \sigma t,$$

with σ being the speed of the wave. The unknowns of the problem are σ and the one-variable functions $\widetilde{S}, \widetilde{N}, \widetilde{\rho}_1, \widetilde{\rho}_2$, where $\widetilde{\rho}_1, \widetilde{\rho}_2$ are pulses as defined below.

Definition
A pulse is defined as a real-valued function which is increasing for negative values of z, decreasing for positive ones and decays to zero at infinity.

Plugging these expressions into Equation (3.3) and dropping the tilde over variables yields

$$\begin{cases} -\sigma(\rho_1)' = D_1(\rho_1)'' - (\rho_1 (u_1[S] + u_1[N]))', \\ -\sigma(\rho_2)' = D_2(\rho_2)'' - (\rho_2 (u_2[S] + u_2[N]))', \\ -\sigma S' = D_S S'' - \alpha S + \rho_1 + \rho_2, \\ -\sigma N' = D_N N'' - \gamma_1 \rho_1 N - \gamma_2 \rho_2 N. \end{cases} \tag{3.8}$$

Looking for a pulse, we prescribe the following boundary conditions

$$\rho_1(\pm\infty) = 0, \quad \rho_2(\pm\infty) = 0, \quad S(\pm\infty) = 0. \tag{3.9}$$

The fact that ρ_i are pulses implies that (see supplementary material 3.5.1)

$$\begin{cases} (\rho_i)'(\pm\infty) = 0, \quad S'(\pm\infty) = 0, \\ \partial_z S > 0 \quad \text{for } z > 0, \quad \partial_z S < 0 \quad \text{for } z > 0, \\ \partial_z N > 0 \quad \text{for } z \in \mathbb{R}. \end{cases} \tag{3.10}$$

Therefore, $u_i[N]$ and $u_i[S]$ are given by

$$u_i[S] = -\chi_i^S \operatorname{sgn}(z), \quad u_i[N] = \chi_i^N \quad \text{for } i = 1, 2.$$

We integrate equations for ρ_i in (3.8) and use (3.10) to obtain

$$\begin{cases} D_1 \rho_1{}' = (u_1[S] + u_1[N] - \sigma)\, \rho_1, \\ D_2 \rho_2{}' = (u_2[S] + u_2[N] - \sigma)\, \rho_2. \end{cases} \tag{3.11}$$

We deduce the analytical forms of ρ_i for $i = 1, 2$ and S.

$$\rho_i = \begin{cases} \rho_i^M \exp(\lambda_i^- z), \quad \lambda_i^- = \dfrac{\chi_i^N + \chi_i^S - \sigma}{D_i} > 0, \quad \text{for } z < 0, \\ \rho_i^M \exp(\lambda_i^+ z), \quad \lambda_i^+ = \dfrac{\chi_i^N - \chi_i^S - \sigma}{D_i} < 0, \quad \text{for } z > 0, \end{cases} \qquad i = 1, 2. \tag{3.12}$$

From the equation satisfied by S, we deduce that

$$S(z) = \int_{-\infty}^{+\infty} K(z - y)\, (\rho_1(y) + \rho_2(y))\, dy, \tag{3.13}$$

where K is given by

$$K = \exp\left(-\frac{\sigma}{2D_S} z - \frac{\sqrt{\sigma^2 + 4\alpha D_S}}{2D_S} |z| \right). \tag{3.14}$$

3.4.5 Speed of the wave σ

Since S is maximal at $z = 0$, by definition of a pulse, we should have $S'(0) = 0$. Differentiating S in (3.13) gives

$$S'(0) = \int_{-\infty}^{+\infty} K'(x)(\rho_1(-x) + \rho_2(-x))dx.$$

We split this integral into two parts S'_- and S'_+:

$$\begin{aligned} S'(0) &= \int_{-\infty}^{0} K'(x)(\rho_1(-x) + \rho_2(-x))dx + \int_{0}^{+\infty} K'(x)(\rho_1(-x) + \rho_2(-x))dx. \\ S'(0) &= S'_- + S'_+. \end{aligned}$$

From the supplementary materials (see 3.5.2), S'_- and S'_+ are given by

$$S'_- = \rho_1^M \frac{-\sigma + \sqrt{\sigma^2 + 4\alpha D_S}}{-\sigma + \sqrt{\sigma^2 + 4\alpha D_S} - 2D_S\lambda_1^+} + \rho_2^M \frac{-\sigma + \sqrt{\sigma^2 + 4\alpha D_S}}{-\sigma + \sqrt{\sigma^2 + 4\alpha D_S} - 2D_S\lambda_2^+},$$
$$S'_+ = \rho_1^M \frac{\sigma + \sqrt{\sigma^2 + 4\alpha D_S}}{-\sigma - \sqrt{\sigma^2 + 4\alpha D_S} - 2D_S\lambda_1^-} + \rho_2^M \frac{\sigma + \sqrt{\sigma^2 + 4\alpha D_S}}{-\sigma - \sqrt{\sigma^2 + 4\alpha D_S} - 2D_S\lambda_2^-}.$$

Putting together S'_- and S'_+ gives

$$\begin{aligned} S'(0) =& \rho_1^M \frac{c_1}{\left(-\sigma - \sqrt{\sigma^2 + 4\alpha D_S} - 2D_S\lambda_1^-\right)\left(-\sigma + \sqrt{\sigma^2 + 4\alpha D_S} - 2D_S\lambda_1^+\right)} \\ &+ \rho_2^M \frac{c_2}{\left(-\sigma - \sqrt{\sigma^2 + 4\alpha D_S} - 2D_S\lambda_2^-\right)\left(-\sigma + \sqrt{\sigma^2 + 4\alpha D_S} - 2D_S\lambda_2^+\right)}, \end{aligned}$$

with c_i given by

$$c_i = 4\frac{D_S}{D_i}\left(\chi_i^S\sigma + \left(\sigma - \chi_i^N\right)\sqrt{\sigma^2 + 4\alpha D_S}\right), \quad i = 1, 2. \tag{3.15}$$

Due to (3.10), S is maximal for $z = 0$, then S' vanishes at 0 and we obtain the equation for σ

$$\begin{aligned} &\left(\chi_1^S\sigma + (\sigma - \chi_1^N)\sqrt{\sigma^2 + 4\alpha D_S}\right) + \left(\chi_2^S\sigma + (\sigma - \chi_2^N)\sqrt{\sigma^2 + 4\alpha D_S}\right) \times \\ &\qquad \frac{D_1\rho_2^M}{D_2\rho_1^M} \frac{\left(-\sigma - \sqrt{\sigma^2 + 4\alpha D_S} - 2D_S\lambda_1^-\right)\left(-\sigma + \sqrt{\sigma^2 + 4\alpha D_S} - 2D_S\lambda_1^+\right)}{\left(-\sigma - \sqrt{\sigma^2 + 4\alpha D_S} - 2D_S\lambda_2^-\right)\left(-\sigma + \sqrt{\sigma^2 + 4\alpha D_S} - 2D_S\lambda_2^+\right)} = 0. \end{aligned} \tag{3.16}$$

We recall that $\lambda_i^\pm$ are given by (3.12). Unknowns ρ_i^M are obtained thanks to the conservation of the total subpopulation M_i. Indeed, from the conservative form of equations for ρ_i (3.3), it follows that for all $t \geq 0$

$$M_i = \int_{-\infty}^{+\infty} \rho_i(x,t)dx = \int_{-\infty}^{+\infty} \rho_i^{ini}(x)dx, \quad i = 1, 2,$$

with $\rho_i^{ini} = \rho_i(x, t = 0)$ the initial profile of ρ_i. We deduce

$$M_i = \int_{-\infty}^{+\infty} \rho_i(z)dz = \rho_i^M \frac{\chi_i^S D_i}{(\chi_i^S)^2 - (\sigma - \chi_i^N)^2}.$$

Replacing λ_i^+, λ_i^- by their values in (3.12) and using the previous relationship, (3.16) becomes

$$(\sigma - \chi_1^N) + \chi_1^S \frac{\sigma}{\sqrt{\sigma^2 + 4\alpha D_S}} + \frac{\phi_{red}}{1 - \phi_{red}} H(\sigma)\left((\sigma - \chi_2^N) + \chi_2^S \frac{\sigma}{\sqrt{\sigma^2 + 4\alpha D_S}}\right) = 0, \tag{3.17}$$

with

$$\begin{aligned} H(\sigma) &= \frac{\chi_1^S D_1}{\chi_2^S D_2} \frac{(\chi_2^S)^2 - (\sigma - \chi_2^N)^2}{(\chi_1^S)^2 - (\sigma - \chi_1^N)^2} \frac{h_1(\sigma)}{h_2(\sigma)}, \\ h_i(\sigma) &= \sigma^2\left(\frac{D_S}{D_i} - 1\right) + \left(1 - 2\frac{D_S}{D_i}\right)\sigma\chi_i^N - \chi_i^S\sqrt{\sigma^2 + 4\alpha D_S} + \frac{D_S}{D_i}\left((\chi_i^N)^2 - (\chi_i^S)^2\right) - \alpha D_i, \quad i = 1, 2. \end{aligned} \tag{3.18}$$

From the supplementary materials (see 3.5.3), we have that σ belongs to $\Omega = I_1 \cap I_2 \cap (\sigma_1, \sigma_2)$. Since σ_2 and $\chi_2^N - \chi_2^S$ do not belong to Ω, then (3.17) rewrites

$$G(\sigma) = \frac{\phi_{red}}{1 - \phi_{red}},$$

where G is a positive function bounded over Ω given by

$$G(\sigma) = -\frac{\chi_1^S\sigma + (\sigma - \chi_1^N)\sqrt{\sigma^2 + 4\alpha D_S}}{H(\sigma)\left(\chi_2^S\sigma + (\sigma - \chi_2^N)\sqrt{\sigma^2 + 4\alpha D_S}\right)}.$$

The function G admits a maximum which is finite. Therefore, there exists $\phi^*_{red} \in (0,1)$ such that

$$\max_{\Omega} G(\sigma) = \frac{\phi^*_{red}}{1-\phi^*_{red}}.$$

For more details, we refer to parts 3.5.2, 3.5.3 in the supplementary material.

3.4.6 Derivation of the two-species macroscopic model

In this section, we derive formally macroscopic equations (3.3) from the kinetic descriptions of individual motion of bacteria [100, 28, 73]. This motion is a succession of run and tumble phases as observed in [72]. During the run phase, bacteria move in straight lines and change their direction during the tumble phase. The Othmer-Dunbar-Alt model (see [99, 3, 116]) gives the mathematical description of the individual behaviour. It describes the dynamics of the distribution density $f_i(x,v,t)$ of cells at position $x \in \mathbb{R}^d$ at time t having speed $v \in V$, where V is a bounded, symmetric and rotationally invariant domain of $\mathbb{R}^d$. It reads

$$\begin{aligned} \partial_t f_i + v\cdot\nabla_x f_i = &\frac{1}{2}\int_V \left(T_i[S](x,v,v',t)f_i(x,v',t) - T_i[S](x,v',v,t)f_i(x,v,t)\right)dv' \\ &+ \frac{1}{2}\int_V \left(T_i[N](x,v,v',t)f_i(x,v',t) - T_i[N](x,v',v,t)f_i(x,v,t)\right)dv', \quad \text{for } i=1,2, \end{aligned} \tag{3.19}$$

where $T_i[S](x,v,v',t)$, $T_i[N](x,v,v',t)$ stand for the amount of bacteria reorienting from the direction v' to v under the influence of the chemoattractant and the nutrient. They are usually called tumbling kernels.
From the definition of the tumbling kernels (see [40]), we can consider that $T_i[S]$ and $T_i[N]$ are given by

$$\begin{cases} T_i[S] = \Phi_i[S](\partial_t S + v'\cdot\nabla_x S), \\ T_i[N] = \Phi_i[N](\partial_t N + v'\cdot\nabla_x N), \end{cases}$$

We perform a diffusive scaling ($\widetilde{x} = \varepsilon x, \widetilde{t} = \varepsilon^2 t$) where $\varepsilon > 0$ is a small parameter and get

$$\begin{aligned} \partial_t f_i^\varepsilon + \frac{v}{\varepsilon}\cdot\nabla_x f_i^\varepsilon = &\frac{1}{2\varepsilon^2}\int_V \Phi_i^\varepsilon[S](\partial_t S + v'\cdot\nabla_x S)f_i^\varepsilon(x,v',t)dv' - |V|\,\Phi_i^\varepsilon[S](\partial_t S + v\cdot\nabla_x S)f_i^\varepsilon(x,v,t), \\ &+ \frac{1}{2\varepsilon^2}\int_V \Phi_i^\varepsilon[N](\partial_t N + v'\cdot\nabla_x N)f_i^\varepsilon(x,v',t)dv' - |V|\,\Phi_i^\varepsilon[N](\partial_t N + v\cdot\nabla_x N)f_i^\varepsilon(x,v,t). \end{aligned}$$

Since tumbling kernels are pertubations of constant tumbling rates for E.Coli, we can assume that

$$\begin{cases} \Phi_i^\varepsilon[S](\partial_t S + v\cdot\nabla_x S) = \psi_i\left(1+\varepsilon\phi_i^S(\varepsilon\partial_t S + v\cdot\nabla_x S)\right), \\ \Phi_i^\varepsilon[N](\partial_t N + v\cdot\nabla_x N) = \psi_i\left(1+\varepsilon\phi_i^N(\varepsilon\partial_t N + v\cdot\nabla_x N)\right), \end{cases}$$

where ϕ_i^S, ϕ_i^N are decreasing functions.
We write expansions of f_i^ε when ε tends to zero.

$$f_i^\varepsilon = f_i^0 + \varepsilon f_i^1, \quad \text{for } i=1,2.$$

Plugging these expansions in the equation for f_i^ε gives at the order $1/\varepsilon^2$

$$f_i^0(x,v,t) = \frac{\int_V f_i^0(x,v',t)dv'}{|V|} = \frac{\rho_i^0(x,t)}{|V|}, \quad \text{for } i=1,2.$$

At the order $1/\varepsilon$, we get

$$\begin{aligned} f_i^1 = \frac{1}{|V|}\int_V f_i^1(x,v',t)dv' + \frac{1}{2\,|V|}\int_V \left(\phi_i^S(v\cdot\nabla_x S^0) + \phi_i^N(v\cdot\nabla_x N^0)\right) f_i^0(x,v',t)dv' \\ - \frac{1}{2}\left(\phi_i^S(v\cdot\nabla_x S^0) + \phi_i^N(v\cdot\nabla_x N^0)\right) f_i^0(x,v,t) - \frac{v}{|V|\,\psi_i}\cdot\nabla_x f_i^0, \end{aligned}$$

where S^0 and N^0 are leading order terms of asymptotic expansions of respectively S and N and are solutions to equations (3.3) for S and N with $\rho_i = \rho_i^0$.
Integrating the equation for f_i^ε over V yields the following conservation equation for $\rho_i^\varepsilon = \int_V f_i^\varepsilon dv$

$$\partial_t \int_V f_i^\varepsilon dv + \frac{1}{\varepsilon}\nabla \cdot \left(\int_V v f_i^\varepsilon dv \right) = 0.$$

From the asymptotic analysis carried out before, we have that

$$\int_V f_i^\varepsilon(x,v,t)dv \to \rho_i^0(x,t).$$

Since V is a symmetric bounded domain, we have the convergence of the scaled first moment

$$\frac{1}{\varepsilon}\int_V v f_i^\varepsilon(x,v,t)dv \to \int_V v f_i^1(x,v,t)$$

with

$$\int_V v f_i^1(x,v,t) = -\left(\int_V \frac{v}{2\,|V|}\phi_i^S (v\cdot\nabla_x S^0)dv \right)\rho_i^0(x,t) - \left(\int_V \frac{v}{2\,|V|}\phi_i^N (v\cdot\nabla_x N^0)dv \right)\rho_i^0(x,t) - \int_V \frac{v\otimes v}{|V|^2\,\psi_i}\nabla_x \rho_i^0(x,t).$$

We finally obtain the equation for ρ_i^0 in (3.3). This formal computation has been rigorously established by part of the authors in [43].

3.4.7 Parameter estimation

In this section, we calibrate our model. This means finding values of parameters $D_S, \alpha, \chi_i^N, \chi_i^S, D_i$. Note that D_S and D_i could be measured experimentally (see [72, 114, 71]). Other parameters are determined as in [115]. We remark that our dispersion formula (3.7) for the two species extends the single species formula. The experimental observation of the double exponential shape gives $\lambda_i^\pm$, then $\chi_i^S, \chi_i^N, \alpha$ are deduced.

$$\alpha = (\sigma_i)^2 \frac{-\lambda_i^+\lambda_i^-}{D_S(\lambda_i^+ + \lambda_i^-)^2},$$
$$\chi_i^N = \sigma + \frac{D_i\left(\lambda_i^+ + \lambda_i^-\right)}{2},$$
$$\chi_i^S = \frac{D_i\left(\lambda_i^+ - \lambda_i^-\right)}{2}.$$

Acknowledgments

Authors acknowledge financial support ANR-13-BS01-0004 Kibord from the French Ministry of Research and from the Labex IPGG. We also thank V.Calvez, D.Lopez, J.Saragosti and P.Silberzan for numerous discussions and their help in setting up the experiments.

Tables

3.5 Supplementary material

In this part, we prove several technical results.

Table 3.1: Table of the values of parameters

Effective bacterial diffusion of subpopulation 1 D_1	$1.79 \times 10^{-6}\text{cm}^2.\text{s}^{-1}$	Experimental measurement
Effective bacterial diffusion of subpopulation 2 D_2	$3.29 \times 10^{-6}\text{cm}^2.\text{s}^{-1}$	Experimental measurement
Effective bacterial chemosensivity of subpopulation 1 χ_1^S	$6.49 \times 10^{-5}\text{cm.s}^{-1}$	Experimental fit
Effective bacterial chemosensivity of subpopulation 2 χ_2^S	$2.88 \times 10^{-4}\text{cm.s}^{-1}$	Experimental fit
Effective bacterial chemosensivity of subpopulation 1 χ_1^N	$2.57 \times 10^{-4}\text{cm.s}^{-1}$	Experimental fit
Effective bacterial chemosensivity of subpopulation 2 χ_2^N	$4.74 \times 10^{-4}\text{cm.s}^{-1}$	Experimental fit
Chemical degradation α	$5 \times 10^{-2}\text{s}^{-1}$	Experimental fit
Chemoattractant diffusion D_S	$8 \times 10^{-6}\text{cm}^2.\text{s}^{-1}$	[72]
Nutrient diffusion D_N	$8 \times 10^{-6}\text{cm}^2.\text{s}^{-1}$	[72]

3.5.1 Proof of the result (3.10) on the signs of $\partial_z S$ and $\partial_z N$

We prove that : if ρ_1 and ρ_2 are pulses, then S is also a pulse and we have

$$\begin{cases} \partial_z S > 0, & \text{for } z < 0, \\ \partial_z S < 0, & \text{for } z > 0. \end{cases}$$

Futhermore, we have

$$\partial_z N > 0, \quad \text{for } z \in \mathbb{R}.$$

Let us prove this result. Equation (3.13) says that $S = K * (\rho_1 + \rho_2)$. Since ρ_i decays to zero at infinity, we conclude that S also decays to zero at infinity. The equation for S in (3.3) also implies that S' admits a limit at infinity. This limit has to be zero otherwise S would not have a limit at infinity. Since limits of S are equal to zero at infinity, S' vanishes at least once. Without loss of generality, let us suppose that S' vanishes at $z = 0$ if not, we can do a translation in z. Differentiating the equation for S in (3.3) yields

$$-\sigma \partial_z S' = D_S \partial_{zz}(S') - \alpha S' + \partial_z \rho_1 + \partial_z \rho_2$$

Since ρ_i is a pulse, we have that $\partial_z \rho_i$ is positive in $(-\infty, 0)$. We get that

$$-\sigma \partial_z S' - D_S \partial_{zz} S' + \alpha S' \geq 0 \quad \text{in } (-\infty, 0).$$

Consider $u = -S'$, then u satisfies

$$-\sigma \partial_z u - D_S \partial_{zz} u + \alpha u \leq 0, \quad (-\infty, 0).$$

Multiplying this equation by $u^+ := \max(u, 0)$ and integrating by parts yields

$$-\sigma \int_{-\infty}^{0} \partial_z u^+ u^+ + D_S \int_{-\infty}^{0} \partial_z {u^+}^2 + \alpha \int_{-\infty}^{0} {u^+}^2 \leq 0.$$

Since the first term is zero

$$\int_{-\infty}^{0} \partial_z u^+ u^+ = [(u^+)^2]_{-\infty}^{0} = 0,$$

we get

$$D_S \int_{-\infty}^{0} (\partial_z u^+)^2 + \alpha \int_{-\infty}^{0} (u^+)^2 \leq 0.$$

Since we have the sum of two nonnegative terms, this implies that

$$\int_{-\infty}^{0} (u^+)^2 \leq 0.$$

We have proved that $u^+ = 0$ for $z \in (-\infty, 0)$ which by definition d of u means that $\partial_x S > 0$.
By a similar argument, we show that $\partial_z S < 0$ for $z \in (0, \infty)$.
Now, we prove that $\partial_z N > 0$. By using the same technique, we can show that $\rho_i, i = 1, 2$ and N are positive. Denoting $u = -\partial_z N$ and using the positivity of ρ_i and N gives that

$$-\sigma u - D_N u' \geq 0, \quad \text{in } (-\infty, \infty).$$

By multiplying by u^+ and integrating by parts, one has

$$\sigma \int_{-\infty}^{+\infty} (u^+)^2 \leq 0 \quad \text{which implies that } \partial_z N > 0, \quad \text{in } (-\infty, -\infty).$$

3.5.2 Detailed computation of $S'(0)$

In this part, we provide missing computations of S'_-, S'_+, c_i, h_i which are used to derive the dispersion relation (3.7) in Section 2.

3.5.2.1 Computations of S'_-, S'_+

From the definition of K (3.14), K' reads

$$K' = \begin{cases} \left(-\dfrac{\sigma}{2D_S} + \dfrac{\sqrt{\sigma^2 + 4D_S\alpha}}{2D_S}\right) \exp\left(-\dfrac{\sigma}{2D_S} z + \dfrac{\sqrt{\sigma^2 + 4D_S\alpha}}{2D_S} z\right), & \text{for } z < 0, \\ \left(-\dfrac{\sigma}{2D_S} - \dfrac{\sqrt{\sigma^2 + 4D_S\alpha}}{2D_S}\right) \exp\left(-\dfrac{\sigma}{2D_S} z - \dfrac{\sqrt{\sigma^2 + 4D_S\alpha}}{2D_S} z\right), & \text{for } z > 0. \end{cases}$$

We have

$$\int_{-\infty}^{0} K'(x)\rho_i(-x)dx = \rho_i^M \frac{-\sigma\sqrt{\sigma^2 + 4\alpha D_S}}{2D_S} \int_{-\infty}^{0} \exp\left(-\frac{\sigma}{2D_S} x + \frac{\sqrt{\sigma^2 + 4D_S\alpha}}{2D_S} x - \lambda_i^+ x\right) dx.$$

It follows that

$$\int_{-\infty}^{0} K'(x)\rho_i(-x)dx = \rho_i^M \frac{\frac{-\sigma+\sqrt{\sigma^2+4\alpha D_S}}{2D_S}}{\frac{-\sigma+\sqrt{\sigma^2+4\alpha D_S}}{2D_S} - \lambda_i^+} \times \left[\exp\left(-\frac{\sigma}{2D_S} x + \frac{\sqrt{\sigma^2 + 4D_S\alpha}}{2D_S} x - \lambda_i^+ x\right)\right]_{-\infty}^{0}.$$

We conclude that

$$\int_{-\infty}^{0} K'(x)\rho_i(-x)dx = \rho_i^M \frac{-\sigma + \sqrt{\sigma^2 + 4\alpha D_S}}{-\sigma + \sqrt{\sigma^2 + 4\alpha D_S} - 2D_S\lambda_i^+}.$$

In the same way, we can prove that

$$\int_{0}^{+\infty} K'(x)\rho_i(-x)dx = \rho_i^M \frac{\sigma + \sqrt{\sigma^2 + 4\alpha D_S}}{-\sigma - \sqrt{\sigma^2 + 4\alpha D_S} - 2D_S\lambda_i^-}.$$

Finally, S'_- and S'_+ read

$$\begin{aligned} S'_- &= \int_{-\infty}^{0} K'(x)(\rho_1(-x) + \rho_2(-x))dx, \\ &= \rho_1^M \frac{-\sigma + \sqrt{\sigma^2 + 4\alpha D_S}}{-\sigma + \sqrt{\sigma^2 + 4\alpha D_S} - 2D_S\lambda_1^+} + \rho_2^M \frac{-\sigma + \sqrt{\sigma^2 + 4\alpha D_S}}{-\sigma + \sqrt{\sigma^2 + 4\alpha D_S} - 2D_S\lambda_2^+}, \\ S'_+ &= \int_{0}^{\infty} K'(x)(\rho_1(-x) + \rho_2(-x))dx \\ &= \rho_1^M \frac{\sigma + \sqrt{\sigma^2 + 4\alpha D_S}}{-\sigma - \sqrt{\sigma^2 + 4\alpha D_S} - 2D_S\lambda_1^-} + \rho_2^M \frac{\sigma + \sqrt{\sigma^2 + 4\alpha D_S}}{-\sigma - \sqrt{\sigma^2 + 4\alpha D_S} - 2D_S\lambda_2^-}. \end{aligned}$$

3.5.2.2 Computations of c_i and h_i

Coefficients c_i are defined in (3.15)

$$c_i = \left(-\sigma + \sqrt{\sigma_2 + 4\alpha D_S}\right)\left(-\sigma - \sqrt{\sigma^2 + 4\alpha D_S} - 2D_S\lambda_i^-\right) + \left(\sigma + \sqrt{\sigma^2 + 4\alpha D_S}\right)\left(-\sigma + \sqrt{\sigma^2 + 4\alpha D_S} - 2D_S\lambda_i^+\right).$$

Expanding c_i yields

$$c_i = (-\sigma + \sqrt{\sigma^2 + 4\alpha D_S})(-\sigma - \sqrt{\sigma^2 + 4\alpha D_S}) + (\sigma + \sqrt{\sigma^2 + 4\alpha D_S})(-\sigma + \sqrt{\sigma^2 + 4\alpha D_S}) + 2D_S(\sigma - \sqrt{\sigma^2 + 4\alpha D_S})\lambda_i^- - 2D_S(\sigma + \sqrt{\sigma^2 + 4\alpha D_S})\lambda_i^+.$$

Recalling expressions of $\lambda_i^\pm$

$$\begin{cases} \lambda_i^- = \dfrac{\chi_i^N + \chi_i^S - \sigma}{D_i}, \\ \lambda_i^+ = \dfrac{\chi_i^N - \chi_i^S - \sigma}{D_i}, \end{cases}$$

we can write

$$c_i = 2D_S(\sigma - \sqrt{\sigma^2 + 4\alpha D_S})\left\{\frac{\chi_i^N - \sigma}{D_i} + \frac{\chi_i^S}{D_i}\right\} - 2D_S(\sigma + \sqrt{\sigma^2 + 4\alpha D_S})\left\{\frac{\chi_i^N - \sigma}{D_i} - \frac{\chi_i^S}{D_i}\right\}.$$

After simplification, we obtain

$$c_i = -4\frac{D_S}{D_i}(\chi_i^N - \sigma)\sqrt{\sigma^2 + 4\alpha D_S} + 4\frac{D_S}{D_i}\chi_i^S\sigma.$$

We now compute the functions h_i defined by:

$$h_i(\sigma) := \left(-\sigma - \sqrt{\sigma^2 + 4\alpha D_S} - 2D_S\lambda_i^-\right)\left(-\sigma + \sqrt{\sigma^2 + 4\alpha D_S} - 2D_S\lambda_i^+\right).$$

The expansion of h_i leads to

$$h_i(\sigma) = \left(-\sigma - \sqrt{\sigma^2 + 4\alpha D_S}\right)\left(-\sigma + \sqrt{\sigma^2 + 4\alpha D_S}\right) + 2D_S\lambda_i^+\left(\sigma + \sqrt{\sigma^2 + 4\alpha D_S}\right) + 2D_S\lambda_i^-\left(\sigma - \sqrt{\sigma^2 + 4\alpha D_S}\right) + 4D_S^2\lambda_i^+\lambda_i^-.$$

Straightforward computations give

$$h_i(\sigma) = -4\alpha D_S + 4\frac{D_S}{D_i}\sigma(\chi_i^N - \sigma) - 4\frac{D_S}{D_i}\chi_i^S\sqrt{\sigma^2 + 4\alpha D_S} + 4(\frac{D_S}{D_\rho^i})^2\left((\chi_i^N - \sigma)^2 - (\chi_i^S)^2\right).$$

We obtain after further simplifications

$$h_i(\sigma) = 4\frac{D_S}{D_i}\left(\sigma^2(\frac{D_S}{D_i} - 1) + \chi_i^N\sigma(1 - 2\frac{D_S}{D_i}) - \chi_i^S\sqrt{\sigma^2 + 4\alpha D_S} + \frac{D_S}{D_i}\left((\chi_i^N)^2 - (\chi_i^S)^2\right) - \alpha D_i\right).$$

3.5.3 Complete analysis of traveling pulses

In this part, the study of the dispersion relation presented briefly in the second section is detailed. We suppose the existence of traveling pulses, which implies the double exponential shapes of ρ_i as given in (3.12) with

$$\begin{cases} \lambda_i^- = \dfrac{\chi_i^N - \sigma + \chi_i^S}{D_\rho^i} > 0 \\ \lambda_i^+ = \dfrac{\chi_i^N - \sigma - \chi_i^S}{D_\rho^i} < 0 \end{cases} \Rightarrow \chi_i^N - \chi_i^S < \sigma < \chi_i^N + \chi_i^S$$

The non-nullity of the intersection of I_1 and I_2 in assumption (3.6) is the first condition to have the existence of traveling pulses. This gives the interval to which σ must belong. The dispersion relation will be studied in this interval. For σ in this interval, λ_i^- is positive and λ_i^+ negative, then

$$h_i(\sigma) = \left(\underbrace{-\sigma - \sqrt{\sigma^2 + 4\alpha D_S}}_{<0} - 2D_S\lambda_i^- \right) \left(\underbrace{-\sigma + \sqrt{\sigma^2 + 4\alpha D_S}}_{>0} - 2D_S\lambda_i^+ \right) < 0.$$

Moreover,

$$\chi_i^N - \sigma \in (-\chi_i^S, \chi_i^S) \Rightarrow (\chi_i^S)^2 - (\chi_i^N - \sigma)^2 > 0.$$

Therefore,

$$H(\sigma) = \frac{\chi_1^S D_1}{\chi_2^S D_2} \frac{(\chi_2^S)^2 - (\chi_2^N - \sigma)^2}{(\chi_1^S)^2 - (\chi_1^N - \sigma)^2} \frac{h_1(\sigma)}{h_2(\sigma)} > 0.$$

We recall the dispersion relation (3.7) obtained in the second section

$$\left((\sigma - \chi_1^N) + \chi_1^S \frac{\sigma}{\sqrt{\sigma^2 + 4\alpha D_S}} \right) + \frac{\phi_{red}}{1 - \phi_{red}} H(\sigma) \left((\sigma - \chi_2^N) + \chi_2^S \frac{\sigma}{\sqrt{\sigma^2 + 4\alpha D_S}} \right) = 0.$$

Denoting g_i the mapping $\sigma \longmapsto (\sigma - \chi_i^N) + \chi_i^S \frac{\sigma}{\sqrt{\sigma^2 + 4\alpha D_S}}$ defined over I_i. Then g_i is an increasing mapping

$$(g_i)'(\sigma) = 1 + \frac{4\alpha D_S}{(\sigma^2 + 4\alpha D_S)\sqrt{\sigma^2 + 4\alpha D_S}} > 0.$$

Moreover

$$g_i(\chi_i^N - \chi_i^S) = -\chi_i^S + \underbrace{\frac{\chi_i^N - \chi_i^S}{(\chi_i^N - \chi_i^S)^2 + 4\alpha D_S}}_{\leq 1} \chi_i^S < 0,$$

$$g_i(\chi_i^N + \chi_i^S) = \chi_i^S + \frac{\chi_i^N + \chi_i^S}{(\chi_i^N + \chi_i^S)^2 + 4\alpha D_S} \chi_i^S > 0.$$

By a monotonicity argument, there exists a unique $\sigma_i \in I_i$ such that $g_i(\sigma_i) = 0$. This corresponds to the individual speed of subpopulation i.
From the hypothesis that subpopulation 2 moves faster than subpopulation 1, we have $\sigma_1 < \sigma_2$ From the dispersion relation (3.7), $g_1(\sigma)$ and $g_2(\sigma)$ are of opposite signs. Thus, from the monotony of g_i, we deduce that

$$\sigma \in (\sigma_1, \sigma_2).$$

Putting together the two conditions, we get

$$\sigma \in (\sigma_1, \sigma_2) \cap (I_1 \cap I_2).$$

If the two following conditions hold

$$\begin{array}{r} \chi_2^N - \chi_2^S \notin I_1 \cap I_2 \\ \sigma_2 \notin I_1 \cap I_2 \end{array} \Rightarrow (\sigma_1, \sigma_2) \cap (I_1 \cap I_2) = (\sigma_1, \chi_1^N + \chi_1^S).$$

The dispersion relation (3.7) is equivalent to

$$G(\sigma) = \frac{\phi_{red}}{1 - \phi_{red}},$$

where G is defined by

$$G(\sigma) := -\frac{\chi_2^S D_2}{\chi_1^S D_1} \frac{g_1(\sigma)}{g_2(\sigma)} \frac{h_2(\sigma)}{h_1(\sigma)} \frac{(\chi_1^S)^2 - (\chi_1^N - \sigma)^2}{(\chi_2^S)^2 - (\chi_2^N - \sigma)^2}.$$

Since $\sigma_2 \notin (I_1 \cap I_2)$, we have $\chi_2^N + \chi_2^S \notin (I_1 \cap I_2)$ and the denominator of G does not vanish on $[\sigma_1, \chi_1^S + \chi_1^N]$. We conclude that the function G is a bounded and positive continuous function over $[\sigma_1, \chi_1^S + \chi_1^N]$. G attains its maximum over $[\sigma_1, \chi_1^S + \chi_1^N]$ denoted λ^* and we get

$$\frac{\phi_{red}}{1 - \phi_{red}} \leq \lambda^* \quad \Rightarrow \quad \phi_{red} \leq \phi_{red}^* = \frac{\lambda^*}{1 + \lambda^*}.$$

This leads to the following conclusion

— $\phi_{red} \leq \phi_{red}^* \Rightarrow$ Existence of a speed σ satisfying the dispersion relation (3.7)

— $\phi_{red} > \phi_{red}^* \Rightarrow$ Non-existence of a σ.

Well-balanced and asymptotic preserving scheme for kinetic models

Ce travail est réalisé en collaboration avec Min Tang de l'Institut de Sciences Naturelles de l'Université de Shanghai Jiao Tong. Il propose une méthode pour construire des schémas numériques de modèles cinétiques qui préservent à la fois le comportement en temps long et le comportement asymptotique (pour ε petit). Cette méthode a été appliquée aux modèles cinétiques de chimiotactisme et de transfert radiatif.
Article soumis.

Chapter 4

Well-balanced and asymptotic preserving scheme for kinetic models

Abstract

In this chapter, we propose a general framework for designing numerical schemes that have both well-balanced (WB) and asymptotic preserving (AP) properties, for various kinds of kinetic models. We are interested in two different parameter regimes, 1) When the ratio between the mean free path and the characteristic macroscopic length ε tends to zero, the density can be described by (advection) diffusion type (linear or nonlinear) macroscopic models; 2) When $\varepsilon = O(1)$, the models behave like hyperbolic equations with source terms and we are interested in their steady states. We apply the framework to three different kinetic models: neutron transport equation and its diffusion limit, the transport equation for chemotaxis and its Keller-Segel limit, and grey radiative transfer equation and its nonlinear diffusion limit. Numerical examples are given to demonstrate the scheme properties.

Contents

4.1 Introduction

Transport equations are important since they arise in many important applications, ranging from neutron transport, radiative transfer, semiconductor device simulation to E.coli chemotaxis. These models describe particles that travel freely for a certain distance and then change their directions by scattering,

interacting with background media or tumbling. The mean free path (the average distance a particle travels between two successive velocity changes) is an important parameter, when it is small compared to the typical length scales, various macroscopic model can be derived asymptotically or analytically [28, 91, 100].

Let the dimensionless parameter ε denote the ratio of the mean free path and the typical length scale. Numerical solutions to the transport equation are challenging when ε is small, since it requires the numerical resolution of the small scale. To develop a multi-scale scheme whose stability and convergence are independent of ε refers to the asymptotic preserving (AP) property. When $\varepsilon = O(1)$, the models behave like hyperbolic equations with source terms. When the source terms in the system become stiff, the usual numerical methods may give poor approximations to the steady state solutions [13, 92]. To maintain the steady states or to achieve them in the long time limit with an acceptable level of accuracy refers to the well balanced (WB) property.

In this work, we present a general framework to build schemes that have both properties. Two different kinetic models are considered to illustrate the idea of our proposed framework

Transport equation for Chemotaxis and its Keller-Segel limit
Bacteria undergo run and tumble process as mentioned in [72, 115, 116]. During the run phase, bacteria move along a straight line and change their directions during the tumble phase. This individual motion is called the velocity jump process and modeled by the so-called Othmer-Dunbar-Alt model [4, 99] which reads

$$\begin{cases} \partial_t f^\varepsilon + \dfrac{v}{\varepsilon}\cdot\nabla_x f^\varepsilon = \dfrac{1}{\varepsilon^2}\left(\dfrac{1}{|V|}\displaystyle\int_V \big(1+\varepsilon\phi(v'\cdot\nabla_x S)\big) f^\varepsilon(v')dv' - \big(1+\varepsilon\phi(v\cdot\nabla_x S)\big) f^\varepsilon(v)\right), \\ \partial_t S^\varepsilon - D\Delta S^\varepsilon + \alpha S^\varepsilon = \beta\rho^\varepsilon(x,t) := \dfrac{1}{|V|}\displaystyle\int_V f^\varepsilon dv. \end{cases} \tag{4.1}$$

Here $f^\varepsilon(x,v,t)$ is the amount of cells with velocity $v \in V$ (V is a sphere) at position x and time $t>0$, $\phi(u)$ is a decreasing function in u, $S^\varepsilon(x,t)$ is the concentration of the chemical substance. The parameters D, α, β are positive constants and ε is the ratio of the average run distance between two successive tumbles and the characteristic macroscopic length.

When $\epsilon \to 0$, the solution of (4.1) $f^\varepsilon(x,v,t)$ tends to $\rho^0(x,t)$, which is independent of v and satisfies the following Keller-Segel type equation [28, 43, 73, 85, 100] :

$$\begin{cases} \partial_t \rho = \dfrac{1}{3}\Delta\rho + \nabla\left(\Big(\dfrac{1}{|V|}\displaystyle\int_V v\phi(v\partial_x S)dv\Big)\rho\right), \\ \partial_t S - D\Delta S + \alpha S = \beta\rho. \end{cases} \tag{4.2}$$

Many numerical schemes have been proposed to study (4.1) [25, 52, 56].

Gray radiative transfer equation and its nonlinear diffusion limit:
The gray radiative transfer equation concerns photon transport and its interaction with the background material. It has wide application in astrophysics and inertial confinement fusion. The system for the radiative intensity I and the material temperature is

$$\begin{cases} \dfrac{1}{c}\partial_t I + \dfrac{1}{\varepsilon}v\cdot\nabla_x I = \dfrac{\sigma}{\varepsilon^2}\left(\dfrac{1}{|V|}acT^4 - I\right) + q(v), \\ C_v\partial_t T = \dfrac{\sigma}{\varepsilon^2}(\rho - acT^4), \end{cases} \tag{4.3}$$

where $\rho := \int_V I dv$, $\sigma(x,T)$ is the opacity and a, c, C_v are positive constants represent the radiation constant, light speed and heat capacity respectively. Similar to the chemotaxis case, when ε goes to

zero, the radiative intensity I approaches a Planckian at the local temperature $\frac{1}{|V|}acT^4$ and the photon temperature satisfies the following nonlinear diffusion equation:

$$a\partial_t T^4 + C_v \partial_t T = \nabla_x (\frac{ac}{3\sigma} \nabla_x T^4) + \int_V q\, dv. \tag{4.4}$$

It is important to preserve the steady state temperature distribution when $t \to \infty$.

A scheme for such problems is AP if it preserves the limiting equation (4.2) or (4.4) when $\varepsilon \to 0$ at the discrete level. AP schemes were first designed for the neutron transport equation to use unresolved cells to capture the macroscopic diffusion limit model [90, 91]. It has been successfully extended to a lot of applications, we refer to the review paper [78] for more discussions. In the literature, many papers have been devoted to build AP schemes for diffusion limit of the transport equations, for example [1, 25, 38, 95].

WB schemes are developed for hyperbolic equations with source terms. They have been proposed for various applications, including the Saint-Venant system with a source term, the non-isothermal nozzle flow equations, etc. By balancing the numerical flux with the source term, WB schemes can capture the steady state solutions exactly or with at least a second order accuracy [83]. A very limited list of such references includes but not limits to quasi-steady scheme [92], kinetic schemes [104, 133], central schemes [88], interface scheme [83], and other references there in [11].

Recently designing schemes that are either AP or WB, or have both properties attracts a lot of interests, both for kinetic chemotaxi model [56, 58, ?] and grey radiative transfer equation [55, 120]. Generally, it is very hard to have a scheme that have both properties and this is the goal of our present paper.

The paper is organized as follows: In section 2, the scheme framework composed of two steps: prediction step and steady problem step, is described and we show that the AP and WB properties can be achieved. Section 3 and 4 are respectively devoted to the construction of AP and WB schemes for the transport equation for chemotaxis and the gray radiative transfer equation. In the prediction step, we first extend the unified gas approach for neutron transport equation [95] to the chemotaxis model (4.1) and construct a new AP scheme for E.coli chemotaxis, while, for the gray radiative transfer equation, the scheme in [120] is employed. Then, in the steady problem step, we use the numerical results obtained by an AP scheme for the steady state equation of (4.1) or (4.3) to modify the numerical flux. The performances of the proposed schemes are presented in section 5 and we conclude with some discussion in section 6.

4.2 The scheme framework and its WB and AP properties

In this part, we introduce a general framework of designing WB and AP schemes, while the details of the discretization are given in section 3 and section 4. In the subsequent part of the paper, we consider the one dimensional problem and use a uniform grid with

$$x_i = i\Delta x, \quad i \in \mathbb{Z}, \qquad t^n = n\Delta t, \quad n \in \mathbb{N}.$$

Extensions to the two dimensional case are straightforward.

To illustrate the idea, we consider the following simplest one dimensional neutron transport equation

$$\partial_t f + \frac{1}{\varepsilon} v \partial_x f = \frac{\sigma_T}{\varepsilon^2} (\rho - f) - \sigma_a \rho + q, \tag{4.5}$$

with $\rho := \frac{1}{2}\int_{-1}^{1} f dv$. When $\varepsilon \to 0$, the solution of the above equation tends to ρ_0 which satisfies the following diffusion equation

$$\partial_t \rho_0 - \partial_x \big(\frac{1}{3\sigma_T} \partial_x \rho_0\big) + \sigma_a \rho_0 = q.$$

The formal derivation is standard by substituting the Chapman-Enskog expansion

$$f = f^{(0)} + \varepsilon f^{(1)} + \varepsilon^2 f^{(2)} + \cdots$$

into (4.5). When ε is small, the solution to (4.5) f can be approximated by

$$f = \rho^{(0)} - \frac{\varepsilon}{\sigma_T} v \partial_x \rho^{(0)} + O(\varepsilon^2). \tag{4.6}$$

We are interested in ε ranging from $O(1)$ to very small, the numerical scheme writes:

$$\begin{aligned} &\frac{f_i^{n+1} - f_i^n}{\Delta t} + \frac{v}{\varepsilon \Delta x}\left((1-\widetilde{\alpha}) f_i^n + \widetilde{\alpha} f_i^{n+1} - \hat{f}_{i-1/2}^n\right) = 0, \quad v > 0, \\ &\frac{f_i^{n+1} - f_i^n}{\Delta t} + \frac{v}{\varepsilon \Delta x}\left(\hat{f}_{i+1/2}^n - \left((1-\widetilde{\alpha}) f_i^n + \widetilde{\alpha} f_i^{n+1}\right)\right) = 0, \quad v < 0, \end{aligned} \tag{4.7}$$

where f_i^n are the approximation of the average $f(x, t^n)$ in the interval $(x_{i-1/2}, x_{i+1/2}) = (x_i - \Delta x/2, x_i + \Delta x/2)$ and

$$\widetilde{\alpha} = \min\left(1, \frac{\Delta t}{\varepsilon}\right). \tag{4.8}$$

The determination of $\hat{f}_{i+1/2}^n$ consists of two steps: the prediction step and the steady problem step.

Prediction step: The prediction step is to evolve the equation (4.5) for one time step by an AP scheme. Starting from f_i^n obtained from the nth iteration, the predictions $\widetilde{f}_i^{n+1}$ and $\widetilde{\rho}_i^{n+1} = \frac{1}{2}\int_{-1}^{1} f_i^{n+1} dv$ can be found by any scheme that is AP. The requirement that, when $\varepsilon \to 0$, the scheme preserves the diffusion limit at the discrete level can only be achieved when

$$\widetilde{f}_i^{n+1} \approx \widetilde{\rho}_i^{n+1} + O(\varepsilon) \tag{4.9}$$

and $\widetilde{\rho}_i^n$ is a discretization of the limiting diffusion equation. Here in this paper we use the unified gas approach developed in [95, 132, 120] for various kinetic models.

Steady problem step: The second step is devoted to the computation of the steady state problem. On each cell $[x_i, x_{i+1}]$, we solve the following stationary problem:

$$v \cdot \partial_x \hat{f} = \frac{\sigma_T}{\varepsilon}\left(\hat{\rho} - \hat{f}\right) - \varepsilon \sigma_a \hat{\rho} + \varepsilon q \tag{4.10}$$

together with inflow boundary conditions

$$\begin{cases} \hat{f}(x_i, v) = (1-\widetilde{\alpha}) f_i^n + \widetilde{\alpha} \widetilde{f}_i^{n+1}, & v > 0, \\ \hat{f}(x_{i+1}, v) = (1-\widetilde{\alpha}) f_{i+1}^n + \widetilde{\alpha} \widetilde{f}_{i+1}^{n+1}, & v < 0. \end{cases} \tag{4.11}$$

Here $\widetilde{f}_i^{n+1}$ is determined by the prediction step. Then $\hat{f}_{i+1/2}^n$ in (4.7) is given by the outflow of the above steady state problem in each cell such that

$$\hat{f}_{i+1/2}^n(v) = \hat{f}(x_{i+1}, v), \quad v > 0 \qquad \hat{f}_{i+1/2}^n(v) = \hat{f}(x_i, v), \quad v < 0. \tag{4.12}$$

First of all, when ϵ is at $O(1)$ or $\Delta x, \Delta t \ll \varepsilon$, i.e. $\widetilde{\alpha} = \Delta t/\varepsilon$, we show that (4.7) is a consist discretization for (4.5). We only consider the case when $v > 0$. Since $\hat{f}_{i-1/2}^n$ is obtained from the steady problem step, it can be approximated by

$$\begin{aligned} &(1 - \Delta t/\varepsilon) f_{i-1}^n + \Delta t/\varepsilon \widetilde{f}_{i-1}^{n+1} + \Delta x \partial_x \hat{f}^n(x_{i-1}, v) \\ =&(1 - \Delta t/\varepsilon) f_{i-1}^n + \Delta t/\varepsilon \widetilde{f}_{i-1}^{n+1} + \frac{\Delta x}{v}\Big(\frac{\sigma_T}{\varepsilon}\left(\hat{\rho}_{i-1}^n - \hat{f}_{i-1}^n\right) - \varepsilon \sigma_a \hat{\rho}_{i-1}^n + \varepsilon q\Big) \\ =&f_{i-1}^n + \frac{\Delta x}{v}\Big(\frac{\sigma_T}{\varepsilon}\left(\rho_{i-1}^n - f_{i-1}^n\right) - \varepsilon \sigma_a \rho_{i-1}^n + \varepsilon q\Big) + O(\Delta t^2) + \frac{\Delta x}{v} O(\Delta x). \end{aligned}$$

From the CFL condition, $\Delta t < \frac{\epsilon}{\max|v|}\Delta x$, (4.7) can then be approximated by

$$\frac{f_i^{n+1}-f_i^n}{\Delta t}+\frac{v}{\varepsilon\Delta x}\left(f_i^n-f_{i-1}^n\right)=\frac{\sigma_T}{\varepsilon^2}\left(\rho_{i-1}^n-f_{i-1}^n\right)-\sigma_a\rho_{i-1}^n+q+O(\Delta x).$$

The derivation for $v<0$ is the same.

Moreover, we have the following proposition:

Proposition 4.2.1. *When AP schemes are used in the prediction step and steady problem, the numerical scheme given in* (4.7) *has both WB and AP properties.*

Proof. **AP property:** When ε tends to zero, since AP schemes are used for the prediction step, we have (4.9). From (4.8), when ε is small, $\widetilde{\alpha}=1$, then the boundary conditions for the steady state problem (4.10) on each cell becomes

$$\hat{f}(x_i,v)=\widetilde{\rho}_i^{n+1}+O(\varepsilon),\quad v>0,\qquad \hat{f}(x_{i+1},v)=\widetilde{\rho}_{i+1}^{n+1}+O(\varepsilon),\quad v<0.$$

When ε is small, at the leading order, the boundary conditions for the steady state problem (4.10) are isotropic. Therefore we have

$$\hat{f}=\hat{\rho}+O(\varepsilon)$$

and

$$\hat{f}_{i+1/2}^n=\hat{f}(x_{i+1},v)=\widetilde{\rho}_{i+1}^{n+1}+O(\varepsilon),\quad v>0,$$
$$\hat{f}_{i+1/2}^n=\hat{f}(x_i,v)=\widetilde{\rho}_i^{n+1}+O(\varepsilon),\quad v<0.$$

Then from (4.7),

$$f_i^{n+1}=\frac{\hat{f}_{i-\frac{1}{2}}+\frac{\varepsilon\Delta x}{v\Delta t}f_i^n}{1+\frac{\varepsilon\Delta x}{v\Delta t}}=\hat{f}_{i-\frac{1}{2}}^n+O(\varepsilon)=\widetilde{\rho}_i^{n+1}+O(\varepsilon),\quad v>v_0,$$
$$f_i^{n+1}=\frac{\hat{f}_{i+\frac{1}{2}}-\frac{\varepsilon\Delta x}{v\Delta t}f_i^n}{1-\frac{\varepsilon\Delta x}{v\Delta t}}=\hat{f}_{i+\frac{1}{2}}^n+O(\varepsilon)=\widetilde{\rho}_i^{n+1}+O(\varepsilon),\quad v<-v_0.$$

with v_0 small positive value away from 0. Therefore, we get

$$\rho_i^{n+1}=\widetilde{\rho}_i^{n+1}+O(\varepsilon).$$

Since $\widetilde{\rho}_i^{n+1}$ satisfy the macroscopic equation at the discrete level, i.e. the leading order of f_i^{n+1} evolves according to a discrete diffusion equation, which gives the AP property of the proposed scheme (4.7).

WB property: To prove the WB property, we assume that at time t^n, $f_i^n=\overline{f}(x_i,v)$ where $\overline{f}(x,v)$ is the solution to the steady state equation (4.10) with given inflow boundary conditions on the whole computational domain. We need to show that when Δx, Δt are small enough, $f_i^{n+1}=f_i^n+O(\Delta x\Delta t)$. For the resolved case under consideration,

$$\widetilde{\alpha}=\frac{\Delta t}{\varepsilon}.$$

Since the scheme at the prediction step is consistent, consider the simplest first order method, we have

$$\widetilde{f}_i^{n+1}=f_i^n+O(\Delta x,\Delta t).$$

The inflow boundary conditions in (4.11) becomes

$$\begin{cases}\hat{f}(x_i,v)=(1-\widetilde{\alpha})f_i^n+\widetilde{\alpha}\widetilde{f}_i^{n+1}=f_i^n+O(\Delta x\Delta t),\quad v>0,\\ \hat{f}(x_{i+1},v)=(1-\widetilde{\alpha})f_{i+1}^n+\widetilde{\alpha}\widetilde{f}_{i+1}^{n+1}=f_{i+1}^n+O(\Delta x\Delta t),\quad v<0.\end{cases}$$

Since the steady state problem is solved in a cell of size Δx, by the simplest Taylor expansion, the out flow can be approximated by at least second order accuracy, so that

$$\hat{f}^n_{i+1/2} = \overline{f}(x_{i+1}, v) + O(\Delta x \Delta t, \Delta x^2), \quad v > 0;$$
$$\hat{f}^n_{i+1/2} = \overline{f}(x_i, v) + O(\Delta x \Delta t, \Delta x^2), \quad v < 0.$$

Thus, (4.7) yields

$$\begin{aligned} f_i^{n+1} &= \frac{\hat{f}_{i-\frac{1}{2}} + \frac{\varepsilon \Delta x}{v \Delta t} f_i^n}{1 + \frac{\varepsilon \Delta x}{v \Delta t}} = \overline{f}(x_i, v) + O(\Delta x \Delta t, \Delta x^2), \quad v > 0, \\ f_i^{n+1} &= \frac{\hat{f}_{i+\frac{1}{2}} - \frac{\varepsilon \Delta x}{v \Delta t} f_i^n}{1 - \frac{\varepsilon \Delta x}{v \Delta t}} = \overline{f}(x_i, v) + O(\Delta x \Delta t, \Delta x^2), \quad v < 0. \end{aligned} \tag{4.13}$$

Due to the CFL condition, $O(\Delta t) = O(\Delta x)$, the solution approximate the steady state $\overline{f}$ with a formally second order accuracy $O(\Delta x^2)$. □

Remark 4.2.2. *The framework in this section does not depend on specific AP methods for the time evolutionary problem and the steady state problem, we can choose any scheme in the literature that has been proved to be AP for various kinetic models.*

Remark 4.2.3. *The accuracy of preserving the steady state problem can be improved by using higher order method in space and time, or we can repeat once the steady problem step by replacing $\widetilde{f}_i^{n+1}$ from the prediction step by f_i^{n+1} obtained in* (4.13).

4.3 The chemotaxis kinetic model

In this section, we apply the framework in section 2 to the chemotaxis kinetic model (4.1). Two specific AP schemes are respectively chosen for the time evolutionary problem and steady state problem. We first extend the unified gas kinetic scheme (UGKS) in [95, 134, 132] to get an AP scheme for the time evolutionary problem, then solve the steady state equation by extending the scheme in [82] which was originally designed for the isotropic neutron transport equation. In [25], the authors have proposed AP schemes for the chemotaxis kinetic model, our approach is different. The details are described below.

As in [95], the UGKS is a finite volume approach of integrating (4.1) over $[x_{i-1/2}, x_{i+1/2}] \times [t^n, t^{n+1}] \times V$. Let

$$f_i^n = \frac{1}{\Delta x} \int_{x_{i-1/2}}^{x_{i+1/2}} f(x, v, t^n)\, dx, \qquad \rho_i^n = \frac{1}{|V|} \int_V f_i^n\, dv.$$

ρ_i^{n+1} and f_i^{n+1} are updated as follows

$$\frac{\rho_i^{n+1} - \rho_i^n}{\Delta t} + \frac{F^n_{i+1/2} - F^n_{i-1/2}}{\Delta x} = 0, \tag{4.14}$$

$$\begin{aligned} \frac{f_i^{n+1} - f_i^n}{\Delta t} + \frac{\Phi^n_{i+1/2} - \Phi^n_{i-1/2}}{\Delta x} &= \frac{1}{\varepsilon^2} \left(\rho_i^{n+1} - f_i^{n+1}\right) \\ &\quad + \frac{1}{\varepsilon} \left(\frac{1}{|V|} \int_V \phi(v\sigma_{i+1/2}) f_i^n - \phi(v\sigma_{i+1/2}) f_i^n \right). \end{aligned} \tag{4.15}$$

Here the numerical flux

$$\begin{aligned} \Phi^n_{i+1/2} &\approx \frac{1}{\varepsilon \Delta t} \int_{t^n}^{t^{n+1}} v f(x_{i+1/2}, v, t)\, dt, \\ F^n_{i+1/2} &\approx \frac{1}{|V|} \int_V \Big(\frac{1}{\varepsilon \Delta t} \int_{t^n}^{t^{n+1}} v f(x_{i+1/2}, v, t)\, dt \Big)\, dv. \end{aligned} \tag{4.16}$$

Since one dimensional problem is considered here, we use discrete ordinate method for the velocity discretization. The most crucial step for UGKS is to determine $\Phi^n_{i+1/2}$ and $F^n_{i+1/2}$. The details are as below:

4.3.1 Determine $\Phi^n_{i+1/2}$, $F^n_{i+1/2}$

In one dimensional space, the chemotaxis model (4.1) can be rewritten as follows:

$$\partial_t f^\varepsilon + \frac{1+\varepsilon\phi(v\partial_x S^\varepsilon)}{\varepsilon^2} f^\varepsilon + \frac{v}{\varepsilon}\partial_x f^\varepsilon = \frac{1}{\varepsilon^2}\mathcal{T}^1 f, \tag{4.17}$$

where $(\mathcal{T}^1 f)(x,t) := \dfrac{1}{|V|}\displaystyle\int_V \big(1+\varepsilon\phi(v\partial_x S)\big) f(x,v,t)dv$.

To approximate the flux $F^n_{i+1/2}$ in (4.16), we first approximate $\partial_x S$ by a piecewise constant function such that

$$\partial_x S \approx \partial_x S(x_{i+1/2}) := \sigma_{i+1/2}, \quad x \in [x_i, x_{i+1}).$$

It is important to note that $\sigma_{i+1/2}$ approximate $\partial_x S$ in the interval $[x_i, x_{i+1})$ while f^n_i is the density average over the cell $[x_{i-1/2}, x_{i+1/2})$. This choice is important to preserve the advection term in the limiting Keller-Segel model when ε becomes small.

On the interval $[x_i, x_{i+1})$, multiplying both sides of (4.17) by $\exp\left(\frac{(1+\varepsilon\phi(v\sigma_{i+1/2})}{\varepsilon^2}t\right)$ yields

$$\frac{d}{dt}\left[f(x+\frac{v}{\varepsilon}t,v,t)\exp\left(\frac{(1+\varepsilon\phi(v\sigma_{i+1/2})}{\varepsilon^2}t\right)\right] = \frac{\mathcal{T}^1 f(x,t)}{\varepsilon^2}\exp\left(\frac{(1+\varepsilon\phi(v\sigma_{i+1/2})}{\varepsilon^2}t\right).$$

Integrating the above equation over (t^n, t) yields

$$\begin{aligned} f(x_{i+1/2},v,t) = {} & f(x_{i+1/2}-\frac{v}{\varepsilon}(t-t^n),v,t^n)\exp\left(-\frac{(1+\varepsilon\phi(v\sigma_{i+1/2})}{\varepsilon^2}(t-t^n)\right) \\ & + \frac{1}{\varepsilon^2}\int_{t^n}^t \mathcal{T}^1 f(x_{i+1/2}-\frac{v}{\varepsilon}(t-s),s)\exp\left(-\frac{(1+\varepsilon\phi(v\sigma_{i+1/2})}{\varepsilon^2}(t-s)\right)ds. \end{aligned} \tag{4.18}$$

This is an exact expression for $f(x_{i+1/2},v,t)$ that will be used to determine $\Phi^n_{i+1/2}$, $F^n_{i+1/2}$ in (4.16). At this stage, we need to approximate $f(x,v,t^n)$ and $\mathcal{T}^1 f(x,t)$ on the right hand side of (4.18). f is approximated by a piecewise constant function and $\mathcal{T}^1 f$ by a piecewise linear function as follows:

$$f(x,v,t^n) = \begin{cases} f^n_i, & x < x_{i+1/2}, \\ f^n_{i+1}, & x > x_{i+1/2}, \end{cases}$$

$$\mathcal{T}^1 f(x,t) = \begin{cases} \mathcal{T}^1 f^n_{i+1/2} + \delta^L \mathcal{T}^1 f^n_{i+1/2}(x-x_{i+1/2}), & x < x_{i+1/2}, \\ \mathcal{T}^1 f^n_{i+1/2} + \delta^R \mathcal{T}^1 f^n_{i+1/2}(x-x_{i+1/2}), & x > x_{i+1/2}. \end{cases}$$

Here $\mathcal{T}^1 f^n_{i+1/2}$, $\delta^L \mathcal{T}^1 f^n_{i+1/2}$, $\delta^R \mathcal{T}^1 f^n_{i+1/2}$ are defined by:

$$\begin{cases} \mathcal{T}^1 f^n_{i+1/2} := \dfrac{1}{|V|}\displaystyle\int_{V^-}(1+\varepsilon\phi(v\sigma_{i+1/2}))f^n_{i+1} + \frac{1}{|V|}\int_{V^+}(1+\varepsilon\phi(v\sigma_{i+1/2}))f^n_i, \\ \delta^L \mathcal{T}^1 f^n_{i+1/2} := \dfrac{\mathcal{T}^1 f^n_{i+1/2} - \mathcal{T}^1 f^n_i}{\Delta x/2}, \\ \delta^R \mathcal{T}^1 f^n_{i+1/2} := \dfrac{\mathcal{T}^1 f^n_{i+1} - \mathcal{T}^1 f^n_{i+1/2}}{\Delta x/2}, \end{cases}$$

with $V^+ = V \cap \mathbb{R}^+$ and $V^- = V \cap \mathbb{R}^-$.
Substituting the above approximations into (4.18) yields an expression for $f(x_{i+1/2}, v, t)$ such that:
For $v > 0$,

$$\begin{aligned} f(x_{i+1/2}, v, t) &= f_i^n \exp\left(-\frac{(1+\varepsilon\phi(v\sigma_{i+1/2})}{\varepsilon^2}(t-t^n)\right) \\ &+ \frac{\mathcal{T}^1 f_{i+1/2}^n}{1+\varepsilon\phi(v\sigma_{i+1/2})}\left(1-\exp\left(-\frac{(1+\varepsilon\phi(v\sigma_{i+1/2})}{\varepsilon^2}(t-t^n)\right)\right) + v\varepsilon\frac{\delta^L\mathcal{T}^1 f_{i+1/2}^n}{(1+\varepsilon\phi(v\sigma_{i+1/2}))^2} \\ &\cdot\left[\left(1+\frac{1+\varepsilon\phi(v\sigma_{i+1/2})}{\varepsilon^2}(t-t^n)\right)\exp\left(-\frac{(1+\varepsilon\phi(v\sigma_{i+1/2})}{\varepsilon^2}(t-t^n)\right)-1\right], \end{aligned} \tag{4.19}$$

and for $v < 0$,

$$\begin{aligned} f(x_{i+1/2}, v, t) &= f_{i+1}^n \exp\left(-\frac{(1+\varepsilon\phi(v\sigma_{i+1/2})}{\varepsilon^2}(t-t^n)\right) \\ &+ \frac{\mathcal{T}^1 f_{i+1/2}^n}{1+\varepsilon\phi(v\sigma_{i+1/2})}\left(1-\exp\left(-\frac{(1+\varepsilon\phi(v\sigma_{i+1/2})}{\varepsilon^2}(t-t^n)\right)\right) + v\varepsilon\frac{\delta^R\mathcal{T}^1 f_{i+1/2}^n}{(1+\varepsilon\phi(v\sigma_{i+1/2}))^2} \\ &\cdot\left[\left(1+\frac{1+\varepsilon\phi(v\sigma_{i+1/2})}{\varepsilon^2}(t-t^n)\right)\exp\left(-\frac{(1+\varepsilon\phi(v\sigma_{i+1/2})}{\varepsilon^2}(t-t^n)\right)-1\right]. \end{aligned} \tag{4.20}$$

Then the flux $\Phi_{i+1/2}^n(v)$ in (4.16) can be approximated by

$$\begin{aligned} \Phi_{i+1/2}(v) &= Av f_{i+1}^n + Bv\mathcal{T}^1 f_{i+1/2}^n + Cv^2\delta^R\mathcal{T}^1 f_{i+1/2}^n, \quad \text{for } v<0, \\ \Phi_{i+1/2}(v) &= Av f_i^n + Bv\mathcal{T}^1 f_{i+1/2}^n + Cv^2\delta^L\mathcal{T}^1 f_{i+1/2}^n, \quad \text{for } v>0, \end{aligned} \tag{4.21}$$

where the coefficients $A(v,\varepsilon,\Delta t), B(v,\varepsilon,\Delta t), C(v,\varepsilon,\Delta t)$ can be determined explicitly such that

$$\begin{aligned} A(v,\varepsilon,\Delta t) :&= \frac{\varepsilon}{\Delta t\big(1+\varepsilon\phi(v\sigma_{i+1/2})\big)}\left(1-\exp\big(-\frac{1+\varepsilon\phi(v\sigma_{i+1/2})}{\varepsilon^2}\Delta t\big)\right), \\ B(v,\varepsilon,\Delta t) :&= \frac{1}{\varepsilon(1+\varepsilon\phi(v\sigma_{i+1/2}))} \\ &\quad - \frac{\varepsilon}{\Delta t(1+\varepsilon\phi(v\sigma_{i+1/2}))^2}\left(1-\exp\big(-\frac{1+\varepsilon\phi(v\sigma_{i+1/2})}{\varepsilon^2}\Delta t\big)\right), \\ C(v,\varepsilon,\Delta t) :&= \frac{2\varepsilon^2}{\Delta t(1+\varepsilon\phi(v\sigma_{i+1/2}))^3}\left(1-\exp\big(-\frac{1+\varepsilon\phi(v\sigma_{i+1/2})}{\varepsilon^2}\Delta t\big)\right) \\ &\quad - \frac{1}{(1+\varepsilon\phi(v\sigma_{i+1/2}))^2}\left(1+\exp\big(-\frac{1+\varepsilon\phi(v\sigma_{i+1/2})}{\varepsilon^2}\Delta t\big)\right). \end{aligned} \tag{4.22}$$

Furthermore, $F_{i+1/2}^n$ in (4.16) is given by

$$\begin{aligned} F_{i+1/2}^n = \frac{1}{|V|}\int_{V^-} Av f_{i+1}^n dv + \frac{1}{|V|}\int_{V^+} Av f_i^n dv + \frac{1}{|V|}\mathcal{T}^1 f_{i+1/2}^n \int_V vB dv \\ + \frac{1}{|V|}\delta^R\mathcal{T}^1 f_{i+1/2}^n \int_{V^-} Cv^2 dv + \frac{1}{|V|}\delta^L\mathcal{T}^1 f_{i+1/2}^n \int_{V^+} Cv^2 dv. \end{aligned} \tag{4.23}$$

and we complete the construction of the scheme. We can prove that the scheme is AP by employing similar approach as in [95].

4.3.2 AP property

In this part, we give a formal derivation of the AP property for the UGKS proposed in (4.14)–(4.15). When ε goes to zero, asymptotic expansions of A, B, C given in (4.22) read

$$A = O(\varepsilon), \qquad B = \frac{1}{\varepsilon} - \phi(v\sigma_{i+1/2}) + O(\varepsilon), \qquad C = -1 + O(\varepsilon).$$

The leading order term of (4.15) yields $f_i^{n+1} = \rho_i^{n+1} + O(\varepsilon)$ and we only need to show that (4.14) satisfies the equation for ρ in (4.2), at the discrete level. Suppose that $f_i^n = \rho_i^n + O(\varepsilon)$, then

$$\begin{cases} \mathcal{T}^1 f_{i+1/2}^n = \dfrac{1}{2}\left(\rho_i^n + \rho_{i+1}^n\right) + O(\varepsilon), \\ \delta^L \mathcal{T}^1 f_{i+1/2}^n = \dfrac{\rho_{i+1}^n - \rho_i^n}{\Delta x} + O(\varepsilon), \\ \delta^R \mathcal{T}^1 f_{i+1/2}^n = \dfrac{\rho_{i+1}^n - \rho_i^n}{\Delta x} + O(\varepsilon). \end{cases}$$

We deduce that the expansion of $F_{i+1/2}^n$ reads:

$$F_{i+1/2}^n = -\frac{\rho_i^n + \rho_{i+1}^n}{2\,|V|}\left(\int_V v\phi(v\sigma_{i+1/2})dv\right) - \frac{\rho_{i+1}^n - \rho_i^n}{3\Delta x} + O(\varepsilon).$$

Therefore,

$$\begin{aligned} &\frac{F_{i+1/2}^n - F_{i-1/2}^n}{\Delta x} \\ =& -\frac{\rho_{i+1}^n - 2\rho_i^n + \rho_{i-1}^n}{3(\Delta x)^2} + \Big(-\Big(\frac{1}{|V|}\int_V v\phi(v\sigma_{i+1/2})dv\Big)\frac{\rho_i^n + \rho_{i+1}^n}{2} \\ &\qquad + \Big(\frac{1}{|V|}\int_V v\phi(v\sigma_{i-1/2})dv\Big)\frac{\rho_i^n + \rho_{i-1}^n}{2}\Big) + O(\varepsilon). \end{aligned}$$

In the limit of $\varepsilon \to 0$, the discretization (4.14) becomes

$$\begin{aligned} \frac{\rho_i^{n+1} - \rho_i^n}{\Delta t} = &\frac{\rho_{i+1}^n - 2\rho_i^n + \rho_{i-1}^n}{3(\Delta x)^2} \\ &+ \left(\frac{1}{|V|}\left(\int_V v\phi(v\sigma_{i+1/2})dv\right)\frac{\rho_i^n + \rho_{i+1}^n}{2} - \frac{1}{|V|}\left(\int_V v\phi(v\sigma_{i-1/2})dv\right)\frac{\rho_i^n + \rho_{i-1}^n}{2}\right). \end{aligned}$$

which is a consistent discretization of the equation for ρ in (4.2). The proposed scheme is AP.

4.3.3 Steady state problem for the chemotaxis kinetic model

To solve the steady state problem, we start from the most used discrete ordinate method [29, 87]. The discrete ordinate method is to discretize the velocity space $V = [-1, 1]$ by a quadrature set $\{\mu_m, \omega_m\}$ ($m \in V_m = \{-N, \cdots, -1, 1, \cdots, N\}$). In one dimensional case, the most used and well accepted quadrature is the Gaussian quadrature. In order to preserve the diffusion limit equation, the points μ_m and weights ω_m satisfy

$$\begin{aligned} &\mu_{-m} = -\mu_m, \quad \omega_{-m} = \omega_m, \quad m \in 1 \cdots N, \\ &\sum_m \omega_m = 2, \quad \sum_m \omega_m \mu_m^2 = \frac{2}{3}. \end{aligned}$$

The discrete ordinate method for the steady state chemotaxis kinetic model on each cell $[x_i, x_{i+1})$ writes

$$\mu_m \partial_x f_m = \frac{1}{2\varepsilon}\sum_{n\in V}\omega_n\left(1 + \varepsilon\phi(\mu_n\sigma_{i+1/2})\right)f_n - \frac{1}{\varepsilon}\left(1 + \varepsilon\phi(\mu_m\sigma_{i+1/2})\right)f_m, \quad m \in V_m. \tag{4.24}$$

This is a linear ODE system with constant matrix coefficient. Together with the inflow boundary conditions, the exact solution can be obtained analytically. We use the following procedure to construct the general solution on each interval $[x_i, x_{i+1})$. We seek eigenfunctions of the form

$$l_m \exp(-\frac{\zeta}{\varepsilon}x). \tag{4.25}$$

By substituting this form into (4.24), one obtains

$$\big[\big(1+\varepsilon\phi(\mu_m\sigma_{i+1/2})\big)-\mu_m\zeta\big]\, l_m = \frac{1}{2}\sum_{n\in V}\omega_n\big(1+\varepsilon\phi(\mu_m\sigma_{i+1/2})\big)\, l_m. \tag{4.26}$$

The above equation holds for all $m \in V_m$ which indicates that ζ is the eigenvalue of the matrix

$$E = U^{-1}\big(I-\frac{1}{2}W\big)\big(I+\varepsilon\phi(U\sigma_{i+1/2})\big). \tag{4.27}$$

Here $U = \mathrm{Diag}(\mu_m)_{m\in V_m}$ and $\phi(U\sigma_{i+1/2}) = \mathrm{Diag}\big(\phi(\mu_m\sigma_{i+1/2})\big)_{m\in V_m}$ are diagonal matrixes, W is a rank 1 matrix whose rows are $(\omega_m)_{m\in V_m}$. Due to (4.26), ζ is the root of

$$\frac{1}{2}\sum_{m\in V_m}\frac{\big(1+\varepsilon\phi(\mu_m\sigma_{i+1/2})\big)\omega_m}{1+\varepsilon\phi(\mu_m\sigma_{i+1/2})-\mu_m\zeta} = 1 \tag{4.28}$$

and the eigenvector associated to ζ can be given by

$$l_m = \frac{1}{1+\varepsilon\phi(\mu_m\sigma_{i+1/2})-\mu_m\zeta}, \qquad m\in V_m. \tag{4.29}$$

It is easy to check that when $\varepsilon \neq 0$, $\zeta = 0$ is a simple root if $\phi(u) = -\phi(-u)$. Besides if $\nu_m = \frac{1+\varepsilon\phi(\mu_m\sigma_{i+1/2})}{\mu_m}$ $(m \in V_m)$ are different from each other, since the sign of ν_m are determined by μ_m, the functional $\frac{1}{2}\sum_{m\in V_m}\frac{\big(1+\varepsilon\phi(\mu_m\sigma_{i+1/2})\big)\omega_m}{1+\varepsilon\phi(\mu_m\sigma_{i+1/2})-\mu_m\zeta}$ tends to plus or minus infinity when ζ approaches ν_m from left or right. Therefore, (4.28) has $2N$ simple roots when ε is away from zero. However when $\varepsilon \to 0$, E becomes $U^{-1}(I - W/2)$ whose eigenvalues admit a zero double root [29, 82]. The general solutions to (4.24) are different for these two different cases, we discuss them separately in the subsequent part.

Case I: If (4.28) has $2N$ different simple roots, we can find $2N$ linearly independent eigenfunctions of the form $l_m \exp(-\frac{\zeta}{\varepsilon}x)$. Then the general solution to (4.24) can be written as

$$f_m(x) = \sum_{\zeta_n<0} B^n l_m^n \exp\big(-\frac{\zeta_n}{\varepsilon}(x-x_{i+1})\big) + \sum_{\zeta_n>0} A^n l_m^n \exp\big(-\frac{\zeta_n}{\varepsilon}(x-x_i)\big),$$

The coefficients B^n, A^n can be determined by the inflow boundary conditions

$$\begin{cases} f_m(x_{i+1}) = f_m^R, & m<0,\\ f_m(x_i) = f_m^L, & m>0. \end{cases}$$

Then the outflows are given by

$$f_m(x_i) = \sum_{\zeta_n<0} B^n l_m^n \exp\big(\frac{\zeta_n}{\varepsilon}\Delta x\big) + \sum_{\zeta_n>0} A^n l_m^n, \quad m<0,$$

$$f_m(x_{i+1}) = \sum_{\zeta_n<0} B^n l_m^n + \sum_{\zeta_n>0} A^n l_m^n \exp\big(-\frac{\zeta_n}{\varepsilon}\Delta x\big), \quad m>0.$$

Case II: We consider the limiting case when $E = U^{-1}(I - W/2)$, the eigenvalues for this matrix have been proved in [82] to have the following propperty

Theorem 4.3.1. *The equation*

$$\frac{1}{2}\sum_{m\in V_m}\frac{\omega_m}{1-\mu_m\zeta}=1$$

has $2(N-1)$ *simple roots appear in positive/negative paris while* 0 *is a double root.*

We set the double zero eigenvalue ζ_N and ζ_{-N} and rearrange eigenvalues ζ_n from the lowest to the highest.

$$\zeta_{1-N}<\cdots<\zeta_{-1}<0<\zeta_1<\cdots<\zeta_{N-1}.$$

For eigenvalues different of zero, eigenfunctions are exponential functions as in (4.25). Let us find eigenfunctions corresponding to the zero eigenvalue. By using the same token as in [82], we are looking for solution of the form $\alpha_m x+\beta_m$.

Injecting $\alpha_m x+\beta_m$ into (4.24) gives two solutions

$$\frac{1}{1+\varepsilon\phi(\mu_m\sigma_{i+1/2})},\qquad \frac{x}{1+\varepsilon\phi(\mu_m\sigma_{i+1/2})}-\frac{\varepsilon\mu_m}{\big(1+\varepsilon\phi(\mu_m\sigma_{i+1/2})\big)^2}.$$

Finally the general solution of (4.24) writes

$$\begin{aligned}f_m(x)=&\frac{c_N}{1+\varepsilon\phi(\mu_m\sigma_{i+1/2})}+\frac{c_{-N}}{1+\varepsilon\phi(\mu_m\sigma_{i+1/2})}\big(x-\frac{\varepsilon\mu_m}{1+\varepsilon\phi(\mu_m\sigma_{i+1/2})}\big)\\&+\sum_{1\le|n|\le N-1}c_n l_m^n\exp\left(-\frac{\zeta_n}{\varepsilon}x\right),\end{aligned}$$

where c_n $(1\le|n|\le N)$ are constants to be determined by the boundary conditions. Since ε can become very small, overflow may occur when evaluating $\exp\big(-\xi_n x/\varepsilon\big)$. In order to have c_n at the same scale as $f_m(x)$, we rewrite the general solution in the interval (x_i,x_{i+1}) into

$$\begin{aligned}f_m(x)=&\frac{c_1}{1+\varepsilon\phi(\mu_m\sigma_{i+1/2})}+\frac{c_2}{1+\varepsilon\phi(\mu_m\sigma_{i+1/2})}\Big((x-x_i)-\frac{\mu_m\varepsilon}{1+\varepsilon\phi(\mu_m\sigma_{i+1/2})}\Big)\\&+\sum_{n<0}B^n l_m^n\exp\big(-\frac{\zeta_n}{\varepsilon}(x-x_{i+1})\big)+\sum_{n>0}A^n l_m^n\exp\big(-\frac{\zeta_n}{\varepsilon}(x-x_i)\big),\end{aligned}\tag{4.30}$$

with c_1,c_2,B^n,A^n constants. Then we can determine c_1,c_2,B^n,A^n by the inflow boundary condition, so that the outflow.

4.4 The radiative transport equation

For the radiative transport equation (4.3), the same as in the previous section, we can choose two specific AP schemes respectively for the time evolutionary problem and steady state problem. For the time evolutionary problem, the UGKS scheme proposed in [120] is employed, while similar discretization as in subsection 3.3 can be used to solve the steady state problem. We sketch the discretization used in [120] in the subsequent part and for more details and the proof of AP, one can refer to [120].

4.4.1 The AP UGKS for the grey radiative transport equation

The idea is to first introduce $\psi=acT^4$ and rewrite the system (4.3) into

$$\begin{cases}\dfrac{1}{c}\partial_t I+\dfrac{1}{\varepsilon}v\partial_x I=\dfrac{\sigma}{\varepsilon^2}\left(\dfrac{1}{|V|}\psi-I\right)+q(x,v),\\ \varepsilon^2\partial_t\psi=\beta(\psi)\sigma(\rho-\psi),\end{cases}\tag{4.31}$$

where $\rho := \int_V I dv$ is the total radiation intensity and β is a function of ψ given by

$$\beta(\psi) = \frac{4ac}{C_v}\left(\frac{\psi}{ac}\right)^{3/4}.$$

Then we take the integral with respect to v in (4.31) and get a system for ρ, ψ, with an advection term depending on $\int_V vI\,dv$. Similar as the UGKS for the chemotaxis model, the first step is to get a prediction for ρ^{n+1} by

$$\begin{cases} \rho_i^{n+1} = \rho_i^n + \dfrac{\Delta t}{\Delta x}\left(F_{i-1/2}^n - F_{i+1/2}^n\right) + \dfrac{\sigma c\Delta t}{\varepsilon^2}(\psi_i^{n+1} - \rho_i^{n+1}) + c\Delta t\displaystyle\int_V q_i dv, \\ \psi_i^{n+1} = \psi_i^n + \dfrac{\sigma\beta_i^{n+1}\Delta t}{\varepsilon^2}\left(\rho_i^{n+1} - \psi_i^{n+1}\right), \end{cases} \tag{4.32}$$

where

$$F_{i+1/2}^n := \frac{c}{|V|}\int_V \left(\frac{1}{\varepsilon\Delta t}\int_{t^n}^{t^{n+1}} vI(x_{i+1/2}, v, t)\,dt\right)dv, \quad q_i(v) := \frac{1}{\Delta x}\int_{x_{i-1/2}}^{x_{i+1/2}} q(x,v)dx.$$

After discretizing the velocity space by discrete-ordinate method, the numerical flux $F_{i-1/2}^n$ and source term are approximated by

$$\begin{aligned} F_{i-1/2}^n \approx{}& A\sum_{m=-N}^{N}\omega_m\mu_m(I_{i-1/2,m}^{n-}\mathbf{1}_{\mu_m>0} + I_{i-1/2,m}^{n+}\mathbf{1}_{\mu_m<0}) + \frac{2D}{3\Delta x}(\psi_i^{n+1} - \psi_{i-1}^{n+1}) \\ &+B\sum_{m=-N}^{N}\omega_m\mu_m^2(\delta_x I_{i-1,m}^n\mathbf{1}_{\mu_m>0} + \delta_x I_{i,m}^n\mathbf{1}_{\mu_m<0}) + |V|\,\varepsilon^2\frac{C}{\sigma}\sum_{m\in V_m}\omega_m\mu_m q_{i,m}, \\ \int_V q_i dv \approx{}& \sum_{m\in V_m}\omega_m q_{i,m} = \sum_{m\in V_m}\omega_m q_i(\mu_m). \end{aligned}$$

Here $\mathbf{1}_{\mu_m<0}$, $\mathbf{1}_{\mu_m>0}$ are the characteristic functions, $\delta_x I_{i,m}^n$ are the approximations to $\partial_x I(x_i, \mu_m, t^n)$ by the slope limiters and $I_{i-1/2,m}^{n\pm}$ are given by

$$I_{i-1/2,m}^{n-} = I_{i-1,m}^n + \frac{\Delta x}{2}\delta_x I_{i-1,m}^n, \quad I_{i-1/2,m}^{n+} = I_{i,m}^n - \frac{\Delta x}{2}\delta_x I_{i,m}^n.$$

The coefficients A, B, C, D depend on ε and Δt, which will be specified later.

After obtaining the macroscopic variables $\rho_i^{n+1}, \psi_i^{n+1}$ from (4.32), $I_{i,m}^{n+1}$ are computed by

$$I_{i,m}^{n+1} = I_{i,m}^n + \frac{\Delta t}{\Delta x}\left(\Phi_{i-1/2,m}^n - \Phi_{i+1/2,m}^n\right) + \frac{\sigma c\Delta t}{\varepsilon^2}\left(\frac{\psi_i^{n+1}}{|V|} - I_{i,m}^{n+1}\right) + c\Delta t q_{i,m}, \tag{4.33}$$

where $\Phi_{i-1/2,m}^n$ are given by

$$\begin{aligned} \Phi_{i-1/2,m}^n ={}& A\mu_m\left(I_{i-1/2,m}^{n-}\mathbf{1}_{\mu_m>0} + I_{i-1/2,m}^{n+}\mathbf{1}_{\mu_m<0}\right) + C\mu_m\psi_{i-1/2}^{n+1} \\ &+D\left(\mu_m^2\delta_x\psi_{i-1/2}^{n+1,L}\mathbf{1}_{\mu_m>0} + \mu_m^2\delta_x\psi_{i-1/2}^{n+1,R}\mathbf{1}_{\mu_m<0}\right) \\ &+B\left(\mu_m^2\delta_x I_{i-1,m}^n\mathbf{1}_{\mu_m>0} + \mu_m^2\delta_x I_{i,m}^n\mathbf{1}_{\mu_m<0}\right) \\ &+E\delta_t\psi_{i-1/2}^{n+1} + \frac{|V|\,\varepsilon^2 C}{\sigma}\mu_m q_{i,m}, \end{aligned}$$

with $\psi^{n+1}_{i+1/2}$, $\delta_x\psi^{n+1,R}_{i-1/2}$, $\delta_x\psi^{n+1,L}_{i-1/2}$, $\delta_t\psi^{n+1}_{i-1/2}$ being defined by

$$\psi^{n+1}_{i+1/2} = \frac{1}{2}(\psi^{n+1}_i + \psi^{n+1}_{i+1}). \qquad \delta_x\psi^{n+1,L}_{i-1/2} = \frac{\psi^{n+1}_{i-1/2} - \psi^{n+1}_{i-1}}{\Delta x/2},$$
$$\delta_t\psi^{n+1}_{i-1/2} = \frac{\psi^{n+1}_{i-1/2} - \psi^{n}_{i-1/2}}{\Delta t}, \qquad \delta_x\psi^{n+1,R}_{i-1/2} = \frac{\psi^{n+1}_{i} - \psi^{n+1}_{i-1/2}}{\Delta x/2}.$$

$\delta_x\psi^{n+1,L}_{i-1/2}$ and $\delta_x\psi^{n+1,R}_{i-1/2}$ are the same and we use different notations in order to be consistent with notations in [120]. In [120], different notations are used for $\delta_x\psi^{n+1,R}_{i-1/2}$ and $\delta_x\psi^{n+1,L}_{i-1/2}$ in order to consider different approximations for $\psi^{n+1}_{i-1/2}$. Some of them can lead to the case when $\delta_x\psi^{n+1,R}_{i-1/2}$ and $\delta_x\psi^{n+1,L}_{i-1/2}$ are different.

Let $\nu = \frac{c\sigma}{\varepsilon^2}$, the coefficients A, B, C, D, E appeared in all above formula are given by

$$\begin{aligned}
A &= \frac{c}{\varepsilon\Delta t\nu}\left(1 - \exp -(\nu\Delta t)\right),\\
C &= \frac{c^2\sigma}{|V|\,\varepsilon^3\Delta t\nu}\left(\Delta t - \frac{1}{\nu}(1 - \exp(-\nu\Delta t))\right),\\
D &= -\frac{c^3\sigma}{|V|\,\varepsilon^4\Delta t\nu^2}\left(\Delta t(1 + \exp(-\nu\Delta t)) - \frac{2}{\nu}(1 - \exp(-\nu\Delta t))\right),\\
B &= -\frac{c^2}{\varepsilon^2\nu^2\Delta t}\left(1 - \exp(-\nu\Delta t) - \nu\Delta t\exp(-\nu\Delta t)\right),\\
E &= \frac{c^2\sigma}{|V|\,\varepsilon^3\nu^3\Delta t}\left(1 - \exp(-\nu\Delta t) - \nu\Delta t\exp(-\nu\Delta t) - \frac{1}{2}(\nu\Delta t)^2\right).
\end{aligned}$$

4.4.2 Steady states for the radiative transport equation

We use the discrete ordinate method similar as in subsection 3.3 and refer to [55] for more details. The one dimensional discrete ordinate steady state problem for (4.31) reads

$$\mu_m\partial_x I_m = \frac{\sigma}{\varepsilon}(\sum_m \omega_m I_m - I_m) + \varepsilon q_m. \tag{4.34}$$

We use the same AP scheme as in subsection 3.3 and the above equation falls into the category of Case II. The only difference is that there exists a source term q_m, which can be easily built into the scheme by constructing an approximated particular solution. The general solution with source term q_m can be given by the summation of the general solution of the homogeneous problem and the approximated particular solution. Then the coefficients in front of the general solutions of the homogeneous equation can be determined by the continuity of solution at the cell edge. For more details, we refer to [82].

4.5 Numerical simulations

In this section, we apply the well-balanced and AP scheme designed in Section 2 to two test cases: kinetic chemotaxis and radiative transport models.

4.5.1 Chemotaxis model

The first simulation concerns the chemotaxis model (4.1). Simulations are set on $x \in [-1, 1]$ and $v \in [-1, 1]$. We take $N_v = 32$ points for the velocity and $N_x = 500$ points for the space discretization.

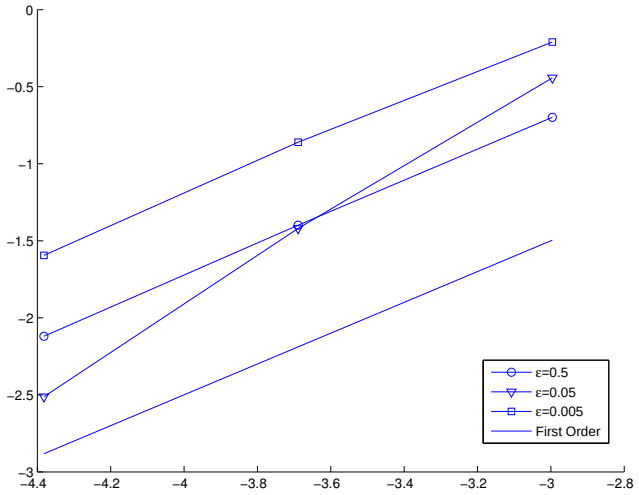

Figure 4.1: Convergence order with respect to Δx. Here the log-log plot of the mesh sizes with respect to the L^1 norm of the probability density error in all directions is displayed. The mesh sizes are 1/20, 1/40, 1/80, 1/160 and $e_{\Delta x} := \max_{x\in(-1,1)} \|f_{\Delta x}(x,t) - f_{2\Delta x}(x,t)\|_1$ are plotted for different ε.

Parameters in (4.1) are chosen as in [58] such that

$$\chi_S = 1, D = 15, \beta = 60, \alpha = 3.$$

and ϕ is of the form

$$\phi(x) = -\chi_S \tanh \frac{x}{\delta}, \qquad \text{with } \delta = 1.$$

We impose specular boundary conditions for f^ε and Dirichlet conditions for S^ε. The initial condition is composed of two bumps in x located at ± 0.65 such that

$$f^0(x,v) = 5\exp\left(-10(x-0.65)^2 - 10(x+0.65)^2\right)\exp\left(-20(v-0.5)^2 - 20(v+0.5)^2\right).$$

To ensure the stability of the numerical scheme, the time step Δt is chosen as follows

$$\Delta t = \begin{cases} \Delta x^2, & \text{for } \varepsilon < \Delta x^2, \\ \epsilon \Delta x, & \text{else.} \end{cases}$$

The requirement for the time step can be improved if the limiting discretization is implicit, the strategy of constructing an implicit limiting discretization has been discussed in [120]. The goal of our present paper is to illustrate the idea of the AP-WB framework and thus we keep using the simple scheme.

4.5.1.1 AP property

In order to verify the AP property of our scheme, we show that the convergence order of the scheme is independent of ε. In figure 4.1, we plot $e_{\Delta x} := \|f_{\Delta x}(t) - f_{2\Delta x}(t)\|_1$ with respect to Δx for different values of ε and uniform convergence with respect to ϵ can be observed numerically. This guarantees the AP property.

4.5.1.2 Model convergence in ε

As predicted by the theoretical analysis, when $\varepsilon \to 0$,

$$f^\varepsilon \to \rho^0 \mathbf{1}_{v \in V},$$

where ρ^0 is the solution to the limiting Keller-Segel equation. To verify the above convergence, the total densities ρ^ε are displayed in Figure 4.2 for different values of ε ranging from 10^{-1} to 10^{-6}. As a comparison, we plot the solution of the limiting model in Figure 4.2 and can observe that ρ^ε get closer to ρ^0 as ε goes to zero.

The convergence order in ε can be seen in Figure 4.3, where we have plotted $\|f^\varepsilon(x,v) - \rho^\varepsilon(x)\mathbf{1}_{v\in V}\|_2$ for different ε in the logarithm scale. The numerical results indicate that the order of convergence is close to 1.

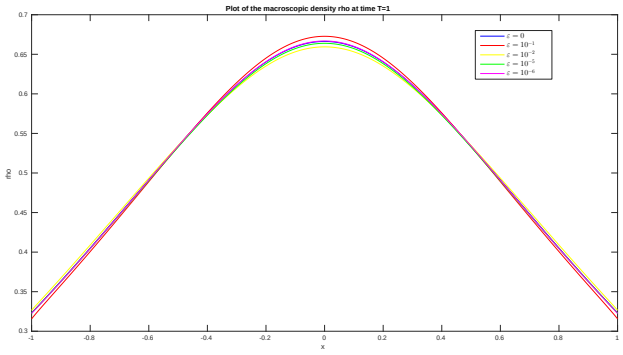

Figure 4.2: Plot of the macroscopic density for different values of ε. $\varepsilon = 0$ is the solution to the macroscopic Keller-Segel equation.

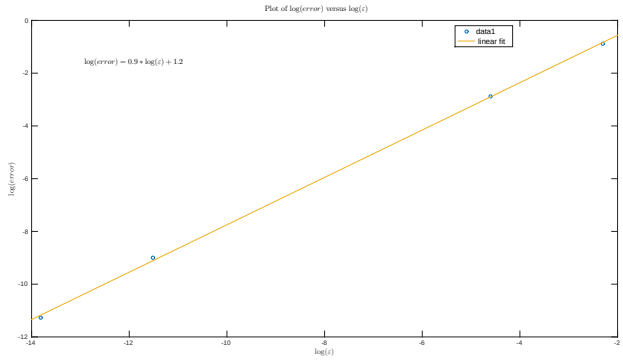

Figure 4.3: Convergence order in ε of the chemotaxi model (4.1).

4.5.1.3 WB property

In order to check the WB property, we calculate the long time behavior of the kinetic scheme for $\varepsilon = 1$. The steady state is characterised by the vanishing of the macroscopic flux J. A way to measure whether the steady state is reached is to look at the evolution of the residues r^n at a given time t^n defined

by

$$r^n := \left\| \sum_{m \in V} \omega_m \left| f^{n+1}(\mu_m) - f^n(\mu_m) \right| \right\|_2 .$$

Figure 4.4 shows the decrease of the residues and its stabilization when the steady state is reached. In addition, the flux J is of order Δx^2 at this steady state as displayed in Figure 4.5.

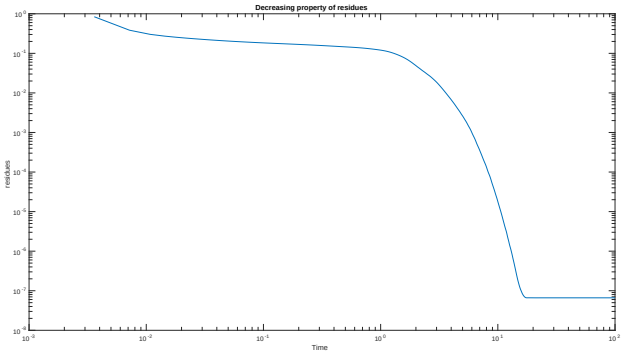

Figure 4.4: The evolution of residues with respect to time.

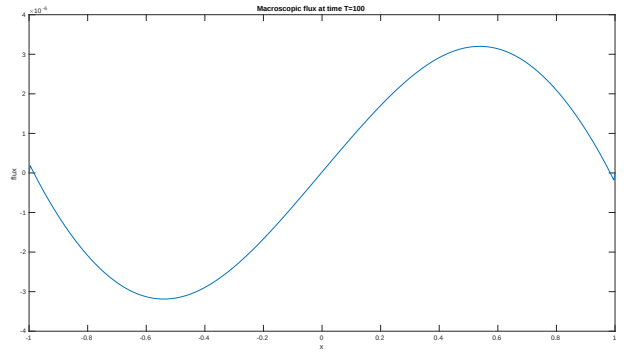

Figure 4.5: The macroscopic flux J at time $T = 100$.

4.5.2 Test case 2 : Radiative transport

We consider the radiative transport equation (4.3) on $x \in [0, 1]$ and $v \in [-1, 1]$. The source term q is given by

$$q(x, v) = v\,|v| + \sigma x \left(|v| - \frac{1}{2} \right). \tag{4.35}$$

When $\varepsilon = 1$, we can have analytical nonzero steady state for this choice of $q(x, v)$. Though $q(x, v)$ in (4.35) can take negative values, which is non-physical, it can be used to test the scheme performance. We use uniform grids in x with $N_x = 400$ and 32 Gaussian quadrature for the velocity space. The parameters are set to be

$$\sigma = 1, a = 0.01372, c = 29.98, C_v = 0.01.$$

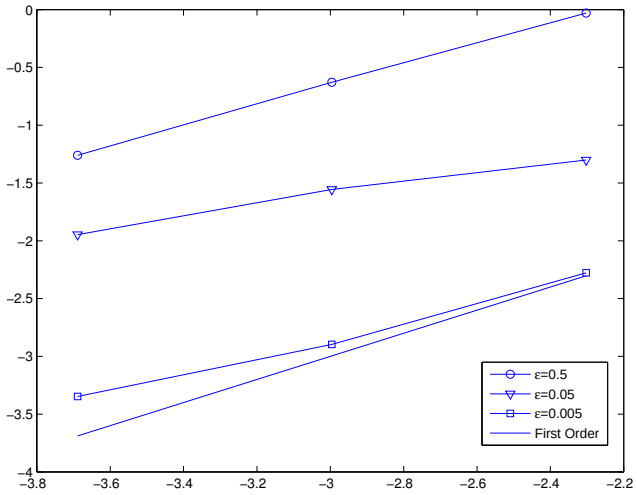

Figure 4.6: Convergence order with respect to Δx. Here the log-log plot of the mesh sizes with respect to the L^1 norm of the probability density error in all directions is displayed. The mesh sizes are 1/10, 1/20, 1/40, 1/80 and $e_{\Delta x} := \max_{x\in(0,1)} \|I_{\Delta x}(x,t) - I_{2\Delta x}(x,t)\|_1$ are plotted for different ε.

For I, Dirichelet boundary condition on the left and specular reflection on the right are prescribed. To guarantee the stability, the time step is given by

$$\Delta t = \begin{cases} 0.95\dfrac{\Delta x^2}{c}, & \text{for } \varepsilon < 0.95\frac{\Delta x}{c}, \\ 0.95\varepsilon\dfrac{\Delta x}{c}, & \text{else.} \end{cases}$$

4.5.2.1 AP property

In this part, we show that the convergence order of the scheme is independent of ε. In Figure 4.7, we plot $e_{\Delta x} := \max_{x\in(0,1)} \|I_{\Delta x}(x,t) - I_{2\Delta x}(x,t)\|_1$ with respect to Δx for different values of ε. Uniform convergence can be observed which confirms the AP property of the scheme.

4.5.2.2 Model convergence with respect to ε

The theoretical analysis indicates that

$$I^\varepsilon \to \frac{\psi^0}{2}\mathbf{1}_{v\in V}, \quad \varepsilon \to 0,$$

where $\psi^0 = ac(T^0)^4$ and T^0 is the solution to the limiting equation (4.4). To verify the above convergence, the total densities ρ^ε are displayed in Figure 4.7 for different values of ε ranging from 10^{-1} to 10^{-6}. As a comparison, we plot the solution of the limiting model in Figure 4.2 and can observe that I^ε get closer to $\psi^0/2$ as ε goes to zero.

The convergence order in ε can be seen in Figure 4.8, where we have plotted $\|I^\varepsilon(x,v) - \rho^\varepsilon \mathbf{1}_{v\in V}\|_2$, for different ε in the logarithm scale. The numerical results indicate that the order of convergence is close to 0.6.

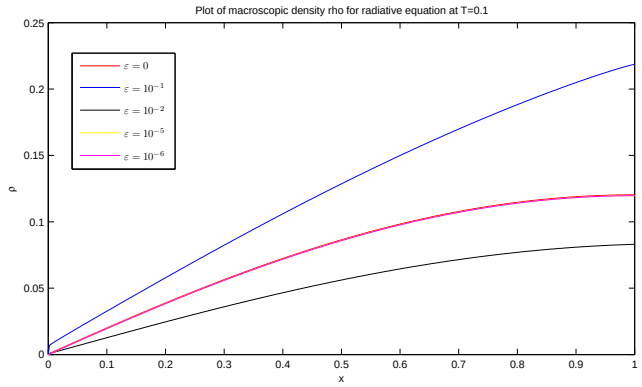

Figure 4.7: Total density for different values of ε. $\varepsilon = 0$ corresponds to the limiting nonlinear diffusion model (4.4).

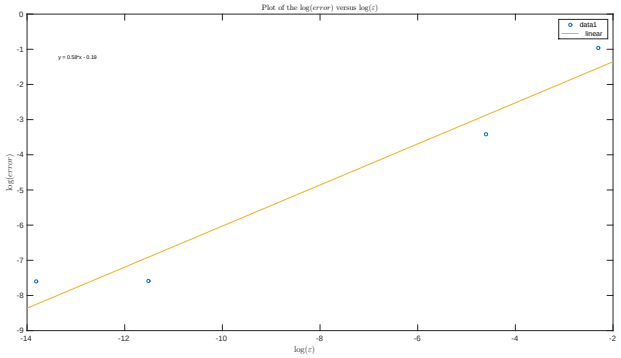

Figure 4.8: Convergence order in ε of the grey radiative transport model (4.3).

4.5.2.3 WB property

For the source term q as in (4.35), when $\varepsilon = 1$, the steady state is given by

$$I(x, v) = |v|x, \quad \rho = x.$$

The time evolution of the residues r^n is given in Figure 4.9, it decrease and stabilize at $T = 1$. In Figure 4.10, the captured steady state is plotted.

4.6 Conclusion

A general framework of developing AP and WB schemes is proposed in this paper. Two parameter regimes are considered: the (advection) diffusion type (linear or nonlinear) limit when $\varepsilon << 1$ and the long time behavior of the hyperbolic equations with source terms when $\varepsilon = O(1)$. The framework is composed of two steps. We first calculate a prediction with an AP scheme for the time evolutionary problem and then use the prediction to set up the inflow boundary conditions for the steady state problem in each cell. The steady state problem in each cell is solved by an AP scheme for the steady state equation, then the obtained outflows in each cell are used for modifying the numerical flux to achieve WB.

The details of the discretizations for transport equations for chemotaxis and gray radiative transfer are given. The numerical results in section 5 verify the AP and WB properties of our proposed scheme.

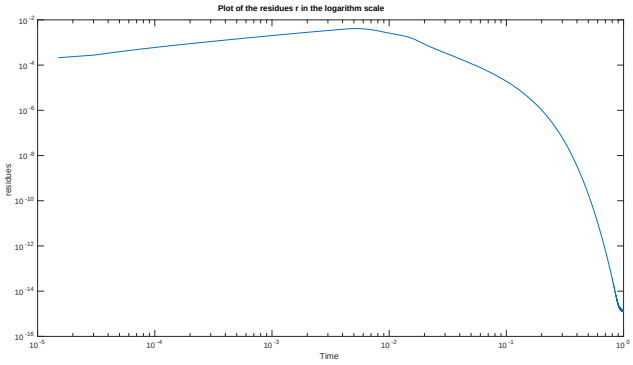

Figure 4.9: Evolution of residues with respect to time.

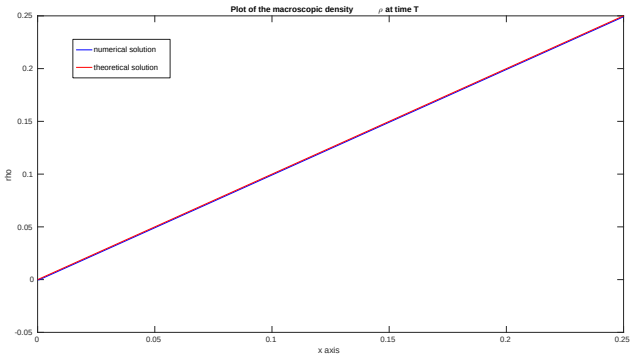

Figure 4.10: The total density of the steady state at time $T = 1$ when $\varepsilon = 1$.

In particular, the AP schemes for the time evolutionary transport equation for chemotaxis and the corresponding steady state equation are new.

One may argue about the computational cost of our proposed framework, the advantage is that, any AP schemes for the time evolutionary problem and steady state problem are applicable, thus we can choose those simple ones. First of all, the key principle underlying most WB schemes consists of using values constructed from a local discrete equilibrium, therefore if we are interested in unknown steady states, it is hard to avoid the steady problem step. On the other hand, in the prediction step, we can use those AP scheme that can implement the implicit stiff terms explicitly as in [49], or at least more efficient than using the Newton type solvers for nonlinear algebraic systems. (4.7) can be updated explicitly afterwards, the total computational cost is composed of some explicit calculations plus solving the steady state problems.

The proposed framework can be extended to the hyperbolic system with relaxations, we will pursue more applications in the future.

Annexes

Cette annexe présente le travail effectué durant le CEMRACS 2013 intitulé “Modélisation et simulation de systèmes complexes”. Ce travail a été réalisé en collaboration avec trois autres doctorants : Viviana Letizia, Nadezda Petrova, Rémi Sainct encadrés par Roland Duclous et Olivier Soulard, chercheurs au CEA.

Article publié dans *ESAIM Proceedings*, Vol. 48 (2015), pp 400-419
http ://dx.doi.org/10.1051/proc/201448019

Appendix A

Diffusion limit of the simplified Langevin PDF model in weakly inhomogeneous turbulence

Abstract

In this work, we discuss the modelling of transport in Langevin probability density function (PDF) models used to predict turbulent flows [109]. Our focus is on the diffusion limit of these models, i.e. when advection and dissipation are the only active physical processes. In this limit, we show that Langevin PDF models allow for an asymptotic expansion in terms of the ratio of the integral length to the mean gradient length. The main contribution of this expansion yields an evolution of the turbulent kinetic energy equivalent to that given by a $k-\varepsilon$ model. In particular, the transport of kinetic energy is given by a gradient diffusion term. Interestingly, the identification between PDF and $\overline{k}-\overline{\varepsilon}$ models raises a number of questions concerning the way turbulent transport is closed in PDF models. In order to validate the asymptotic solution, several numerical simulations are performed, with a Monte Carlo solver and also with a deterministic code.

Contents

Since the early work of Pope [109], the so-called probability density function (PDF) approach has proved to be an efficient tool for predicting turbulent flows. In this approach, one derives and solves a modelled transport equation for the one-point PDF of the fluctuating velocity field and, when necessary, of additional variables describing the state of the flow, such as concentration, temperature or density. In the modelling process of the flow one-point statistics, closures must be applied to the turbulent acceleration

as well as to molecular diffusion terms. Most of these closures yield a PDF transport equation of the Langevin type [109, 108, 110, 53]. In this work, we will only focus on this class of models.

While mostly used to predict turbulent reactive flows, the PDF approach has also demonstrated its utility for solving incompressible inert flows. In this context, Langevin PDF models have been shown [108] to be connected to simpler turbulent models which focus solely on the second-order one-point correlation tensor of the velocity field, also called Reynolds stress tensor. These Reynolds stress models (RSM) revert to the well known $k-\varepsilon$ model when turbulence is isotropic. The PDF/RSM equivalence encompasses most physical processes at work in incompressible flows, including production, non-linear redistribution and dissipation effects. However, strong differences exist in the way both approaches deal with the transport of the turbulent kinetic energy and of its anisotropy.

In RSM, turbulent transport is usually modelled by a gradient diffusion assumption. Many variants of this closure exist, but most are found to yield similar results in practical situations [6, 124]. In the PDF approach, the situation is different. The advection term appearing in the Navier-Stokes equations does not require any closure. In that sense, turbulent advection is often said to be treated "exactly" or "without assumption" [125, 53]. However, such statements might be somewhat misleading. Indeed, the overall process of turbulent transport is not exact since the statistics of the velocity field are affected by the Langevin closures used in the remaining parts of the PDF transport equation.

Thus, turbulent transport and Langevin closures are interacting in PDF models. This interaction is flow-dependent and cannot be made explicit in the general case. Yet, when non-equilibrium/production effects become negligible, the PDF equation is expected to degenerate and to yield a gradient diffusion formulation for the transport of Reynolds stresses. This is suggested by several works, for instance [108, 64, 6], which focus on triple velocity correlations and on their expression in the absence of production. As a consequence, in this diffusion limit, a PDF/RSM equivalence should exist for the turbulent transport term. Then, significant knowledge could be gained by comparing the two families of models, just as it was done in the homogeneous case by Pope [108].

However, the diffusion limit of PDF models has never been looked at thoroughly. The precise conditions under which it occurs have not been made explicit. Besides, the influence of dissipation processes are usually discarded while they are expected to play a significant role. Finally and more importantly, the study of the diffusion limit has been limited to considerations on the sole triple velocity correlations and not on the PDF itself.

Thus, the purpose of this work is to study the diffusion limit of PDF Langevin models and to explicit the connection with RSM models in that particular case. To this end, we consider a simplified setting in which diffusion and dissipation are the only active physical mechanisms. Besides, we restrict our attention to the simplified Langevin model described for instance in [110]. Then, we look for an asymptotic expansion of the Eulerian Langevin PDF equation in terms of the ratio of the integral length to the mean gradient length. The relevance of this expansion is verified on several simulations. Finally, its implications in terms of physical models are discussed.

A.1 Simplified Langevin PDF model applied to a turbulent zone

Throughout this work, we will consider a canonical turbulent flow consisting in a 1D slab of turbulence that decays and diffuses with time, and has no mean velocity. This flow is sketched in Figure A.1 and will be referred to as turbulent zone (TZ). The inhomogeneous direction is denoted by x_1 and the length of the TZ by L_{TZ}. Our interest lies in finding the properties of the Eulerian PDF $f(\mathbf{u}; x_1, t)$ of the velocity field $\mathbf{u} = (u_1, u_2, u_3)$ at point x_1 and time t when modelled by the simplified Langevin model (SLM) [109]. The PDF f is defined as:

$$f(\mathbf{u}; x_1, t) = \overline{\delta(\boldsymbol{v}(\boldsymbol{x}, t) - \mathbf{u})} \quad ,$$

where $\boldsymbol{v}(\boldsymbol{x}, t)$ is the instantaneous value of the velocity field, δ is the Dirac delta function and where, for any quantity a, $\overline{a}$ represents the averaging operator. Note that the PDF f depends on x_1 instead

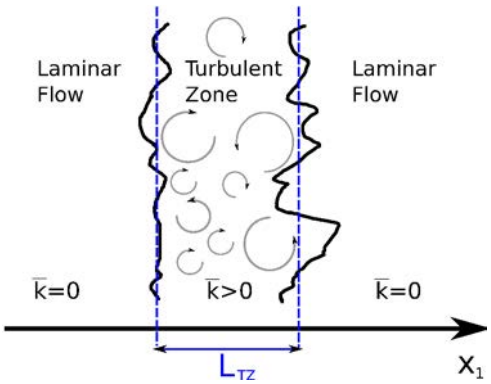

Figure A.1: Sketch of a turbulent zone as studied in this work.

of $\boldsymbol{x}$ because of the assumed statistical homogeneity of the flow in the directions x_2 and x_3. In the TZ configuration and with the SLM, the evolution of f is given by:

$$\frac{\partial f}{\partial t} + u_1 \frac{\partial f}{\partial x_1} = -\frac{\partial}{\partial u_j}\left[\left(\frac{\partial R_{1j}}{\partial x_1} - \frac{C_1}{2}\overline{\omega} u_j\right) f\right] + \frac{C_0}{2}\overline{\varepsilon}\frac{\partial^2 f}{\partial u_j \partial u_j} \ , \tag{A.1}$$

where C_0 and C_1 are model constants, $R_{ij} = \overline{u_i u_j}$ is the Reynolds stress tensor, $\overline{k}$ is the mean turbulent kinetic energy, $\overline{\omega}$ is the mean dissipation frequency and $\overline{\varepsilon}$ is the mean dissipation rate. Note the presence of the gradient of the Reynolds stress tensor in the right-hand side of Equation (A.1). This is due to the fact that the mean velocity is null and that the first moment of f is zero: $\int u_i f(\mathbf{u}; x_1, t) d\mathbf{u} = 0$ (see eq. (12.19) in [110]). The Reynolds stress tensor R_{ij} and $\overline{k}$ are obtained directly from the PDF by the relations:

$$\overline{k}(x_1,t) = \frac{1}{2} R_{ii}(x_1,t) = \frac{1}{2}\overline{u_i u_i}(x_1,t) \quad \text{and} \quad R_{ij}(x_1,t) = \overline{u_i u_j}(x_1,t) = \int_{\mathbb{R}^3} u_i u_j f(\mathbf{u}; x_1, t) d\mathbf{u} \, . \tag{A.2}$$

In these expressions, the Einstein summation convention on indices is used. The mean dissipation rate and mean frequency are linked by the relation:

$$\overline{\omega}(x_1,t) = \frac{\overline{\varepsilon}(x_1,t)}{\overline{k}(x_1,t)} \, . \tag{A.3}$$

An additional equation for the dissipation is required to close the system. As in standard $\overline{k} - \overline{\varepsilon}$ models, this equation is obtained by direct analogy with the equation of $\overline{k}$. The evolution of $\overline{k}$ deduced from the PDF equation (A.1) is:

$$\frac{\partial \overline{k}}{\partial t} + \frac{\partial}{\partial x_1}\left(\overline{u_1 k}\right) = -\overline{\varepsilon} \, . \tag{A.4}$$

The evolution of $\overline{\varepsilon}$ is then set to:

$$\frac{\partial \overline{\varepsilon}}{\partial t} + \frac{\partial}{\partial x_1}\left(C_\varepsilon \overline{\omega}\, \overline{u_1 k}\right) = -C_{\varepsilon_2} \overline{\omega}\, \overline{\varepsilon} \quad , \tag{A.5}$$

where C_ε and C_{ε_2} are model constants and where $\overline{u_i k}$ is the following triple velocity correlation:

$$\overline{u_i k} = \frac{1}{2}\overline{u_i u_p u_p} \, .$$

The values of the different constants appearing in the above equations are given in table A.1. These values are taken from the literature [109, 108, 110, 53].

C_0	C_1	C_ε	C_{ε_2}
$\frac{2}{3}(C_1-1)$	$[1.5,5]$	1	1.9

Table A.1: Model constants

Note that C_0 and C_1 are not independent: in order to ensure that $\overline{\varepsilon}$ is the dissipation rate of $\overline{k}$ one must have $C_0 = \frac{2}{3}(C_1 - 1)$. As noted in [108], the value of C_1 varies significantly in the literature. It mostly depends on whether the SLM is used to model both the non-linear redistribution of energy and the rapid contribution of the pressure gradient, or whether it is associated with an additional component modelling the rapid pressure part. In the former case, the value of C_1 is usually set to higher values, typically $C_1 = 4.15$. In the latter case, it is set to lower values, typically $C_1 = 1.8$. In the absence of production, as in the TZ case considered here, there is no rapid pressure term and both low and high values of C_1 are acceptable.

A.2 Weakly inhomogeneous limit and diffusion regime

A.2.1 Main assumption

Two main lengths characterize the turbulent field in the TZ configuration, the integral length ℓ and the gradient length L. They are respectively defined as:

$$\ell = \frac{\overline{k}^{3/2}}{\overline{\varepsilon}} \quad \text{and} \quad L = \left[\frac{1}{\overline{k}}\frac{\partial \overline{k}}{\partial x_1}\right]^{-1} .$$

The integral length ℓ is representative of the size of the turbulent eddies present in the turbulent zone, while L measures the inhomogeneity of the turbulent field. Its maximum is expected to be roughly on the order of the turbulent zone size L_{TZ}.

We now make the assumption that the flow is weakly inhomogeneous, i.e. that turbulent eddies are much smaller than L. More precisely, we assume that:

$$\frac{\ell}{L} \leq \epsilon_a \ll 1 \quad , \tag{A.6}$$

where ϵ_a is a constant. Anticipating on a configuration where the PDF remains close to a Gaussian, this assumption can be incorporated in Equations (A.1) and (A.5) by introducing a rescaled spatial coordinate:

$$z = \frac{x_1}{\epsilon_a} .$$

With this definition, Equations (A.1) and (A.5) can be rewritten as:

$$\frac{\partial f}{\partial t} + \epsilon_a u_1 \frac{\partial f}{\partial z} = -\frac{\partial}{\partial u_j}\left[\left(\epsilon_a \frac{\partial R_{1j}}{\partial z} - \frac{C_1}{2}\overline{\omega} u_j\right) f\right] + \frac{C_0}{2}\overline{\varepsilon}\frac{\partial^2 f}{\partial u_j \partial u_j} \quad , \tag{A.7}$$

$$\frac{\partial \overline{\varepsilon}}{\partial t} + \epsilon_a \frac{\partial}{\partial z}\left(C_\varepsilon \overline{\omega}\, \overline{u_1 k}\right) = -C_{\varepsilon_2}\overline{\omega}\,\overline{\varepsilon} . \tag{A.8}$$

A.2.2 Asymptotic expansion

We look for a solution of Equations (A.7) and (A.8) as an expansion of the small parameter ϵ_a:

$$f = f^{(0)} + \epsilon_a f^{(1)} + \epsilon_a^2 f^{(2)} + \dots , \tag{A.9}$$

$$\overline{\varepsilon} = \overline{\varepsilon}^{(0)} + \epsilon_a \overline{\varepsilon}^{(1)} + \epsilon_a^2 \overline{\varepsilon}^{(2)} + \dots , \tag{A.10}$$

where we impose $\int_{\mathbb{R}^3} f^{(0)}(\mathbf{u};z,t)d\mathbf{u} = 1$ and $\forall i \geq 1, \int_{\mathbb{R}^3} f^{(i)}(\mathbf{u};z,t)d\mathbf{u} = 0$, without loss of generality. The zeroth order of the expansion for f obeys the following Fokker-Planck equation:

$$\frac{\partial f^{(0)}}{\partial t} = \frac{\partial}{\partial u_j}\left[\frac{C_1}{2}\overline{\omega}^{(0)}u_j f^{(0)}\right] + \frac{C_0}{2}\overline{\varepsilon}^{(0)}\frac{\partial^2 f^{(0)}}{\partial u_j \partial u_j}$$

with $\overline{\omega}^{(0)} = \overline{\varepsilon}^{(0)}/\overline{k}^{(0)}$. Besides, the zeroth order kinetic energy and its dissipation evolve according to:

$$\frac{\partial \overline{k}^{(0)}}{\partial t} = -\overline{\varepsilon}^{(0)} \quad , \quad \frac{\partial \overline{\varepsilon}^{(0)}}{\partial t} = -C_{\varepsilon_2}\frac{{\overline{\varepsilon}^{(0)}}^2}{\overline{k}^{(0)}} \, .$$

From these equations, it can be shown that the long-time solution of the PDF $f^{(0)}$ is an isotropic Gaussian of variance $\sigma^2 = 2\overline{k}^{(0)}/3$. We hereafter assume that time is large enough so that this long-time solution is reached. Equivalently, we can assume that the initial condition of f is an isotropic Gaussian and that we look at the development of a perturbation around this initial state. In either case, we hereafter consider that:

$$f^{(0)}(\mathbf{u};z,t) = \frac{e^{-\frac{u_i u_i}{2\sigma^2}}}{(2\pi\sigma^2)^{3/2}} \quad \text{with} \quad \sigma^2 = \frac{2}{3}\overline{k}^{(0)} \, .$$

The derivation of the first order of the expansion is detailed in appendix .1. The central result is that, for large times, $f^{(1)}$ takes the following form:

$$f^{(1)} = C_g \frac{\sigma}{\overline{\omega}}\frac{\partial_z \sigma^2}{\sigma^2}\ \frac{u_1}{\sigma}\left(5 - \frac{u_i u_i}{\sigma^2}\right) f^{(0)} \qquad \text{with } C_g = \frac{1}{3C_1 + 2C_{\varepsilon_2} - 6} \, . \tag{A.11}$$

The first order perturbation $f^{(1)}$ does not contribute to the Reynolds stresses:

$$\overline{u_i u_j}^{(1)} = 0 \, .$$

However, it yields the main contribution to the third order moments. From the previous formula, one has:

$$\overline{u_i u_j u_k}^{(1)} = -2C_g \frac{\sigma^2}{\overline{\omega}}\frac{\partial \sigma^2}{\partial z}\left(\delta_{1i}\delta_{jk} + \delta_{1j}\delta_{ik} + \delta_{1k}\delta_{ij}\right) \, . \tag{A.12}$$

In particular, the flux of kinetic energy is given by:

$$\overline{u_i k}^{(1)} = -5C_g \frac{\sigma^2}{\overline{\omega}}\frac{\partial \sigma^2}{\partial z}\delta_{i1} \, . \tag{A.13}$$

The second order is not detailed here. It yields an anisotropic contribution to the Reynolds stresses and an even contribution to the PDF, with a dependency on the gradient of σ^2 and on its Laplacian.

A.2.3 Main result: approximate PDF solution in the weakly inhomogeneous regime

A.2.3.1 Main result

We now collect the zeroth and first orders of the expansion. Besides, we also go back to the original spatial coordinate $x_1 = \epsilon_a z$. Then, we obtain that:

$$\text{For } \frac{\ell}{L} \ll 1 \quad , \quad f(\mathbf{u};x_1,t) = \left[1 + \sqrt{2/3}C_g\, \ell \frac{1}{\overline{k}}\frac{\partial \overline{k}}{\partial x_1}\ \frac{u_1}{\sqrt{2\overline{k}/3}}\left(5 - \frac{u_i u_i}{2\overline{k}/3}\right)\right] \frac{e^{-u_i u_i/(4\overline{k}/3)}}{(4\pi\overline{k}/3)^{3/2}} \quad , \tag{A.14}$$

where $\overline{k}$ is solution of a $\overline{k}-\overline{\varepsilon}$-like system:

$$\text{For } \frac{\ell}{L} \ll 1 \quad , \quad \frac{\partial \overline{k}}{\partial t} = \frac{\partial}{\partial x_1}\left(C_k \frac{\overline{k}^2}{\overline{\varepsilon}} \frac{\partial \overline{k}}{\partial x_1} \right) - \overline{\varepsilon} \quad , \tag{A.15}$$

$$\frac{\partial \overline{\varepsilon}}{\partial t} = \frac{\partial}{\partial x_1}\left(C_\varepsilon C_k \frac{\overline{k}^2}{\overline{\varepsilon}} \left(\frac{\partial \overline{\varepsilon}}{\partial x_1} - \overline{k} \frac{\partial \overline{\omega}}{\partial x_1} \right) \right) - C_{\varepsilon_2} \overline{\omega}\, \overline{\varepsilon} \quad , \tag{A.16}$$

with:

$$C_k = \frac{20}{9} C_g = \frac{20}{9\,(3C_1 + 2C_{\varepsilon_2} - 6)} \, .$$

To obtain these expressions, we used the relations $\ell = \overline{k}^{3/2}/\overline{\varepsilon} = \sqrt{3/2}\,\sigma/\overline{\omega}$ and $\sigma^2 = 2\overline{k}/3$. We also injected relation (A.13) into the evolution Equations (A.4)-(A.5) of $\overline{k}$ and $\overline{\varepsilon}$.

Equations (A.14)-(A.16) are the main result of this work. They show that, in the weakly inhomogeneous regime, the simplified Langevin PDF model behaves as a standard $\overline{k}-\overline{\varepsilon}$ model. In particular, turbulent transport is given on first order by a diffusion term which coefficient depends explicitly on two model constants: C_1 and C_{ε_2}. The physical implications of this finding will be discussed in section A.4.

A.2.3.2 Comment on the domain of validity of the main result

The asymptotic expansion of the PDF eq. (A.14) and the ensuing $\overline{k}-\overline{\varepsilon}$ system (A.15)-(A.16) are valid in weakly inhomogeneous turbulence, i.e. for $\ell/L \ll 1$. Let us assume that this condition is indeed verified on the whole spatial domain. Then, when $C_\varepsilon = 1$, the $\overline{k}-\overline{\varepsilon}$ system (A.15)-(A.16) admits a self-similar solution, first found by Barenblatt & co-workers [7] and later by Cherfils & Harrison [31]. This solution is reached for asymptotically large times for arbitrary initial conditions. For initial conditions that are compatible with the self-similar solution, the self-similar regime is immediately reached. It is given by:

$$\overline{k}(x_1,t) = \overline{k}_0\,(1+t/\tau_0)^{-2+2\beta}\left(1-\left[x_1/\Lambda(t)\right]^2\right) \quad , \quad \varepsilon(x_1,t) = \overline{\varepsilon}_0\,(1+t/\tau_0)^{-3+2\beta}\left(1-\left[x_1/\Lambda(t)\right]^2\right) \, , \tag{A.17a}$$

$$\text{with } \Lambda(t) = \Lambda_0\,(1+t/\tau_0)^{\beta} \quad \text{and} \quad \beta = \frac{2C_{\varepsilon_2}-3}{3(C_{\varepsilon_2}-1)} \, . \tag{A.17b}$$

The values of $\overline{k}$ and $\overline{\varepsilon}$ at $t=0$ and $x_1=0$ are related to the two free parameters defining the initial length of the profile Λ_0 and the initial turbulent time τ_0:

$$\tau_0 = \frac{1}{C_{\varepsilon_2}-1}\frac{\overline{k}_0}{\overline{\varepsilon}_0} \quad , \quad \Lambda_0 = \sqrt{\frac{2C_k}{\beta(C_{\varepsilon_2}-1)}}\frac{\overline{k}_0^{3/2}}{\overline{\varepsilon}_0} \, . \tag{A.18}$$

From this analytical solution, we can compute the small parameter on which the asymptotic expansion is based: $\ell/L = (\overline{k}^{3/2}/\overline{\varepsilon})(\partial_{x_1}\overline{k}/\overline{k})$. We find that:

$$\frac{\ell}{L} = \sqrt{2\beta(C_{\varepsilon_2}-1)/C_k}\,\frac{x_1/\Lambda}{\sqrt{1-(x_1/\Lambda)^2}} \, .$$

This ratio is equal to 0 at the center of the mixing zone and grows to infinity at the edges of the mixing zone. The condition $\ell/L \ll 1$ is met only for:

$$\frac{|x_1|}{\Lambda} \ll \frac{x_{10}}{\Lambda} = \frac{1}{\sqrt{1+2\beta(C_{\varepsilon_2}-1)/C_k}} \quad ,$$

where the value of x_{10}/Λ is on the order of 1.

As a result, we deduce that the initial hypothesis of this reasoning, according to which the weakly inhomogeneous limit $\ell/L \ll 1$ is met on the whole spatial domain, cannot be fulfilled. Because of this,

differences will exist between the solution of the actual f and $\overline{\varepsilon}$ equations (A.1)-(A.5) and the solution of the approximate system (A.14)-(A.16), when applied to the whole domain, instead of being restricted to is domain of validity.

The question that follows is whether these differences will affect significantly the overall dynamical evolution of the mixing zone or not. In particular, it is important to know whether the evolution of $\overline{k}$ and $\overline{\varepsilon}$ obtained from the initial equations (A.1)-(A.5) differs substantially or not from the evolution of the approximate $\overline{k}$-$\overline{\varepsilon}$ model (A.15)-(A.16) applied to the whole domain. If the two remain close, the weakly inhomogeneous asymptotic expansion will not only yield a local approximation of the PDF and its moments, but also provide a global approximation of the evolution of the mixing zone.

The answer to these questions cannot be determined beforehand with the present analysis. Instead, numerical simulations are performed in the next section to give elements of discussion.

A.3 Numerical simulations

The purpose of the simulations is two-fold. First, when the parameter for the asymptotic expansion is small (eq. (A.6)), we want to corroborate numerically the analytical asymptotic expansion of the PDF (eq. (A.14)). Second, we would like to check whether or not the actual evolution of the mixing zone given by Equations (A.1) and (A.5) remains close to the approximate evolution given by System (A.14)-(A.16). Indeed, as noted in section A.2.3.2, the weakly inhomogeneous condition (A.6) and the ensuing approximation (A.14)-(A.16) cannot apply on the whole spatial domain, but fail close to the mixing zone edges.

To achieve those objectives, we propose two types of numerical reference solutions for the PDF equations (A.1) and (A.5). On the one hand, we consider a Eulerian Monte Carlo (EMC) solver. EMC methods have been introduced for scalar PDFs in [123, 113] and have been extended to include the velocity field in [119]. They are described in appendix .2. On the other hand, we use a direct deterministic solver based on finite volume approximations, described in appendix .3. Given the high number of dimensions of Equation (A.1), the computational cost of a deterministic method is too expensive. Hence, we decide to apply the deterministic method to a simplified version of Equations (A.1) and (A.5). This simplified system is described in section A.3.2.

In all simulations, we will restrict our attention to the case $C_\varepsilon = 1$ which allows for the analytical solution (A.17).

A.3.1 Eulerian Monte Carlo simulations

First, we solve Equations (A.1) and (A.5) with the Eulerian Monte Carlo (EMC) solver which principle is detailed in appendix .2. The parameters of the simulation are the following. The computational domain $[x_{min}, x_{max}]$ is set to $[-80, 80]$. It is discretized with $N_x = 256$ points. The number of stochastic fields is set to $N_f = 16000$. The initial conditions are set according to the expected solution (A.17):

$$\overline{k}(x_1, t=0) = \overline{k}_0 \left(1 - \left[\frac{x_1}{\Lambda_0}\right]^2\right) \quad , \quad \overline{\varepsilon}(x_1, t=0) = \overline{\varepsilon}_0 \left(1 - \left[\frac{x_1}{\Lambda_0}\right]^2\right) \quad ,$$

where we set the values $\Lambda_0 = 10$ and $\overline{k}_0 = 1.5$ and where the values of τ_0 and $\overline{\varepsilon}_0$ are given by Formula (A.18). Two calculations are done: one with $C_1 = 4.15$ and one with $C_1 = 1.8$. For $C_1 = 1.8$, one has $\tau_0 = 2.0$ and $\overline{\varepsilon}_0 = 0.84$ and for $C_1 = 4.15$, one has $\tau_0 = 3.6$ and $\overline{\varepsilon}_0 = 0.47$.

A.3.1.1 Validity of the asymptotic expansion

The first point we examine is whether the validity conditions of the asymptotic expansion are met and, if it is the case, whether the asymptotic expansion is indeed obtained. Figure A.2 shows the profiles

of ℓ/L at $t/\tau_0 = 10$. It can be seen that this ratio is $\ell/L = \mathcal{O}(1)$ at $1/2 \lesssim x/L_k(t) \lesssim 1$, and falls close to zero at $x/L_k(t) = 0$. It can also be seen that ℓ/L slowly goes back to zero at the edges of the mixing zone for $\ell/L_k(t) \geq 1$. The length L_k is defined as:

$$L_k(t) = \frac{3}{4} \frac{\int \overline{k}(x_1,t) dx_1}{\max_{x_1 \in \mathbb{R}} \left(\overline{k}(x_1,t)\right)} \, .$$

It is equal to $\Lambda(t)$ when $\overline{k}$ and $\overline{\varepsilon}$ obey the self-similar solution (A.17). While other definitions are possible, we will hereafter consider that L_k defines the size of the mixing zone: $L_{TZ} = L_k$.

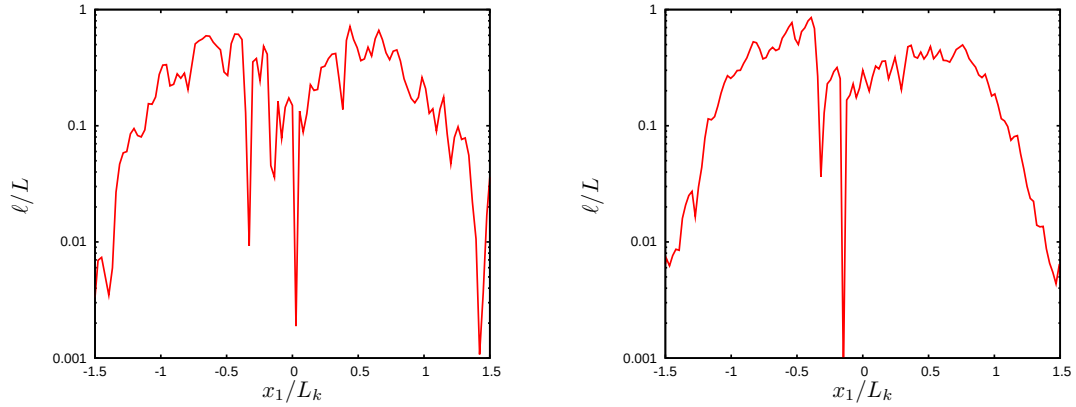

(a) $C_1 = 1.8$ (b) $C_1 = 4.15$

Figure A.2: ℓ/L as a function of x_1/L_k at time $t/\tau_0 = 10$

The estimate of the PDF obtained from the EMC code is too noisy to be compared directly to the analytical form (A.14). Direct comparisons will be made with the deterministic code. However, we can compare predicted and computed moments. In particular, Figure A.3 shows a comparison of the third order moment $\overline{u_1 k}$ against its predicted value given by Equation (A.13). More precisely, Figure A.3 shows the quantity:

$$\Delta F = \frac{\left| \overline{u_1 k} + C_k \frac{\overline{k}^2}{\overline{\varepsilon}} \frac{\partial \overline{k}}{\partial x_1} \right|}{\overline{k}^{3/2}}$$

The main observation is that predicted and computed third order moments are close to one another in the central part of the mixing zone, approximately for $|x_1|/L_k \leq 0.5$. Their difference is maximum for $|x_1|/L_k \approx 1$ and decreases slowly beyond this point. These observations are in agreement with the expected domain of validity of the asymptotic expansion, as commented from Figure A.2.

A.3.1.2 Evolution of the mixing zone

We now turn our attention to the question asked at the end of section A.2.3.2: whether the evolution of $\overline{k}$ and $\overline{\varepsilon}$ differs substantially or not from the analytical prediction (A.17). To do so, we first assess the self-similarity of the solution. In addition to L_k, we introduce the following two parameters:

$$\overline{k}_{max}(t) = \max_{x_1 \in \mathbb{R}} \left(\overline{k}(x_1,t)\right) \quad , \quad \overline{\varepsilon}_{max}(t) = \max_{x_1 \in \mathbb{R}} \left(\overline{\varepsilon}(x_1,t)\right) \, .$$

We first consider the time evolutions of the three parameters $\overline{k}_{max}(t)$, $\overline{\varepsilon}_{max}(t)$ and $L_k(t)$ and compare them against their predicted values given by the self-similar solution (A.17). To this end, we introduce

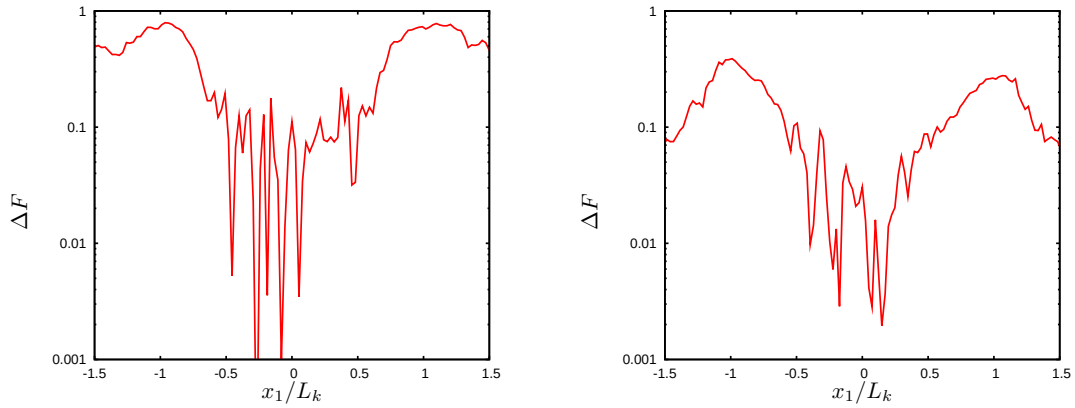

(a) $C_1 = 1.8$ (b) $C_1 = 4.15$

Figure A.3: ΔF as a function of x_1/L_k at time $t/\tau_0 = 10$

the three ratios R_k, R_ε and R_L defined by:

$$R_k = \frac{\overline{k}_{max}}{\overline{k}_0 \left(1 + {}^{t}/_{\tau_0}\right)^{-2+2\beta}} \quad , \quad R_\varepsilon = \frac{\overline{\varepsilon}_{max}}{\overline{\varepsilon}_0 \left(1 + {}^{t}/_{\tau_0}\right)^{-3+2\beta}} \quad , \quad R_L = \frac{L_k}{\Lambda_0 \left(1 + {}^{t}/_{\tau_0}\right)^{\beta}} \, .$$

If the solution remains close to the self-similar solution (A.17), then R_k, R_ε and R_L should become independent of time. Besides, given that the initial condition was chosen close to a self-similar solution, one should have $R_k = R_\varepsilon = R_L \approx 1$. A strict equality is not expected since the asymptotic expansion is not valid on the whole domain and since the initial condition is not fully coherent with the self-similar state. In particular, the initial PDF is a Gaussian, whereas the self-similar PDF deviates from Gaussianity.

The three ratios R_k, R_ε and R_L are displayed in Figure A.4. It can be seen that they indeed remain approximately constant and stay close to one for the two simulations respectively performed with $C_1 = 1.8$ and $C_1 = 4.15$.

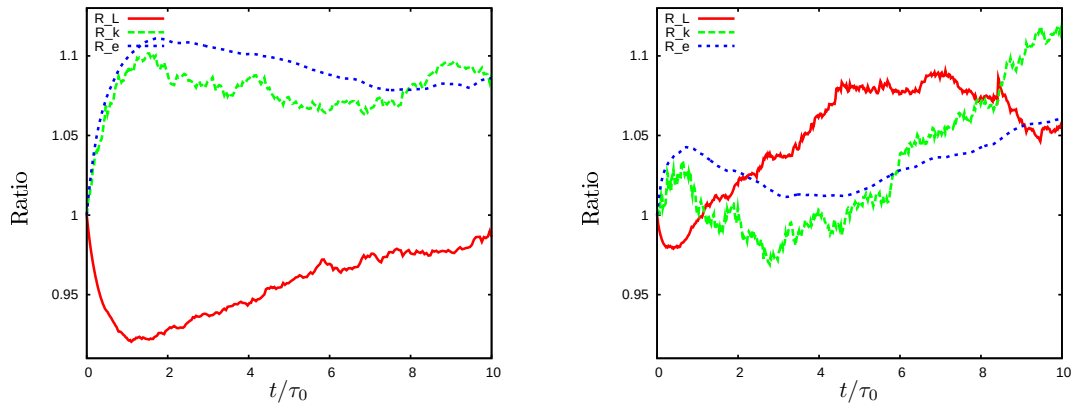

(a) $C_1 = 1.8$ (b) $C_1 = 4.15$

Figure A.4: Evolution of R_k, R_ε and R_L as a function of time.

We now consider the ratio $\overline{k}/k_{max}$ taken at different times is displayed in Figure A.5 as a function of x_1/L_k and for two values of C_1. It can be seen that the respective profiles of the two ratios fall approximately on a single curve. This indicates that $\overline{k}$ is close to a self-similar state. Besides, the collapsed curves

remain close to parabolas as predicted by solution (A.17). The main difference with this solution occurs at the edges of the turbulent zone : while Equation (A.17) predicts a compactly supported turbulent kinetic energy $\overline{k}$, the simulation yields a non-compact one. Compactly supported initial conditions indeed lead to compactly supported solutions for the system (A.15)-(A.16). The departure of the simulation results from the self-similar compactly supported solution can be explained by the high values of the expansion parameter ℓ/L at the edges of the TZ. At these locations, the asymptotic expansion ceases to be valid and $\overline{k}$ and $\overline{\varepsilon}$ cease to be governed by Equations (A.15)-(A.16).

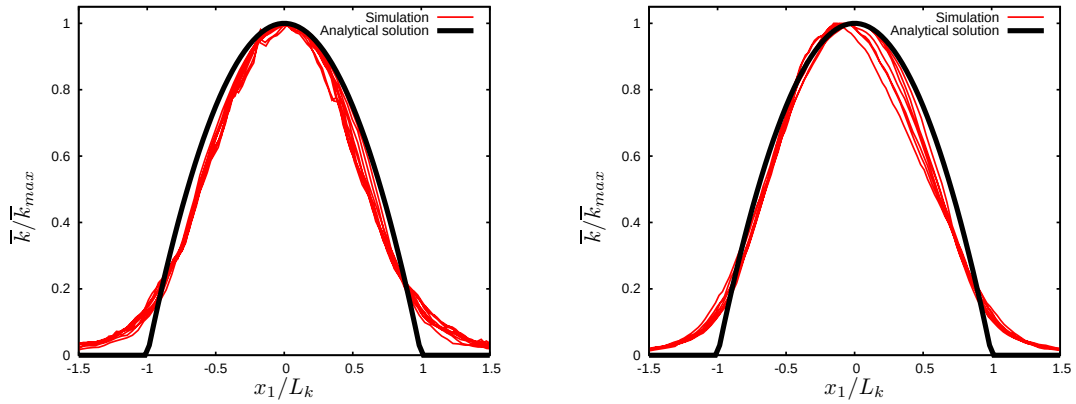

(a) $C_1 = 1.8$ (b) $C_1 = 4.15$

Figure A.5: $\overline{k}/\overline{k}_{max}$ as a function of x_1/L_k at different times from $t/\tau_0 = 2$ to $t/\tau_0 = 10$

The existence and properties of the self-similar solution arise in part from the approximation of the flux of kinetic energy given by Formula (A.13). This approximation has been checked directly in Figure A.3. Here, we would like make an additional comparison against the self-similar prediction corresponding to Equation (A.17). To this end, we introduce the non-dimensional flux :

$$F^*(x_1,t) = \frac{\overline{u_1 k}}{\overline{k}_{max}^{3/2}\sqrt{2\beta C_k(C_{\varepsilon_2}-1)}}\,.$$

According to Formula (A.13) and (A.17), F^* should be equal to $x_1/L_k(1-[x_1/L_k]^2)$. The comparison between the two functions is displayed at Figure A.6 for different times. It can be seen that both simulation and prediction are in good agreement in the central part of the mixing zone, for $x_1/L_k \in [-0.5, 0.5]$. Outside, the gradient diffusion assumption ceases to be relevant: the predicted flux of kinetic energy becomes much smaller than the simulated flux. This observation is consistent with the one made on the non-compactness of the $\overline{k}-\overline{\varepsilon}$ supports observed in Figure A.5.

As a conclusion, the simulation results appear to be in good agreement with the self-similar solution (A.17) of the $\overline{k}$-$\overline{\varepsilon}$ system (A.15)-(A.16). Thus, these simulations suggest that the asymptotic expansion of the PDF eq. (A.14) and the ensuing $\overline{k}-\overline{\varepsilon}$ system (A.15)-(A.16) offer a good estimate of the overall evolution of the mixing zone given by the full PDF system (A.1) and (A.5).

A.3.2 Deterministic finite volume simulations

The Eulerian Monte Carlo method has allowed to study some properties of the second and third order moments of the velocity field. However, its intrinsic noise is too high to directly study the PDF. To circumvent this deficiency, we propose to use a deterministic solver described in appendix .3.

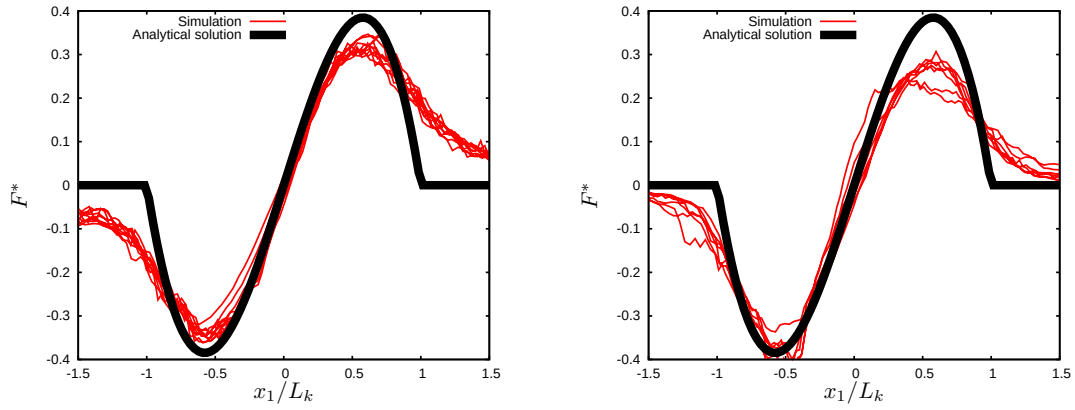

(a) $C_1 = 1.8$ (b) $C_1 = 4.15$

Figure A.6: F^* as a function of x_1/L_k at different times from $t/\tau_0 = 2$ to $t/\tau_0 = 10$.

A.3.2.1 Simplification of System (A.1)-(A.5)

The basic configuration studied hereafter is the same TZ configuration introduced in section A.1 and governed by Equations (A.1)-(A.5). As explained above, Equations (A.1)-(A.5) have a high number of dimensions : 1 in time and 4 in velocity and physical space. The computational cost of a deterministic method is too expensive so that we propose to simplify these equations in order to reduce their dimensionality. More precisely, we focus on the marginal PDF f_1 of u_1. By integrating Equation (A.1) over u_2 and u_3, one obtains that f_1 evolves as:

$$\frac{\partial f_1}{\partial t} + u_1 \frac{\partial f_1}{\partial x_1} = -\frac{\partial}{\partial u_1}\left[\left(\frac{\partial \overline{u_1^2}}{\partial x_1} - \frac{C_1}{2}\overline{\omega} u_1\right) f_1\right] + \frac{C_1 - 1}{2}\overline{\varepsilon}^* \frac{\partial^2 f_1}{\partial u_1 u_1} \ , \tag{A.19}$$

where $\overline{\varepsilon}^* = \frac{2}{3}\overline{\varepsilon}$ is the dissipation of $\overline{u_1^2}$. This equation is closed provided the evolution of $\overline{\varepsilon}^*$ is known in terms of the statistics of u_1. This is not the case of Equation (A.5) which is related to $\overline{k}$. Hence, we propose to simplify this equation. Namely, we assume that the Reynolds stresses are strictly isotropic. Then, the turbulent frequency can be related to $\overline{u_1^2}$ according to: $\overline{\omega} = \overline{\varepsilon}/\overline{k} = \overline{\varepsilon}^*/\overline{u_1^2}$. Besides, we assume that $\overline{u_1 u_i u_j}$ is also an isotropic tensor, which yields $\overline{u_1 k} = 3\overline{u_1^3}/2$. With these assumptions, one deduces from Equation (A.5) the following simplified evolution for $\overline{\varepsilon}^*$:

$$\frac{\partial \overline{\varepsilon}^*}{\partial t} + \frac{\partial}{\partial x_1}\left(C_\varepsilon \overline{\omega}\, \overline{u_1^3}\right) = -C_{\varepsilon 2}\overline{\omega}\, \overline{\varepsilon}^* \ . \tag{A.20}$$

Equations (A.19)-(A.20) are three dimensional and can be solved with the deterministic solver. They share the same properties as Equations (A.1)-(A.5) but present a slight variation in the weakly inhomogeneous limit. The limit of f_1 is, as expected, the integral of the limit of f (A.14) over u_2 and u_3:

$$f_1(u_1; x_1, t) = \frac{e^{-u_1^2/(2\overline{u_1^2})}}{\sqrt{2\pi \overline{u_1^2}}}\left(1 + C_g\left(\frac{1}{\sqrt{\overline{u_1^2}\,\overline{\omega}}}\frac{\partial \overline{u_1^2}}{\partial x_1}\right)\frac{u_1}{\sqrt{\overline{u_1^2}}}\left(3 - \frac{u_1^2}{\overline{u_1^2}}\right)\right) \ , \tag{A.21}$$

However, the value of $\overline{u_1^3}$ is not given by Formula (A.12) but by:

$$\overline{u_1^3} = -C_k \frac{\overline{u_1^2}}{\overline{\omega}}\frac{\partial \overline{u_1^2}}{\partial x_1} \ ,$$

with $C_k = 6C_g$. The notation C_k has been retained here because in the diffusion limit, $\overline{u_1^2}$ and $\overline{\varepsilon}^*$ obey a $\overline{k} - \overline{\varepsilon}$ like system similar to Equations (A.15)-(A.16). The solution of this system is then obtained directly from Equations (A.17) by replacing $\overline{k}$ by $\overline{u_1^2}$ and $\overline{\varepsilon}$ by $\overline{\varepsilon}^*$.

A.3.2.2 Set-up

The computational domain is defined by $[x_{min}, x_{max}] = [-30, 30]$ and $[u_{min}, u_{max}] = [-6, 6]$. It is discretized with $(n_x, n_{vx}) = 256^2$ points and the time step is set to $dt = 2 \cdot 10^{-3}$. The initial conditions are set according to

$$\overline{u_1^2}(x_1, t=0) = \overline{k}_0 \left(1 - \left[\frac{x_1}{\Lambda_0}\right]^2\right) + \overline{k}_{min} \quad , \quad \overline{\varepsilon}^*(x_1, t=0) = \overline{\varepsilon}_0 \left(1 - \left[\frac{x_1}{\Lambda_0}\right]^2\right) \quad ,$$

where $\overline{k}_0 = 1$ and $\Lambda_0 = 10$ and where the values of τ_0 and $\overline{\varepsilon}_0$ are given by Formula (A.18). The additional parameter $\overline{k}_{min}$ is set to $\overline{k}_{min} = 10^{-2}$. It is required because Diracs cannot be represented in a deterministic method. They are here replaced by a Gaussian with a sufficiently small variance for the PDF to approximate a Dirac, and sufficiently large to obtain a numerical resolution of the PDF with a reasonable number of velocity points. The coefficient of the model is set to $C_1 = 2.73$, in order to recover $C_k = 1$.

A.3.2.3 Validity of the asymptotic expansion

The value of the small expansion parameter stabilizes at $\ell/L = 5.10^{-3}$ at the center of the TZ, and $\ell/L = 0.8$ at the edge of the TZ. As expected, the validity range of the expansion is therefore not verified *a posteriori* at all points of the domain, but only in the bulk of the mixing zone. This is similar to what was observed in the EMC simulation.

Then, we can analyse the anisotropic odd part of the PDF, with respect to the analytical one (denoted as $\epsilon_a f^1$ in Section A.2.2). The comparison between the numerical and analytical PDF is shown in Figure A.7, respectively at the center and at the edge of the TZ. It can be seen that the predicted and simulated PDF shapes are close to one another. This gives confidence in the asymptotic expansion derived in section A.2.2.

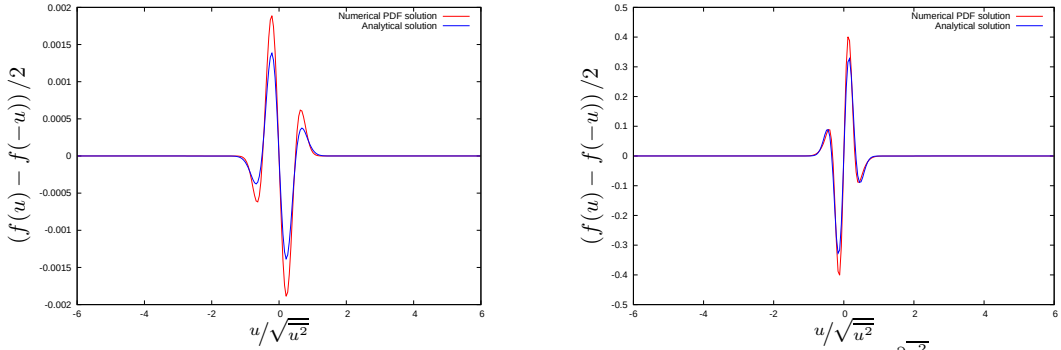

(a) PDF at the TZ center (b) PDF at the point where $\frac{\partial \overline{u^2}}{\partial x}$ is maximum

Figure A.7: Odd part of the PDF. Comparison between the numerical PDF and the solution obtained from the asymptotic development, at $t/\tau_0 = 5$.

A.3.2.4 Evolution of the mixing zone

For the TZ configuration described in section A.3.2, we first compare the diffusion solution (A.17), and the numerical solution of Equations (A.19)-(A.20). In Figures A.8(a) and A.8(b), we observe a good agreement between the numerical and the analytical solutions, for the second and third moments of the PDF. Moreover, in Figure A.9, the self-similarity of the solution is checked, with respect to the quantities

R_k, R_ϵ and R_L (that are defined in Section A.3.1.2). This shows that the PDF solution operates close to the diffusion regime, for which asymptotic PDF solutions have been derived in Section A.2.2.

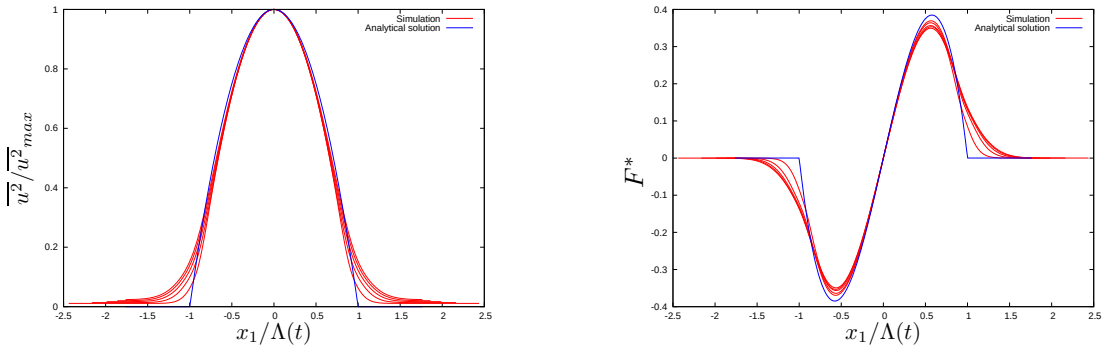

(a) Turbulent kinetic energy (b) Normalized third order moment

Figure A.8: Comparison between Barenblatt analytical solution (A.17) and the numerical PDF solution from $t/\tau_0 = 1$ to $t/\tau_0 = 5$. The TZ support increases as time increases.

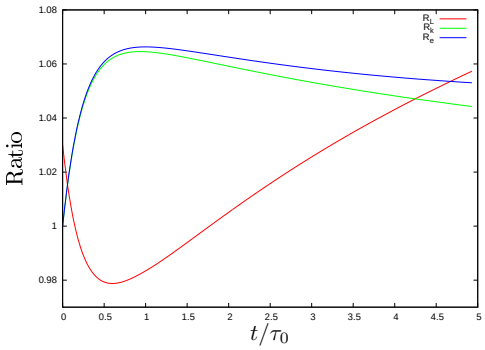

Figure A.9: Evolution of R_k, R_ϵ, and R_L as a function of time.

A.4 Discussion and conclusions

In section A.2, we showed that, in the weakly inhomogeneous limit, the simplified Langevin model (SLM) gives rise to diffusion approximation for turbulent transport and behaves as a standard $\overline{k}-\overline{\varepsilon}$ model. In section A.3, we performed numerical simulations of a turbulent mixing zone and showed that the weakly inhomogeneous limit and the diffusion approximation were relevant to describe the diffusion and decay of turbulence in this configuration. These results have been obtained for the SLM. However, they should also apply to a broader class of Langevin models, including most of those described in [108, 110] and called Generalized Langevin models (GLM). Indeed, in the turbulent mixing zone configuration, these models only differ from the SLM by correction due the anisotropy tensor. In the weakly inhomogeneous expansion, this quantity is of order 2. Consequently, it will not modify the orders 0 and 1 on which the present discussion is based.

The results obtained in sections A.2 and A.3 raise a number of questions concerning the way turbulent transport is effectively modelled in Langevin PDF models. First, the transport of kinetic energy is given on first order by a gradient diffusion approximation. The corresponding diffusion coefficient C_k is found to depend explicitly on two model constants: C_1 and C_{ε_2}. We recall that the constant C_{ε_2} is set in

order to reproduce the correct decay of kinetic energy in homogeneous isotropic turbulence. As for the constant C_1, it is set in order to specify the decay of the anisotropy tensor $b_{ij} = R_{ij} - 2\overline{k}/3\delta_{ij}$ in homogeneous turbulence. Hence, one is faced with an apparent contradiction : the coefficient controlling turbulent transport in Langevin PDF methods is set by observations and reasonings made in homogeneous turbulence, which by definition is devoid of turbulent transport.

Second, the value of C_1 varies in the literature and so does the value of the diffusion coefficient C_k. For $C_1 = 1.8$, one has $C_k = 0.7$ and for $C_1 = 4.15$, one has $C_k = 0.22$. These values have to be compared with the usual value retained in $\overline{k} - \overline{\varepsilon}$ models $C_k^{\overline{k}-\overline{\varepsilon}} = 0.15 - 0.22$. Thus, if one wants to obtain results close to a standard $\overline{k} - \overline{\varepsilon}$ model in the diffusion-dissipation regime, one should rather choose a value of $C_1 = 4.15$. However, as explained in section A.1, higher values of C_1 are usually associated with simpler models discarding the rapid contribution of the pressure gradient. For more realistic models, it is the value $C_1 = 1.8$ which is relevant. Hence, one is left to choose between a value of C_1 that captures correctly turbulent transport and a value that is compatible with the presence of a rapid pressure model. In addition to the first comment, this second remark tends to indicate that the definition of C_1 and the term it controls in the simplified Langevin model is overloaded. It looks as if the C_1 term in Equation (A.1) had to represent two distinct physical mechanisms: return to isotropy and turbulent transport.

Finally, a last remark must be made. While the Langevin PDF and $\overline{k} - \overline{\varepsilon}$ models behave alike in the diffusion limit, there is still a fundamental difference between the two. In the $\overline{k} - \overline{\varepsilon}$ model, the gradient diffusion term models turbulent advection and also turbulent transport by the pressure: $-C_k^{\overline{k}-\varepsilon}\frac{\overline{k}^2}{\overline{\varepsilon}}\partial_{x_i}\overline{k} = \overline{u_i k} + \overline{u_i p}$. By contrast, in the simplified Langevin PDF model, pressure transport is neglected. This can be seen in Equation (A.4) where only the flux of $\overline{k}$ appears. For the simplified Langevin model, one has: $-C_k\frac{\overline{k}^2}{\overline{\varepsilon}}\partial_{x_i}\overline{k} = \overline{u_i k}$. This relation could be justified if $\overline{u_i p}$ was negligible. However, this is not the case. In isotropic turbulence, one has exactly: $\overline{u_i p} = -2/5\overline{u_i k}$ [94]. Therefore, an important part of turbulent transport is missing in PDF models. Still, the fact that $\overline{u_i p}$ and $\overline{u_i k}$ are proportional allows for an effective definition of C_k which accounts for the missing term and give an overall correct transport in the diffusion regime. In that case, the value of $\overline{u_i k}$ is overestimated by a factor $5/3 \approx 1.7$.

All these remarks point to some deficiencies in the way turbulent transport is represented in PDF models. We hope to address some of these deficiencies in a forthcoming paper.

.1 Derivation of the first order of the asymptotic expansion

First of all, we note that $\overline{k}^{(1)}$ and $\overline{\varepsilon}^{(1)}$ obey a system of equations independent of higher orders:

$$\frac{\partial\overline{k}^{(1)}}{\partial t} = -\overline{\varepsilon}^{(1)} \quad , \quad \frac{\partial\overline{\varepsilon}^{(1)}}{\partial t} = -C_{\varepsilon_2}\overline{\omega}^{(0)}\,\overline{\varepsilon}^{(0)}\left(2\frac{\overline{\varepsilon}^{(1)}}{\overline{\varepsilon}^{(0)}} - \frac{\overline{k}^{(1)}}{\overline{k}^{(0)}}\right) .$$

Zero being a particular solution of it, we can set, without loss of generality:

$$\overline{k}^{(1)} = 0 \text{ and } \overline{\varepsilon}^{(1)} = 0\,.$$

Then, the equation for $f^{(1)}$ becomes:

$$\frac{\partial f^{(1)}}{\partial t} - \frac{\partial}{\partial u_j}\left[\frac{C_1}{2}\overline{\omega}^{(0)}u_j f^{(1)}\right] - \frac{C_0}{2}\overline{\varepsilon}^{(0)}\frac{\partial^2 f^{(0)}}{\partial u_j\partial u_j} = -u_1\frac{\partial f^{(0)}}{\partial z} - \frac{\partial}{\partial u_1}\left[\frac{\partial\sigma^2}{\partial z}f^{(0)}\right] .$$

A particular form $f^{(1)} = f^{(0)}\frac{u_1}{\overline{\omega}^{(0)}}g\left(\|\boldsymbol{u}\|^2/\sigma^2\right)\frac{1}{\sigma^2}\frac{\partial\sigma^2}{\partial z}$ is injected in this equation (we recall that $\sigma^2 = 2\overline{k}^{(0)}/3$). We find that the function $g(y)$ is solution of the following second order ODE:

$$2y\frac{d^2g}{dy^2}(y) + (5-y)\frac{dg}{dy}(y) - \frac{C_{\varepsilon_2} + C_1/2 - 2 - \Gamma}{C_1 - 1}g(y) = -\frac{1}{2}\frac{5-y}{C_1-1} \quad ,$$

where $\Gamma = \left[\frac{1}{\overline{\omega}^{(0)}}\frac{\partial\overline{\omega}^{(0)}}{\partial z}\right] / \left[\frac{1}{\sigma^2}\frac{\partial\sigma^2}{\partial z}\right]$. The solution of this equation is:

$$g(y) = \frac{5-y}{3C_1 + 2C_{\varepsilon_2} - 6 - 2\Gamma} \quad ,$$

so that we obtain:

$$f^{(1)} = \widetilde{C}_g \frac{\sigma}{\overline{\omega}} \frac{\partial_z \sigma^2}{\sigma^2} \quad \frac{u_1}{\sigma}\left(5 - \frac{u_i u_i}{\sigma^2}\right) f^{(0)} \qquad \text{with } \widetilde{C}_g = \frac{1}{3C_1 + 2C_{\varepsilon_2} - 6 - 2\Gamma} \, .$$

The evolution of Γ is given by: $\frac{\partial\Gamma}{\partial t} = \overline{\omega}^{(0)}\Gamma^2 - (C_{\varepsilon_2} - 1)\overline{\omega}^{(0)}\Gamma$, which solution is:

$$\Gamma = \frac{\Gamma_0 (C_{\varepsilon_2} - 1)}{\Gamma_0 + (C_{\varepsilon_2} - 1 - \Gamma_0) e^{(C_{\varepsilon_2} - 1)\int_0^t \overline{\omega}^{(0)}(s) ds}} \quad ,$$

with Γ_0 the initial condition of Γ. For physical reasons, we are only interested in solutions for which $\overline{k}^{(0)}$ and $\overline{\varepsilon}^{(0)}$ have approximately the same spatial profiles. In that case, Γ_0 remains small. In this work, we will more specifically restrict our attention to cases for which Γ_0 is smaller that $(C_{\varepsilon_2} - 1)$. Then, Γ tends to 0, so that, for long times, we can neglect its contribution in the final expression of $\widetilde{C}_g$. The PDF $f^{(1)}$ is then given by Equation (A.11). Note that the case Γ_0 larger than $(C_{\varepsilon_2} - 1)$ would yield an infinite value of Γ which is not physically relevant in the present context. The only other relevant case would be $(C_{\varepsilon_2} - 1) = \Gamma_0$, which is a special limit not treated in this work.

.2 Eulerian Monte Carlo solver

Following [119], a statistical equivalence can be found between the PDF equation (A.1) and the following system of stochastic partial differential equations (SPDE):

$$\frac{\partial r}{\partial t} + \frac{\partial}{\partial x_1}(r u_1) = 0 \quad , \tag{.22a}$$

$$\frac{\partial v_i}{\partial t} dt + v_1 \frac{\partial v_i}{\partial x_1} dt = \frac{\partial R_{1i}}{\partial x_1} dt - \frac{C_1}{2}\overline{\omega} v_i dt + \sqrt{C_0 \overline{\varepsilon}} dW_i \quad , \tag{.22b}$$

where W_i are independent Wiener processes. More precisely, the weighted PDF:

$$\widetilde{f} = \frac{\overline{r(x_1,t)\delta(\boldsymbol{v}(x_1,t) - \mathbf{u})}}{\overline{r}(x_1,t)}$$

has an evolution equation identical to equation (A.1). Then provided the right boundary and initial conditions are chosen, system (.22) will allow to solve PDF equation (A.1).

From a numerical point of view, the main difficulty lies in solving the advection part of the equation: $\frac{\partial v_i}{\partial t} + v_1 \frac{\partial v_i}{\partial x_1}$. In the PDF equation the equivalent of this term corresponds to purely linear advection and this property should be preserved in the interpretation of the SPDEs. Thus, the latter should be interpreted as quasi-linear hyperbolic equations: characteristic curves of the SPDEs can cross, which results in a multivalued solutions. At points where the solution of the velocity is multivalued, the corresponding density also becomes a multivalued function. This kind of properties also arises in different contexts. See for instance [30].

Traditional numerical schemes which satisfy an entropy increase condition are not appropriate for the description of multivalued solutions. Instead, one can use a level-set based method as in [30]. Alternatively, given the stochastic nature of our problem, on can devise a variation on the Random Choice Method (RCM) [54]. The details of the derivation of these methods will be given in a forthcoming article. We only give here its final expression.

Space is discretized with a uniform mesh $x_j = j\Delta x, j = 1 \cdots N_x$. Time is discretized on intervals $[t^n, t^{n+1} = t^n + \Delta t]$. N_s stochastic fields are solved simultaneously. They are each indexed by the superscript (s). For the sake of simplicity, we will only use this index when necessary. For a given stochastic field, the numerical scheme is the following:

$$\begin{aligned} r_j^{n+1} =& r_j^n - \frac{\Delta t}{\Delta x}\left[|(v_1)_j^n|\, r_j^n - v_{j+1}^- r_{j+1}^n - v_{j-1}^+ r_{j-1}^n\right] \quad , \\ v_i|_j^{n+1} =& S_i^n + v_i|_{j+1}^n \eta_j^+ + v_i|_{j-1}^n \eta_j^- + v_i|_j^n \eta_j^0 \quad , \end{aligned}$$

where $v_{j-1}^+ = \max(v_1|_{j-1}^n, 0)$, $v_{j+1}^- = -\min(v_1|_{j+1}^n, 0)$ and where $\eta_j^{\{+,-,0\}}$ are random numbers defined by:

$$\left(\eta_j^+, \eta_j^-, \eta_j^0\right) = \begin{cases} (1,0,0)\,, & \text{with probability} \quad P_j^+ \\ (0,1,0)\,, & \text{with probability} \quad P_j^- \\ (0,0,1)\,, & \text{with probability} \quad P_j^0 = 1 - P_j^+ - P_j^- \end{cases} .$$

The probabilities P_j^0, P_j^- and P_j^+ define the random choice method. They are given by:

$$\begin{aligned} P_j^+ =& \frac{r_{j+1}^n}{r_j^{n+1}} v_{j+1}^+ \frac{\Delta t}{\Delta x} \quad , \\ P_j^- =& \frac{r_{j-1}^n}{r_j^{n+1}} v_{j-1}^- \frac{\Delta t}{\Delta x} \quad , \\ P_j^0 =& \frac{r_j^n}{r_j^{n+1}} \left(1 - |(v_1)_j^n| \frac{\Delta t}{\Delta x}\right) . \end{aligned}$$

To guarantee that the probability P_j^0 is positive, one must enforce the following CFL condition:

$$|(v_1)_j^n| \frac{\Delta t}{\Delta x} \leq 1 .$$

Finally, the source term S_i^n is defined as:

$$S_i^n = -\frac{C_1}{2}\overline{\omega}^n v_i^n \Delta t + \sqrt{C_0 \overline{\varepsilon}^n \Delta t}\xi_i^n - \left\langle v_i|_{j+1}^n \eta_i^+ + v_i|_{j-1}^n \eta_i^- + v_i|_j^n \eta_i^0 \right\rangle_{N_s} \quad , \tag{.23}$$

where ξ_i^n are random independent Gaussian noises with variance 1 and mean 0 and where, for any quantity q, $\langle q \rangle_{N_s}$ represents the weighted mean on the stochastic field:

$$\langle q \rangle_{N_s} = \frac{\sum_{s=1}^{N_s} r^{(s)} q^{(s)}}{\sum_{s=1}^{N_s} r^{(s)}} .$$

The last term in equation (.23) is a discretization of $\frac{\partial R_{1i}}{\partial x_1}$ that guarantees that advection has a zero contribution to the evolution of the mean, as should be the case.

The numerical scheme described here can be shown to be first order in time and in space when stochastic convergence is achieved.

.3 Deterministic direct method

We propose here a Finite Volume numerical method to discretize the equation (A.19), where the space, velocity fluctuation and time dimensions are discretized to yield a unique value of the PDF $f_1(u_1; x_1, t)$. This numerical scheme should allow to satisfy the following constraints:

$$f_1(u_1; x_1, t) \geq 0 , \tag{.24}$$

$$\int_{\mathbb{R}} f_1(u_1; x_1, t) du_1 = 1 , \tag{.25}$$

$$\int_{\mathbb{R}} u_1 f_1(u_1; x_1, t) du_1 = 0 . \tag{.26}$$

To simplify notations, we will hereafter drop the index 1 from x_1 and f_1.

We introduce a Cartesian, uniform mesh, defined by the control volumes $\mathcal{C}_{i,j} = \left[x_{i-1/2}, x_{i+1/2}\right]\left[u_{j-1/2}, u_{j+1/2}\right]$, where $(i,j) \in I \times J \subset \mathbb{N} \times \mathbb{Z}$. We define Δx and Δv as the sizes of the space and velocity control volumes, respectively. $x_i = i\Delta x$ and $u_j = j\Delta v$ here refer to the cell centres, whereas $x_{i+1/2} = (i+1/2)\Delta x$ and $u_{j+1/2} = (j+1/2)\Delta u$ refer to the volume control boundaries.
Let $f_{i,j}^n$ be an average approximation of the PDF on the control volume at time $t^n = n\Delta t$, $n \in \mathbb{N}$,

$$f_{i,j}^n = \frac{1}{\Delta x \Delta v} \int_{\mathcal{C}_{i,j}} f(x,u,t^n) du dx \ . \tag{.27}$$

We start from the Finite Volume scheme originally derived in [51]. We recall the basic steps leading to its construction on the simplified advection equation

$$\frac{\partial f}{\partial t} + u\frac{\partial f}{\partial x} = 0 \ , u > 0 \ , \tag{.28}$$

for the sake of simplicity. Its extension by symmetry to the negative velocity space is straightforward. Its application to the right-hand side, velocity drift terms, in Equation (A.19), will be discussed hereafter. First, a time explicit Euler scheme is employed to discretize the Equation (.28) as

$$f_i^{n+1} = f_i^n + u\frac{\Delta t}{\Delta x}\left(F_{i+1/2}^n - F_{i-1/2}^n\right) \ , \tag{.29}$$

where $F_{i+1/2}^n = F(x_{i+1/2}, t^n)$ stands as a discrete conservative approximation of $f(x,t)$ on the boundary of the control volume $\left[x_{i-1/2}, x_{i+1/2}\right]$. Second, following [51], a second order MUSCL reconstruction technique (by primitive), leads to the approximation

$$F(x,t^n) = \left[f_i^n + \epsilon^+ \frac{x - x_i}{\Delta x}\left(f_{i+1}^n - f_i^n\right)\right] \ , \ \forall x \in \left[x_{i-1/2}, x_{i+1/2}\right] \ . \tag{.30}$$

The slope limiter ϵ^+ is introduced in order to recover the maximum principle $0 \leq f_i^n \leq \|f\|_\infty$ under the CFL condition $u\frac{\Delta t}{\Delta x} \leq 1$. Its expression, given by

$$\epsilon^+ = \begin{cases} 0 \ , \text{if } \left(f_{i+1}^n - f_i^n\right)\left(f_i^n - f_{i-1}^n\right) < 0 \\ \min\left(1, \dfrac{2\left(\|f\|_\infty - f_i^n\right)}{f_i^n - f_{i+1}^n}\right) \ , \text{if } \left(f_{i+1}^n - f_i^n\right) < 0 \\ \min\left(1, \dfrac{2f_i^n}{f_{i+1}^n - f_i^n}\right) \ , \text{else} \end{cases} \tag{.31}$$

leads to a non-linear expression for the numerical flux.

This approximation procedure can be further extended to evaluate the velocity drift term in the right hand side of Equation (A.19), which involves the velocity variance gradient $\frac{\partial \overline{u^2}}{\partial x}$. This drift term should balance with the advection term in the left hand side of Equation (A.19), in order to guarantee the zero mean velocity conservation (.26). At the discrete level, this requirement is met with a re-definition of $\left.\frac{\partial \overline{u^2}}{\partial x}\right|_i^n$ as a function of the discrete, reconstructed, numerical flux obtained for the advection term (left hand side of Equation (A.19))

$$\left.\frac{\partial \overline{u^2}}{\partial x}\right|_i^n = \sum_j u_j^2 \frac{F_{i+1/2,j}^n - F_{i-1/2,j}^n}{\Delta x}\Delta v \Bigg/ \left(-\sum_j u_j \frac{F_{i,j+1/2}^n - F_{i,j-1/2}^n}{\Delta v}\Delta v\right) \ , \tag{.32}$$

which is the analogous of the continuous relation, obtained by integration by parts,

$$\frac{\partial \overline{u^2}}{\partial x} = \int_{\mathbb{R}} du u^2 \frac{\partial f}{\partial x} \Bigg/ \left(-\int_{\mathbb{R}} du u \frac{\partial f}{\partial u}\right) \ . \tag{.33}$$

The chosen discrete definition (.32) mimics the integration by part (.33) required to satisty the zero mean velocity conservation (.26), that is $\overline{u} = 0$.
A similar procedure is now applied to the C_1 term in the right hand side of Equation (A.19), which is rewritten as

$$\frac{\partial}{\partial u}\left(\frac{C_1}{2}\overline{\omega}uf\right) \rightarrow \frac{\partial}{\partial u}\left(\frac{C_1}{2}\overline{\omega}\left(u-\overline{u}\right)f\right) \ . \tag{.34}$$

An extension of the Finite Volume scheme (.29)-(.30)-(.31) is employed here, to the more general case where the fluxes depend on the drift variable u. This dependence is treated with a conservative centered discretization of the velocity variable in the flux uf. A discrete definition for $\overline{u}$ is required at this point in (.34). We introduce an approximation that satisfies the zero mean velocity conservation in a discrete manner on the discrete analogous of the Equation (.34)

$$\overline{u}_i^n = \sum_j u_j \frac{F^n_{i,j+1/2} - F^n_{i,j-1/2}}{\Delta v}\Delta v \Bigg/ \left(\sum_j u_j \frac{u_{j+1/2}F^n_{i,j+1/2} - u_{j-1/2}F^n_{i,j-1/2}}{\Delta v}\Delta v\right) \ , \tag{.35}$$

which is the discrete analogous of the continuous expression

$$\overline{u} = \int_{\mathbb{R}} duu\frac{\partial f}{\partial u} \Bigg/ \int_{\mathbb{R}} du\frac{\partial}{\partial u}\left(uf\right) = 0 \ . \tag{.36}$$

We finally obtain an unsplit discretization for all the advection terms in Equation (A.19). The discrete analogous of the probability density conservation (.25) is satisfied if the slope limiters are not active for the advection term $u\dfrac{\partial f}{\partial x}$. In this case, we indeed obtain a centered discretization whatever the sign of the velocity is. We accept a small deviation from the probability density conservation, where the limiters are active to guarantee the maximum principle.

We now turn to the discretization of the C_0 operator in the right hand side of Equation (A.19). This term is splitted and discretized with an centered, implicit scheme, with net flux boundary conditions on the velocity space. This ensures the respect of the conservations (.25) and (.26), at the discrete level. Moreover, we obtain a M-matrix with a positive right hand side, leading to a positive PDF.
Finally, we remark that the splitting of the C_0 operator is convenient in the sense that it allows both the implicitation of this term and an easy implementation of a parallelisation on the space dimension x with good expected scalability. We have made use of the MPI parallelisation protocol to do so.

Bibliography

[1] M.L. Adams. Discontinuous finite element transport solutions in thick diffusive problems. *Nuclear Science and Engineering*, 137:298–333, 2001.

[2] Julius Adler. Chemotaxis in bacteria. *Science*, 153(3737):708–716, 1966.

[3] Wolgang Alt. Biased random walk models for chemotaxis and related diffusion approximations. *Journal of Mathematical Biology*, 9(2):147–177, 1980.

[4] Wolgang Alt. Biased random walk models for chemotaxis and related diffusion approximations. *Journal of Mathematical Biology*, 9(2):147–177, 1980.

[5] Luigi Ambrosio, Nicola Gigli, and Giuseppe Savaré. *Gradient flows in metric spaces and in the space of probability measures.* Lectures in Mathematics ETH Zürich. Birkhäuser Verlag, Basel, second edition, 2008.

[6] T.B. Gatski B.A. Younis and C.G. Speziale. Towards a rational model for the triple velocity correlations of turbulence. *Technical Report TM-1999-209134*, 1999.

[7] G.I Barenblatt. Self-similar turbulence propagation from an instantaneous plane source. *Nonlinear Dynamics and Turbulence*, pages 48–60, 1983.

[8] Nicola Bellomo, Abdelghani Bellouquid, Juan Nieto, and Juan Soler. Multicellular biological growing systems: hyperbolic limits towards macroscopic description. *Math. Models Methods Appl. Sci.*, 17(suppl.):1675–1692, 2007.

[9] Nicola Bellomo, Abdelghani Bellouquid, Juan Nieto, and Juan Soler. Multiscale biological tissue models and flux-limited chemotaxis for multicellular growing systems. *Math. Models Methods Appl. Sci.*, 20(7):1179–1207, 2010.

[10] Andrea Louise Bertozzi and Jeremy Brandman. Finite-time blow-up of L^∞-weak solutions of an aggregation equation. *Commun. Math. Sci.*, 8(1):45–65, 2010.

[11] Georgij Bispen, K. R. Arun, Mária Luká?ová-Medvid?ová, and Sebastian Noelle. Imex large time step finite volume methods for low froude number shallow water flows. *Communications in Computational Physics*, 16:307–347, 8 2014.

[12] Adrien Blanchet, Jean Dolbeault, and Benoît Perthame. Two-dimensional Keller-Segel model: optimal critical mass and qualitative properties of the solutions. *Electron. J. Differential Equations*, pages No. 44, 32 pp. (electronic), 2006.

[13] Ramaz Botchorishvili, Benoit Perthame, and Alexis Vasseur. Equilibrium schemes for scalar conservation laws with stiff sources. *Math. Comp.*, 72(241):131–157 (electronic), 2003.

[14] François Bouchut and François James. One-dimensional transport equations with discontinuous coefficients. *Nonlinear Anal.*, 32(7):891–933, 1998.

[15] François Bouchut. *Nonlinear stability of finite volume methods for hyperbolic conservation laws and well-balanced schemes for sources.* Frontiers in Mathematics. Birkhäuser Verlag, Basel, 2004.

[16] François Bouchut and François James. Duality solutions for pressureless gases, monotone scalar conservation laws, and uniqueness. *Comm. Partial Differential Equations*, 24(11-12):2173–2189, 1999.

[17] Nikolaos Bournaveas and Vincent Calvez. Critical mass phenomenon for a chemotaxis kinetic model with spherically symmetric initial data. *Ann. Inst. H. Poincaré Anal. Non Linéaire*, 26(5):1871–1895, 2009.

[18] Nikolaos Bournaveas, Vincent Calvez, Susana Gutiérrez, and Benoît Perthame. Global existence for a kinetic model of chemotaxis via dispersion and Strichartz estimates. *Comm. Partial Differential Equations*, 33(1-3):79–95, 2008.

[19] D Bray, RB Bourret, and MI Simon. Computer simulation of the phosphorylation cascade controlling bacterial chemotaxis. *Molecular biology of the cell*, 4(5):469–482, May 1993.

[20] Haïm Brezis. *Analyse fonctionnelle*. Collection Mathématiques Appliquées pour la Maîtrise. [Collection of Applied Mathematics for the Master's Degree]. Masson, Paris, 1983. Théorie et applications. [Theory and applications].

[21] Vincent Calvez, Lucilla Corrias, and Mohamed Abderrahman Ebde. Blow-up, concentration phenomenon and global existence for the keller–segel model in high dimension. *Communications in Partial Differential Equations*, 37(4):561–584, 2012.

[22] Vincent Calvez, Gaël Raoul, and Christian Schmeiser. Confinement by biased velocity jumps: Aggregation of escherichia coli. *Kinetic and Related Models*, 8(4):651?666, 2015.

[23] Jose Carrillo, Marco Di Francesco, Alessio Figalli, Thomas Laurent, and Dejan Slepčev. Global-in-time weak measure solutions and finite-time aggregation for nonlocal interaction equations. *Duke Math. J.*, 156(2):229–271, 2011.

[24] José A. Carrillo, James François, Frédéric Lagoutière, and Nicolas Vauchelet. The filippov characteristic flow for the aggregation equation with mildly singular potentials. *Arxiv preprint*, 2014.

[25] José A. Carrillo and Bokai Yan. An asymptotic preserving scheme for the diffusive limit of kinetic systems for chemotaxis. *Multiscale Model. Simul.*, 11(1):336–361, 2013.

[26] José Antonio Carrillo, Frédérique Charles, Young-Pil Choi, and Martin Campos-Pinto. Convergence of linearly transformed particle methods for the aggregation equation. *in preparation*.

[27] José Antonio Carrillo, Alina Chertock, and Yanghong Huang. A finite-volume method for nonlinear nonlocal equations with a gradient flow structure. *Communications in Computational Physics*, 17:233–258, 1 2015.

[28] Fabio Chalub, Peter Markowich, Benoît Perthame, and Christian Schmeiser. Kinetic models for chemotaxis and their drift-diffusion limits. *Monatsh. Math.*, 142(1-2):123–141, 2004.

[29] Subrahmanyan Chandrasekhar. *Radiative transfer*. Dover Publications, Inc., New York, 1960.

[30] Li-Tien Cheng, Hailiang Liu, and Stanley Osher. Computational high-frequency wave propogation using the level-set method with applications to the semi-classical limit of the schrödinger equations. *Commun. Math. Sci.*, 1(3):593–621, 09 2003.

[31] C. Cherfils and A.K Harrison. Comparison of different statistical models of turbulence by similarity methods. *Proceedings of the Fluids Engineering Division Summer Meeting, Incline Village, Nevada, USA*, 1994.

[32] Alina Chertock, Alexander Kurganov, Xuefeng Wang, and Yaping Wu. On a chemotaxis model with saturated chemotactic flux. *Kinet. Relat. Models*, 5(1):51–95, 2012.

[33] Carlos Conca, Elio Espejo, and Karina Vilches. Remarks on the blowup and global existence for a two species chemotactic Keller-Segel system in $\mathbb{R}^2$. *European J. Appl. Math.*, 22(6):553–580, 2011.

[34] Katy Craig and Andrea Bertozzi. A blob method for the aggregation equation. *to appear in Math. Comp.*, 2015.

[35] Gianluca Crippa and Magali Lécureux-Mercier. Existence and uniqueness of measure solutions for a system of continuity equations with non-local flow. *Nonlinear Differential Equations and Applications NoDEA*, 20(3):523–537, 2013.

[36] Marco Di Francesco and Simone Fagioli. Measure solutions for non-local interaction PDEs with two species. *Nonlinearity*, 26(10):2777–2808, 2013.

[37] Marco Di Francesco and Simone Fagioli. Measure solutions for non-local interaction PDEs with two species. *Nonlinearity*, 26(10):2777–2808, 2013.

[38] Cristiana Di Russo, Roberto Natalini, and Magali Ribot. Global existence of smooth solutions to a two-dimensional hyperbolic model of chemotaxis. *Commun. Appl. Ind. Math.*, 1(1):92–109, 2010.

[39] Giacomo Dimarco and Lorenzo Pareschi. Asymptotic preserving implicit-explicit Runge-Kutta methods for nonlinear kinetic equations. *SIAM J. Numer. Anal.*, 51(2):1064–1087, 2013.

[40] Yasmin Dolak and Christian Schmeiser. Kinetic models for chemotaxis: hydrodynamic limits and spatio-temporal mechanisms. *J. Math. Biol.*, 51(6):595–615, 2005.

[41] Budrene Elena and Berg Howard. Dynamics of formation of symmetrical patterns by chemotactic bacteria. *Nature*, 6(376), 1995.

[42] Casimir Emako, Charlène Gayrard, Nicolas Vauchelet, Luis Neves de Almeida, and Axel Buguin. Traveling pulses for a two-species chemotaxis model. *in preparation*.

[43] Casimir Emako, Luis Neves de Almeida, and Nicolas Vauchelet. Existence and diffusive limit of a two-species kinetic model of chemotaxis. *Kinetic and Related Models*, 8(2):359–380, 2015.

[44] Radek Erban and Hans G. Othmer. From individual to collective behavior in bacterial chemotaxis. *SIAM Journal on Applied Mathematics*, 65(2):361–391, 2004.

[45] Elio Eduardo Espejo Arenas, Angela Stevens, and Juan J. L. Velázquez. Simultaneous finite time blow-up in a two-species model for chemotaxis. *Analysis (Munich)*, 29(3):317–338, 2009.

[46] Lawrence C. Evans. *Partial differential equations*, volume 19 of *Graduate Studies in Mathematics*. American Mathematical Society, Providence, RI, 1998.

[47] Antonio Fasano, Alberto Mancini, and Mario Primicerio. Equilibruim of two populations subject to chemotaxis. *Mathematical Models and Methods in Applied Sciences*, 14(04):503–533, 2004.

[48] Francis Filbet and Shi Jin. A class of asymptotic-preserving schemes for kinetic equations and related problems with stiff sources. *J. Comput. Phys.*, 229(20):7625–7648, 2010.

[49] Francis Filbet and Shi Jin. A class of asymptotic-preserving schemes for kinetic equations and related problems with stiff sources. *Journal of Computational Physics*, 229(20):7625–7648, 2010.

[50] Francis Filbet, Philippe Laurençot, and Benoît Perthame. Derivation of hyperbolic models for chemosensitive movement. *J. Math. Biol.*, 50(2):189–207, 2005.

[51] Francis Filbet, Eric Sonnendrücker, and Pierre Bertrand. Conservative numerical schemes for the vlasov equation. *Journal of Computational Physics*, 172(1):166 – 187, 2001.

[52] Francis Filbet and Chang Yang. Numerical simulations of kinetic models for chemotaxis. *SIAM J. Sci. Comput.*, 36(3):B348–B366, 2014.

[53] R. O. Fox and P. K. Yeung. Improved lagrangian mixing models for passive scalars in isotropic turbulence. *Physics of Fluids*, 15(4):961–985, 2003.

[54] James Glimm. Solutions in the large for nonlinear hyperbolic systems of equations. *Communications on Pure and Applied Mathematics*, 18(4):697–715, 1965.

[55] Laurent Gosse. Transient radiative transfer in the grey case: Well-balanced and asymptotic-preserving schemes built on case's elementary solutions. *Journal of Quantitative Spectroscopy and Radiative Transfer*, 112(12):1995?2012, 2011.

[56] Laurent Gosse. Asymptotic-preserving and well-balanced schemes for the 1D Cattaneo model of chemotaxis movement in both hyperbolic and diffusive regimes. *J. Math. Anal. Appl.*, 388(2):964–983, 2012.

[57] Laurent Gosse. *Computing qualitatively correct approximations of balance laws*, volume 2 of *SIMAI Springer Series*. Springer, Milan, 2013. Exponential-fit, well-balanced and asymptotic-preserving.

[58] Laurent Gosse. A well-balanced scheme for kinetic models of chemotaxis derived from one-dimensional local forward-backward problems. *Math. Biosci.*, 242(2):117–128, 2013.

[59] Laurent Gosse and François James. Numerical approximations of one-dimensional linear conservation equations with discontinuous coefficients. *Math. Comp.*, 69(231):987–1015, 2000.

[60] Laurent Gosse and Alain-Yves Leroux. Un schéma-équilibre adapté aux lois de conservation scalaires non-homogènes. *C. R. Acad. Sci. Paris Sér. I Math.*, 323(5):543–546, 1996.

[61] Laurent Gosse and Giuseppe Toscani. Asymptotic-preserving & well-balanced schemes for radiative transfer and the Rosseland approximation. *Numer. Math.*, 98(2):223–250, 2004.

[62] J. M. Greenberg and A. Y. Leroux. A well-balanced scheme for the numerical processing of source terms in hyperbolic equations. *SIAM J. Numer. Anal.*, 33(1):1–16, 1996.

[63] James M. Greenberg and Wolfgang Alt. Stability results for a diffusion equation with functional drift approximating a chemotaxis model. *Trans. Amer. Math. Soc.*, 300(1):235–258, 1987.

[64] K. Hanjalic and B. E. Launder. A reynolds stress model of turbulence and its application to thin shear flows. *Journal of Fluid Mechanics*, 52:609–638, 4 1972.

[65] Dirk Helbing, Wenjian Yu, and Heiko Rauhut. Self-organization and emergence in social systems: modeling the coevolution of social environments and cooperative behavior. *J. Math. Sociol.*, 35(1-3):177–208, 2011.

[66] Thomas Hillen. Hyperbolic models for chemosensitive movement. *Math. Models Methods Appl. Sci.*, 12(7):1007–1034, 2002. Special issue on kinetic theory.

[67] Thomas Hillen and Angela Stevens. Hyperbolic models for chemotaxis in 1-D. *Nonlinear Anal. Real World Appl.*, 1(3):409–433, 2000.

[68] Thomas Hofer, Jonathan A. Sherratt, and Philip K. Maini. Dictyostelium discoideum: Cellular self-organization in an excitable biological medium. *Proceedings of the Royal Society of London. Series B: Biological Sciences*, 259(1356):249–257, 1995.

[69] D. Horstmann and A. Stevens. A constructive approach to traveling waves in chemotaxis. *J. Nonlinear Sci.*, 14(1):1–25, 2004.

[70] Dirk Horstmann. Generalizing the Keller-Segel model: Lyapunov functionals, steady state analysis, and blow-up results for multi-species chemotaxis models in the presence of attraction and repulsion between competitive interacting species. *J. Nonlinear Sci.*, 21(2):231–270, 2011.

[71] Berg Howard. *Random walks in biology*. Princeton University Press, 1993.

[72] Berg Howard. *E. coli in Motion*. Biological and Medical Physics, Biomedical Engineering. Springer, 2004.

[73] Hyung Ju Hwang, Kyungkeun Kang, and Angela Stevens. Drift-diffusion limits of kinetic models for chemotaxis: a generalization. *Discrete Contin. Dyn. Syst. Ser. B*, 5(2):319–334, 2005.

[74] Hyung Ju Hwang, Kyungkeun Kang, and Angela Stevens. Global solutions of nonlinear transport equations for chemosensitive movement. *SIAM J. Math. Anal.*, 36(4):1177–1199 (electronic), 2005.

[75] François James and Nicolas Vauchelet. Equivalence between duality and gradient flow solutions for one-dimensional aggregation equations. *in preparation*.

[76] François James and Nicolas Vauchelet. Chemotaxis: from kinetic equations to aggregate dynamics. *NoDEA Nonlinear Differential Equations Appl.*, 20(1):101–127, 2013.

[77] François James and Nicolas Vauchelet. Numerical methods for one-dimensional aggregation equations. *SIAM Journal on Numerical Analysis*, 53(2):895–916, 2015.

[78] Shi Jin. Asymptotic preserving (ap) schemes for multiscale kinetic and hyperbolic equations: a review. lecture notes for summer school on Ómethods and models of kinetic theory. *Rivista di Mathematica della Universita di Parma, Porto Ercole (Grosseto, Italy)*, 2010.

[79] Shi Jin. Asymptotic preserving (AP) schemes for multiscale kinetic and hyperbolic equations: a review. *Riv. Math. Univ. Parma (N.S.)*, 3(2):177–216, 2012.

[80] Shi Jin and C. David Levermore. Numerical schemes for hyperbolic conservation laws with stiff relaxation terms. *J. Comput. Phys.*, 126(2):449–467, 1996.

[81] Shi Jin, Lorenzo Pareschi, and Giuseppe Toscani. Diffusive relaxation schemes for multiscale discrete-velocity kinetic equations. *SIAM J. Numer. Anal.*, 35(6):2405–2439 (electronic), 1998.

[82] Shi Jin, Min Tang, and Houde Han. A uniformly second order numerical method for the one-dimensional discrete-ordinate transport equation and its diffusion limit with interface. *Netw. Heterog. Media*, 4(1):35–65, 2009.

[83] Shi Jin and Xin Wen. An efficient method for computing hyperbolic systems with geometrical source terms having concentrations. *J. Comput. Math.*, 22(2):230–249, 2004. Special issue dedicated to the 70th birthday of Professor Zhong-Ci Shi.

[84] Evelyn Keller and Lee Segel. Initiation of slime mold aggregation viewed as an instability. *Journal of Theoretical Biology*, 26(3):399–415, 1970.

[85] Evelyn F. Keller and Lee A. Segel. Model for chemotaxis. *Journal of Theoretical Biology*, 30(2):225–234, 1971.

[86] Evelyn F. Keller and Lee A. Segel. Model for chemotaxis. *Journal of Theoretical Biology*, 30(2):225–234, 1971.

[87] Paul Kubelka. New contributions to the optics of intensely light-scattering materials. I. *J. Opt. Soc. Amer.*, 38:448–457, 1948.

[88] Alexander Kurganov and Doron Levy. Central-upwind schemes for the saint-venant system. *ESAIM: Mathematical Modelling and Numerical Analysis*, 36:397–425, 5 2002.

[89] Alexander Kurganov and Maria Lukacova-Medvidova. Numerical study of two-species chemotaxis models. *Discrete and Continuous Dynamical Systems. Series B*, 19(1):131–152, 2014.

[90] E. W. Larsen and J. E. Morel. Asymptotic solutions of numerical transport problems in optically thick,diffusive regimes ii. *J. Comput. Phys.*, 69:212–236, 1989.

[91] Edward W Larsen, J.E Morel, and Warren F Miller Jr. Asymptotic solutions of numerical transport problems in optically thick, diffusive regimes. *Journal of Computational Physics*, 69(2):283 – 324, 1987.

[92] Randall J. LeVeque. Balancing source terms and flux gradients in high-resolution godunov methods: The quasi-steady wave-propagation algorithm. *Journal of Computational Physics*, 146(1):346–365, 1998.

[93] Tai-Chia Lin and Zhi-An Wang. Development of traveling waves in an interacting two-species chemotaxis model. *Discrete Continuous Dynamical Systems Series A*, 34(7):2907–2927, 2014.

[94] John L. Lumley. Computational modeling of turbulent flows. 18:123 – 176, 1979.

[95] Luc Mieussens. On the asymptotic preserving property of the unified gas kinetic scheme for the diffusion limit of linear kinetic models. *J. Comput. Phys.*, 253:138–156, 2013.

[96] Nikhil Mittal, Elena O. Budrene, Michael P. Brenner, and Alexander van Oudenaarden. Motility of escherichia coli cells in clusters formed by chemotactic aggregation. *Proceedings of the National Academy of Sciences*, 100(23):13259–13263, 2003.

[97] Toshitaka Nagai and Tsutomu Ikeda. Traveling waves in a chemotactic model. *Journal of Mathematical Biology*, 30(2):169–184, 1991.

[98] Roberto Natalini, Magali Ribot, and Monika Twarogowska. A well-balanced numerical scheme for a one dimensional quasilinear hyperbolic model of chemotaxis. *Commun. Math. Sci.*, 12(1):13–39, 2014.

[99] Hans Othmer, Stevens Dunbar, and Wolfgang Alt. Models of dispersal in biological systems. *J. Math. Biol.*, 26(3):263–298, 1988.

[100] Hans Othmer and Thomas Hillen. The diffusion limit of transport equations. II. Chemotaxis equations. *SIAM J. Appl. Math.*, 62(4):1222–1250 (electronic), 2002.

[101] Sungsu Park, Peter M. Wolanin, Emil A. Yuzbashyan, Hai Lin, Nicholas C. Darnton, Jeffry B. Stock, Pascal Silberzan, and Robert Austin. Influence of topology on bacterial social interaction. *Proceedings of the National Academy of Sciences*, 100(24):13910–13915, 2003.

[102] CliffordS. Patlak. Random walk with persistence and external bias. *The bulletin of mathematical biophysics*, 15(3):311–338, 1953.

[103] B. Perthame and C. Simeoni. A kinetic scheme for the Saint-Venant system with a source term. *Calcolo*, 38(4):201–231, 2001.

[104] B. Perthame and C. Simeoni. A kinetic scheme for the saint-venant system with a source term. *CALCOLO*, 38(4):201–231, 2001.

[105] Benoit Perthame. PDE models for chemotactic movements: parabolic, hyperbolic and kinetic. *Appl. Math.*, 49(6):539–564, 2004.

[106] Benoît Perthame. *Transport equations in biology*. Frontiers in Mathematics. Birkhäuser Verlag, Basel, 2007.

[107] Benoit Perthame, Min Tang, and Nicolas Vauchelet. Derivation of the bacterial run-and-tumble kinetic equation from a model with biochemical pathway. *Arxiv preprints*, 2015.

[108] S. B. Pope. On the relationship between stochastic lagrangian models of turbulence and second?-moment closures. *Physics of Fluids*, 6(2):973–985, 1994.

[109] S.B Pope. Pdf methods for turbulent reactive flows. *Progress in Energy and Combustion Science*, 11(2):119–192, 1985.

[110] S.B Pope. *Turbulent flows*. Cambridge University Press, 2000.

[111] Frédéric Poupaud. Diagonal defect measures, adhesion dynamics and Euler equation. *Methods Appl. Anal.*, 9(4):533–561, 2002.

[112] Svetlozar T. Rachev and Ludger Rüschendorf. *Mass transportation problems. Vol. II*. Probability and its Applications (New York). Springer-Verlag, New York, 1998. Applications.

[113] Vladimir Sabelnikov and Olivier Soulard. Rapidly decorrelating velocity-field model as a tool for solving one-point fokker-planck equations for probability density functions of turbulent reactive scalars. *Phys. Rev. E*, 72:016301, Jul 2005.

[114] H. Salman, A. Zilman, C. Loverdo, M. Jeffroy, and A. Libchaber. Solitary modes of bacterial culture in a temperature gradient. *Phys. Rev. Lett.*, 97:118101, Sep 2006.

[115] Jonathan Saragosti, Vincent Calvez, Nikolaos Bournaveas, Axel Buguin, Pascal Silberzan, and Benoît Perthame. Mathematical description of bacterial traveling pulses. *PLoS Comput. Biol.*, 6(8):e1000890, 12, 2010.

[116] Jonathan Saragosti, Vincent Calvez, Nikolaos Bournaveas, Benoît Perthame, Axel Buguin, and Pascal Silberzan. Directional persistence of chemotactic bacteria in a traveling concentration wave. *Proceedings of the National Academy of Sciences*, 108(39):16235–16240, 2011.

[117] Guangwei Si, Min Tang, and Xu Yang. A pathway-based mean-field model for *e. coli* chemotaxis: mathematical derivation and its hyperbolic and parabolic limits. *Multiscale Model. Simul.*, 12(2):907–926, 2014.

[118] Jacques Simon. Compact sets in the space $L^p(0,T;B)$. *Ann. Mat. Pura Appl. (4)*, 146:65–96, 1987.

[119] O. Soulard and V.A. Sabelnikov. Eulerian monte carlo method for the joint velocity and mass-fraction probability density function in turbulent reactive gas flows. *Combustion, Explosion and Shock Waves*, 42(6):753–762, 2006.

[120] Wenjun Sun, Song Jiang, and Kun Xu. Asymptotic preserving unified gas kinetic scheme for grey radiative transfer equations. *J Comput. Physics*, 285:265–279, 2015.

[121] Katarzyna Sznajd-Weron and Jozef Sznajd. Opinion evolution in closed community. *International Journal of Modern Physics C*, 11(06):1157–1165, 2000.

[122] M. J. Tindall, P. K. Maini, S. L. Porter, and J. P. Armitage. Overview of mathematical approaches used to model bacterial chemotaxis. II. Bacterial populations. *Bull. Math. Biol.*, 70(6):1570–1607, 2008.

[123] Luis Valino. A field monte carlo formulation for calculating the probability density function of a single scalar in a turbulent flow. *Flow, Turbulence and Combustion*, 60(2):157–172, 1998.

[124] I. Vallet. Reynolds stress modeling of three-dimensional secondary flows with emphasis on turbulent diffusion closure. *Journal of Applied Mechanics*, 74(6):1142–1156, 2007.

[125] P. R. Van Slooten, Jayesh, and S. B. Pope. Advances in pdf modeling for inhomogeneous turbulent flows. *Physics of Fluids*, 10(1):246–265, 1998.

[126] Nicolas Vauchelet. Numerical simulation of a kinetic model for chemotaxis. *Kinet. Relat. Models*, 3(3):501–528, 2010.

[127] Cédric Villani. *Topics in optimal transportation*, volume 58 of *Graduate Studies in Mathematics*. American Mathematical Society, Providence, RI, 2003.

[128] Cédric Villani. *Optimal transport, old and new*, volume 338 of *Grundlehren der Mathematischen Wissenschaften [Fundamental Principles of Mathematical Sciences]*. Springer-Verlag, Berlin, 2009.

[129] Michael Winkler. Finite-time blow-up in the higher-dimensional parabolic–parabolic keller–segel system. *Journal de Mathématiques Pures et Appliquées*, 100(5):748–767, 2013.

[130] Gershon Wolansky. Multi-components chemotactic system in the absence of conflicts. *European J. Appl. Math.*, 13(6):641–661, 2002.

[131] Yang Xia and George Whitesides. Soft lithography. *Angewandte Chemie*, 37:550, 1998.

[132] Kun Xu. A gas-kinetic bgk scheme for the navier-stokes equations and its connection with artificial dissipation and godunov method. *Journal of Computational Physics*, 171(1):289–335, 2001.

[133] Kun Xu. A well-balanced gas-kinetic scheme for the shallow-water equations with source terms. *Journal of Computational Physics*, 178(2):533 – 562, 2002.

[134] Kun Xu and Juan-Chen Huang. A unified gas-kinetic scheme for continuum and rarefied flows. *Journal of Computational Physics*, 229(20):7747–7764, 2010.

Résumé

Cette thèse s'intéresse à la migration cellulaire d'une population composée de deux espèces qui interagissent par le biais de signaux chimiques. Ces signaux chimiques auxquels sont soumis les deux espèces sont de nature différente. Ils sont soit intérieur (produit par les deux espèces) ou bien extérieur (apporté par le milieu et consommé par les deux espèces). On observe le phénomène de synchronisation et de désynchronisation lors de la migration d'une population composée de deux espèces différentes d'E.Coli. Séparément, les bactéries rouges d'E.Coli se déplacent deux fois plus vite que les bactéries vertes. Cependant dans le cas d'une population mixte composée de rouges et de vertes, les bactéries rouges et vertes se déplacent ensemble ou séparément en fonction de la proportion de la bactérie la plus rapide rouge dans la population. Cette observation expérimentale est interprétée par un modèle macroscopique parabolique de chimiotactisme à deux espèces pour lequel l'existence et la non-existence des ondes de concentration sont prouvées. Ce modèle macroscopique parabolique à deux espèces est construit à partir des modèles microscopiques qui traduisent le mouvement individuel des cellules. Ce phénomène de synchronisation et de désynchronisation est aussi présent dans la dynamique des masses de dirac des deux espèces après l'explosion des solutions classiques dans un modèle d'agrégation à deux espèces avec une seule substance chimique. Nous proposons aussi dans cette thèse une méthode pour obtenir des schémas numériques préservant à la fois l'équilibre et l'asymptotique. Cette méthode est testée aux modèles cinétiques de chimiotactisme et de transfert radiatif.

Abstract

This thesis is concerned about cellular motion of a population composed of two species in interaction through chemical cues. The chemical cues to which the two species are subject are of different kind. They can be internal (produced by the two species) or external (present in the meduim and consommed by the two species). Synchronising and non-synchronising effects are observed during the migration of the population formed by two different strains of E.Coli. Although separately, red bacteria E.Coli travel twice as fast as green bacteria E.Coli, put together, they travel or split depending on the percentage of the faster bacteria in the population. This experimental result is explained by a two-species parabolic macroscopic chemotaxis model for which the existence and non-existence of traveling pulses are showed. The parabolic macroscopic model is derived from microscopic models which describe the individual motion of cells. The synchronising and non-synchronising effect is also encountered in dynamics of the two-species dirac masses after blow-up of classical solutions in a two-species model for aggregation. A method to design both well-balanced and asymptotic preserving schemes is proposed. This method is tested to chemotaxis and radiative transport kinetic models.